Hierarchically Structured Superomniphobic Coatings

DEVELOPING HIERARCHICALLY STRUCTURED SUPER-REPELLENT COATINGS FOR THE REDUCED ADHESION OF BIOLOGICAL CONTAMINATES

BY RODERICK DAVID MACLACHLAN

B.ENG. (McMaster University)

A Thesis Submitted to the School of Graduate Studies in Partial Fulfillment of the requirements for the Degree Doctor of Philosophy in Engineering Physics

McMaster University, Doctor of Philosophy (2022) Hamilton, Ontario

(Engineering Physics)

TITLE: Developing Hierarchically Structured Super-Repellent Coatings for the Reduced Physical Transmission of Pathogens

AUTHOR: Roderick David MacLachlan, B.Eng., Engineering physics (McMaster University)

SUPERVISORS: Leyla Soleymani, Associate Professor, Department of Engineering Physics, McMaster University and Tohid F. Didar, Associate Professor, Department of Mechanical Engineering, McMaster University

NUMBER OF PAGES: XVIII, 184

Lay Abstract

The interaction of pathogens with surfaces in our environment has significant implications for human health and contributes significantly to infections acquired in the community or in hospitals. In the past decade, enormous efforts have been put towards reducing the surface-mediated spread of pathogens. As a result, engineered surfaces with repellent properties that prevent biofouling and contamination have gained significant traction. Repellent surfaces typically work based on the superhydrophobic effect, trapping air within their surface structure, and limiting the interacting surface area of the interface. In this thesis, we developed a simple and scalable method for creating superhydrophobic materials and investigate the ability of this surface in repelling various biological contaminants including: blood, feces, bacteria and viruses. To characterize the repellant properties, multiple experimental methods were developed to analyze the biofouling ability of the surfaces and physical transfer of pathogens between different materials. We also further develop these repellant surfaces to have the additional ability to deactivate pathogens on their surfaces under light exposure.

Abstract

Recently, the rise and appearance of antibiotic resistant pathogenic bacteria, and pathogenic viruses have resulted in significant economic and societal repercussions. The spread of pathogens has led to increases in the prevalence of infections acquired from contaminated surface, especially within healthcare environments. In response to these issues, many new technologies have been developed to address the spread of these pathogens. Repellent and antipathogenic materials have been developed to reduce the levels of contamination seen on surfaces and the ability for these surfaces to transmit pathogens. In this thesis, we developed pathogen-repellent surfaces, which significantly reduce biofouling on their surface by reducing bacterial adhesion due to their omniphobic properties and deactivating the adhered pathogens *via* the production or Radical Oxygen Specie (ROS).

Superhydrophobic wetting states have been shown to reduce the adhesion of biological contaminants and prevent biofouling at the surface. However, the performance of these repellent properties is dependent on the stability of the wetting states. Hierarchical structured surfaces with topography in both the micro- and nano-scale increase the stability of these wetting states when compared to structures at each individual length scale, and thus show potential in further increasing the repellency of surfaces in response to biological contaminants. To create a superhydrophobic and repellent surface with a hierarchically structured surface, we developed an all solution-based technique for depositing nanoparticle (NP) films. This method utilized self-assembled monolayers of ((3-Aminopropyl)triethoxysilane (APTES). The positive charge of the uniform amine monolayer was able to then ionically bond to negatively charged gold nanoparticles

(AuNP) and silica nanoparticles (SiNP). This was combined with pre-strained polymer substrates which allowed for the formation of a wrinkled microstructure when shrunk, resulting in nanotextured microscale wrinkles. These Structures were then paired with a self-assembled coating of Fluorosilane (FS), which greatly reduced the surface energy of the surface and formed robust superhydrophobic states.

To characterize the resistance of the surfaces to biofouling, we explored the interaction of the surface to blood staining and thrombosis under both static and dynamic conditions and found a greater than 90% reduction in contamination for all cases. To quantify the adhesion of pathogens to the repellant surfaces, a touch transfer assay was designed, which simulated the transmission from contaminated human hands to sterile surfaces. Two viral pathogens, Herpes Simplex Virus 2 (HSV2) and Human Coronavirus 229E (HuCoV), were tested under single and multiple contamination events, and the surfaces were imaged using SEM to confirm the levels of viral contamination, and showed a reduction greater than 4-log to the adhesion of both viruses. Bacterial contamination was tested for multiple different bacterial pathogens: *Escherichia coli* (*E. coli)*, *Bacillus subtilis (B. subtilis)*, *Pseudomonas aeruginosa* (*P. aeruginosa)* and Methicillin-Resistance *Staphylococcus aureus* (MRSA)). The omniphobic surface here showed a reduction of all bacterial pathogen species of roughly 2.77-log, both individually and in combination. To further reduce the contamination of the surface with pathogens, the repellant surface structures were modified with photoactive TiO_2 nanoparticles, to introduce antipathogenic properties into the films. These surfaces were able to reduce the initial adhesion of bacteria pathogens by 2.77-log while also being able to decrease surface contamination by another2.5-log after exposure to ultra-violet (UV) light.

Acknowledgements

First, I would like to give my deepest gratitude to my supervisors Dr. Leyla Soleymani and Dr. Tohid F. Didar for their combined guidance, advice, and mentorship though the work. While completing my studies both Dr. Soleymani and Dr. Didar inspired as well as encouraged me to pursue new and interesting ideas. I would also like to thank Dr. Katherine Grandfield (Bernar) for her insights and feedback during her role in my supervisory committee.

I would like to also express my thanks to all the members of Dr. Soleymani and Dr. Didar's lab for making my time during the research more enjoyable. Specifically, I would like to thank Dr. Sara Imani who I collaborated with closely on several aspects of this work. Specifically, I acknowledge her for help in blood related bioassays, and the development and guidance in the design of virus and bacteria assays.

Many thanks to the several of the incredible graduate and undergraduate students to whom I worked closely with, including, Amanda Victorious, Sudip Saha, Sadman Sakib, Noor Abu Jarad, Liane Ladouceur, Amid Shakeri and Shadman Khan. All my lab mates for the support, insights and discussions though the research work, which aided my understanding in several aspects of my projects.

I would like to thank my parents, Donna Rae Rowlands and Howard MacLachlan for their continuous support and encouragement though both easy and difficult times.

Finally, I would like to acknowledge the Natural Sciences and Engineering Research Council of Canada (NSERC), and McMaster University for their Financial support.

Table of Contents

Lay Abstract iii
Abstract iv
Acknowledgements vi
List of Figures x
List of Tables xiv
List of Abbreviations and Symbols xv
Declaration of Academic Achievement xvii
Chapter 1 Introduction 1
1.1 Impact of Biological Contamination of Surfaces 1
1.1.1 Pathogen Transmission *via* Surfaces 1
1.1.2 Blood Related Biofouling of Surfaces 5
1.2 Engineered Materials for Reducing the Biological Contamination of Surfaces 6
1.2.1 Importance of developing repellent materials 6
1.2.2 Repellent surfaces 7
1.2.3 Pathogen Repellency 9
1.2.4 Blood Repellency 14
1.2.5 Dual-Functional Surfaces: Combined Repellency and Antimicrobial Properties 16
1.3 Research Objectives 23
1.4 Thesis Overview 26
Chapter 2 Background on Surface Wetting, Biological Contamination, Repellent Wrinkled Hierarchical Structures and Antimicrobial Action of TiO_2 29
2.1 Principles of Surface Wettability and Adhesion 29
2.2 Theoretical Implications of Wettability for Repellant Surfaces 34
2.2.1 Bacteria Adhesion 35
2.2.2 Blood Adhesion 36
2.2.3 Robustness of Repellent Properties 37
2.3 Design of Hierarchically Structured Omniphobic Surfaces 39
2.4 Thin Film Wrinkling for Hierarchical Structure Formation 43
2.5 Deactivation of Pathogens 46
2.5.1 Antipathogenic Compounds 46
2.5.2 Anti-microbial Effects of TiO_2 48
2.6 Conclusion 52

Chapter 3 Hierarchical Structures, with Submillimeter Patterns, Micrometer Wrinkles, and Nanoscale Decorations, Suppress Biofouling and Enable Rapid Droplet Digitization 53

3.1 Abstract 56

3.2 Introduction 56

3.3 Materials and Methods 60

3.4 Results and discussion 65

3.4.1 Fabrication and characterization of hierarchical liquid repellant surfaces 65

3.4.2 Interaction of hierarchical surfaces with human whole blood 70

3.4.3 Patterned structures for digitizing droplets and dip-based bioassays 75

3.5 Conclusion 77

3.6 Acknowledgements 78

3.7 Supplementary Information 79

Chapter 4 A Repellent Plastic Wrap With Built-In Hierarchical Structuring Prevents the Contamination of Surfaces with Coronaviruses 81

4.1 Abstract 83

4.2 Introduction 84

4.3 Methods 89

4.4 Results and Discussion 93

4.4.1 RepelWrap Fabrication and Quantification of Surface Repellency and Durability 93

4.4.2 Evaluation of RepelWrap in reducing viral contamination using an enveloped virus (HSV-2) as a model 99

4.4.3 RepelWrap significantly reduces contamination with coronaviruses 101

4.5 Conclusion 104

4.6 Acknowledgments 105

4.7 Supplementary Information 105

4.7.1 Inactivation of viruses from Fluorosilane 105

4.7.2 Partial wetting of surface structure with different liquids 106

4.7.3 Tunable Wetting with change in nanoparticle size 107

4.7.4 Surface Durability to shearing 111

Chapter 5 A Super-Omniphobic and Photoactive Surface Presents Antimicrobial Properties by Repelling and Killing Pathogens 113

5.1 Abstract 115

5.2 Introduction 116

5.3 Methods 121

5.4 Results and Discussion 124
5.4.1 Manufacturing and Wettability of the Omniphobic Wrap 124
5.4.2 Interaction of Omniphobic Hierarchical structures with Pathogens 129
5.4.3 Testing of Anti-Pathogenic Properties in Real-World Conditions 133
5.6 Conclusion 136
5.7 Acknowledgements 137
5.8 Supplementary Information 138
5.8.1 EDX Data on the surfaces 138
5.8.2 Properties of Probing Liquids 138
5.8.3 Fraction of Surface Wetting 138
5.8.4 Surface Durability 140
5.8.5 Mixed Bacteria Transfer Assay 141
5.8.6 Determination of Fecal Bacteria Strains 142
Chapter 6 Summary, Conclusions, Limitations, and Future Work 146
6.1 Thesis Summary 146
6.2 Thesis Conclusions 147
6.3 Contributions to the Field 150
6.4 Future Work 153
6.5 References 159

List of Figures

Figure 1-1: Flowchart showing the pathways of transmission between an infected host and a healthy individual. 3
Figure 1-2: Schematic of liquid droplet interacting with a) hierarchically structured and b) lubricant infused omniphobic surface. i) and ii) represent the static interaction of water and hexadecane with the surface respectively. iii) and iv) represent the dynamic interaction of water and hexadecane sliding across the surface respectively. 8
Figure 1-3: Schematic showing the function of pathogen repellent, antipathogenic and dual-functional surface. Pathogen repellent surfaces a) superhydrophobic surface and b) lubricant infused surface. Antipathogenic surfaces c) contact killing surface and d) biocide releasing surface. Dual-functional surface e) co-deposited repellent and antipathogenic functionalized surface and f) repellent surface structure with biocide releasing surface. 17
Figure 2-1: Contact angle and droplet geometry on surfaces with different surface energy and surface topography. a) The contact angle on a smooth homogenous coating, the red arrow denotes the different forces interacting at the three-phase line. The droplet geometry of b) hydrophobic and c) hydrophilic materials under different wetting states; i) Young wetting, ii) Wenzel wetting and iii) Cassie-Baxter Wetting. 31
Figure 2-2: Surface Biofouling of planar and superhydrophobic surface by bacteria (a, b) and whole blood (c, d). 36
Figure *2-3*: Schematic showing the difference in wetting state of water (blue) and hexadecane (green) for a) superhydrophobic-oleophilic, b) superhydrophobic-oleophobic and c) omniphobic surfaces. 39
Figure 2-4: Schematic drawing of the thin film deposited on the substrate a) before and b) after shrinking. 45
Figure 2-5: Schematic of the antimicrobial action of TiO2. a) Photoactive production of ROS by TiO2, b) transport and attack of ROS to the live bacteria cell wall, and c) bacterial deactivation after oxidation of cell wall and internal cellular components. 50
Figure 3-1: Schematic depicting the fabrication process of liquid repellant surfaces and corresponding SEM images. a) Process steps for the formation of the AuNP decorated surface and the hierarchically structured surfaces. b) SEM images depicting the untreated PS (i), AuNP decorated PS (ii, PS-AuNP-Planar), and final hierarchically-structured PS (iii, PS-AuNP-Shrunk). The scale bars in the larger SEM images represent 1 μm and those in the insets represent 100 nm. 65
Figure 3-2: Surface Repellency. a) Graph depicting the contact angle of different surfaces for water (blue), hexadecane (orange), and whole blood (red). Representative SEM images are also shown on the top with an image of the water droplet on the surface. The table shows the sliding angles of the different control groups. b) Graph showing the change in contact angle with varying ethanol concentrations in water. Dotted line at 90 degrees shows the point where surfaces enter the hydrophilic regime. 67
Figure 3-3: Study of blood repellency on the hierarchical surfaces. a) All surfaces were incubated with blood for 30 minutes and after two washes, they were transferred to well plates containing water (transfer solution). The absorbance of the transfer solution was measured at 450 nm wavelength and normalized to the value obtained from PS-Planar. Representative images of the transfer wells corresponding to PS-Planar and PS-AuNP-Shrunk are shown at the top right of the figure. The representative images of the surfaces incubated in blood are shown at the bottom of the figure. b) Relative clot weight adhered to each surface is normalized to the

adhered clot to the PS-Planar and compared to the other control groups. Representative images of samples are shown after being exposed to the clotting assay after a 2X PBS wash. Error bars represent standard deviation from the mean for the clot assay performed on at least three surfaces for each class. c) SEM images of the surfaces after the clotting assay and 2X PBS washes followed by fixation in 4% formaldehyde performed on the PS-Planar (i) and PS-AuNP-Shrunk (ii), demonstrating blood adherence to the planar surface. The scale bars represent 1 μm in (i) and (ii).....72
Figure 3-4: Dynamic conditions for blood adhesion tests. a) number of blood cells per mm^2 in microfluidics channel subjected to heparinized blood flow and subsequent washing for both PS-Planar and PS-AuNP-Shrunk. b) Optical images showing blood adhesion in (i) PS-Planar and (ii) PS-AuNP-Shrunk. c) Bright-field microscope images comparing (i) PS-Planar (ii) PS-AuNP-Shrunk. Blood cells are visible in (i) and wrinkles are visible with no presence of blood cells in (ii).....74
Figure 3-5: Digitization strategy enabled by patterning hydrophilic and liquid repellant areas a) (i) the substrate is covered with a vinyl mask, (ii) the vinyl mask is patterned to create hydrophilic wells, (iii) the substrate is modified with nanoparticles and coated with fluorosilane, (iv) the mask is removed, (v) the substrate is shrunk. b) SEM images of the fabricated wells showing the planar (hydrophilic) and hierarchical liquid repellant regions (scale bar 1 μm). c) (i) shows patterned wells with planar (inside the squares) and modified regions. (ii) shows the patterned well after being dipped in blue dyed water, demonstrating digitization of water droplets (iii) digitizing Cy5-tagged anti IL-6 antibody on the patterned wells. d) IL-6 assay performed using 2500 pg/mL of target solution compared to control solutions by dipping the wells in solutions containing the assay components. Briefly, capture antibody was deposited on the wells through EDC-NHS chemistry, and then dipped in solution containing 2500 pg/mL IL-6. Subsequently, the sample was subjected in biotinylated IL-6 antibody and streptavidin dye. And for blank, all the steps were kept the same but for the IL-6 incubation. e) Representative fluorescent images of the assay used in (d). 76
Figure 4-1: RepelWrap and its role in reducing viral transmission. (a) schematic illustration of person-to-person transfer of viruses through common (i) and RepelWrap-coated (ii) high touch surfaces. (b) Schematic diagram illustrating the manufacturing process of the RepelWrap (c) Scanning electron micrograph of i) polyethylene, ii) aluminum and iii) RepelWrap. The scale bars represent 1 μm. The inset provides a high magnification image of the surface with a scale bar of 100 nm.....94
Figure 4-2: Evaluation of surface repellency and durability. (a) Graph displaying the contact angle (bars) and contact angle hysteresis (cross) of different surfaces with water (blue), hexadecane (green), glycerol (orange), and ethylene glycol (yellow). Images of water CA are inserted blow. (b) Schematic representation of the stability testing experiments where the contact angle of a newly fabricated surface was evaluated (i), the surface was physically contacted using an elastomeric stamp or a human finger (ii), and the physical characteristics of the surface were re-evaluated (iii). (c) Graph demonstrating the change in contact angle and contact angle hysteresis of water and hexadecane after repeated contact with an elastomeric stamp. (d) Graph demonstrating the change in contact angle and contact angle hysteresis of water and hexadecane after repeated touches with a human finger. All error bars represent the standard deviation from the mean. 97
Figure 4-3: Evaluation of the viral titer of RepelWrap after exposure to stamps contaminated with HSV-2. (a) schematic showing the stamp-based surface contamination assay (b) image showing the plaque assay performed on the three surfaces (c) Quantification of viral load on

different surfaces after contamination using the stamping technique depicted in (a), the red line represents the concentration of viruses deposited onto the stamp prior to contact with the surface. 101
Figure 4-4: Evaluation of the viral titer of RepelWrap after exposure to stamps contaminated with HuCoV-229E (a) The amount of viral titer measured on surfaces after contact with stamps contaminated with HuCov-229E. The red and blue line shows the total concentration of viral samples deposited on the stamp before contact with the surface. (b) SEMs of aluminum (i, ii), polyethylene (iii, iv) and RepelWrap (v, vi) after contact with contaminated HuCov-229E stamps. The scale bars represent 1 µm (i, iii, v) and 10 µm (ii, iv, vi). 103
Figure 5-1: Fabrication and characterization of the OmniKill Wrap. a) Schematic diagram depicting the manufacturing process of the OmniKill Wrap: i) oxygen Plasma treatment of the polyolefin substrate, ii) dip-coating of the substrate into a TiO_2 nanoparticle suspension, iii) fluorosilanization of nanoparticles on the substrate, and iv) formation of microstructure through shrinking of the polymer substrate, along with the corresponding SEM images. e) Surface repellency of the OmniKill Wrap with various liquids (water, glycerol, ethylene glycol, formamide and hexadecane). The static contact angles for each liquid are denoted in the table above the graph while the colour boxes in the graph represent the contact angle hysteresis. Dynamics of liquids bouncing on the surface of OmniKill Wrap using f) water and g) hexadecane. Scale bars on the SEM images are 3 µm. 125
Figure 5-2: Characterization of the pathogen repellency of the OmniKill Wrap. a) Log-plot depicting the number of bacteria transferred between a contaminated stamp and sterile surface after physical contact. Red lines indicate the initial concentration of bacteria on the contaminating stamp. b) SEMs of bacteria (E. coli; i, ii, iii. B. subtilis; iv, v, vi. P. aeruginosa; vii, viii, ix. MRSA; x, xi, xii) on surface after contamination through physical contact. Scale bars on the SEM images are 3µm. 129
Figure 5-3: Antimicrobial properties due to the photoactivity of TiO_2. Concentration of live a) P. aeruginosa and b) MRSA on the surfaces after exposure to UV light. Red lines indicate the initial concentration of bacteria on the stamp before contamination. SEMs of the surfaces contaminated with c) P. aeruginosa and d) MRSA after 1h exposure to UV light; i) PO+TiO_2+FS, ii) PO+TiO_2, iii) PO, and in the dark; iv) PO+TiO_2+FS, v) PO+TiO_2, vi) PO. Scale bars on the SEM images represent 3 µm. 131
Figure 5-4: Multi-pathogen assay characterizing the simultaneous contamination of surfaces with multiple bacteria. a) contamination of the surfaces using the stamp assay inoculated with a mixed culture of E. coli, B. subtilis, P. aeruginosa and MRSA. b) contamination of the surfaces with mouse feces containing two types of bacteria (Bacillus cereus and Lactobacillus murinus. c) images showing the staining of i) PO, ii) PO+TiO_2 and iii) PO+TiO_2+FS with mouse feces before (left) and after (right) contact with the contaminated stamp. d) decontamination of the surfaces with UV light after contamination with feces containing Bacillus cereus. Red lines indicate the initial concentration on the stamp prior to contamination. 133
Figure 6-1: Modification of TiO_2 coated PO with catechols a) Schematic of the surface manufacturing b) TiO_2 surface modified with different catechols c) SEM of CA modified TiO_2 surface. 156

Supplementary Figure 3-1: a) Adhesion test on the patterned hierarchical surface, demonstrating the 5B class b) Classification table Adapted from [205] 79
Supplementary Figure 3-2: IL-6 assay components. 80

Supplementary Figure 4-1: Effect of fluorosilane on HSV-2 proliferation. Various concentrations (3%, 0.3%, 0.03%) of fluorosilane solution (blue) and different surfaces(unmodified glass (red), fluorosilane modified glass (white) and fluorosilane modified polyethylene (yellow)) after incubation with 6µL of 10^6 pfu/mL virus solution for 20min. 106
Supplementary Figure 4-2: SEM images of RepelWrap surfaces created from nanoparticles having diameters of a) 27 nm, b) 100 nm and c) 200 nm. Scale bar represents 1 µm. (d), (e)Wettability analysis of RepelWrap surfaces created from nanoparticles in (a)-(c). 109
Supplementary Figure 4-3: Surface structure before (a,b) and after repeated stamping (c,d) and repeated touching with a finger (e,f) for 90 and 300 times respectively. The scale represents 1 µm (a,c,e) and 10 µm (b,d,f)..... 110
Supplementary Figure 4-4: Polyethylene Surface after stamping with culture media at two separate locations demonstrating debris (a,c) and surface defects (b,d). 111
Supplementary Figure 4-5: Contact angle after surface sheering with different weights 112
Supplementary Figure 5-1: EDS images of the Fluorine coverage of the a) microstructure and b) nanostructure 138
Supplementary Figure 5-2: Static Contact angle for surface before and after formation of the microstructure. 139
Supplementary Figure 5-3: Fraction of surface wetting for PO+TiO_2 and PO+TiO_2+FS surfaces 140
Supplementary Figure 5-4: Stability of the omniphobic properties to a) surface compression and b) mechanical abrasion. 140
Supplementary Figure 5-5: Total contamination of Surface After mixed assay transfer..... 141
Supplementary Figure 5-6: Different colony morphologies of the various bacterial strains, a) TSB-NXA plates and b) TSB plates. 142
Supplementary Figure 5-7: Different colonies found in mouse fecal samples 143

List of Tables

Table 1-1: Summary of blood and pathogen repellent surfaces' technologies. 11
Table 1-2: Summary of the best preforming dual-functional antimicrobial and pathogen repellant surface technologies 20
Table 2-1: Summary of the liquid repellant properties of hierarchically structured wrinkled surfaces. 42

Supplementary Table 5-1: Surface Tension Components of Probe Liquids 138

List of Abbreviations and Symbols

APTES	(3-Aminopropyl)triethoxysilane
AuNP	Gold Nanoparticle
BSA	Bovine Serum Albumin
CA	Contact Angle
CAH	Contact Angle Hysteresis
DMEM	Dulbecco's Minimum Egal Medium
EDS	Energy Dispersive Spectroscopy
EDC	(N-ethyl-N'-(3-(dimethylomino)propyl)carbodiimide
EPS	Extracellular Polymeric Substances
FS	Fluorosilane
HuCoV	Human Corona Virus
IL6	Interlukin-6
MERS	Middle East Respiratory Virus
MES	2-(N-morpholino)ethanesulfonic acid
MRSA	Methicillin-Resistant *Staphylococcus aureus*
NHS	N-hydroxysuccinimide
NMW	Nanoparticle induced Micro Wrinkling
NP	Nanoparticle

OTS	Trichloro(octadecyl)silane
PBS	Phosphate Buffer Silane
PDMS	Polydimethylsiloxane
PFA	Paraformaldehyde
PO	Polyolefin
PS	Polystyrene
PTFE	Polytetrafluoroethylene
ROS	Reactive Oxygen Species
SA	Sliding Angle
SAM	Self-Assembled Monolayer
SEM	Scanning Electron Microscopy
SiNP	Silica Nanoparticle
TSB	Tryptic Soy Broth
UV	Ultraviolet
UVO	Ultraviolet Ozone

Declaration of Academic Achievement

This dissertation was written to fulfill the requirements of the doctoral degree in the department of Engineering Physics at McMaster University. The work described here was preformed from September 2018 to March 2023.

The majority of the work in this written document was conducted, conceived, analyzed and written by the author of this thesis, in consultation with the supervisor Dr. Leyla Soleymani and the Co-supervisor Dr. Tohid F. Didar, with the following exceptions:

Chapter 1: “Introduction” was drafted by Roderick David MacLachlan and reviewed to the final version by Dr. Tohid Didar and Dr. Leyla Soleymani.

Chapter 2: “Background on Surface Wetting, Biological Contamination, Repellent Wrinkled Hierarchical Structures and Antimicrobial Action of TiO_2” was drafted by Roderick David MacLachlan and reviewed to the final version by Dr. Tohid Didar and Dr. Leyla Soleymani

Chapter 3: For “Hierarchical Structures, with Submillimeter Patterns, Micrometer Wrinkles, and Nanoscale Decorations, Suppress Biofouling and Enable Rapid Droplet Digitization”, Dr. Sara Imani performed the blood staining and coagulation assays and contributed equally in the writing of the manuscript. The manuscript was reviewed to the final version by Dr. Tohid Didar and Dr. Leyla Soleymani

Chapter 4: “Repellent Plastic Wrap with Built-In Hierarchical Structures Prevents the Contamination of Surfaces with Coronaviruses” was drafted by Roderick David MacLachlan and reviewed to the final version by Dr. Tohid Didar and Dr. Leyla Soleymani. Fatema Vahedi conducted the virus transmission assays.

Chapter 5: “A Super-Omniphobic and Photoactive Surface Presents Antimicrobial Properties by Repelling and Killing Pathogens” was drafted by Roderick David MacLachlan and reviewed to the final version by Dr. Tohid Didar and Dr. Leyla Soleymani. Farhaan Kanji ran the multi-pathogen transmission assay.

Chapter 1 Introduction

Preface:

This chapter outlines the challenges caused by the contamination of surfaces with biological materials. It also reviews the current strategies and technologies used for addressing the concerns related to biological contamination. More specifically, the chapter reviews the scientific literature on the role of pathogen-repellant, antipathogenic, and dual functional materials in reducing biological contamination. The final portion of this chapter is dedicated to the organization and objectives of this thesis.

1.1 Impact of Biological Contamination of Surfaces

1.1.1 Pathogen Transmission *via* Surfaces

Pathogens are microorganisms, such as bacteria and fungi,[1] or biological materials like viruses, which produce infection or disease in a host organism.[2] The prevalence of pathogens in the healthcare system and the transmission between patients, workers and visitors have significant implications on human health. Hospital acquired (nosocomial) infections occur in approximately 5-10% of all hospital visits in developed countries, while occurring in 40% of all visits in low-income countries.[3,4] Pathogens are transmitted through the following means: indirect or direct physical contact, droplet transmission, airborne transmission, or fecal-oral transmission.[5] Indirect contact transmission involves the transfer of pathogens from inanimate objects to the hands of an individual, while droplet transmission is generated by coughing, sneezing or talking.[6–8] Once present on hands or airborne, the released pathogens can then be deposited onto inanimate surfaces in the environment, creating fomites. Fomites are contaminated inanimate

surfaces or materials that cause infection, and are created through three distinct pathways; droplet transmission,[5,9] direct contact transmission, and indirect contact transmission (Figure 1-1).[5,10] Droplet transmission occurs through the settlement of aerosols or airborne droplets on surfaces.[11,12] This process is dependent on the size of the droplet, as large airborne droplets settle on surfaces faster than smaller ones.[13] During direct and indirect contact transmission, pathogens are physically transferred from one surface to another. Direct transmission occurs from physical contact with the pathogen source,[5] while indirect transfer occurs from physical contact with an already contaminated material.[5] Once fomites are formed in the environment, a healthy individual may come in contact with them leading to the onset of an infectious disease. The contamination of healthy individuals occurs through contact with inanimate surfaces (fomites); inhalation of contaminate aerosols, secondary contact with a fomite (indirect contact transmission), or direct contact with an infected individual (direct contact transmission).[5] Once in the host, pathogens begin to grow and proliferate increasing their numbers and causing infection. Eventually, the pathogen will shed from the infected host and the process of transmission begins.

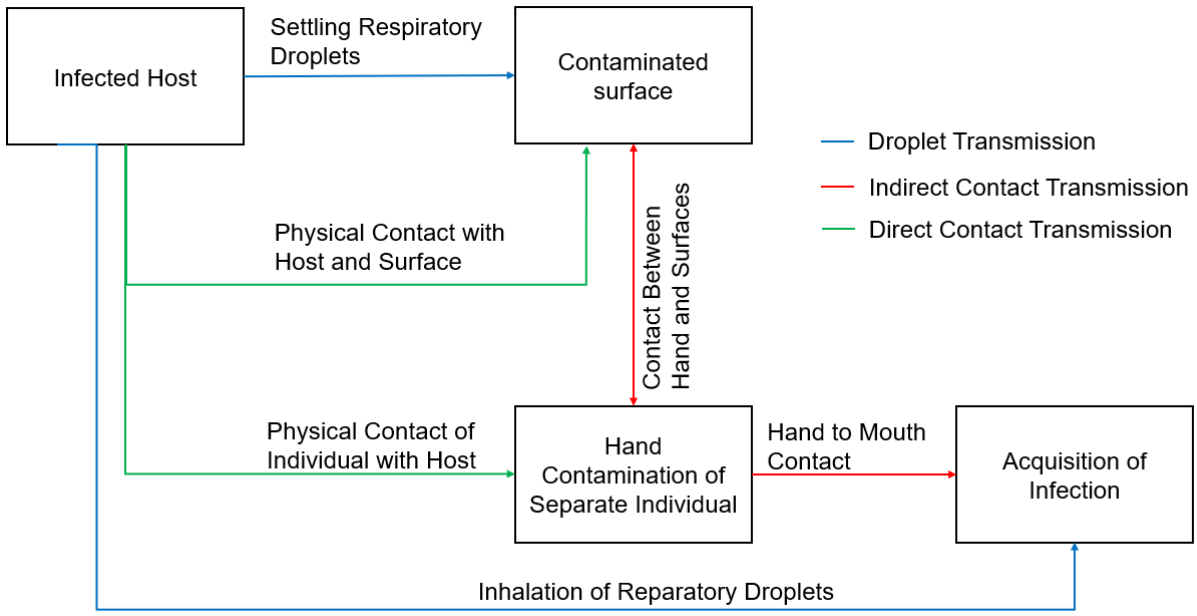

Figure 1-1: Flowchart showing the pathways of transmission between an infected host and a healthy individual.

Most of the pathogens responsible for the prevalence of nosocomial infections are bacterial pathogens and are transmitted through physical contact between healthcare workers, patients and surfaces/equipment in their environment.[3] Methicillin-Resistant *Staphylococcus aureus* (MRSA) is the most significant nosocomial pathogen, responsible for up to 60% of all nosocomial infections found in hospital intensive care units.[4] Within these environments, MRSA has been found to contaminate various surfaces including hospital beds, supply carts and door handles,[3,14] where it has been shown to stay viable for long periods of time, ranging from several weeks to several months.[15] Other notable pathogens transmitted from person to person and environment to person through physical contact are *P. aeruginosa*, *E. coli* and vancomycin-resistant *enterococci*.[3] Fungi are the second most common classes of pathogens responsible for nosocomial infections,[1] with

the two most common species being *Candida* and *Aspergillus*.[16] *Candida* species in particular have been shown to significantly contaminate surfaces around infected patients and have demonstrated survivability and viability for periods ranging from 14 days to 4 weeks.[17] Viruses make up the smallest contributor of nosocomial infections,[18] and mostly spread through air-born transmission (influenza and corona virus);[16] however, some viruses have been shown to transmit though contaminated surfaces.[19] Human Norovirus and Hepatitis A Virus are found in high concentrations in infected fecal matter and are able to transmit between people through fomites.[16,19]

Reducing the number of fomites is important in reducing the spread of pathogens between individuals within an environment. This can be achieved in two ways: preventing the initial contamination of the surfaces and decontaminating the material after contamination. The decontamination of surfaces is usually done using strong disinfectants (for the cleaning of surfaces) and hygiene protocols (for the cleaning of hands).[1,3] However, many nosocomial pathogens have shown resistance to the effects of disinfectants and persist on surfaces after decontamination is carried out,[20] and the effectiveness of the widespread use of disinfectants has been debated.[1,17] In addition, there are concerns with the environmental and worker health risks associated with high exposure to chemical disinfectants such as ortho-phthalaldehyde, hydrogen peroxide - peracetic acid mixtures, and chlorine based disinfectants.[21,22] This highlights the importance robust and safe contamination prevention methods.

1.1.2 Blood Related Biofouling of Surfaces

The contamination of surfaces with blood has a significant impact on the performance of medical devices and the transmission of pathogens in hospitals. Blood is a complex liquid made up of many different proteins (platelets and fibrin) and cells (red blood cells and while blood cells).[23] The contamination of a surface with blood begins with the adhesion of proteins and cells to an inanimate surface.[23] As soon as blood comes into physical contact with a surface, proteins from the blood plasma begin to adhere to the solid interface.[24] This begins a series of complex interactions known as the coagulation cascade and ends with the formation of Thrombi (blood clots).[23] This process has a significant impact on the performance of medical devices such as stents, vascular grafts, pacemakers, tubing and catheters. [24] Blood coagulation in these devices often leads to thrombotic complications and has the potential to be lethal.[24,25] As such methods for preventing the formation of thrombi in these devices have gained significant traction in recent year.[26]

In addition to medical devices, the contamination of surfaces in human made environments (*i.e.* built environments) with blood also has significant health implications, both inside and outside of healthcare settings. Both wet and dry blood interacting with surfaces have been shown to transmit blood borne pathogens such as Human Immunodeficiency Virus, Hepatitis B Virus, and *S. aureus*.[27–29] Blood released from a contaminated individual via open lesions or excretions can spread and contaminate both medical devices and surfaces in the environment,[27] aiding in the adhesion of pathogens to those materials.[24] For bacterial pathogens, the presence of blood can facilitate the formation of biofilms and supply the pathogen with nutrients,[14] creating long lasting

contamination of the surface.[14,24,27] While whole blood is a highly contaminating and complex liquid which can quickly adhere to various surfaces, repellent surface technologies have been developed and studied in recent years in order to combat this form of contamination.[30]

1.2 Engineered Materials for Reducing the Biological Contamination of Surfaces

1.2.1 Importance of developing repellent materials

In recent years, novel material systems that reduce the adhesion, viability, and spread of pathogens have been developed. Materials that prevent the initial contamination of pathogens are known as pathogen-repellent materials, while materials that disinfect their surface after contamination are known as antipathogenic materials.[31] Of significant interest is the ability of pathogen repellent materials to significantly reduce the transmitted/inoculating concentration of pathogens on the surface. This has significant effects on the lifetime of pathogens on the surface, as high concentrations of pathogens on surfaces are associated with increased lifetime and survivability.[14] Pathogen-repellent surfaces have the added benefit of preventing the development of antimicrobial resistance, as they do not rely on biocidal agents for their reduction in contamination.[14] Furthermore, pathogen repellent surfaces also display resistance to the adhesion of extra-cellular proteins and metabolic biproducts produced by pathogens, such as biofilms,[32] that increase pathogen adhesion, longevity and proliferation on a contaminated surface.[33] In addition to biofilm resistance, many pathogen-repellent materials repel other contaminating matter/materials that may contain pathogens such as fecal matter and respiratory droplets.[31] Pathogen containing feces, respiratory droplets, dust, and

biological liquids (blood, urine, and saliva) enable the formation and increase the lifetime of fomites.[1,14,34] As a result, developing materials with both pathogen repellent and broad-spectrum repellent properties to a wide variety of biological contaminates is important in limiting the transmission of pathogens.

1.2.2 Repellent surfaces

Surfaces with broad spectrum repellency can be broken down into two subcategories: 1) hierarchically structured superhydrophobic coatings, or 2) lubricant infused coatings. The classification of the repellent surface depends on the material, surface structure and repellent mechanism of the surface.

Hierarchically structured surfaces are materials with structures that exist across multiple length scales, typically incorporating structures at the nano and microscale.[35] As such, they have high surface roughness allowing for large quantities of air to be entrapped within the surface structure, forming superhydrophobic (Cassie-Baxter) states. For surfaces experiencing superhydrophobicity, the quality/strength of the repellent properties is determined from contact angle (CA) measurements, which characterizes the profile of a droplet on the solid interface.[36] When superhydrophobic wetting states are present, the contact angle (θ_c) of the droplet is greater than 150^o and displays a spherical profile indicating poor adhesion to the surface (Figure 1-2a, i).[36,37] As a result of the spherical droplet profile, water droplets on superhydrophobic surfaces roll/slide across the surface (Figure 1-2a, iii). The roll off angle or sliding angle (SA) is often used as another metric for determining the repellency of the surface.[36]

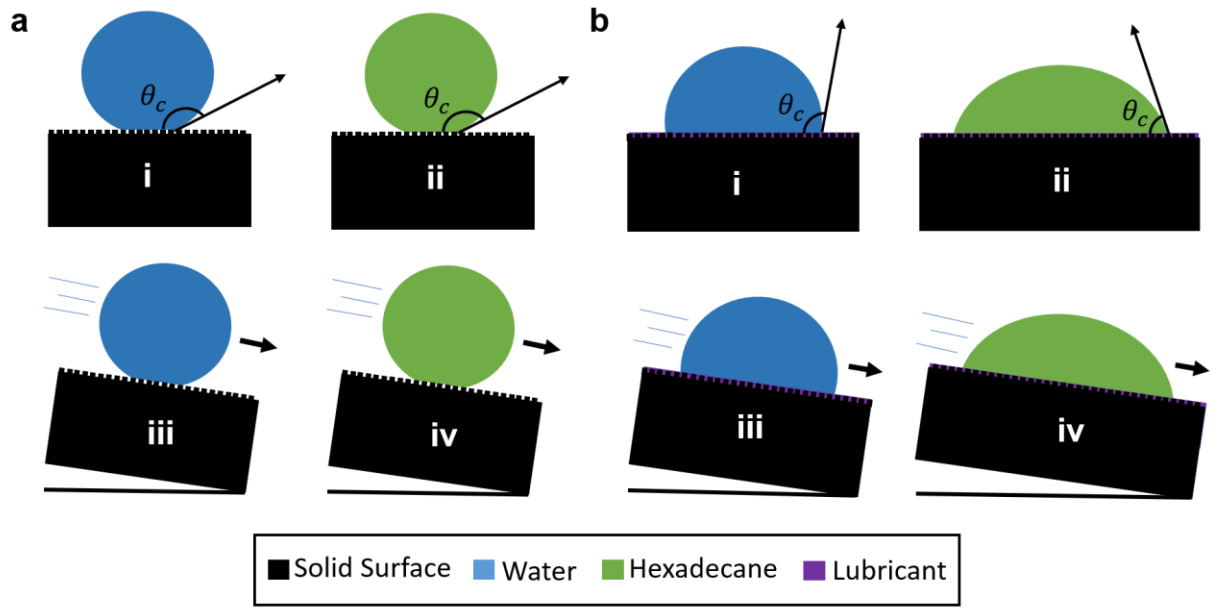

Figure 1-2: Schematic of liquid droplet interacting with a) hierarchically structured and b) lubricant infused omniphobic surface. i) and ii) represent the static interaction of water and hexadecane with the surface respectively. iii) and iv) represent the dynamic interaction of water and hexadecane sliding across the surface respectively.

Lubricant infused surfaces are materials with a liquid lubricant trapped on or within their solid surface.[36] This lubricant acts as a barrier and prevents the interaction and adhesion between the solid surface and contaminating matter (solid or liquid).[38] The lubricating liquid is bound/held near the surface by a chemical monolayer with high affinity for the lubricant.[36,38] Furthermore, lubricant infused surface can have a variety of surface structures and topographies being planar, porous, or hierarchical structured.[35,39–42] For lubricant infused surfaces, the level of repellency is no longer quantified by the CA, as liquids with CA both greater or less than 90^o can easily slide across the surface (Figure 1-2b). Lubricant infused surfaces, unlike superhydrophobic surfaces, rely on the

immiscibility of the contaminate with the lubricating layer. As a result, CAH and SA are more important indicators of repellency.[38]

For both hierarchically structured superhydrophobic and lubricant infused surfaces, those with the highest and broadest repellent properties display omniphobicity. Omniphobicity is the ability for a solid interface to prevent the adhesion or wetting of all liquids,[43] including those with low surface tension such as hexadecane (27.5 $mN \cdot m^{-1}$).[44] For repellent surfaces (hierarchically structured and liquid infused), those which exhibit omniphobic properties are characterized by low (<1º) SA and CAH for all liquids interacting with the surface (Figure 1-2).[45–49] For hierarchically structured surfaces to be considered omniphobic, they have the additional requirement that the CA for all liquids must be greater than 150º (Figure 1-2a, i, ii), indicating that there are robust Cassie-Baxter wetting states regardless of the contaminating liquid.[45]

1.2.3 Pathogen Repellency

Hierarchically structured superhydrophobic surfaces

Hierarchical structured surfaces have shown great performance in reducing the adhesion of pathogens to surfaces in aqueous environments (Table 1-1). Work by Tingting Ren et al. created a hierarchically structured nanocomposite comprised of fluorinated SiO_2 and CuO NP, with a thickness of 290 nm. This repellent surface structure showed high levels of water repellency (CA of 163º) while also displaying a 3.2-log reduction in the adherence of *Escherichia coli* (*E. coli*).[50] Other notable hierarchical structures have also shown significant reduction 1-log to 2-log (90-99%) in pathogen adherence such as, SiO_2 micro

pillars modified with fluorinated ZnO nanoneedles (Jiang et al.) which showed a >98% (~2-log) reduction in *E. coli* adherence, [51] and hierarchical diamond like carbon films (Wang et al.), which showed reductions of 99% (2-log) and 90% (1-log) for *E. coli* and *P. aeruginosa* respectively.[52] In addition to pathogen repulsion, hierarchically structured surfaces have shown good immunity to the formation of biofilms (MRSA, *P. aeruginosa*)[53,54] on their surfaces. Work by Ekrem Ozkan et al. created a polyurethane sponge functionalized with a mixture of polydimethylsiloxane (PDMS), ZnO, Cu NP and fluorosilane (FS), which is capable of reducing the formation of S*. aureus* biofilm by 99.94% (~3-log) after four days of exposure.[53] While the structures perform well in aqueous environments, they fail to mimic/replicate the real-world transfer of pathogens under physical contact in open air conditions. Work by our lab demonstrated a hierarchically structured wrinkled polymer film showing over 85% reduction in the formation for both MRSA and *P. aeruginosa*.[54] Unlike previous examples from literature, this work conducted pathogen adhesion studies in an open air environment, displaying ~1-log reduction in the adhesion of *E. coli*,[54] demonstrating one of the first examples of repellent materials reducing the physical contact transmission of pathogens in open air.[31]

Table 1-1: Summary of blood and pathogen repellent surfaces' technologies.

Surface Properties		**Surface Wettability**			**Repellency of Biological Contaminates**	
Classification	*Materials and manufacturing*	*CA*	*SA*	*CAH*	*Blood*	*Pathogens*
Hierarchically Structured Surface	Polyurethane sponge coated with fluorinated ZnO and Cu NP.[53]	Water: 160º Blood: 160º	Water: <5º	Water: 0.8º	Fibrinogen adsorption assay showed 76.62% reduction in adhesion	99.94% reduction of *S. aureus* after 4-day drip-flow assay when compared to control surfaces
	Glass substrate coated with silica nanoparticles and Fluorinated CuO nanoparticles.[50]	Water: 163º	-	-	-	3.2-log reduction in adhered *E. coli* from suspension, compared to glass control
	Mussel-inspired dendritic polymer functionalized with gold and silver nanoparticles.[55]	Water: 173º Serum: 166º Ethylene Glycol: 157º SDS (4%): 156º Hexadecane: 148º	Water: <2º Serum: 5º Ethylene Glycol: 10º SDS (4%): 10º Hexadecane: -	Water: <1º	Protein adhesion assay from blood serum showed significant contamination of control surfaces, glass (1.6ug/cm^2) and polystyrene (2.4ug/cm^2), while no contamination was seen on the repellent coating (contamination below LOD)	-
	Polydimethylsiloxane casted on hierarchically wrinkled surfaces and functionalized with silica nanoparticles and fluorosilane.[42]	Water: 166.7º Blood: 143.2º Hexadecane: 100.0º	Water: <5º	-	Showed increase in blood staining of 7%	Showed persistence of MRSA *and P. aeruginosa* on the surface
	Hierarchical diamond like carbon film, with (top) and without (Bottom) Fluorosilane modification.[52]	Water: 148-151º	Water: 2º	Water: 4º	-	Reduced *E. coli* and *P aeruginosa* adhesion by 99% and 90 % respectively
		Water: 170º	Water: 3º	Water: 3º	-	
	Polymer substrate functionalized with silica nanoparticles and fluorosilane, with strain induced hierarchical wrinkle structures.[54]	Water: 154º Blood: 144º Hexadecane: 124º	Water: <5º	Water: 10º	Blood contact angle of 142º	~85% reduction in biofilm formation of both MRSA and *P. aeruginosa*. 20-fold decrease in the fluorescence signal of GFP expressing *E. coli* on hierarchically structured

						surface compared to the bare polymer surface.
	Fluorosilane coated ZnO nanoneedles grown on SiO_2 micropillars.[51]	Water: 174°	Water: <1°	-	-	>98% reduction in the adherence of *E. coli* to the surface. ~140-fold decrease in bacterial contamination after 24 hours incubation in bacteria culture when compared to control surface
Lubricant Infused Surface	Titanium surface microscale features were made though laser ablation of the surface, coated with a fluorinate polymer and infused with perfluoropolyether lubricants.[56]	Water: ~100°	-	Water: <5°	-	~100-fold (2-log) reduction in biofilm volume produced by *S. aureus* on the surface.
	Electrodeposited nano-porous tungstite, infused with perfluoropolyether lubricant.[40]	Water: 124°	Water: 3°	Water: 1.4°	Blood staining assay showed little to no signs of surface contamination	Submersion in10^8 CFU/mL of *E. coli* showed a ~2-fold reduction in the attachment of bacteria cells
	Polydimethylsiloxane casted on hierarchically wrinkled surfaces and functionalized with silica nanoparticles and fluorosilane.[42]	-	Water: <5°	-	95-95% decrease in blood staining of the surface, significant delay in thrombin generation of lubricant infused surface when compared to control surfaces	86% reduction in the adherence of MRSA and 98.5% reduction in the adherence *of P. aeruginosa* to the surface
	Porous amine-reactive films with integrated silver nanoparticles and silicon oil lubricant.[41]	-	Water: 8.7° Ethanol: 8.0°	-	-	75% reduction in *E. coli* biofilm adherence to surface
	Perfluorocarbon functionalized surfaces with infused perfluorodecalin lubricant.[57]	-	Blood: 0.6°	-	Prevented the formation of fibrin networks on the surface. Displayed significant reduction in platelet adhesion (27- and 4- fold reduction for acrylate and polysulfone substrates respectively)	Showed an 8-fold reduction in the formation of *P. aeruginosa* biofilms when compared to the control after 6.5 weeks

Lubricant infused surfaces

Lubricant infused surfaces have also shown the ability to significantly reduce the adhesion of pathogens to their surfaces, displaying reductions of ~2-log for both *P. aeruginosa* and *S. aureus*. [42,56] Lubricant infused surfaces can have a variety of underlying surface structures such as molecular monolayers (on planar substrates),[39] porous coatings (micro- and nano-pores) [40,41] and hierarchically structured surfaces, [35,42] all of which can be infused with lubricant, creating a slippery structure. Tesler et al. electrodeposited nano-porous Tungstite onto surgical grade stainless steel scalpels, which were infused with perfluoropolyether lubricant and capable of reducing *E. coli* cell adhesion to the surface by ~2-fold.[40] Work by Khan et al. created wrinkled structures on a PDMS substrate via casting on a hierarchically structured wrinkled mold, PDMS was then functionalized with SiNP and fluorosilane to create a highly repellent (water SA < 5º) hierarchical wrinkled structure on a flexible substrate. When these structures were infused with lubricant, they displayed a 98.5% (1.51-log) reduction in the adhesion of *P. aeruginosa*.[42] This work along with others has also shown lubricant infused surfaces outperforming their non-lubricated hierarchically structured counterparts.[40,42] Doll et al. developed a slippery lubricant infused porous surface on titanium substrates. The porous microstructure was formed through laser ablation of the surface using a 800 nm Ti-Sapphire femtosecond laser, after which the Titanium surface was functionalized with a fluorinated polymer (Antispread E 2/30 FE 60). Krytox GPL 106 lubricant was then infused into the coating, which displayed significant anti-fouling properties, showing upwards of 2-log reduction in the formation of biofilms (*S. aureus*).[56] While these lubricant infused surfaces have shown remarkable reductions in the adhesion of pathogens and biofilm formation on their

surface, almost all studies have been performed in aqueous environments and there is a significant lack of characterization in open air environments (Table 1-1). [40,42,56,57] Furthermore, most studies investigating the pathogen repellent properties of repellent surfaces (hierarchically structured and lubricant infused) have only been conducted with bacterial pathogens and there is limited research on their ability to prevent the adhesion of viruses.[40,41,57,42,50–56]

1.2.4 Blood Repellency

Hierarchically structured superhydrophobic surfaces

Hierarchically structured surfaces have also shown antifouling properties towards blood staining[40,58], as well as reduced adhesion of fibrinogen and platelets,[53,55] which are involved in the initial steps in thrombosis (blood clot formation).[59] Hierarchically structured surfaces which display broad and strong repellency to liquids (high CA for water, ethylene glycol and hexadecane) have shown the lowest amount of surface blood contamination (Table 1-1).[51,52,54,55] Particularly the work by Christoph Schlaich et al. created a mussel-inspired dendritic polymer coating which displayed omniphobicity with CA of 173º, 157º and 148º for water, ethylene glycol, and hexadecane respectively.[55] A platelet adhesion assay was performed on these surfaces as well as control glass and polystyrene surfaces. The control surfaces showed contamination of 1.6ug/cm^2 (glass) and 2.4ug/cm^2 (polystyrene), while no adhesion was demonstrated on hierarchically structured surfaces (the levels of contamination were below the limit of detection for the assay).[55] Ekrem Ozkan et al. created a hierarchically structured sponge surfaces with

high water and blood CAs of 161.6º and 165.4º, respectively, and reduced fibrinogen adsorption by 76.62%.[53]

Liquid infused surfaces

Similar to hierarchically structured surfaces, lubricant infused surfaces have displayed significant reduction of blood staining and platelet adhesion. Leslie et al. created a coating using perfluorocarbon monolayers infused with perfluorodecalin lubricant.[57] This coating showed low sliding angle of blood (0.6º) and was capable of reducing the adhesion of platelets to the surface by 27-fold.[57] Khan et al. discussed above, also characterized their repellant surfaces with blood contamination in addition to pathogen work. Interestingly, their lubricant infused versions of their hierarchically structured surfaces significantly outperformed their non-lubricant infused ones, showing reduced blood staining of greater than 95% compared to planar PDMS. However, the non-lubricated versions of their hierarchical surfaces showed increases in adhesion when compared to planar surfaces.[42] Lubricant infused surfaces have shown better performance than hierarchically structured surfaces in resisting blood related fouling of surfaces (Table 1-1). However, the performance of hierarchically structured surfaces toward blood adhesion is highly dependent on their omniphobicity. Surfaces with omniphobic properties have demonstrated similar levels of repellency to lubricant infused surfaces.[55]

A summary of the different surface technologies available from the scientific literature, hierarchically structured and liquid infused surfaces, and their corresponding repellency to liquids and biological contaminates such as blood, viruses and bacteria are found in Table 1-1.

1.2.5 Dual-Functional Surfaces: Combined Repellency and Antimicrobial Properties

In the previous section, we discussed different classes of repellent surfaces (Figure 1-3a and Figure 1-3b) and their performance toward repelling various biological contaminates. Even though pathogen and broad spectrum repellent surfaces are highly effective, they are not sufficient in completely eliminating the formation of fomites because surface defects or damage can lead to pathogen adhesion.[60] As such, some have proposed the use of antipathogenic surfaces, which deactivate pathogens when they come near or make contact with the solid interface.[31,61] Antipathogenic surfaces (Figure 1-3c & Figure 1-3d) contain chemically- or physically-bound biocidal agents,[62] that are either static and participate in contact killing (Figure 1-3c) or have controlled release over time (Figure 1-3d).[63] Antipathogenic materials have some major drawbacks compared to pathogen repellent materials. The antimicrobial properties of these materials decline significantly over time due to depletion of their antimicrobial compounds, build-up of dead pathogens on the surface or the development of antimicrobial reistance.[63,64] To overcome the limitations of pathogen repellent and antipathogenic material, dual-functional material systems with both antipathogenic and pathogen repellent properties have been developed.[61,65]

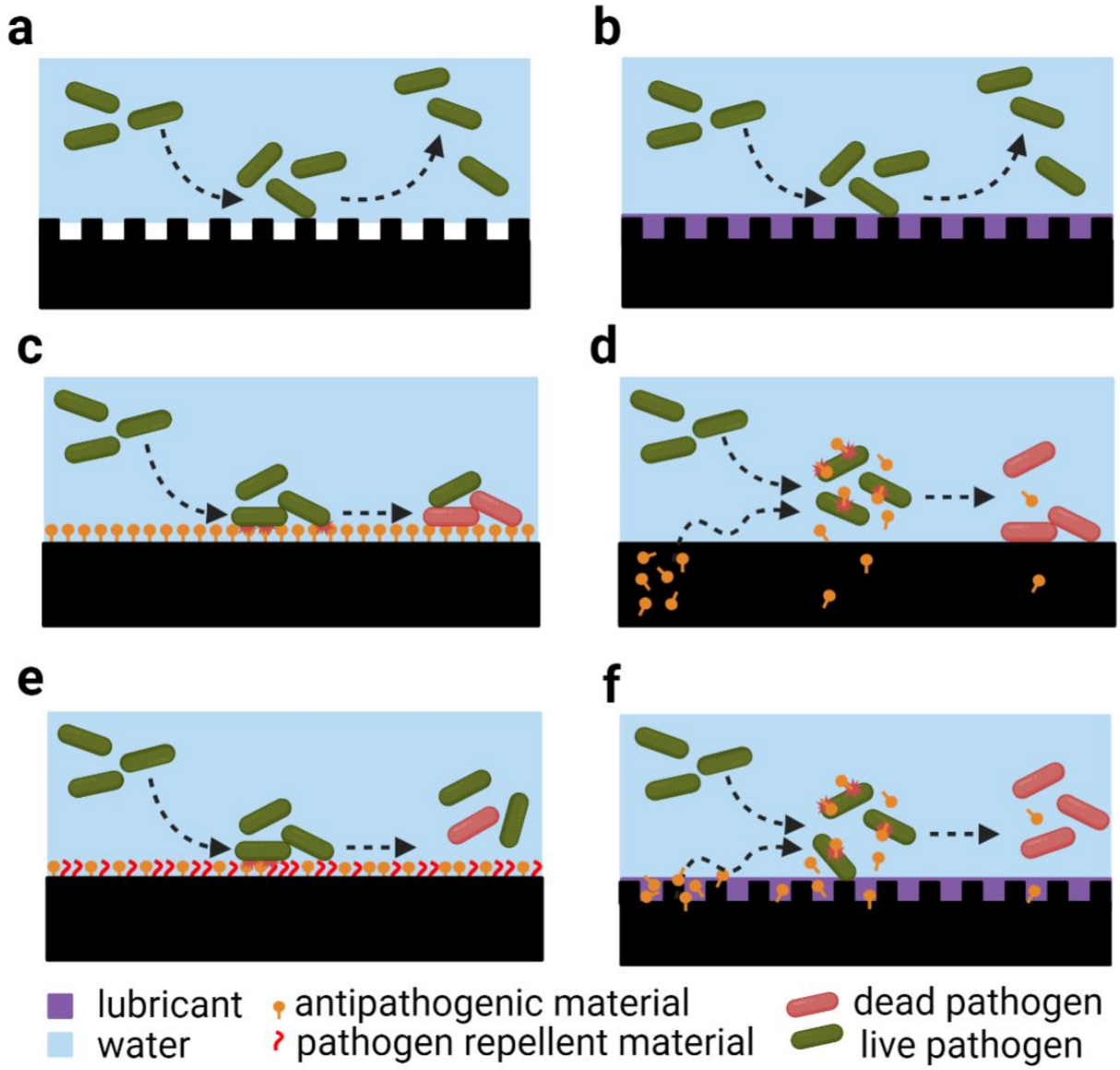

Figure 1-3: Schematic showing the function of pathogen repellent, antipathogenic and dual-functional surface. Pathogen repellent surfaces a) superhydrophobic surface and b) lubricant infused surface. Antipathogenic surfaces c) contact killing surface and d) biocide releasing surface. Dual-functional surface e) co-deposited repellent and antipathogenic functionalized surface and f) repellent surface structure with biocide releasing surface.

Dual-functional materials are typically developed by either co-depositing antipathogenic and pathogen-repellent coatings,[63,66,67] impregnating a repellant surface with antipathogenic materials,[41] or using switchable/stimulated materials.[31,61,68,69] Co-deposited materials provide both pathogen repellency and antipathogenic properties simultaneously (Figure 1-3e). These surfaces have been shown to provide high levels of repellency, greater then ~3-log reduction,[50,60] and robust deactivation of pathogens adhered to the surface, greater than 90%.[50,60,70] These material systems are usually made by depositing antimicrobial materials such as lysosomes,[60] silver nanoparticles (AgNP)[41] or CuO[50] and functionalizing them with a repellent monolayer such as fluorosilane (FS)[60] or infusing them with a slippery lubricant (Table 1-2).[41] Another common approach is the co-deposition of a repellent and antimicrobial polymer brush for the simultaneous repelling and killing of pathogens.[61,70] Yanhong Fu et al. created a mixed polymer brush coating comprised of poly(N-hydroxylethyl acrylamide) and poly(trimethylamine) ethyl methacrylate chloride with pathogen repellent and antimicrobial properties, respectively. These co-polymer brushes reduced the initial adhesion of bacteria and deactivated the adhered bacteria by greater than 90% (1-log) for *E. coli* and *S. aureus*.[70] Impregnation of antipathogenic materials (AgNP, antibiotics) into repellent surfaces is typically achieved with porous repellant materials, which allows for the slow and consistent release of the antimicrobial agents into the environment (Figure 1-3f). For example, Jieun Lee et al created a lubricant infused porous surface (pour size of 1-3μm) based on amine-reactive films, which were then functionalized with AgNPs and infused with silicone oil. The silicon oil lubricant layer allowed for a 75% reduction in biofilm formation over 48 hours, while the release of Ag^{+} ions from the AgNP

resulted in ~3-log reduction in bacterial activity of *E. coli*, *S. aureus* and *B. cereus* over 6 hours.[41] Yi Zou et al. created a copolymer brush (2-hydroxyethyl methacrylate and 2-(acrylamide)-phenylboronic acid) that was impregnated with quercetin.[71] This material has the ability to sustain antimicrobial effects (~1.3-log reduction) for more than 3 days, preventing cell adhesion while simultaneously preventing biofilm formation by releasing quercetin when bacteria bind to the surface .[71]

Table 1-2: Summary of the best preforming dual-functional antimicrobial and pathogen repellant surface technologies

Dual-Functionality Method	**Material**	**Repellent Properties**	**Antimicrobial Properties**
Biocide releasing	Copolymer brushes functionalized with quercetin. Decreases in the pH at the surface of the co-polymer brushes allows for the release of the quercetin.[71]	The polymer brush structure displayed a decrease in the surface density of *S. aureus* and *P. aeruginosa*	Reduction in the proliferation of *S. aureus* and *P. aeruginosa* by 1.31-log and 1.35-log respectively. Also showed reduction of biofilm biomass of 74% and 77% for each bacterium after 3 days.
	Polydopamine- coated porous sulfonated polyetheretherketone, impregnated with moxifloxacin hydrochloride and osteogenic growth peptide for release.[72]	Showed a >97% reduction in the number of adhered bacteria	Almost complete elimination of planktonic cells (*S. aureus* and *E. coli*
Co-deposited	Lysosome functionalized fluorinated silica nanoparticles.[60]	2.7 log reduction due to the presence of superhydrophobic wetting states	6.5 and 4.0 log reduction in the adhesion of *S. Typhimurium* and *L. innocua*
	Silver nanoparticles decorated dopamine functionalized poly(pentafluorophenyl acrylate) porous microstructure infused with silicone oil.[41]	Presence of the lubricant showed a 75% reduction in crystal violet staining of the surface when compared to the non-lubricated surfaces	~3-log reductions in the viability and activity of *E. coli*, *S. aureus* and *B. cereus*
	Mixed polymer brush comprised of poly(N-hydroxyethyl acrylamide) and poly(trimethylamine)	Reduced adhesion of live and dead *E. coli* and *S. aureus* by 99% and 90%	92% and 90% killing of adhered *E. coli* and *S. aureus*, respectively

	ethyl methacrylate chloride.[70]	after 72 hours respectively	
	CuO nanoparticles coated surface functionalized with fluorosilane.[50]	Showed a 3.2-log reduction in the adherence of *E. coli*	Live-dead assay of *E. coli* adhered to the surface showed significant deactivation after 24 hours
Environmentally stimulated	Copolymer with zwitterionic inner and polycationic outer layer. The functionality is switched under dry (kill) and wet (repel) conditions.[73]	Under wet conditions the surface showed a reduction of ~98.3% and ~96.9% for *S. aureus* and *E. coli* surface adherence respectively	Under dry conditions, the surfaces deactivated ~80% and ~96% of the attached *S. aureus* and *E. coli* respectively
	Poly(N-isopropylacrylamide) functionalized with gold NP.[74]	At 4^{O}C the polymer chains swell releasing the dead bacteria	At 37^{O}C attachment of bacteria is favorable and the *E. coli* are deactivated by the gold NP

Switchable/stimulated materials are of particular interest as they only express their antipathogenic properties when stimulated by an environmental condition such as, temperature,[75] hydration[69,76] or light exposure.[66,68] This has advantages over the co-deposition and impregnation material systems as antipathogen properties can be expressed only when necessary, which can help prevent the emergence of antimicrobial resistance.[62] The most prominent switchable dual-functional materials have been those based on switchable polymer brushes, which change state based on the humidity/hydration of the solid interface.[63,71,73] These materials have shown pathogen repellency and pathogen killing effects greater than 99% and 90%, respectively.[70,73] Another method for selectively producing antipathogenic products/conditions is the generation of reactive oxygen species (ROS) by exposing photoactive materials to specific wavelengths of light,[17,77] which degrade pathogens by oxidizing their protective outer layers.[78] The use of photoactive materials for disinfection has been used extensively in water treatment facilities,[79,80] and has gained traction in self-cleaning textiles for medical use.[81] Madson Santos et al. created an industrial varnish comprised of synthetic polymeric biocides and photosensitizer (toluidine blue O, curcumin and proflavine). A varnish (mixture of polymer A200B0 and curcumin) was coated on glass substrates and exposed to both white and blue light, showing a reduced concentration of adhered pathogens by 2-log and 3-log, respectively.[68]

To reduce the widespread contamination of biological contaminates and transmission of pathogens between people, it is important to develop materials with robust repellent and antipathogenic properties. For these materials to be effective in reducing the contamination of biological contaminates and transmission of pathogens, they must also

be easily and quickly manufactured and applied over a wide variety of surfaces, while also withstanding repeated physical contact by human hands. However, many of the existing repellent and antipathogenic surface technologies are manufactured through methods which are expensive or not suitable for large scale manufacturing. To address these concerns, we aim to develop wrinkled hierarchical surface structures with omniphobic wetting properties, though all-solution based processes, that allow for rapid and scalable manufacturing of repellent hierarchical structures. This work will also aim to characterize the repellency of these surface structures to various biological contaminates (blood, feces, virus and bacteria). Furthermore, to create engineered surfaces that can prevent the long-term transmission of pathogens, it is important for them to display not only have repellant properties but also display antipathogenic effects. Materials which can switch between their repellent and antipathogenic properties or display antipathogenic effects when stimulated have been desired due to the rise in antimicrobial resistance in past decades. To address this, we aim to integration of photoactive materials (TiO_2) into the omniphobic repellent surface structures, creating antipathogenic ROS at the surface when surface decontamination is desired.

1.3 Research Objectives

This research aims to develop materials for reducing the surface mediated transmission and contamination of a variety of pathogens such as bacteria and viruses, as well as biological contaminants, specifically blood and feces. To achieve this overarching goal, the following objectives were followed:

I. To develop hierarchically structured wrinkled surfaces for use as omniphobic coatings

Superhydrophobic and omniphobic surfaces, especially those based on hierarchical structures, have been shown to repel a variety of surfaces contaminates.[51–53] To build a robust superhydrophobic and omniphobic surface that can be utilized as protective coatings in built environments, it is important to develop manufacturing methods which are scalable, universal, and easily applied over large surface areas. Hierarchically structured surfaces based on thin film wrinkling of solution deposited NP films have been proposed to solve these manufacturing problems.[82,83] However, there is limited research showing hierarchically structured wrinkled surfaces displaying robust omniphobic properties.[54,84–91] We explore the effects of different nanoparticle (NP) materials, NP sizes, NP deposition techniques and polymer substrates in the structural hierarchy of the wrinkled materials and their associated wettability.

II. To understand the correlation between anti-biofouling and wettability of surfaces developed in objective I.

Analysis of the superhydrophobic and liquid repellant properties of surfaces is typically done by analyzing the droplet profile of various liquids on the solid interface.[36] These liquids are typically selected to have a wide range of differing properties: viscosity, surface tension and intermolecular forces, which give insight into the cohesive and adhesive interactions at the solid-liquid interface.[92] Biological liquids are often much more complex than the usual selected test liquids, containing a variety of salts, proteins, bacteria, and cells. Biological liquids often have complex interactions such as thrombosis and biofouling, resulting to surface contamination.[26,93] Additionally, many studies investigating

the interaction of blood with repellent surfaces present limited insight into the interaction of surfaces with whole blood, and also lack the analysis of these surfaces under dynamic and real-world conditions. We explore how different length scales of surface structures (nano, micro and hierarchical nano-micro) affect the resistance of the surface to blood staining (blood wettability) and thrombosis (blood surface fouling, *i.e.* blood clot formation) under static and dynamic conditions.

III. To understand the physical transmission of pathogens between contaminated and omniphobic surfaces

The transmission of pathogens between individuals occurs through different pathways including inhalation of respiratory droplets,[5,9] contact with mucosal membranes and secretions, and contact with contaminated surfaces.[11,12] In built environments, a significant proportion of pathogen (virus, bacteria and fungi) transmission and contamination is attributed to the physical transmission between inanimate contaminated objects and the hands of indeviduals.[3,4] Omniphobic surfaces have been shown to significantly reduce the adhesion of pathogens in aqueous environments.[94] However, open-air conditions like those in healthcare settings and surfaces in built environments have not seen significant investigation.[95] Furthermore, the studies that investigate the open-air adhesion of pathogens *via* physical contact have only investigated bacterial pathogens,[54] and viruses specifically have not seen any investigation.[31] We develop a series of touch transfer assays for quantifying the physical adsorption of pathogens to solid interfaces. We further explore the ability for hierarchically structured omniphobic surfaces to reduce the physical adsorption/transmission of viral and bacterial (both Gram-negative and Gram-positive) pathogens to their surface in open-air environments.

IV. To Integrate dual functionality into hierarchically structured omniphobic surfaces

Reducing the adhesion of pathogens significantly decreases the level of contamination on surfaces.[50] However, very large loads of pathogens,[14] damage to the repellant surface,[60] and the development of surface defects result in eventual surface contamination. Herein, we sought to use the knowledge obtained in the previous objectives on repellent materials and combine them with antipathogenic materials to create a dual functional wrap, capable of decontaminating the surface if the repellent properties break down. More specifically, we aimed at answering whether it would be possible for photoactive materials integrated into the hierarchically structured repellent surfaces to enable controlled/stimulated dual-functional effects.

1.4 Thesis Overview

The remainder of this thesis is organized as follows:

Chapter 2 "Background on Surface Wetting, Biological Contamination, Repellent Wrinkled Hierarchical Structures and Antimicrobial Action of TiO_2" discusses the theory behind the manufacturing and properties of the repellent surfaces. Specifically, it overviews the theory of surface wetting, the implications of this theory on surface contamination, the formation of micro- and nano-scale surface wrinkling, and the antimicrobial action of TiO_2.

Chapter 3 "Hierarchical structures, with submillimeter patterns, micrometer wrinkles, and nanoscale decorations, suppress biofouling and enable rapid droplet digitization"

discusses the development of a tunable and antifouling hierarchically structured omniphobic surface. Comparison of different surface structure length scales revealed that hierarchically micro- and nano-structured surfaces showed improved liquid repellent properties, as well as antifouling and blood staining resistance when compared to micro and nano structures individually. Blood contact angle measurements, blood staining, clotting assays and scanning electron microscopy (SEM) of the surfaces were performed to quantify the differences in repellency of each of the surface structures. Finally, the application of these surface structures in medical devices was tested by creating a dip-based IL6 biosensor. This article has been published in *Small.*

Chapter 4 "A Repellent plastic wrap with built-in hierarchical structuring prevents the contamination of surfaces with coronaviruses" focuses on improving the wettability of the surface structures seen in chapter 3 and understanding the physical transmission of viruses between contaminated and highly repellent surfaces. In this work, we introduced a new material substrate (PO) and NP material (silica), which displayed improved repellent effects. The virus repellency of this surface was demonstrated through a novel touch-based assay. This assay quantified the number of transferred viruses to sterile surfaces under single and multiple touches, and a comparison of repellent and common hospital surface materials was done. The contamination of the different surfaces with viruses were confirmed *via* culture and SEM. Repellent surfaces were additionally tested for their touch durability, which was quantified through CA measurements and SEM of the surface, after physical contact. This article has been published in *ACS: Applied Materials and Interfaces.*

Chapter 5 "A super-omniphobic and photoactive surface presents antimicrobial properties by repelling and killing pathogens" explores the integration of photoactive TiO_2 into the repellent surfaces and their dual-functionality in both repelling and killing pathogens. New NP deposition techniques were utilized to functionalize the surface with photoactive materials (TiO_2) and displayed robust omniphobic properties. An in-depth analysis of the adhesion of multiple pathogenic strains of bacteria was conducted, analyzing the adhesion of individual and multiple pathogens after a single contamination event. Following the adhesion of pathogens to the material surface, the antipathogenic photoactivity of the surface was characterized for both Gram-negative and Gram-positive bacteria under ultraviolet light exposure.

Chapter 6 discusses the conclusions and the contributions made to the field. It will also summarize the key findings and the potential future work stemming from this research.

Chapter 2 Background on Surface Wetting, Biological Contamination, Repellent Wrinkled Hierarchical Structures and Antimicrobial Action of TiO_2

Preface:

This chapter provides the theoretical background that supports the work performed in the thesis. More specifically, it discusses the theory behind surface wettability, biological contamination of surfaces, the formation of hierarchical structures through thin film wrinkling, and the antimicrobial properties nanomaterials (primarily focusing on the photoactive antimicrobial action of TiO_2), which are utilized and discussed throughout the thesis work. We will begin by reviewing the mechanism of surface wetting and the implications of this theory on the adhesion of biological contaminates, pathogens, and blood onto repellant surfaces, as well as the robustness of the repellent properties. We will then discuss the omniphobic properties of liquid repellent hierarchical structures with a focus on thin film wrinkling. Following this, the theory of thin film wrinkling will be described in order to a better understand how we can utilize these structures for the formation of omniphobic surfaces. Finally, we will discuss the antimicrobial properties of nanomaterials, specifically focusing on the photoactive TiO_2 nanoparticles.

2.1 Principles of Surface Wettability and Adhesion

In this section, we will discuss the interfacial properties of surfaces, factors governing their cohesion with liquid contaminants, and the properties that can be modulated to increase or decrease their repellency towards contaminants. The level of resistance of a surface to contamination is typically quantified through measurement of the surface free energy. This is typically done though measuring the wettability/affinity of various liquids

to the solid liquid interface via contact angle (CA) and contact angle hysteresis (CAH) measurements.[36] CA evaluates the geometry of liquid droplets sitting on a surface under thermodynamic and static equilibrium. Under these conditions, the interfacial forces balance (Figure 2-2a) and we obtain the young equations[37]:

$$\gamma_{sg} - \gamma_{sl} - \gamma_{lg}\cos(\theta_c) = 0 \text{ (Equation 2.1)}$$

where γ_{sg} is the solid-gas interfacial energy, γ_{sl} is the solid-liquid interfacial energy, γ_{lg} is the liquid gas interfacial energy (often referred to as the surface tension), and θ_c is the CA. If the CA > 90^o for a given liquid the surface is considered phobic to the liquid (Figure 1-3b, i) while if CA < 90^o the material is phillic to the liquid (Figure 1-3c, i).[96] When the probing liquid is water, the terms hydrophobic and hydrophilic are used, while if the probing liquid is an oil the term oleophobic and oleophilic are generally used.[96] A more useful way to describe the CA of a solid liquid interaction is in terms of the adhesion energy of the solid-liquid interface (ΔG_{sl}) obtaining the Young-Dupre equation[37]:

$$\Delta G_{sl} = \gamma_{lg}(1 + \cos(\theta_c)) \text{ (Equation 2.2)}$$

Describing the wettability in terms of the adhesion energy of the solid-liquid interface paints a clearer picture of what it means for a surface to be hydrophobic or hydrophilic. When the CA < 90^o, the free energy of adhesion will be greater than the surface tension of the liquid, causing the droplet to spread over the surface (hydrophilicity). If the CA > 90^o the free energy of adhesion will be less than the surface tension of the liquid, causing the droplet to adhere to itself more than the surface (hydrophobicity). While understanding the interaction at a surface under static conditions is useful, a more realistic situation is that of droplets moving along the interface. Under dynamic conditions, such as a droplet

sliding across a solid interface, the CAH and sliding angles (SA) are used.[97] The CAH is defined as the difference between the advancing and the receding CA, $\theta_H = \theta_A - \theta_R$, where θ_A is the advancing CA (representing droplet or solid-liquid cohesion, ΔG_{sl}^{coh}) and θ_R is the receding CA (representing droplet or solid-liquid adhesion, ΔG_{sl}^{adh}).[92] CAH is closely related to the tilting or SA, which is the angle at which the gravitational force acting on a static droplet sitting on a surface will begin to slide across the surface, and is commonly used as a quantifier for the surface adhesion of a droplet, with lower SA indicating a less adhesive interaction between the droplet and the surface.[98]

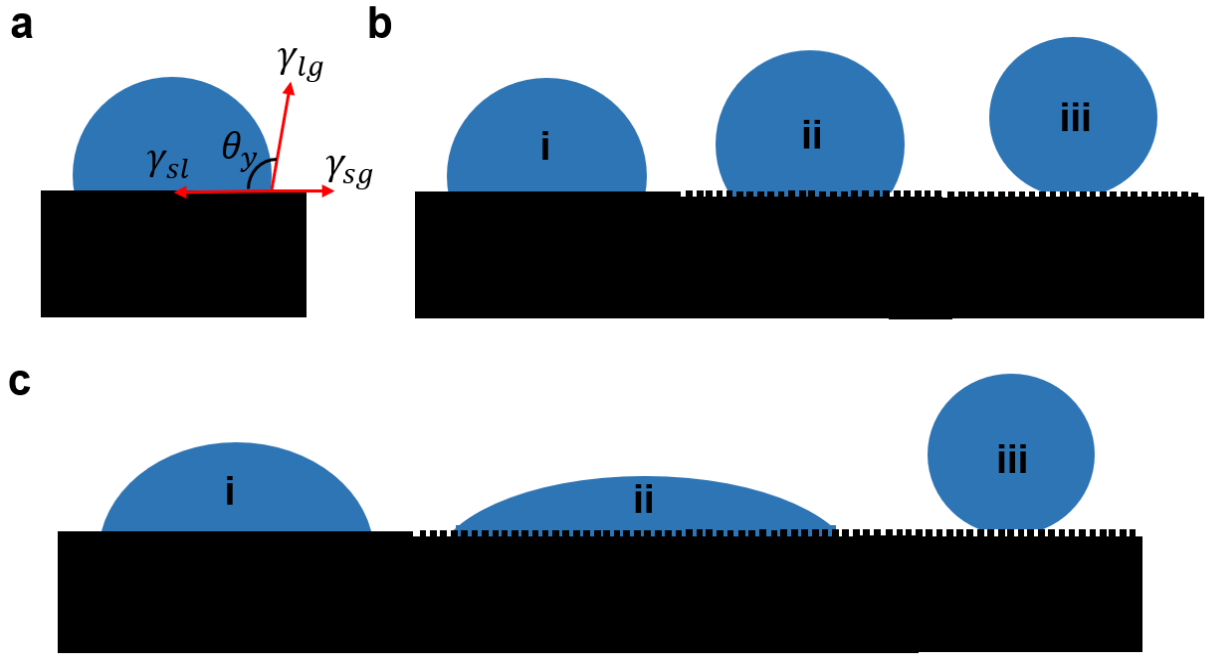

Figure 2-1: Contact angle and droplet geometry on surfaces with different surface energy and surface topography. a) The contact angle on a smooth homogenous coating, the red arrow denotes the different forces interacting at the three-phase line. The droplet geometry of b) hydrophobic and c) hydrophilic materials under different wetting states; i) Young wetting, ii) Wenzel wetting and iii) Cassie-Baxter Wetting.

To improve the liquid repellency of smooth solid interfaces, the material and/or surface energy of the interface needs to be changed. This can be done by depositing a thin coatings of a lower surface energy material onto the surface or by chemically modifying the surface with lower surface energy molecules. Chemical modifications using low surface energy molecules such as Trichloro(octadecyl)silane (OTS),[99] polytetrafluoroethylene (PTFE)[86] and Fluorosilane (FS)[100] have been used extensively for this purpose. Deposition of OTS, PTFE and FS on planar hydrophilic glass substrates have been shown to increase CAs to 98-111°,[99,101] 115-127° [86], and 119° [99] respectively.

Chemically modifying the surfaces can only increase the water CA to a maximum of 120°, thus other surface modification methods need to be adapted in order to achieve higher repellencies.[102] The main method used to increase the repellency of solid-liquid interfaces, aside from chemical modification, is to change the geometry/topography of the interface.[36,102] Once we begin to deform the shape of the solid-liquid interface, the Young-Dupre equation no longer holds true.[103] To address these, two other models have been developed, the Wenzel model for rough surfaces and the Cassie-Baxter model for non-homogenous wetting of the surface.[36,104] Under the conditions of homogeneous wetting of a rough surface (Wenzel wetting) the CA is given by:

$$\cos\theta_W = r\cos\theta_c \quad \text{(Equation 2.3)}$$

where θ_W is the apparent (observed) CA, *r* is the roughness ratio of the surface, and θ_c is the CA of the planar material substrate. This relationship implies that the surface energy of the material scales with increase in surface roughness. As such hydrophilic materials become more hydrophilic (Figure 2-2c, ii), and hydrophobic materials become more hydrophobic (Figure 2-2b, ii) as the surface roughness increases.[36] But what happens if

a surface is not uniformly wetted or is made of multiple materials with different surface energies? In this case, one can use the Cassie-Baxter wetting model to determine the effects of the surface structure on the wettability of the interface.

$$\gamma_l \cos\theta_{CB} = \sum_i^n \varphi_i(\gamma_{s,i} - \gamma_{l,i}) \text{ (Equation 2.4)}$$

where φ_i is the fraction of material i in contact with the liquid media, $\gamma_{s,i}$ is the surface tension of the solid material, $\gamma_{l,i}$ is the surface tension of the liquid interacting with material i, and θ_{CB} is observed CA. For a two-material system ($n = 2$) where the second material is air pockets trapped within the surface structure, the Cassie-Baxter equation takes the form of:

$$\cos\theta_{CB} = \varphi_{SL}(\cos\theta_c + 1) - 1 \text{ (Equation 2.5)}$$

Interestingly, increasing surface roughness and trapping more air in the structure can bring both naturally hydrophilic (Figure 2-2c, iii) and hydrophobic (Figure 2-2b, iii) materials deep into the hydrophobic regime, obtaining CAs with water greater than 150^o, which is known as superhydrophobicity.[36] This effect can be visualized as scaling the free energy of adhesion by the surface area of the solid-liquid interface. As a result, when the surface area of the solid-liquid interface decreases so does the apparent free energy of the surface resulting in an increase in the CA. Furthermore, materials with surface roughness at multiple length scales (micro and nano) may have different wetting states in these regimes. The CA of hierarchical micro- and nano-scale surfaces under different wetting states is given by the following four equations:

$$\cos(\theta_{Cb,Cb}) = \varphi_m\varphi_n(\cos(\theta_c) + 1) \text{ (Equation 2.6)}$$

$$\cos(\theta_{W,Cb}) = r_m(\varphi_n(\cos(\theta_c) + 1) - 1) \quad \text{(Equation 2.7)}$$

$$\cos(\theta_{Cb,W}) = r_n(\varphi_m(\cos(\theta_c) + 1) - 1) \quad \text{(Equation 2.8)}$$

$$\cos(\theta_{W,W}) = r_m r_n \cos(\theta_c) \quad \text{(Equation 2.9)}$$

where $\theta_{i,j}$ is the CA of the micro (i) and nanoscale (j) under Wenzel (W) or Cassie-Baxter (Cb) wetting, r_m and r_n are the roughness ratios of the micro and nano scale respectively, and φ_m and φ_n are the fraction of surface wetting at the micro and nanoscale respectively. Surfaces with Cassie-Baxter states at both the micro- and nano- scale show the best performance. Since CA of the liquid-air interface is essentially 180º, there are no adhesive or cohesive interactions between the two phases. [37] This in conjunction with the high fraction of air inside of surfaces structure, results in hierarchically structured surfaces being some of the best liquid repellent materials,[35,105] and have extremely high water CA and low SA and CAH (CA > 160º, SA < 3º, CAH < 5º) ,[106,107] as well as high CA and low SA and CAH, with low surface tension liquids (hexadecane CA > 150º, SA < 7º, CAH < 10º).[43]

2.2 Theoretical Implications of Wettability for Repellant Surfaces

The extremely high CA and repellent properties seen by the surfaces under Cassie-Baxter (superhydrophobic) wetting states indicates the presence of extremely low adhesive and cohesive interactions at the surface.[36,37] The driving factor for the observed low adhesive and cohesive effects arise due to the high fraction of air at the liquid-surface interface. The air-liquid interface is unique as it has a CA of 180º and thus no cohesive

and adhesive interaction are seen between the two materials.[37] This high fraction of air (>0.9) within superhydrophobic surfaces causes them to not only display high water CA (>150^{o}) but also display small CAH (<1^{o}) as there are small differences between the advancing CA (adhesive interactions) and receding CA (cohesive interactions).[37] In addition to liquid repellant properties, this high fraction of air in the surface has a significant impact on the adhesion of biological contaminates to superhydrophobic surfaces.[26,95]

2.2.1 Bacteria Adhesion

The biological contamination of solid interfaces can best be understood through biofilm and blood clot formation at the surface. The formation of biofilms on planar solid interfaces begins with the adhesion of bacteria to the solid surface (Figure 2-2a). As bacteria get sufficiently close to the surface, they interact through dispersive and polar interactions,[108,109] becoming reversibly adhered to the surface.[32] Bacteria can then interact with the surface through extracellular proteins and extracellular polymeric substances (EPS) such as capsules, pili and slime,[33] resulting in the chemical and irreversible adhesion of the bacteria to the surface.[32] The bacteria continue the production of EPS, eventually forming a biofilm (Figure 2-2a, ii) that aides in the adhesion of more bacteria and creates an ideal environment for bacteria proliferation.[32,33,110] When interacting with hierarchically structured surfaces under superhydrophobic wetting states, bacteria can only interact and adhere to the solid surface which is wetted by the aqueous media.[111,112] As the fraction of solid surface wetted decreases, the probability for the bacteria adhering both reversibly and irreversibly to the solid interface will also decrease.

This results in the bacteria being unable to effectively physiochemically interact with the surface, inhibiting contamination and biofilm formation (Figure 2-2b, ii).[113]

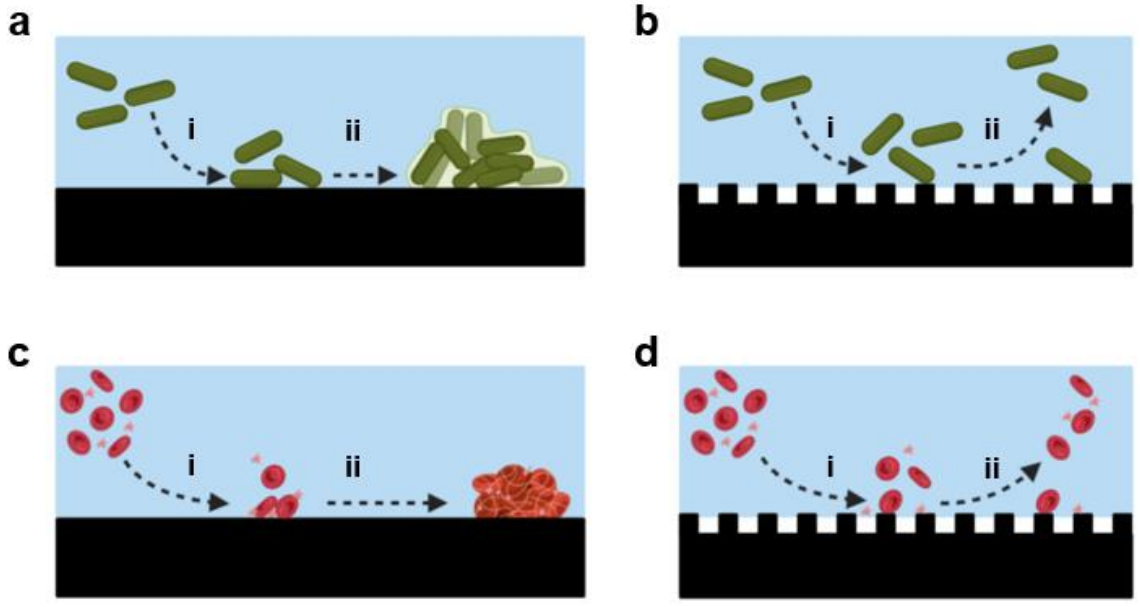

***Figure 2-2*:** Surface Biofouling of planar and superhydrophobic surface by bacteria (a, b) and whole blood (c, d).

2.2.2 Blood Adhesion

The contamination of solid interfaces with blood clots follows similarly to the adhesion of bacterial pathogens. On planar surfaces, blood clot formation (thrombosis) begins with the adhesion of platelets and red blood cells to the solid interface.[26] Once platelets and red blood cells have adhered to the solid interface (Figure 2-2c), they may interact with various proteins and enzymes eventually creating thrombin.[59,114] Thrombin then catalyzes the conversion of fibrinogen into fibrin, which creates a mesh structure that encapsulates platelets, blood cells, and other proteins creating the blood clot (Figure 2-2c, ii).[59]

Hierarchically structured surfaces under superhydrophobic wetting have been shown to reduce the adhesion of platelets and display antithrombin effects,[26] and is attributed to the reduced effective area available for platelet adhesion (Figure 2-2d, ii) and hydrodynamic conditions seen at the solid-liquid interface of superhydrophobic surfaces.[26] If the superhydrophobic wetting state breaks down and transitions into a Wenzel wetting state, the effective area and platelet adhesion to the surface will increase.[26] Under Wenzel wetting, platelet adhesion has been shown to be higher than that of a planar surface with the same footprint, resulting in increased blood clot formation on the surface.[115]

2.2.3 Robustness of Repellent Properties

As seen above, the robustness of the air-pockets trapped within hierarchical surfaces is of key importance for maintaining robust repellency towards biological contaminates. However, many surfaces that display superhydrophobic properties don't display robust air pockets under wetting with liquids of sufficiently low surface tension (Figure 2-3a),[42] which indicates an increase in the adhesive and cohesive interactions under such conditions.[37] The surface tension of liquids can be broken down into several components depending on their types of interactions, liquids are commonly broken down into their dispersive and polar interactions.[109] For example, water (72.8 $mN{\cdot}m^{-1}$) interacts through both polar (57.7 $mN{\cdot}m^{-1}$) and dispersive (22.1 $mN{\cdot}m^{-1}$) forces,[116] while hexadecane only interacts through dispersive interactions (27.5 $mN{\cdot}m^{-1}$).[44] Surfaces that display robust Cassie wetting state, regardless of the surface tension of a liquid, are called omniphobic [96,117] or superomniphobic [45,46] (Figure 2-3c) surfaces, and have gained significant traction

as antifouling surfaces in recent years.[31] Surfaces that display omniphobicity are characterized by CA > 150^{o} and SA or CAH < 10^{o} for all test liquids,[45,46,118] which indicates that there are low dispersive and polar interactions at the solid interface.[37] The improved robustness of Cassie states seen by omniphobic surfaces when compared to superhydrophobic materials, has been directly compared to enhancements in the repellency towards biological contaminates.[26,31]

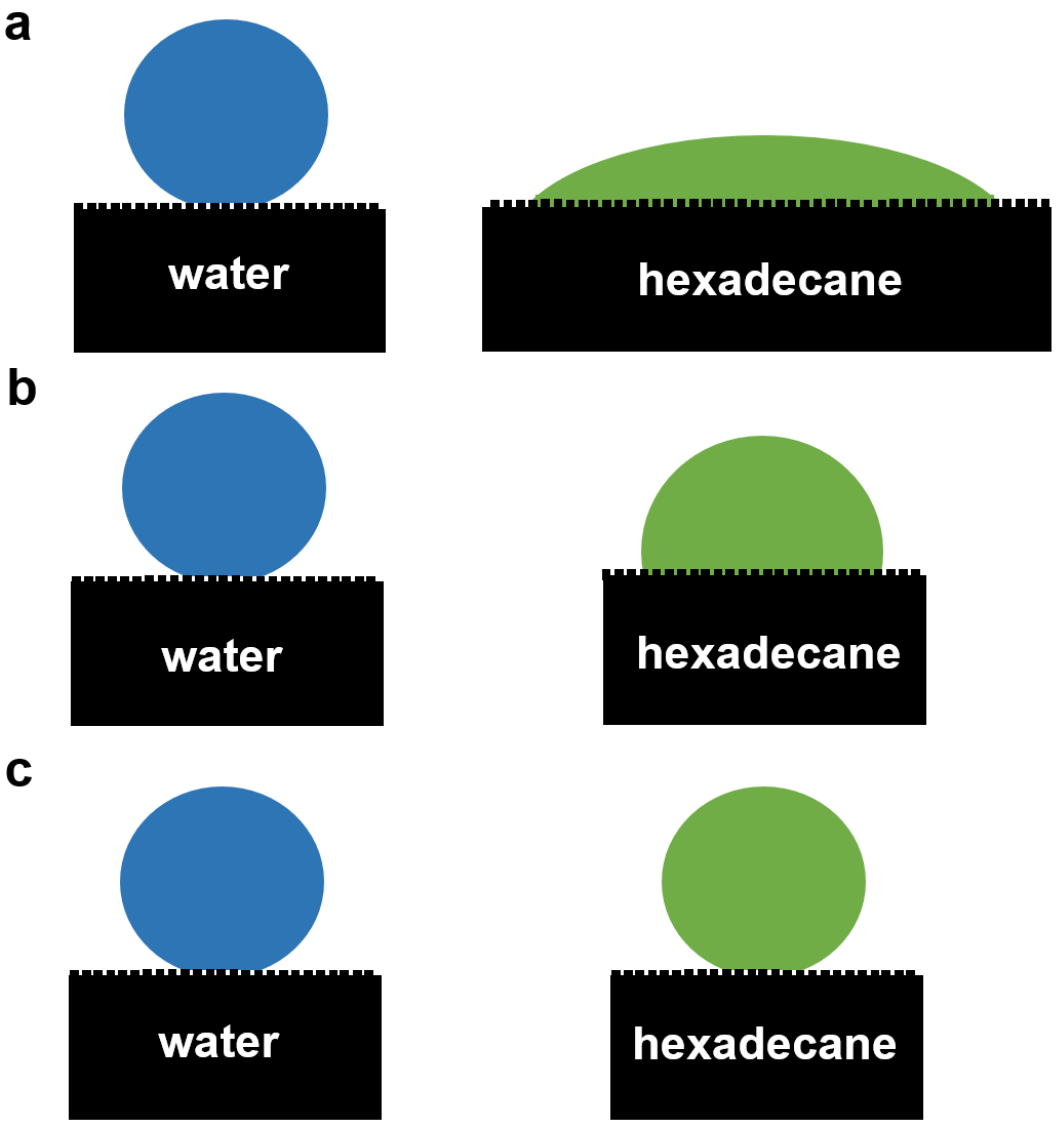

Figure *2-3*: Schematic showing the difference in wetting state of water (blue) and hexadecane (green) for a) superhydrophobic-oleophilic, b) superhydrophobic-oleophobic and c) omniphobic surfaces.

2.3 Design of Hierarchically Structured Omniphobic Surfaces

Hierarchically structured surfaces with superhydrophobic properties have displayed some of the highest levels of repellency toward biological contaminates, for example, reducing the adhesion of pathogens in open air conditions by upwards of 3-log.[50] The

superhydrophobic effect responsible for this repellency, arises from high roughness at the surface- liquid interface, which traps air within the surface structure and prevents/inhibits the full and homogenous wetting of the solid interface.[36] If the quantity and size of the air pockets is sufficiently large, water droplets will be unable to adhere to the surface. A superhydrophobic wetting state is present on a surface if it is displaying a sufficiently high CA (greater than 150^{o}) and low SA (less than 5^{o}). The superhydrophobic effect (*i.e*. Cassie-Baxter wetting) is usually proportional to the surface tension of the interacting liquid, with high surface tension liquids displaying larger air pockets and thus high levels of repellency.[36] If liquids of both high and low surface tensions display high CA (greater than 150^{o}) and low SA (less than 10^{o}), then the material is considered omniphobic.[45,46,118–121] Omniphobic surfaces typically have both hierarchical and re-entrant (concave) surface structures.[31,122,123] Daoai Wang et al. created a controllable omniphobic surface through electrochemical methods, creating a Ti/TiO_2 nanotube array which was capable of switching between repellent and adhesive states under ultraviolet (UV) light and heat exposure.[120] This nanotube array showed water and hexadecane CA of 176^{o} and 155^{o} respectively, and water and hexadecane SA of 2^{o} and 7^{o} respectively.[120] Work by Boxun Leng et al. created a silica nanoparticle (SiNP) textile that was functionalized with FS to give it omniphobic properties.[121] These textiles displayed CA and SA of water of 152^{o} (20µL) and 5^{o} (20µL) respectively while showing hexadecane CA and SA of 153^{o} (5 µL) and 9^{o} (20µL) respectively.[121]

Materials that display omniphobicity are typically manufactured through spin coating,[86,124] photolithography,[45] laser ablation [89,125,126] and electrospinning, which limits the scalability and materials selection to which these coatings can be applied.[54] One approach to

improve the manufacturing of these materials is the wrinkling of thin films, which is a facile way of creating large surface areas of self-induced microstructures on polymer sheets and utilizes scalable manufacturing methods such as roll-to-roll printing[39] and solution deposition.[127–129] Wrinkled surface structures, especially those with hierarchical structures, have shown liquid repellency (Table 2-1). Scarratt et al. created robust microscale wrinkles through spin coating Teflon films (13-718 nm) onto shrinkable plastic substrates. The resultant wrinkled structure displayed superhydrophobic wetting properties (168nm Teflon film) with a water CA of 174°.[86] Lee et al. created multi-generation wrinkled structures through sequential wrinkling of fluorocarbon films, which were deposited though reactive ion etching onto shrinkable polystyrene substrates.[90] These wrinkled surfaces were used as molds for pattern transfer of the hierarchical wrinkles onto flexible PDMS substrates which showed water CA of 160° and extremely low water SA of less than 1° under large substrate deformation.[90] Although wrinkled surface structures have displayed robust superhydrophobic, they have shown weaker performance in the formation of robust omniphobic wetting states, with the highest reported hexadecane CA being 124° and no sliding of the droplets on the surfaces.[54] Yun et al. was able to achieve omniphobicity with wrinkled microstructures. However, in order to achieve this, the structures were combined with T-shaped nanostructures. The combination of micro-wrinkles and T-shaped nanoscale features showed robust omniphobicity with CA of 160°, 150° and 150° for water, ethylene glycol, and ethanol respectively,[91] showing that wrinkled structures can be used in the development of omniphobic surfaces.

Table 2-1: Summary of the liquid repellant properties of hierarchically structured wrinkled surfaces.

Wrinkle Length Scale	Material Description	CA	SA	CAH
Nano	PDMS micro pillars with diamond like carbon wrinkles.[84]	Water: 160º	-	Water: 2.4º-4.2º
	PDMS micro-pyramids coated with perfluorocyclobutane via plasma enhanced chemical vapor deposition.[85]	Water: 171.8º	Water: ~5º	-
Micro	Teflon film (168nm) on polystyrene substrates.[86]	Water: 174º	Water: <5º	Water: 3º
	Mold imprinted nanostructures on wrinkled poly(2-hydroxyethl methacrylate) film.[87]	Water: 160º	Water: 5º	Water: <10º
	SiNP coated Graphene Oxide wrinkled films functionalized with fluorosilane.[88]	Water: 161.4º	Water: 1.2º	Water: 2º
Micro-Nano	Nanoporous Teflon wrinkled film.[89]	Water: 165º	Water: 2-3º	-
	Fluorinated silica nanoparticles on a polyolefin substrate.[54]	Water: 154º Blood: 144º Hexadecane: 124º	Water: <5º Blood: - Hexadecane: -	Water: 10º Blood: - Hexadecane: -
	Polystyrene substrate with Fluorocarbon and SF_6 coatings (deposited through reactive ion etching). Three consecutive deposition and shrinking steps were done to create 3 generations of wrinkles on the surface.[90]	Water: 160º	-	Water: <1º
	T-shaped nanostructures on wrinkled polystyrene substrates.[91]	Water: 160º Ethylene Glycol: 150º Ethanol: 150º	-	-

2.4 Thin Film Wrinkling for Hierarchical Structure Formation

The wrinkling phenomena occurs when films or material interfaces are subjected to internal strain [130] or compressive stress,[131] and is seen in various places and length scales throughout nature such as, papillae on rose petals, fingerprints, and bronchioles.[105,131] The work will focus on the formation of wrinkles though compressive loads, which are achieved by depositing films on stretched elastomeric, or thermally shrinking substrates.[83,129,132] Elastomeric substrates, such as PMDS, have been used extensively to create uniform and periodic wrinkle microstructures,[133] but are not feasible for large-scale coatings. Pre-strained (thermally shrinking) polymers like polystyrene (PS), polyolefin (PO), and polyethylene solve these manufacturing issues, as large areas can be coated through metal evaporation or sputtering,[83] dip-coating,[134] and roll-to-roll printing.[135,136] Once the film is coated, these substrates can shrink resulting in the buckling of the deposited film and the formation of wrinkled surfaces.[83,127]

The simplest model for thin film wrinkling is the uniaxial model for a compressive force acting on a uniform thin film on an infinitely thick elastic substrate.[137]

$$E_f I \frac{d^4 z}{dx^4} + F \frac{d^2 z}{dx^2} + kz = 0 \text{ (Equation 2.10)}$$

where E_f and E_s are the elastic moduli of the film and the substrate respectively, F is the compressive force, k is the Winkler's modulus ($k = E_s w\pi/\lambda$), and I is the moment of inertia of the film ($I = wh^3/12$). [137] Assuming that the resulting surface instability can be described as a sinusoidal deflection, $z(x) = A \sin(2\pi x/\lambda)$,[131] then rearranging for the applied force provides the following equation:

$$F = E_f \left(\frac{wh^3}{3}\right) \left(\frac{\pi}{\lambda}\right)^2 + \frac{E_s w}{4} \left(\frac{\pi}{\lambda}\right)^{-1} \text{ (Equation 2.11)}$$

where w and h are the width and thickness of the film respectively, and λ is the wavelength of the wrinkles (Figure 2-3). The geometric properties of the wrinkles, the wavelength and the amplitude, can be found by minimizing F with respect to the wavelength, $dF/d\lambda = 0$:

$$\lambda = 2\pi h \left(\frac{E_f}{3E_s}\right)^{\frac{1}{3}} \text{ (Equation 2.12)}$$

$$A = h\sqrt{\frac{\varepsilon - \varepsilon_c}{\varepsilon_c}} \text{ (Equation 2.13)}$$

where ε is the applied strain to the substrate and $\varepsilon_c = \left(3E_s/E_f\right)^{\frac{2}{3}}$ is the critical strain at which the wrinkle structure will form. It is clear from these equations that both the amplitude and the wavelength of the final wrinkle structure have a linear relationship with the film's thickness, while the amplitude and wavelength scale by the square and cube root of the material parameters respectively.[131] This allows for the easy tuning of the final structure of the surface by varying the thickness of the deposited film.[131,137] Given a large enough strain applied to the film, the initial wrinkles may begin to act as a stiff layer and buckle themselves into wrinkles, leading to hierarchical wrinkles on wrinkle structures.[131] Furthermore, strain may also be applied biaxially (in two directions), which results in more complex wrinkle structures depending on the interference of the wrinkles in either direction.[137]

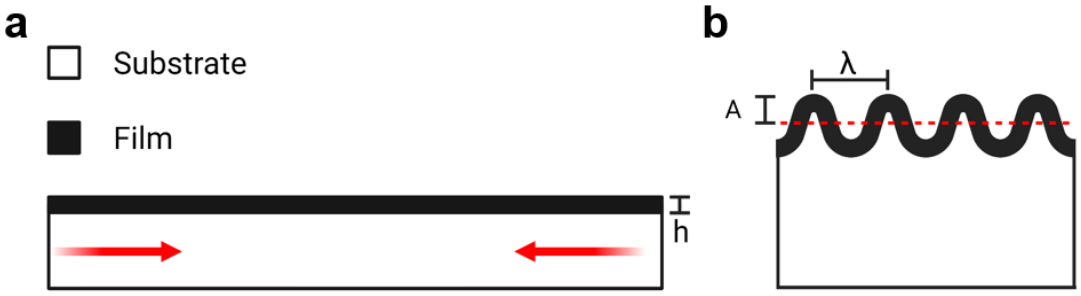

Figure 2-4: Schematic drawing of the thin film deposited on the substrate a) before and b) after shrinking.

Wrinkled surfaces made from polytetrafluoroethylene films have shown significant anti wetting properties with water CA greater than 165°.[86,89] Furthermore, wrinkled surfaces have shown water CAs over 160° without the need for low energy fluorinated coatings.[84] In addition to continuous thin films, NP films have also shown similar wrinkling behavior.[128,129] After shrinking, the buckled NP films follow a linear relationship between wavelength and their apparent film thickness, as predicted by the uniaxial model.[129] The apparent film thickness of these films is dependent on the diameter of the NPs and the number of layers deposited. For example a single layer of 36 nm particles would have the same effective film thickness as 3 layers of 12 nm particles.[129] The deposited NPs add another layer of hierarchy to the structure, which further increases the surface roughness of these coatings. Wrinkled NP films as a result have shown robust Cassie-Baxter wetting states with water CA of 155° ± 4° and hexadecane CA of 124° ± 2°.[54] These NP films (27 nm) have also been tested for their antifouling properties where they showed ~85% reductions in the formation of MRSA and *P. aeruginosa* biofilms on the surfaces.[54] These highly repellent properties are due to the extremely rough surface structure,[54] which is a

result of the small effective film thickness, producing small wavelengths and multiple generations of wrinkles.[138]

2.5 Deactivation of Pathogens

2.5.1 Antipathogenic Compounds

Pathogens may be deactivated by a variety of materials including drugs, polymeric materials, metals and metal ions.[139,140] The most common of these methods is the use of drugs such as antibiotics, antifungal and antiviral medications.[141] However, the widespread use of pharmaceuticals has led to antimicrobial resistance (MRSA and vancomycin-resistant *Enterococcus*) and decreased efficacy.[1,4] As such, other materials with anti-pathogenic properties have been studied in recent years.[139] Of specific interest are the development of nanoparticles and nanocomposites with antipathogenic properties such as metal, organic, and organometallic nanomaterials.[139,142–145] Organic nanomaterials with antipathogenic properties typically function by releasing antipathogenic materials (antibiotics, antimicrobial peptides and antimicrobial agents) or by forming contact killing cationic interfaces (quaternary ammonium compounds, cationic quaternary polyelectrolytes or polycationic nanoparticles).[139] Inorganic nanomaterials with antipathogenic properties are typically broken into two categories, metal nanoparticles and metal oxide nanoparticles.[31,139,140,145] The most common metal nanomaterials with antipathogenic effects are silver, gold and copper.[146,147]

The exact mechanism of antimicrobial action of metal nanomaterials is not precisely known;[142] however, the deactivation of pathogens is generally attributed to the following

pathways. Firstly, metal nanomaterials release metal ions that interact with the cell wall and cytoplasmic membrane via electrostatic and thiol interactions.[139,145] This leads to changes in the membrane potential, membrane depolarization or loss of integrity, eventually leading to cell death.[139] This has been observed with Ag NPs creating pits in the cell membrane of *E. coli,* ultimately leading to the death of the cell.[139] Secondly, the metal ions may bind to proteins and enzymes in the cell membrane, interrupting the metabolism and leading to cell deactivation.[139,145] Finally, the metal nanomaterials or metal ions may interact with pathogen DNA or RNA resulting in the destruction or oxidation of genetic material.[145] Furthermore, unlike antipathogenic drugs, like antibiotics and antivirals, metal nanomaterials have shown to deactivate all classes of pathogens, effectively deactivating bacteria, fungi and viruses.[145] Metal nanomaterials suffer from a few drawbacks, as the release of metal ions from their surface cannot be easily controlled.[63] As a result, they will continuously leach ions into their environment depleting their effectiveness over time,[148] and potentially leading to the development of antimicrobial resistance as seen with antibiotics.[64] Semiconductive metal oxide nanomaterials function differently than that of their metal counterparts. When a semiconductive metal oxide nanomaterial is exposed to specific wavelengths of light, it can produce reactive oxygen species (ROS) that interacts with various components of pathogens, leading to their deactivation.[149] Interestingly, light activation allows for the controlled release of antipathogenic agents from these materials and may solve some issues seen with other antipathogenic nanomaterials.[31]

2.5.2 Anti-microbial Effects of TiO_2

Metal oxide semiconductors such as TiO_2, ZnO, WO_3, Fe_2O_3, and In_2O_3 have shown strong photoactivity and antimicrobial properties,[79,81] and have been researched extensively for use in water treatment facilities/process[79] and self-cleaning textiles.[81] TiO_2 has a few advantages over the other materials, being abundantly available (and inexpensive), stable with and without light, and exhibiting strong reactivity for the generation of reactive oxygen species (ROS).[77,81] The photocatalytic properties of TiO_2 arise from the interactions of electrons and holes with oxidizable materials at the surface of TiO_2. When a photon of appropriate energy (greater than or equal to the band gap) is adsorbed by the TiO_2, an electron is excited into the conduction band leaving a hole behind in the valance band (Figure 2-5a). This electron-hole pair can then either recombine or migrate to the surface where they may participate in oxidation and reduction reactions.[150,151] The size of the band gap is dependent on the crystal structure of the TiO_2, with the two most prevalent crystal phases being the anatase and rutile phase,[81] with band gaps of 3.05 eV and 3.18 eV, respectively.[152] Commonly, the anatase and rutile phases are mixed in different combinations, such as P25 (80% anatase, 20% rutile), which has been used extensively for photooxidation of organic matter.[81] This combination of the two phases in TiO_2 NP allows for lower recombination of electro-hole pairs, increased surface area and increased photoabsorption efficiency at longer wavelengths,[153] which intern increases the number of ROS which can be generated under light absorption.[81]

When electrons and holes migrate to the surface, they can interact in two distinct ways, either producing ROS or directly oxidizing organic matter at the surface. If the TiO_2 is in

an aqueous environment, electron-hole pairs available at the solid-liquid interface can produce ROS. The electron can interact with O_2(oxygen) through photoreduction, producing $\cdot O_2^-$ (superoxide radicals), H_2O_2(Hydrogen peroxide) and $\cdot OH$ (hydroxyl radicals).[150] The hole can interact with H_2O (water) through photooxidation, producing $\cdot OH$ (hydroxyl radicals).[78] All of the ROS species generated by the TiO_2 are active and nonspecifically oxidize most of the organic matter that they interact with,[81] which accounts for TiO_2's robust photocatalytic properties in aqueous environments.[79] If the TiO_2 is not in an aqueous environment but organic or oxidizable materials are attached to the solid interface, then the electron or hole may directly oxidize those materials.[78]

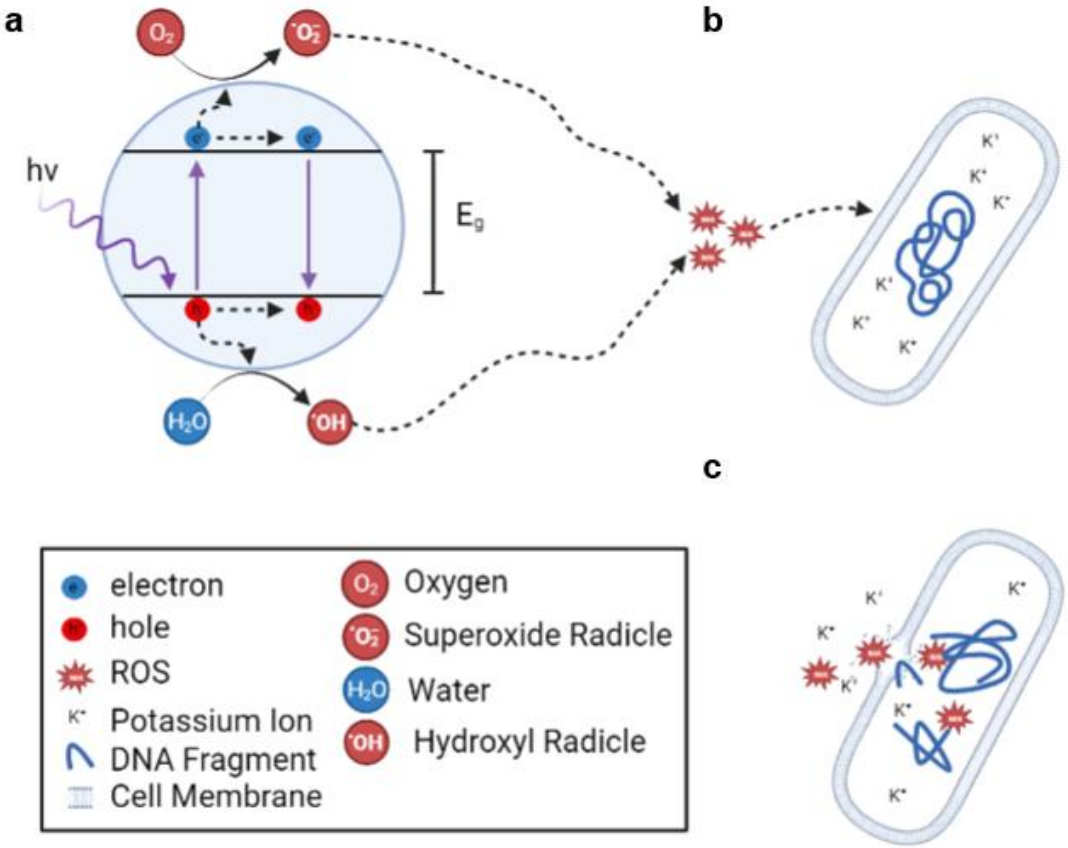

Figure 2-5: Schematic of the antimicrobial action of TiO2. a) Photoactive production of ROS by TiO2, b) transport and attack of ROS to the live bacteria cell wall, and c) bacterial deactivation after oxidation of cell wall and internal cellular components.

TiO_2 can interact and affect pathogens through the pathways mentioned above, directly though the oxidation of organic materials and compounds at the surface of the TiO_2, or indirectly though the production of ROS, which can then oxidize organic matter not bound to the surface of the TiO_2 (Figure 2-5b).[78,81] In both cases, the deactivation of the pathogen occurs through the oxidation of the protective/structural membrane, functional proteins in the membrane, and/or genetic materials (DNA/RNA) inside pathogens (Figure 2-5c).[78] For bacterial pathogens, the oxidation pathway depends on its membrane structure, which is characterized by weather the bacteria are Gram-negative or Gram

positive. Gram-negative bacteria have a cell wall structure comprised of an outer membrane, peptidoglycan layer and inner membrane,[110] while the Gram-positive cell wall is comprised of a thick outer peptidoglycan layer and an inner membrane.[110] It should be noted that Gram-positive bacteria show more resistance to damage from ROS due to their thicker peptidoglycan layer,[151] and ability to form spores,[81] however both types of bacteria are readily deactivated by ROS.[151] Once the cell wall of the bacteria has acquired substantial damage, the intercellular contents such as DNA and K^+ ions begin to leak out (Figure 2-5c).[78] ROS can then interact with the leaking contents of the bacteria or diffuse into the cell, increasing the oxidation of the bacteria and leading to its deactivation (Figure 2-5c).[78,151] Viral pathogens are deactivated in a similar way to that of bacteria, with the ROS created by the TiO_2 surface interacting with and oxidizing the shell/capsid of the virus.[154] This process results in the leaking and oxidation of the genetic material, minerals and proteins within the virus resulting in deactivation.[155]

Ruptured and deactivated pathogens present negative implications for the antimicrobial and photocatalytic properties of the TiO_2. If oxidized and deactivated on the surface of TiO_2, the ruptured membrane will cover the surface and prevent the TiO_2 from being able to directly oxidize other biological material as well as block/inhibit the production ROS,[151] resulting in the surface becoming less antimicrobial over time.[63] Combining photoactive materials with surfaces that prevent or significantly reduce the adhesion of biological contaminate may increase the effectiveness and the productions of ROS over time.

2.6 Conclusion

Throughout this work, wettability is used to characterize and quantify the level of repellency of the different surfaces and structures that are developed. Specifically, it is used to determine whether or not the surface has omniphobic wetting properties. To create these repellent structures, we utilized the phenomena of thin film wrinkling discussed above. In combining these films with fluorinated monolayers, we are able to create omniphobic wrinkle structures on thermally shrinkable polymer substrates. The use of antimicrobial agents is also used in order to improve the antipathogenic properties of the repellent surface. In the work done TiO_2 is integrated into the repellent surface structure and allows for the controlled release or ROS which can actively deactivate pathogens that are able to bind to the surface.

Chapter 3 Hierarchical Structures, with Submillimeter Patterns, Micrometer Wrinkles, and Nanoscale Decorations, Suppress Biofouling and Enable Rapid Droplet Digitization

Preface:

In chapter 2, we provided background on how the modification of both the chemical and topographical features of surfaces, can be leveraged in order to create liquid repellent surface structures. Hierarchically structured materials have gained significant attention in recent years for the development of superhydrophobic, antifouling, and repellant surfaces. One of the major challenges with the deployment of hierarchically structured and repellent surface in the real world is their restrictions in scalability driving by the common manufacturing methods.[45,117,156–158] This chapter focuses on research Objective I and II, by developing of a highly repellant material based off of the wrinkling of NP thin films and characterizing its ability to prevent blood fouling on the surface. The deposition of NP films onto pre-strained polymers using all-solution techniques was utilized to create a surface area independent deposition method for creating large amounts of hierarchically structured repellent surfaces. We begin by optimizing and characterizing the wettability of surface structures at the micro (wrinkles) and the nano (NP films) scale individually. These surfaces structures were then combined and optimized to achieve superhydrophobicity (water CA > 150^{o}) and oleophobicity (hexadecane CA > 90^{o}) (Objective I). With the different surface structures, we were able to investigate how the wetting at different scales affected the adhesion of blood to the surface, under both dynamic and static conditions (Objective II). To quantify any enhancements in the repellant and antifouling properties of hierarchical structures, a comparison of the surface wettability and blood repellency of each of the different surface structures was done. The blood repellency was quantified by testing the resistance of each surface towards blood

staining, blood clot formation (Thrombosis) and red blood cell adhesion. Finally, the patternibility of the superhydrophobic structures was utilized in medical devices by creating a dip-based droplet digitization surface integrated with a fluorescence-based IL-6 biosensor in the non-repellent regions.

Methodology:

The aim of this chapter as discussed above is to develop a scalable method for the manufacturing of ominphobic surfaces, as well as characterize the blood repellent properties of the manufactured materials. Solution-based manufacturing methods were selected as the manufacturing method as they can be scaled by simply increasing the volume of the deposition solutions in order to compensate for larger surfaces. The liquid repellent properties of the surface were characterized through contact angle and sliding angle measurements with water, hexadecane and blood. Water and hexadecane were selected for their differing interfacial properties as water interacts through polar and dispersive effects, while hexadecane only interacts though dispersive effects. The wettability measurements were conducted on the individual micro and nano structures in order to determine their contributions and effect on the wettability of the omniphobic hierarchical structures. To quantify the blood adhesion of the difference surfaces developed, blood staining and blood coagulation assays were developed. These two assays were selected to give insight into the adhesion of blood prior to and after the coagulation process has occurred. One hurdle with the blood staining assay was the visibility of blood on the surface structure with AuNP present. The light absorbing properties (~465nm) of the gold nanoparticles made it difficult to see blood present on the surface. This issue was especially true for the hierarchically structured shrunk surface as

increased the density of the gold nanoparticles and the wrinkled microstructure amplified this effect. As such, in the blood staining assay the surfaces were washed after staining and the amount of blood present in the wash solution was measured. For the blood clotting assay surface were weighed before and after clotting to quantify the amount of contamination. Inconsistencies in the blood staining and clotting assay results were also due to the modification of only one side of the polystyrene surface, thus causing blood to stain the unmodified side and skew the results. To address this, we had to ensure that one side of the surface was in contact with blood, as their difference in repellency between the front and back could significantly skew the results. To prevent this from occurring all samples were secured to the bottom of well plates with double sided tape, ensuring that only the functionalized regions were interacting with blood. Overall, the blood staining and coagulation assays were effective in characterizing the interaction of whole human blood with the different surface structures (planar surfaces, microstructured, nanostructured and hierarchical structures), as well as displaying the repellent properties of the combined hierarchical micro- and nano-structures.

Authors: *Roderick Maclachlan*, Sara M. Imani*, Yuting Chan, Amid Shakeri, Leyla Soleymani, Tohid F. Didar*

* Indicates equal contribution to the work

Publication: Small, 2020, 16, 2004886

Publication Date: 23 November 2020

3.1 Abstract

Liquid repellant surfaces have been shown to play a vital role for eliminating thrombosis on medical devices, minimizing blood contamination on common surfaces as well as preventing non-specific adhesion. Herein, we report an all solution-based, easily scalable method for producing liquid repellant flexible films, fabricated through NP deposition and heat-induced thin film wrinkling that suppress blood adhesion, and clot formation. Furthermore, we have combined superhydrophobic and hydrophilic surfaces onto the same substrate using a facile streamlined process. The patterned superhydrophobic/hydrophilic surfaces showed selective digitization of droplets from various solutions with a single solution dipping step, which provides a route for rapid compartmentalization of solutions into virtual wells needed for high-throughput assays. This rapid solution digitization approach was demonstrated for detection of Interleukin 6. The developed liquid repellant surfaces are expected to find a wide range of applications in high-throughput assays and blood contacting medical devices.

3.2 Introduction

Biofouling, coagulation and thrombosis are undesirable effects that occur when blood comes into contact with the surfaces of *in vitro*, *ex vivo*, and *in vivo* biomedical devices.[159] These processes are initiated by the non-specific adsorption of blood proteins on surfaces and the formation of a complex protein layer.[160] To address this issue, surface modification strategies have focused on using bioinert polymers,[161–164] antithrombotic agents,[165–170] or changing the surface charge, wettability, chemical affinity and hydrophilicity.[171–175] Anticoagulants such as heparin have been widely used as coatings

on biomedical devices to overcome these adverse effects.[176] Heparin-coated surfaces typically operate through either the release of heparin into the blood stream for inhibiting clotting in the vicinity of the device surface or reducing coagulation *via* immobilized heparin on the surface of the device. Anticoagulant coatings fail over time due to leaching and the loss of anticoagulant activity. Furthermore, administration of anticoagulants (*e.g.* heparin) both as a coating and a chronic medication, enters the bloodstream, elevating the risk of life-threatening heparin-induced thrombocytopenia , reported to occur in 1-5% of surgical patients.[25]

Recently, omniphobic coatings have been introduced on the surface of biomedical devices for reducing biofouling and the resultant blood coagulation,[38,54,177–184] while minimizing the administration of anticoagulants.[57] Liquid-infused surfaces are one of the recent classes of omniphobic surfaces which have shown to significantly suppress biofouling and thrombosis with their performances surpassing previous anticoagulant based strategies in terms of longevity under blood flow, and anti-biofouling ability. [38,57,177–184] However, in order for these surfaces to sustain their omniphobic and repellent properties, the lubricant layer must be stable on the surfaces, making them difficult to use in open-air applications where the lubricant is susceptible to evaporation. [35] Another class of omniphobic surfaces are those with structural modifications wherein the micro- and nano-scale topography of the surface provides omniphobic properties. Through the formation of micro, nano and hierarchical structures, air pockets are trapped within the features, leading to the formation of a Cassie wetting state, which reduces the apparent surface energy seen by liquids, [119] resulting in elevated CAs and low SAs which lead to omniphobicity. [119] Additionally, the formation of the Cassie state reduces the effective

surface area to which platelets and proteins in blood can bind to, and decreases shear stress at the surfaces reducing platelet adhesion. These two effects reduce the number of nucleation sights for thrombin generation. [26] Hydrophilic polymer surfaces have also shown significant antifouling properties and blood compatibility through the reduction of fibrinogen and platelet adhesion. As a result of the hydrophilicity of these surfaces, blood can still easily stain them, which can spread blood related pathogens between healthcare workers and patients. [185,186]

In spite of great performance demonstrated by several classes of hierarchically-structured omniphobic surfaces for reducing blood-related contamination (including sand-casting of SiO_2 and Polydimethylsiloxane (PDMS), [187] electrochemical anodization of titania, [115] and laser ablated stainless steel and titanium), [126] these high performance structures are fabricated using molds, electrodeposition or laser ablation, which are material dependent, difficult to scale and/or costly (due to material choice and equipment cost and upkeep). Hierarchical structures have recently been developed using a series of bottom up fabrication processes such as electrophoretic deposition, [156] emulsion templating, [157] electrospinning, [117] electrochemical techniques, [158] and reactive ion etching. [45] Among these, methods that allow for controlling the materials architecture over a range of length scales *and* can be manufactured using easy-to-scale processes are highly desirable for creating application-specific omniphobic materials and translating these to real-life biomedical devices. In response, we sought to develop easy-to-scale hierarchical materials that combine tunable materials in the microscale, nanoscale, and molecular scale.

Nanoparticle-induced microscale wrinkling (NMW) is a process that uses the self-assembly of NPs on pre-strained substrates followed by the application of strain to create microscale wrinkles with nanoscale features. [129] The NP size controls the nanoscale features and the size of the secondary microscale wrinkles, delivering tunability over multiple length scales. Such hierarchical structures, when combined with molecular layers, have demonstrated remarkable omniphobicity (water and hexadecane CAs > 163° and 101° respectively, and SA > 5°). [188,189] Additionally, this method is compatible with batch scale solution-processing, which is widely used for large volume manufacturing.

Herein, we focus on developing liquid repellant hierarchical materials based on NMW and applying these to surfaces for reducing blood adhesion and coagulation with potential for use in *in vivo* systems like catheters and *in vitro* devices such as biosensors. We further tested the developed technology in dynamic systems (*e.g.* microfluidic devices) to assess the extent of blood adhesion. These materials are patterned on surfaces to spatially modulate their repellency for creating biosensing arrays integrating hydrophilic and superhydrophobic regions. This approach led to a strategy for one-step and instrument-free droplet digitization and was used in a proof-of-concept dip-based Interleukin 6 (IL-6) detection chip, demonstrating the application of our approach for use in *in vitro* biomedical devices. This opens up a platform to utilize such devices in in vitro biosensing assays in complex fluids where shorter amount of contact time is needed.

3.3 Materials and Methods

Reagents: (3-Aminopropyl)triethoxysilane (99%) and 1H,1H,2H,2H-Perfluorodecyltriethoxysilane (97%), were purchased from Sigma-Aldrich (Oakville, Onatrio). Ethanol (anhydrous) was purchased from Commercial Alchohols (Brampton, Ontario). Hydrochloric acid (36.5–38%) was purchased from Caledon (Georgetown, Ontario). Milli-Q grade water (18.2 MΩ) was used to prepare all solutions. Whole human blood was collected from healthy donors in BD heparinized tubes. All donors provided signed written consent and the procedures were approved by the McMaster University Research Ethics Board. Self-adhesive vinyl sheets (FDC 4304) were purchased from FDC graphic films (South Bend, Indiana). Streptavidin eFluor 660 was purchased from eBioscience (San Diego, CA). Recombinant human (*E. coli* derived) IL-6 was purchased from R&D systems (Minneapolis, MN). IL-6 monoclonal antibody (MQ2-13A5, capture antibody) and biotinylated IL-6 monoclonal antibody (MQ2-39C3, detector antibody) were purchased from ThermoFisher Scientific (ON, Canada).

Surface Fabrication: Using Robo Pro CE5000-40-CRP cutter (Graphtec America Inc., Irvine, California) pre-strained polystyrene (Graphix Shrink Film, Graphix, Maple Heights, Ohio) was cut into pieces. PS pieces then were cleaned with ethanol and milli-Q water and dried. In a pre-warmed ultraviolet ozone (UVO) cleaner (UVOCS model T0606B, Montgomeryville, Pennsylvania), PS samples were placed and UVO treated for 4 mins. 12 nm gold nanoparticle (AuNPs) were synthesized as described elsewhere and were kept at 4°C until used. [129] Activated PS substrates were incubated on a shaker in 10% aqueous (3-Aminopropyl)triethoxysilane (APTES) (for creating the seed layer for NP solution for respected samples) for 3 hours at room temperature followed by sonication

in water. To coat the AuNPs covered PS with FS, the substrates were first submerged in 10% aqueous APTES for 3 hours with agitation. The substrates were sonicated in milli-Q water for 10 minutes and dried. To fluorosilanize the samples, a solution of ethanol and milli-Q water with volume ratio of 3:1 was prepared. A catalytic amount of hydrochloride acid (0.1 wt%) was added into the solution with 0.5 wt% of FS. The solution was incubated at 40° for an hour before use. [190] Following deposition of coating, the substrates were sonicated in Milli-Q water and subsequent 10 min sonication in ethanol for 10 minutes and dried (PS-AuNP-Planar). To add the microstructures to the NP treated surface, thermal treatment was performed by placing the substrates into an oven at 140°C for 5 minutes (PS-AuNP-Shrunk). As a control FS-treated planar surfaces, PS-Planar surfaces were FS treated in a similar method (PS-FS-Planar).

The patterned surfaces were fabricated in a similar way. Before the modification steps, a vinyl mask was placed on a clean (as described in the previous paragraph) PS sheet and cut in the desired pattern with the craft cutter. The vinyl was then removed from the regions where the treatment was required and the samples were subject to UVO treatment and the subsequent treatments while maintaining the vinyl mask on. After the final FS treatment, the vinyl mask was removed and the samples were subjected to heat treatment as described before. To enhance the hydrophilicity on the untreated regions, a 0.6 µL droplet of 12 M H_2SO_4 was deposited on the untreated regions, incubated for 10 minutes and subsequently washed 2 times with Milli-Q water.

Surface physical characterization: Scanning electron microscopy (SEM) imaging was performed in a JEOL 7000F. Samples were coated with 3 nm of platinum prior to imaging. For CA measurement a goniometer (OCA 20, Future Digital Scientific, Garden City, NY)

was used and water droplets were dispensed by automated syringe and other liquids by using A pipette. The sessile drop CA was provided via image processing software (Dataphysics SCA 20) through ellipse curve fit shape analysis of the droplets. SAs were measured using a digital angle level (ROK, Exeter, UK). Each value was averaged over at least three measurements.

Whole human blood staining assay: Whole human blood was collected from healthy donors in BD heparinized tubes. All donors provided signed written consent and the procedures were approved by the McMaster University Research Ethics Board. Blood sessile drop CA was measured at room temperature using the goniometer. The extent of blood adherence was evaluated by dipping each sample in human whole blood and resuspending the adhered blood to each surface by transferring each substrate in a well and adding 700 µL of water. To ensure the adhered blood was transferred in solution, samples were placed on a shaker for 30 minutes. 200 µL of each well was transferred to a 96 well and the absorbance was measured at 450 nm wavelength on a SpectraMax plate reader. To ensure reproducibility, 6 samples per each condition was evaluated. Samples were also incubated in blood for 30 minutes and washed subsequently by dipping in water two times to evaluate the extent of stickiness of the surfaces.

Whole human blood clotting assay and scanning electron microscopy: In order to investigate the blood clot repellency properties, 500 µL of citrated human whole blood and 500 µL of 25 mM $CaCl_2$ in 1 M HEPES buffer were added to a 24 well containing the treated samples and controls and incubated for 1 hour to allow for complete clot formation. Subsequently, samples were washed 2X with PBS. The quantification of the amount of the adhered clot was done by weighing the samples before and after the clotting assay.

The weight difference was then reported in Figure 3b normalized to PS-Planar. The samples were fixed in 4% formaldehyde for 2 hours and coated with 3 nm Platinum. SEM was conducted to investigate blood clot formation and blood cell attachment.

Microfluidic channel and heparinized blood assay: Molds were created through vinyl (152.4 µm height) masking a PS surface and cutting the pattern for the channels with a craft cutter (2 mm width), then the molds were placed in a petri dish. PDMS (10:1) was poured on the created mold and cured over night at 60 degrees. The PDMS channels were then bonded to the PS-Planar or PS-AuNP-Shrunk through wet bonding. [132] This was done by creating a thin layer of PDMS (10:1) by depositing 400 µL PDMS in a petri dish and spin coating for 30 seconds at 7000 rpm. The PDMS channel was stamped on the spin coated layer then placed carefully on PS-Planar or PS-AuNP-Shrunk and cured overnight. For the heparinized blood assay, at 10 µL/min heparinized blood was flowed on PS-Planar or PS-AuNP-Shrunk for 30 minutes followed by a 10-minute wash. For evaluating the extent of blood adhesion, an optical image and bright field microscope image at 40X was acquired and the cells were counted.

Droplet digitization on patterned surfaces and volume measurement: The patterned surfaces were dipped in blue dyed water allowing the droplets to attach to the hydrophilic patterns. The surfaces were also dipped in 8:1000 Cy5 tagged anti IL-6 antibody allowing the droplets to attach to the hydrophilic sites, this was confirmed by imaging the wells by a Chemidoc imaging system (BioInterface Institute, McMaster University) by Cy5 channel. The volumes were measured using image processing software (Dataphysics SCA 20) on Digital Scientific OCA20 goniometer (Garden City, NY, USA).

Detection of IL-6 on patterned oleophobic surfaces: The patterned hydrophilic wells were treated with 10% APTES solution for 3 hours, followed by 10 min sonication in DI water. This was then followed by treatment in EDC/NHS (2 mM EDC ((N-ethyl-N'-(3-(dimethylomino)propyl)carbodiimide) and 5 mM NHS (N-hydroxysuccinimide) in 0.1 M MES (2-(N-morpholino)ethanesulfonic acid) buffer) mixed with 1:100 ratio of capture antibody to initiate the carbodiimide cross-linking reaction and 1 µl of the solution was pipetted on to each well and was incubated overnight. Subsequently the wells were block by 2% bovine serum albumin (BSA) for an hour. The samples were then dipped into buffer containing 2500 pg mL^{-1} of IL-6 (in sample diluent composed of 1% BSA in phosphate-buffered saline), digitizing the solution on to the substrate. These droplets were let for 1 hour before washing in TBST and TBS. Surfaces were then dried with compressed air and dipped in biotinylated IL-6 monoclonal antibody (1:500 v:v diluted in the sample diluent buffer) for another hour. The samples were again washed using both wash buffers, and dried. Finally, the samples were dipped in the streptavidin dye (8:1000 v:v diluted in the reporter buffer) for 30 minutes in complete darkness, and subsequently washed with the wash buffers before the imaging. The binding of IL6 was confirmed and quantified by imaging the wells using a Chemidoc imaging system (BioInterface Institute, McMaster University) by Cy5 channel. A schematic of the assay component can be found in Figure S2.

3.4 Results and discussion

3.4.1 Fabrication and characterization of hierarchical liquid repellant surfaces

In order to create hierarchically-structured surfaces using NMW, we designed a fabrication process (Figure 3-1a) in which AuNPs modified with a molecular FS layer for reducing surface energy were deposited on the surface of a pre-strained polymer substrate (Figure 1b,i) to create a stiff layer (Figure 1b,ii). Upon shrinking, this stiff layer transformed into a hierarchical surface combining nanoscale features with microscale wrinkles (Figure 1b,iii).

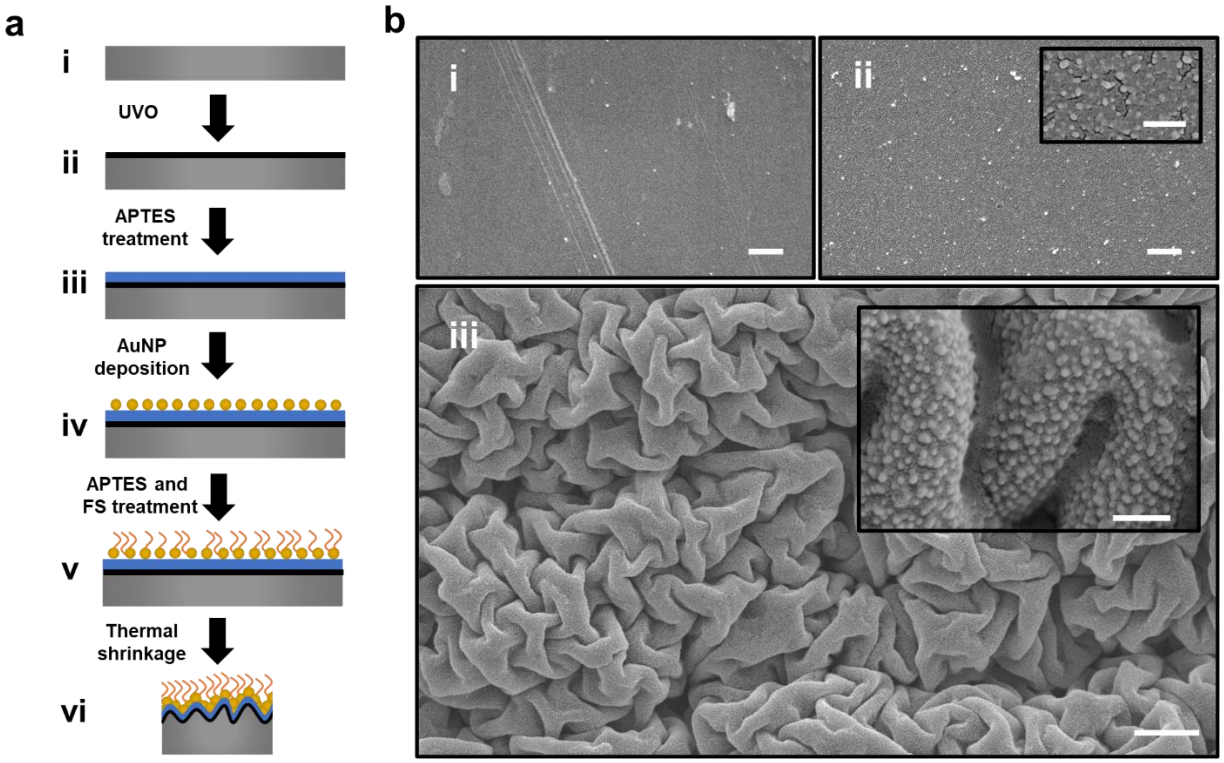

Figure 3-1: Schematic depicting the fabrication process of liquid repellant surfaces and corresponding SEM images. a) Process steps for the formation of the AuNP decorated surface and the hierarchically structured surfaces. b) SEM images depicting the untreated PS (i), AuNP decorated PS (ii, PS-AuNP-Planar), and final hierarchically-structured PS

(iii, PS-AuNP-Shrunk). The scale bars in the larger SEM images represent 1 μm and those in the insets represent 100 nm.

The fabrication process started with surface activation of pre-strained PS using ultraviolet-Ozone (UVO) treatment to induce hydroxyl groups on PS (Figure 1a,ii) for subsequent surface functionalization with APTES (Figure 3-1a,iii). Following APTES deposition, 12 nm AuNPs were bound to the surface through the electrostatic interactions of the amine terminus of APTES and the citrate surfactants present on AuNPs (Figure 1a,iv). [191,192] A self-assembled monolayer (SAM) of FS was then covalently attached to the surface through hydrolysis and condensation reactions using APTES as an intermediate linker (see methods for more information, Figure. 1a,v), which generated a nanostructured surface using AuNPs as building blocks (PS-AuNP-Planar). The PS-AuNP-Planar substrate was then shrunk at 145º C for 10 minutes to induce hierarchical structuring (PS-AuNP-Shrunk, Figure 1a,vi).

The repellency of PS-AuNP-Planar and PS-AuNP-shrunk was evaluated alongside the untreated polystyrene (PS-planar), PS substrate after shrinking (PS-shrunk), and PS substrate after fluorosilinizaiton (PS-FS-Planar) by measuring CA using various test liquids, as well as SA (Figure 3-2a). In order to understand the hydrophobic and oleophobic properties, the CA of the surfaces were assessed using the following test liquids: milli-Q grade water (surface tension of 72.75 mJ/m^2), [193] hexadecane (surface tension of 27.76 mJ/m^2), [193] human whole blood (surface tension of approximately 55 mJ/m^2) [194] and various ethanol/water concentrations (%v/v).

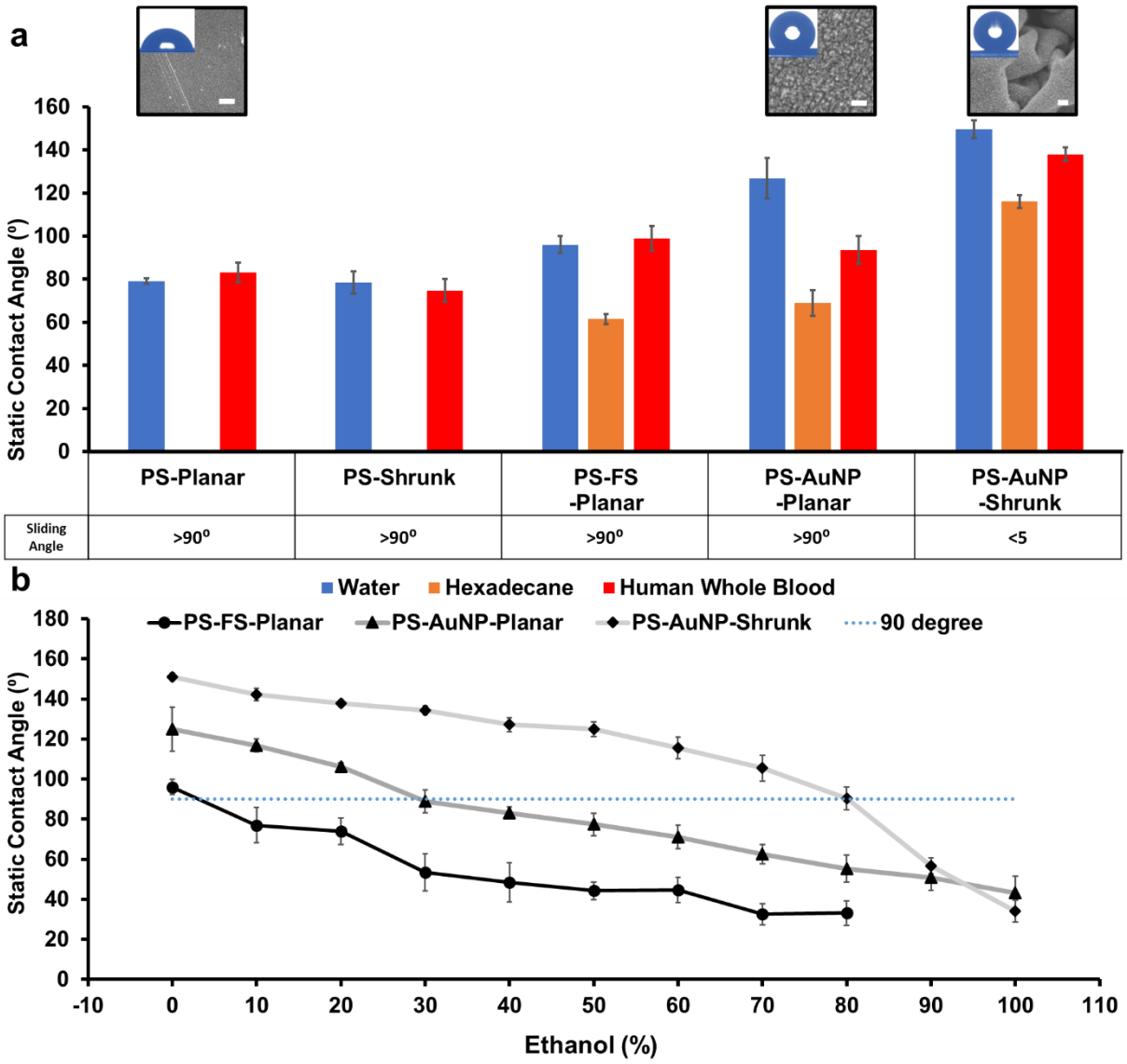

Figure 3-2: Surface Repellency. a) Graph depicting the contact angle of different surfaces for water (blue), hexadecane (orange), and whole blood (red). Representative SEM images are also shown on the top with an image of the water droplet on the surface. The table shows the sliding angles of the different control groups. b) Graph showing the change in contact angle with varying ethanol concentrations in water. Dotted line at 90 degrees shows the point where surfaces enter the hydrophilic regime.

The hydrophobicity of the various surfaces created here was evaluated by measuring the water CA (Figure 3-2a) Both unmodified surfaces, PS-Planar and PS-Shrunk, showed a hydrophilic behavior (CA of 79±1.3° and 78±5.1° respectively). The successful FS

treatment was verified by the observed elevation in the CA for the PS-FS-Planar (96±3.8°) compared to PS-Planar. Coating the substrate with NPs (PS-AuNP-Planar) increased the surface roughness and introduced re-entrant texture. This surface roughness introduced an effective Cassie wetting state and increased the apparent CA (water CA of 127±9.4°). [195,196] The water CA and CAH was then further improved (149.5±4°, 10.7±4.3° with advancing and receding CA of 160.6±0.6 and 149.9±3.7 respectively)) through the formation of hierarchical structures (PS-AuNP-Shrunk). When these surfaces were transformed into a cylinder (radius of curvature o was 5.5 mm), they sustained their CA (154.23±0.55), as well as their slippery behavior (Supplementary Video 1) with a CAH of 9.45±2.7 (advancing and receding CA 148.6±3.93 and 139.2±1.3 respectively). The smallest radius of curvature that was manufacturable with the PS substrates was 2.25 mm radius and the repellent behavior was maintained while showing no fractures on the surface of the bent surfaces.

The hexadecane CA was also evaluated to test for oleophobicity for all the different classes of surfaces. The PS-planar and PS-shrunk surfaces were both completely wetted by hexadecane; however, the introduction of FS (PS-FS-Planar) and NPs to the surface (PS-AuNP-Planar) increased the CA to 62±2.4° and 69±6°, respectively. Through the introduction of hierarchical structures (PS-AuNP -Shrunk), the surfaces were brought into the oleophobic regime with a hexadecane CA of 116±3°.

The heparinized blood CA was also measured to gain insight into the interaction of our oleophobic surfaces with complex liquids. With the introduction of these structures an increase from 83±4.5° (PS-Planar) to 138±3.1°(PS-AuNP-Shrunk) was seen. Overall, the formation of hierarchical structures combined with chemical modification demonstrated

liquid repellency due to the high CAs recorded for this class of surfaces with various test liquids. This effect can be explained by the higher amounts of trapped air within the hierarchical structure compared to the other control groups. [197]

In order to gain a greater understanding and indication of the functional range of repellency with regards to liquid surface tensions for each of the surface topographies, the CA was measured for different water/ethanol concentrations, ranging from the surface tension of water 72.86 mN/m to ethanol 22.39 mN/m (at room temperature). As seen in Figure 2b, the hierarchical surfaces were able to maintain CAs greater than 90° for ethanol concentrations of 80% and lower indicating that the surfaces remain repellent towards liquids with surface tension of 24.32 mN/m (80% ethanol) [198] and above, unlike the PS-FS-Planar and the PS-AuNP-Planar substrates which demonstrated CAs below 90° after 0% and 30% ethanol, respectively. Additionally, for an ethanol/water mixture with similar surface tension to hexadecane (60% ethanol) we can observe a similar CA of ~120º for both liquids using the PS-AuNP-Shrunk surfaces and ~70º for the PS-AuNP-Planar. However, this was not the case for the PS-FS-Planar surfaces, indicating the significance of micro and nanostructures on the generation of oleophobicity.

The ability of the fabricated surfaces in repelling liquid droplets was further assessed by measuring the SA, which is a key metric for classifying surfaces as repellant (Figure 3-2a). Among the investigated surfaces, only PS-AuNP-Shrunk demonstrated droplets sliding off with SA below 5°, which can be attributed to the roughness of the hierarchical surfaces (Figure 3-1b,iii) such that the formation of the Cassie state and the entrapment of air-pockets within the texture allow for the water droplets to only contact discrete sections of the surface. [199] These discrete contact patches decrease the adhesive forces

experienced by the droplets, allowing the droplet to easily detach from the surface. To test the performance of the hierarchical surface for extended amounts of time in heparinized blood, the surfaces were incubated in heparinized blood for 48 hours and subsequently washed twice and dried. The surfaces were examined for their water CA following the blood incubation, demonstrating a water CA of 140.3±8.2 (compared to 149.5±4 before) which is in the hydrophobic region showing that their hydrophobic characteristic is resilient after a long incubation time in blood.

To assess the adhesion of the coating to the substrate and to test the resilience of the coating, we performed an adhesion test according to ASTM standard. In this method, two perpendicular cuts were made and subsequently brushed and taped over to clean the incision parts. Based on the smooth edges following the incision, we concluded that our surfaces demonstrated a 5B classification, which stands for the highest level of adhesion (Supplementary Figure 3-1).

3.4.2 Interaction of hierarchical surfaces with human whole blood

In order to understand the interaction of the various surfaces developed here with anticoagulated whole blood, we evaluated the repellant behavior of the surfaces under conditions that are important for blood contacting medical devices and implants such as clot formation and blood adherence (blood stain). These *in vitro* assays might not completely mimic the complex environment in *in vivo* studies such as animal tests, but still has been proved to be important for assessing surfaces behavior. [200] The staining assay was designed to investigate the amount of blood that was sticking to each surface and see the extent by which the hierarchical surfaces attenuate staining (Figure 3-3a). In

this assay, the surfaces were submerged in heparinized human whole blood (Supplementary Video 2) and were subsequently agitated in PBS to quantify the extent of blood adhesion using spectrophotometry (Figure 3-3a). The results revealed that the hierarchical surfaces (PS-AuNP-Shrunk) reduced blood adherence by over 90% compared to the untreated polystyrene surfaces (PS-Planar and PS-Shrunk). The PS-FS-Planar surface showed a 13% increase in blood adhesion which is due to the hydrophobic-hydrophobic interaction of these class of surfaces with proteins present in blood. [201] Furthermore, PS-AuNP-Planar surfaces reduced blood adhesion by 29% compared to the untreated samples. We also visually inspected these surfaces after incubating them in heparinized human whole blood for 30 minutes followed by rinsing them with water (Figure 3-3a). The blood repellency of the hierarchical surfaces (PS-AuNP-Shrunk) was visually evident. All surfaces remained stained after washing; however, the hierarchical surface did not contain a *visible* stain. It should be noted that the presence of AuNPs on the PS-AuNP-Planar and PS-AuNP-Shrunk surfaces resulted in the substrates having a grey hue, which made precise visual inspection difficult.

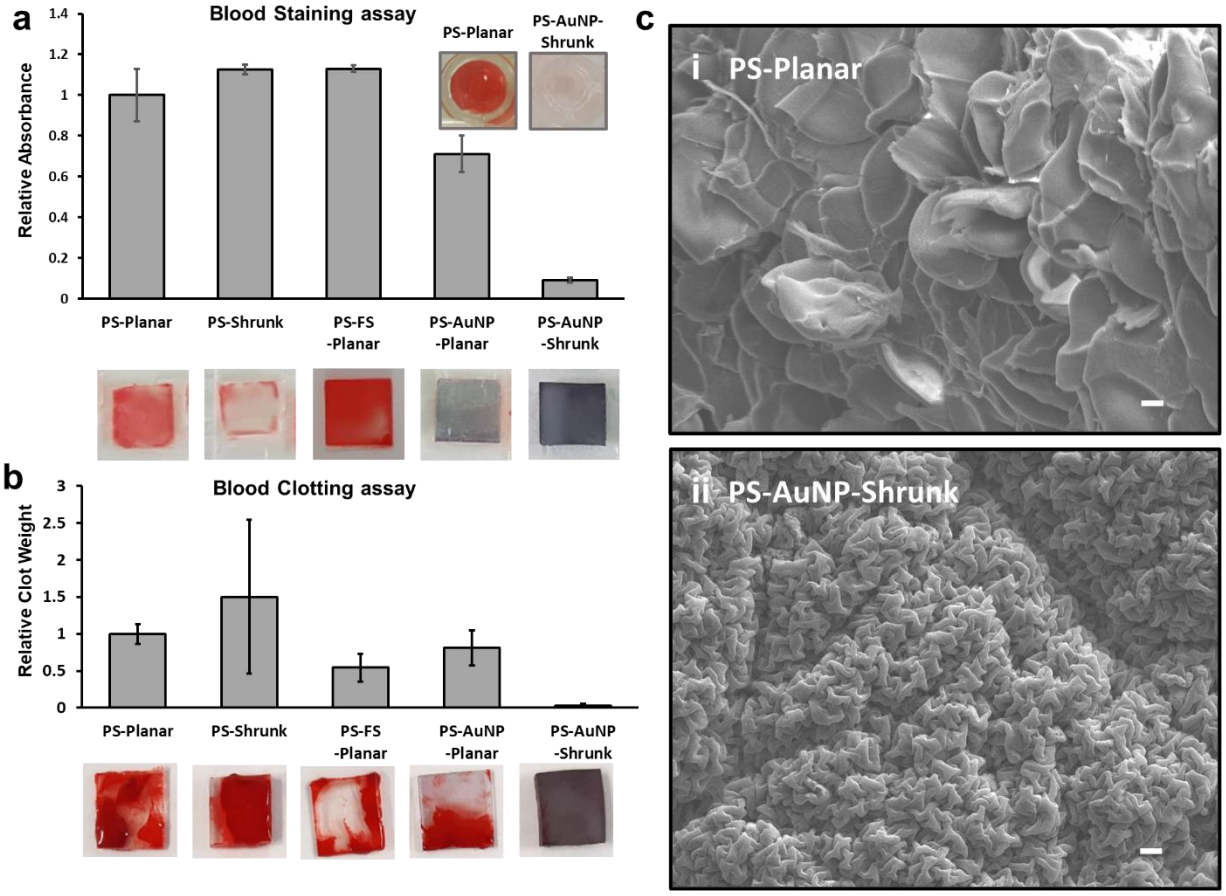

Figure 3-3: Study of blood repellency on the hierarchical surfaces. a) All surfaces were incubated with blood for 30 minutes and after two washes, they were transferred to well plates containing water (transfer solution). The absorbance of the transfer solution was measured at 450 nm wavelength and normalized to the value obtained from PS-Planar. Representative images of the transfer wells corresponding to PS-Planar and PS-AuNP-Shrunk are shown at the top right of the figure. The representative images of the surfaces incubated in blood are shown at the bottom of the figure. b) Relative clot weight adhered to each surface is normalized to the adhered clot to the PS-Planar and compared to the other control groups. Representative images of samples are shown after being exposed to the clotting assay after a 2X PBS wash. Error bars represent standard deviation from the mean for the clot assay performed on at least three surfaces for each class. c) SEM images of the surfaces after the clotting assay and 2X PBS washes followed by fixation in 4% formaldehyde performed on the PS-Planar (i) and PS-AuNP-Shrunk (ii), demonstrating blood adherence to the planar surface. The scale bars represent 1 μm in (i) and (ii).

In order to investigate the anticoagulant properties of the surface, they were subjected to citrated whole blood and the clotting was initiated by the introduction of calcium chloride and two subsequent washes with phosphate buffered saline (PBS). The extent of adhered blood clots to each surface was verified by weighing the surfaces before and after the clotting assay. As shown in Figure 3b**,** the hierarchically-structured samples (PS-AuNP-Shrunk) significantly attenuated the adherence of blood clots compared to the PS-Planar and PS-AuNP-Planar surfaces. SEM imaging of the surfaces after the clotting assay demonstrated significantly lower blood cell accumulation and blood clot formation on hierarchically structured surfaces compared to the untreated surfaces (Figure 3-3cii**)**. These experiments demonstrate that the degree of liquid repellency determines the effectiveness of the surface in blood repellency, with PS-AuNP-Shrunk surfaces demonstrating superior performance in terms of superhydrophobicity, oleophobicity, and blood repellency compared to the other investigated surfaces. Furthermore, covalently coated self-assembled monolayers of FS, has been reported to be harmless [57,202] therefore, making our developed coating a promising candidate for real-life applications. However, long-term *in vivo* studies might be needed in the future to further confirm biocompatibility.

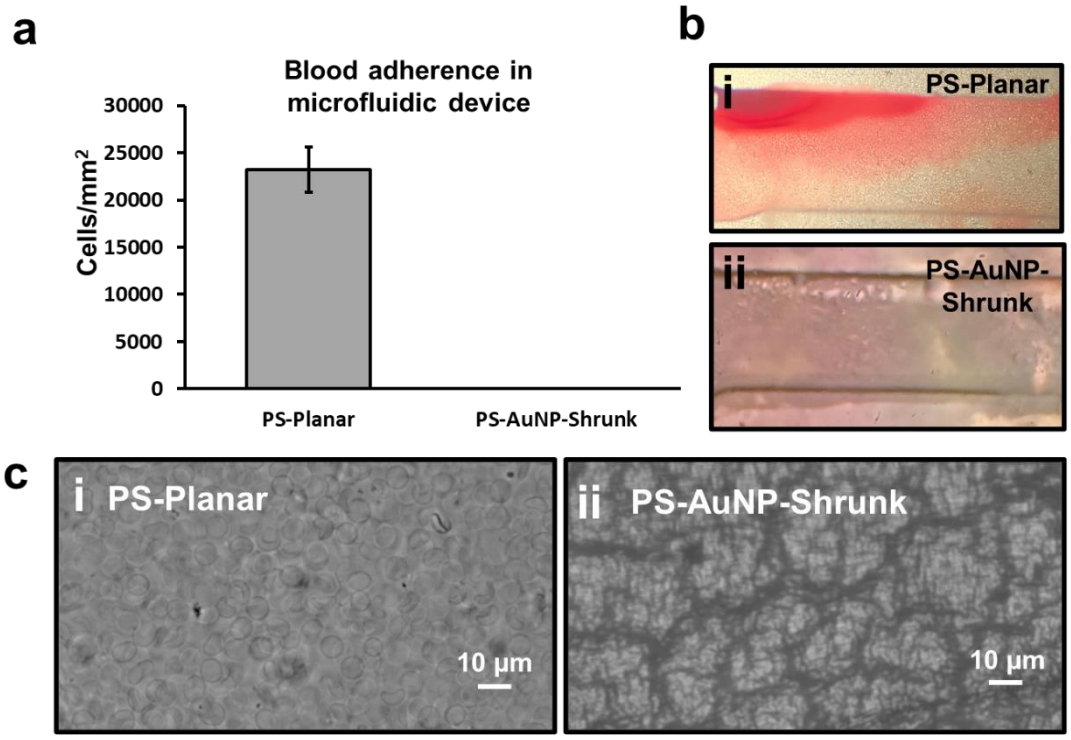

Figure 3-4: Dynamic conditions for blood adhesion tests. a) number of blood cells per mm^2 in microfluidics channel subjected to heparinized blood flow and subsequent washing for both PS-Planar and PS-AuNP-Shrunk. b) Optical images showing blood adhesion in (i) PS-Planar and (ii) PS-AuNP-Shrunk. c) Bright-field microscope images comparing (i) PS-Planar (ii) PS-AuNP-Shrunk. Blood cells are visible in (i) and wrinkles are visible with no presence of blood cells in (ii).

To investigate to behavior of the surfaces in dynamic conditions, we integrated the PS-AuNP-Shrunk surface in a microfluidic device and flowed heparinized blood through the channel. Subsequent to this, the channel was washed and imaged. As a control PS-Planar was also integrated into a microfluidic channel. The results showed significantly higher amount of blood cell adhesion within the channel on PS-Planar (23,200±2414 cell/mm2) than PS-AuNP-Shrunk (no cells were observed) (Figure 3-4a). This is also apparent in the acquired optical images (Figure 3-4a.i,ii) which a clear red stain is left in

the PS-Planar channel. Furthermore, images obtained using optical microscopy indicate that blood cells are visible in PS-Planar channel (Figure 3-4c,i), whereas in the PS-AuNP-Shrunk (Figure 3-4c,ii) the wrinkles are visible but there no blood cells found.

3.4.3 Patterned structures for digitizing droplets and dip-based bioassays

To further expand the application of the developed repellent surfaces, we introduced hydrophilic micro-patterns into the developed superhydrophobic surfaces through a benchtop masking method shown in the schematic in Figure 3-5a,i-v. Briefly, a vinyl mask was patterned on the PS surface using a craft cutter to protect the hydrophilic areas, while the substrate was modified with the NP and FS layers. The mask was then removed before heat shrinking the PS substrates. This method led to the development of hierarchical structures everywhere, except for the masked regions that retained their planar morphology upon shrinking because they did not possess a stiff surface layer. [82,83] The structural difference between the patterned area and the rest of the surface is clearly demonstrated in the SEM images in Figure 5b.

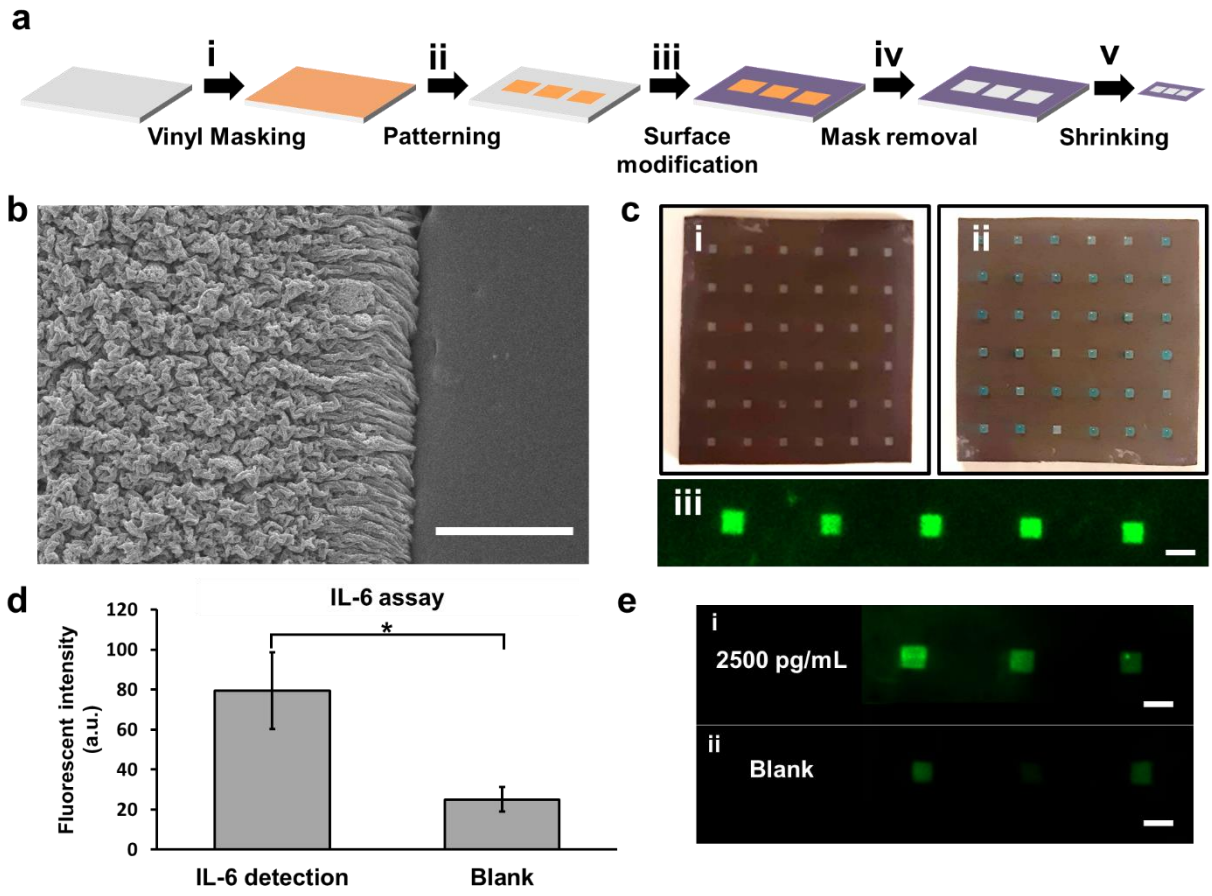

Figure 3-5: Digitization strategy enabled by patterning hydrophilic and liquid repellant areas a) (i) the substrate is covered with a vinyl mask, (ii) the vinyl mask is patterned to create hydrophilic wells, (iii) the substrate is modified with nanoparticles and coated with fluorosilane, (iv) the mask is removed, (v) the substrate is shrunk. b) SEM images of the fabricated wells showing the planar (hydrophilic) and hierarchical liquid repellant regions (scale bar 1 µm). c) (i) shows patterned wells with planar (inside the squares) and modified regions. (ii) shows the patterned well after being dipped in blue dyed water, demonstrating digitization of water droplets (iii) digitizing Cy5-tagged anti IL-6 antibody on the patterned wells. d) IL-6 assay performed using 2500 pg/mL of target solution compared to control solutions by dipping the wells in solutions containing the assay components. Briefly, capture antibody was deposited on the wells through EDC-NHS chemistry, and then dipped in solution containing 2500 pg/mL IL-6. Subsequently, the sample was subjected in biotinylated IL-6 antibody and streptavidin dye. And for blank, all the steps were kept the same but for the IL-6 incubation. e) Representative fluorescent images of the assay used in (d).

To demonstrate the capability of the patterned hydrophilic/superhydrophobic surfaces in digitizing water droplets they were dipped into aqueous solutions containing food colouring and fluorescent dyes (Figure 3-5c.ii-iii). We used this droplet digitization strategy to create a fluorescence biosensor for analyzing IL-6 (Supplementary Figure 3-2). To transform the patterned surfaces to biosensors, we first modified the hydrophilic areas with molecular linkers for antibody binding (APTES modification followed by 1-ethyl-3-(-3-dimethylaminopropyl) carbodiimide (EDC) and N-hydroxysuccinimide (NHS) bonding). [177,203] The hydrophilic areas were then functionalized with anti-IL6 capture antibodies. The assay was performed by dipping the biosensor into the target (IL-6) or control solutions (PBS), incubation for 60 minutes, washing the unreacted analyte, and dipping the biosensor into the solution of secondary antibodies modified with a Cy5 fluorescent label. In this assay, we observed a significant difference between the fluorescence intensity of the target and control solutions (Figure 3-5,e), demonstrating the potential of this materials-inspired digitization strategy for use in biosensing assays.

3.5 Conclusion

We have developed a scalable and low-cost method for producing patterned repellent surfaces. The repellency is created by introducing hierarchical structuring using NMW designed to combine nanoscale features with microscale wrinkles. We demonstrated that hierarchical structuring results in superior performance in reducing blood coagulation and contamination compared to planar and nanostructured surfaces chemically-functionalized using fluorosilane. Furthermore, we introduced hydrophilic patterns into our substrate alongside the superhydrophobic areas, leading to virtual wells that can be used for the

digitization of liquids in high throughput assays. The tunability of these surfaces allows for controlling the volume of the digitized drops as well as the localization of biomolecules. The facile fabrication method developed here can be applied to instances where both repellency and specificity are required for meeting functional requirements. This Cassie-based hierarchical surface (surface having hierarchical structures leading to Cassie state) opens up applications for *in vitro* assays in complex liquids, mainly for shorter periods of contact times (*e.g.* biosensing assays) for which Cassie state is satisfied.

3.6 Acknowledgements

This work was supported by NSERC Discovery and CRD grants, Ontario Early Researcher Award grant and McMaster start-up funds to T.F.D.

3.7 Supplementary Information

a

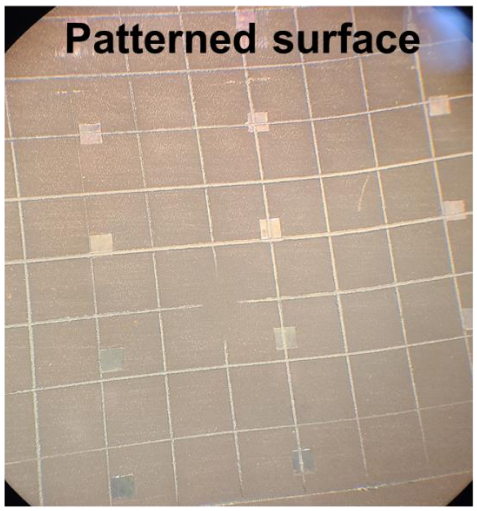

b

Example Appearance		Description	Classification	
Minimum Removal	Maximum Removal		ISO/JIS	ASTM
		The edges of the cuts are completely smooth; none of the squares of the lattice is detached.	0	5B
		Detachment of flakes of the coating at the intersections of the cuts. A cross cut area not greater than 5% is affected.	1	4B
		The coating has flaked along the edges and/or at the intersections of the cuts. A cross cut area greater than 5%, but not greater than 15% is affected.	2	3B
		The coating has flaked along the edges of the cuts partly or wholly in large ribbons, and/or it has flaked partly or wholly on different parts of the squares. A cross cut area greater than 15%, but not greater than 35%, is affected.	3	2B
		The coating has flaked along the edges of the cuts in large ribbons and/or some squares have detached partly or wholly. A cross cut area greater than 35%, but not greater than 65%, is affected.	4	1B
		Any degree of flaking that cannot be classified even by classification 4 or 1B	5	0B

Supplementary Figure 3-1: a) Adhesion test on the patterned hierarchical surface, demonstrating the 5B class b) Classification table Adapted from [204]

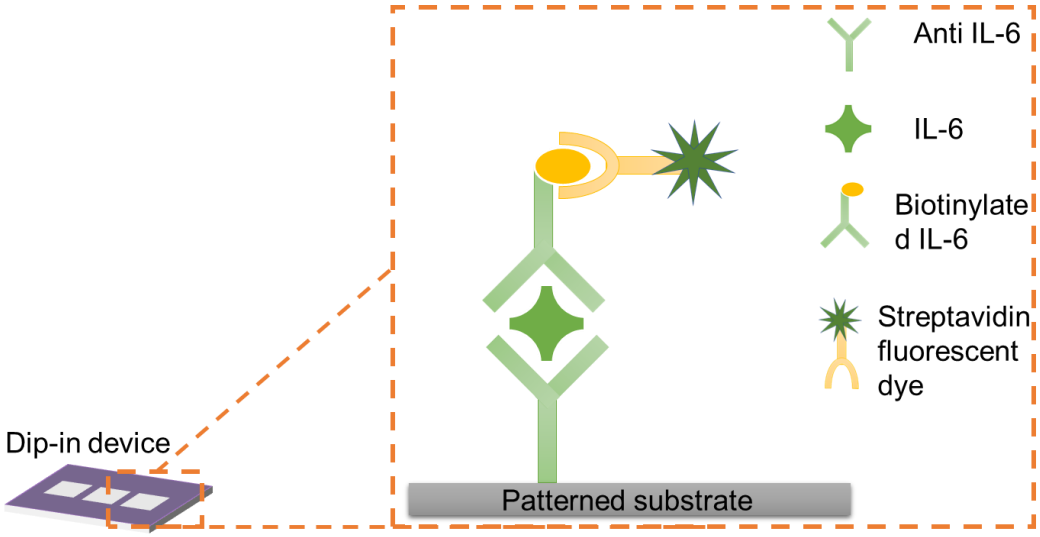

Supplementary Figure 3-2: IL-6 assay components.

Chapter 4 A Repellent Plastic Wrap With Built-In Hierarchical Structuring Prevents the Contamination of Surfaces with Coronaviruses

Preface:

In Chapter 3, we developed a scalable method for creating hierarchically structured surfaces with superhydrophobic and oleophobic properties, that displayed antifouling properties towards whole human blood. One significant drawback of this work was the PS substrate, which suffers from poor material properties. These drawbacks included the need for UVO treatment to assist in the formation of microscale wrinkles and the change in material properties becoming stiff and brittle after shrinking. To address these issues, work with Sara M. Imani was performed to translate this repellent platform to PO substrates, and characterize their bacterial repellency. Within this work, I contributed to the optimization of the repellent surface structure on the PO substrates and the characterization of the surface wettability, which can be found in Appendix A.

Continuing from this work, we hypothesized that the repellant surfaces, in addition to bacterial repellency, would demonstrate virus repellency.[54] To investigate this, a touch-based viral transmission assay was designed with PDMS stamps, to simulate the physical contact of a contaminated finger with a repellent surface (Objective III). This chapter furthers the work in the previous chapter (Objective I) by investigating the liquid repellent properties under dynamic wetting conditions and their durability after repeated physical contact, via CA and CAH measurements respectively. To thoroughly investigate this, the surfaces were tested for both the hydrophobic and oleophobic properties, as well as imaging of the surface to observe any physical damage after repeated physical contact.

Methodology:

Continuing from the work in the previous chapter, we made some modifications to the manufacturing of the repellent coatings by changing the polymer substrate and the type of nanoparticles used. The polystyrene substrates used in the previous chapter (chapter 3) became extremely glassy and stiff after shrinking at 145^{o}C, preventing their use as coatings. The new polyolefin substates used in this chapter remain flexible and compliant after shrinking allowing them to be easily wrapped around objects or surfaces. To reduce the cost of manufacturing, Silica nanoparticles were used instead of gold nanoparticles. The repellency of the developed surface was initially characterized through contact angle and contact angle hysteresis measurements of multiple liquids (water, glycerol, ethylene glycol and hexadecane) with different surface tension properties. Since the surfaces are designed to be used in high touch settings, their durability under repeated physical touches with human hands was extremely important. Therefore, their repellency was measured after a given number of touches or abrasion cycles. Durable surfaces showed sustained repellency, while fragile surfaces revealed a decrease in their liquid repellent properties. Next, viral adhesion was tested on the durable surfaces by simulating the physical contact of a contaminated human finger. PDMS stamps were selected as stamps due to their ability to hold moisture onto their surface, as extensively shown in microcontact printing studies of proteins. [205] Following the stamping of the surfaces with the viruses, the surfaces were washed and plated was conducted to quantify the transferred viruses. To examine whether repeated physical contact with contaminants would lead to increased surface contamination, the viral stamping assay was repeated and multiple touches were performed. Quantification of the transfer of pathogens to the

surfaces was performed using cell culture methods. The results were further validated using SEM imaging to visualize the viruses on different materials.

Authors: Roderick MacLachlan*, Fatemah Vahedi*, Sara M. Imani, Ali A. Ashkar, Tohid F. Didar and Leyla Soleymani

* Indicates equal contribution to the work

Publication: ACS Applied Materials an Interfaces 2022, 14, 9, 11068-11077

Publication Date: February 28, 2022

4.1 Abstract

Amidst the COVID19 pandemic, it is evident that viral spread is mediated through several different transmission pathways. Reduction of these transmission pathways is urgently needed to control the spread of viruses between infected and susceptible individuals. Herein we report the use of repellent plastic wraps (RepelWrap) with engineered surface structure at multiple lengthscales (nanoscale to microscale) as means of reducing the indirect contact transmission of viruses through fomites. To quantify viral repellency, we developed a touch-based viral quantification assay to mimic the interaction of a contaminated human touch with a surface through the modification of traditional viral quantification methods (viral plaque and TCID50 assays). These studies demonstrate that RepelWrap reduced contamination with an enveloped DNA virus as well as the *human coronavirus 229E* (HuCoV 229E) by more than 4 log 10 (>99.99%) compared to a standard commercially-available polyethylene plastic wrap. In addition, RepelWrap maintained its repellent properties after repeated 300 touches and did not show an

accumulation in viral titer after multiple contacts with contaminated surfaces while increases were seen on other commonly-used surfaces. These findings show the potential use of repellent surfaces in reducing viral contamination on surfaces, which could in turn reduce surface-based spread and transmission.

4.2 Introduction

The transfer of viral pathogens from host to a healthy individual is typically broken into three mutually non-exclusive modes of transmission: airborne, droplet, and contact transmission. Airborne and droplet modes of transmission are important for perspired droplets released by the host and are classified by an aerodynamic diameter (d_a) smaller than 100 µm.[5,206] This small size allows the droplets to stay suspended in the air and easily travel deep into the respiratory tract and interact with mucus membranes in the mouth and nose.[5] Alternatively, contact transmission occurs from either direct physical contact with infected individuals (*via* touch, sexual contact, oral secretions, and body lesions) or indirectly through contact with contaminated surfaces.[5] Surfaces may become contaminated through contact with other contaminated materials[206] or through the deposition of large respiratory droplets and the residual solid material from an evaporated droplet.[11,12] Droplets with a d_a > 100 µm settle quickly (<8 seconds)[13] from air onto surfaces and contribute greatly to surface contamination.[9] While the main transmission pathway of SARS-CoV-2 is through the contact of infected respiratory droplets with mucosal membranes[207], there is also a risk of viral transmission with contaminated hands.[207,208] Furthermore, high touch surfaces (keyboards, door handles, telephones and medical equipment) in hospital centers have shown significant contamination.[208]

Inanimate objects, that when contaminated, assist in the transfer of infectious materials to a new host are known as fomites, and play a key role in the spread and transmission of viruses and pathogenic infections *via* direct and indirect contact.[5,10] The indirect contamination pathway of viruses commonly occurs between fomites and hands (Figure 4-1a), and can effectively transfer up to 65% of the virus concentration from the fomite to uncontaminated hands.[10] Contaminated hands can then transfer the virus to the body through the mouth, nose, or eyes.[10,206] In addition to spreading the virus to a new host, fomites also increase the lifetime of viruses outside a host, contributing to increased overall viral transmission rates. Pathogens from the coronavirus family (SARS-CoV-2, Middle East Respiratory Syndrome (MERS) and Human Coronaviruses (HuCoV)) have been shown to remain infective for up to 9 days on common surface materials such as metal glass or plastic.[209] In particular, *human coronavirus 229E* (HuCoV-229E), in low titers (10^3 pfu/mL and 10^2 pfu/mL), stay active and infective for up to 5 days[210], and 4 days[211], respectively when deposited within organic matter/debris (human lung cell debris, in human faeces)[210,212], implying that contaminated organic matter/debris can increase the lifetime and survivability of a virus outside the host.

Engineered Surfaces that prevent or greatly reduce contamination when exposed to viruses show great promise in mitigating the spread of viruses *via* indirect contact transfer. Antiviral Coatings made from disinfectants (ethanol, glutaraldehyde, hydrogen peroxide, sodium hypochlorite)[213] or engineered materials (coper[214], zinc[215], silver[216], TiO_2[217], N,N-Dimethylhexadecylamine[218]) are commonly used to reduce the viral titer on high touch surfaces. These reagents and/or materials are either harmful to the surface (hydrogen peroxide)[219], to the individuals touching them (Peracetic acid)[220], or to the environment

(Sodium hypochlorite)[31,220], or present a delay, in the order of hours (>4h) between contamination and disinfection (TiO_2[221], copper[222]), leading to the spread of viruses during such long transition times.

An alternative rapid and safe way of halting surface-mediated transmission of viruses involves the use of liquid repellent surfaces (repelling high and low surface tension fluids) surfaces that reduce virus binding onto surfaces, the formation of fomites, and contamination of surfaces with potentially contaminated droplets. Two classes of liquid repellent surfaces, liquid-infused [40,179,223–225] and hierarchically-structured surfaces[51,52,54,226,227], have shown to significantly repel contaminating liquids while also preventing the adhesion of pathogens and formation of biofilms at the surface. Liquid infused surfaces integrate a lubricating liquid into a porous or rough surface using the chemical affinity that exists between the surface and the lubricant, causing contaminants to slide away from the surface, resulting in self-cleaning properties.[38] Lubricant infused surfaces significantly reduce the attachment and growth of bacteria and their biofilms by over 90% over the course of multiple days.[228,229] Introduction of antipathogenic materials, such as carvacrol and antibiotics, into the lubricant has also been utilized to reducing the transmissibility of bacteria (*Staphylococcus aureus* and *Pseudomonas aeruginosa*), fungi (*Bacillus subtilis*) and viruses (Zika Virus) by nearly 100%.[230,231] Lubricant infused surfaces have also displayed self-healing properties through the swelling of the surface structure in the presence of the lubricant,[232] however the number of healing cycles is limited by the amount of lubricant trapped in the surfaces. [230] Despite high performance in liquid[40,187] and pathogen[223,228,230,233] repellency, liquid infused surfaces are difficult to operate in open-air conditions due to the evaporation of the liquid layer and the limited

stability of such surfaces.[35] On the other hand, hierarchically-structured surfaces do not rely on liquid infusion and provide liquid repellent properties by reducing the apparent surface energy through the formation of unique wetting states by trapping air pockets within their surface structure (Cassie state).[119,234–236] This effect is enhanced through chemical modification with hydrocarbon and fluorocarbon chains,[101] improving repellency with low surfaces tension liquids[237] and resulting in liquid repellent properties.

Hierarchically-structured surfaces with an extremely high liquid repellency have demonstrated significant pathogen repellency[238]. Among these surfaces, a hierarchically-structured surface with diamond architecture, created through hot Filament chemical vapor deposition, reduced the adherence of *Pseudomonas aeruginosa* and *Escherichia Coli* on the surface by >90%.[52] Similar performance has also been achieved through the use of photoablation[226] and photolithographic techniques[51] to achieve >89% and 99% reduction in the adhesion of *E. coli* respectively. In addition bacterial repellency, reduced adhesion of adenoviruses HAdv4 (2.10 log) and Hadv7a (1.62 log) has also been demonstrated with superhydrophobic textiles modified with fluorinated polytetrafluoroethylene NPs.[227] While having high performance, many of these surfaces are fabricated using difficult-to-scale and expensive methods such as photolithography[51], chemical vapor deposition[52] or photoablation[226]. In response, we have developed a facile and scalable method, based on all-solution-processing and heat shrinking, to create hierarchically-structured surfaces on flexible substrates.[54,129] These surfaces decreased the formation of biofilms of pathogenic Gram negative (*P. aeruginosa*) and positive (Methicillin-Resistant Staph a*ureus* (MRSA)) bacteria by ~85%, and demonstrated a 20-fold decrease in bacterial (*E. coli*) adhesion.[54] These surfaces have also significant

repellency toward biological liquids (whole blood CA 144±2^{o} [54] and Fetal Bovine Serum CA 158.3±2.6^{o} [227]) which can mediate the transmission of pathogens.[10] Recent studies have also displayed superhydrophobic surfaces having significant reduction in viral contamination when interacting with virus laten droplets.[239,240] These surfaces can significantly reduce the contamination from air born droplet during sneezing or the interaction of the surface with bodily fluids.[239] However, these studies have only looked at the interaction of surfaces with the liquid phase and data is still missing on how liquid repellent surfaces interact under direct contact (ie surface to surface) transmission of viruses.

In this work, we evaluate a hierarchically-structured superhydrophobic flexible plastic that has been previously shown to repel low and high surface energy liquids and reduce the adhesion of bacteria and formation of biofilms[54,238] in its ability to reduce the adhesion of viruses. To model the transfer of viruses between surfaces, we developed a touch assay coupled with viral quantification to detect the presence of active viral particles transferred to surfaces with high sensitivity. To stablish the assay, we first used an enveloped virus, *Herpes Simplex Virus 2* (HSV-2) with a similar size as SARS-CoV-2, we then used Hu-Cov-229E, a coronavirus from the same family as SARS-CoV-2, to evaluate the viral repellency of the engineered surfaces. Our experiments demonstrate that such engineered surfaces, when placed on regular surfaces, can greatly reduce the level of viral contamination.

4.3 Methods

Reagents: (3-Aminopropyl)triethoxysilane (APTES, 99%), 1H,1H,2H,2H-Perfluorodecyltriethoxysilane (FS, 97%), and Ludox TMA colloidal silica were purchased from Sigma-Aldrich (Oakville, Ontario). Ethanol (anhydrous) was purchased from Green Field global (Mississauga, Ontario). Polydimethylsiloxane, elastomer and curing agent, were purchased from Ellsworth Adhesives (Stoney Creek, Ontario). Hydrochloric acid (36.5-38%) was purchased from Caledon (Georgetown, Ontario). Milli-Q grade water (18.2 MΩ) was used to prepare all solutions. HSV-2 Thymidine kinase- deficient (TK2/2) HSV-2 ATCC, Vero cell line Vero (ATCC® CCL-81™), Human coronavirus 229E (ATCC® VR-740™) were purchased from ATCC (Manassas, Virginia). Huh7.5 cells were kindly provided by Dr. Charles M. Rice (Rockefeller University, New York City, NY, USA)

Surface Fabrication: Polyolefin (PO) (Cryovac D-955) was cut into 15 mm discs and subsequently cleaned with ethanol and milli-Q water and dried with compressed air. The PO substrates were then exposed to air-plasma in an expanded plasma cleaner (Harrick Plasma) on HIGH RF power for 1 min. The surfaces were then immediately placed into a 10% aqueous APTES solution for 18 h. Following the deposition of APTES, the surfaces were rinsed with Milli-Q water and sonicated for 10 min in milli-Q water, and dried with compressed air. The silica nanoparticle (SiNP) solution was then prepared by mixing 1-part Ludox TMA colloidal silica with 2-parts milli-Q water and sonicated for 30 min, the diameter of the SiNP is 27nm. The substrates were then placed into the SiNP solution for 3 h followed by sonication in Milli-Q Water and dried with compressed air. The SiNP-modified surfaces were placed in the FS. The FS solution was prepared by mixing ethanol and Milli-Q water in a 3:1 ratio, followed by the addition of a catalytic amount of

hydrochloric acid (0.1%wt) into the solution with 0.5%wt of FS. This solution was heated at 40^{o} C for 1 hr before use. The surfaces were rinsed with ethanol followed by sonication in both ethanol and Milli-Q water for 10 min then dried with compressed air. These surfaces were then shrunk in an oven for 10 min at 145^{o} C.

Surface Physics Characterization: SEMs imaging was performed on a JEOL 70000F. Samples were coated with 5 nm of platinum before imaging. CA, CAH and SA measurements were taken on a KRUSS DSA30S Drop Shape Analyzer (Hamburg, Germany) with droplets of water (5 µL) and hexadecane (5 µL).

Durability to Physical Contact Test: CA and CAH were measured on RepelWrap with KRUSS DSA30S Drop Shape Analyzer (Hamburg, Germany) to characterize the wettability of the surfaces. PDMS stamps and human fingers were repeatedly brought into contact with the hierarchically structured surfaces for a given number of contacts (30 and 150 for the PDMS stamp and human finger, respectively). This process was then repeated several times for each surface.

PDMS Stamp Fabrication: Sylgard 184 silicone elastomer base and elastomer curing agent were mixed in a ratio of 10:1. Once fully mixed, the elastomer was cured overnight in an oven at 60 ^{o} C. The elastomer was then cut into their final shape, 1 cmx1 cm cubes, and sonicated in ethanol for 10 min followed by drying with compressed air.

Cell cultures: Human hepatoma cells, Huh7.5, were maintained in Dulbecco's modified Eagle medium (DMEM) supplemented with 10% heat-inactivated fetal bovine serum (FBS), (Life Technologies Inc.), 100 μg mL^{-1} penicillin, 100 mg mL^{-1} streptomycin (Sigma-Aldrich, Oakville, ON, Canada), 10 µM of 4-(2-hydroxyethyl)-1-

piperazineethanesulfonic acid (HEPES) (McMaster University) and 2 μM L-glutamine (L-glu) (Life Technologies Inc.). Experiments were performed with cells at passages 2–6. All cells were incubated at 37 °C in a humidified 5% CO_2 incubator.

Vero cells (ATCC) were cultured in Minimum Essential Medium Eagle- Alpha Modification (α-MEM) media supplemented with 5% FBS in addition to all the additives mentioned above for DMEM.

Virus Contact Transfer Assay: The Stamping surface was contaminated by pipetting 20 μL of DMEM + 10% FBS with a viral load of 1 x 10^5 pfu/mL, onto the stamp, this was then followed by placing a glass coverslip on the contaminated side of the stamp to evenly disperse the solution across the surfaces and left for 10 min. After removal of the glass slide, the stamps were left until the remaining excess solution was adsorbed or evaporated from the now contaminated surface. Before stamping, the high touch surface models were disinfected with 70% ethanol for 5 min and then dried with compressed air to ensure no contaminants were present on the surfaces. The virus-contaminated stamps were then placed, contaminated side down, onto the surfaces for 1 min with a 70g weight on their non-contaminated side. The stamp was then removed, and the surfaces were placed into a 12-well plate containing 400 μL DMEM 10%FBS. This solution was then used for titration.

HSV-2 Titration (Plaque assay): A Vero-cell plaque assay, previously described elsewhere[241], was used to quantify the virus concentration on the touch transferred surfaces.

huCov229e Titration (TCID50): Huh-7.5 Cells in a 96-well plate at a seeding density of $5x10^4$ cells per well were cultured in DMEM 10% FBS. The cells were then left in the incubator until 100% confluency was reached. The virus-containing solution was then serially diluted in DMEM and 0% FBS and 50 µl of each viral dilution was added to the corresponding well of confluent cells, starting at the highest dilution. The plate was left for 2 h in 37 °C, in a 5% CO_2 incubator and was shaken every 15 min. Then 150 μL of DMEM and 10% FBS solution was added to each well. The cells were incubated for 6 days and finally stained using crystal violet solution. The Reed and Muench method was used for the calculation of the virus titer.[242]

Viral Infectivity of Fluorosilane: FS solutions were made by adding 2 µl of DMSO to 30 µl of FS stock (30%). The solutions were diluted using a-MEM 0%. The FS surfaces were manufactured using the protocol discussed above. A 60 µL viral solution was added to the FS solutions. These were then incubated for 20 minutes before the virus concentration was quantified. In the surface assays, 6 µL of the viral solution was added to the surfaces and incubated for 20 minutes. These surfaces were then washed with cell media and viral concentration was quantified. The initial viral titer (HSV-2) of 10^6 pfu/ml was used for both the FS solutions and surfaces. This experiment was repeated two times and the results were consistent.

Scanning Electron Microscopy – Virus Fixation: The Hu-Cov-229E were stamped onto the polymer and metallic surfaces as described in the previous section. The stamped surfaces were then incubated in 4% Paraformaldehyde (PFA) (EM grade) in Phosphate Buffer Silane (PBS) to fix the viruses. Then surfaces were rinsed with Milli-Q water and

air-dried, and afterwards coated with 3 nm of platinum for imaging using a JEOL 70000F (JEOL, Peabody).

4.4 Results and Discussion

4.4.1 RepelWrap Fabrication and Quantification of Surface Repellency and Durability

The repellent plastic wrap (RepelWrap) was created by coating the surface of a shrinkable plastic wrap with an aminosilane linker (APTES) for binding the plastic to the NP layer; depositing a layer of SiNP as a stiff layer needed for wrinkle generation; and a adding a molecular layer of FS as the hydrophobic chemistry (Figure 4-1b). Following the coating of the plastic wrap with the desired materials, it was heat shrunk to form hierarchical micro/nanoscale wrinkles decorated with SiNP (Figure 4-1c, i).[54,82,83,129] The RepelWrap combines a unique physical structure, microscale wrinkles with SiNP building blocks, with chemical functionalization for achieving repellency.[54]

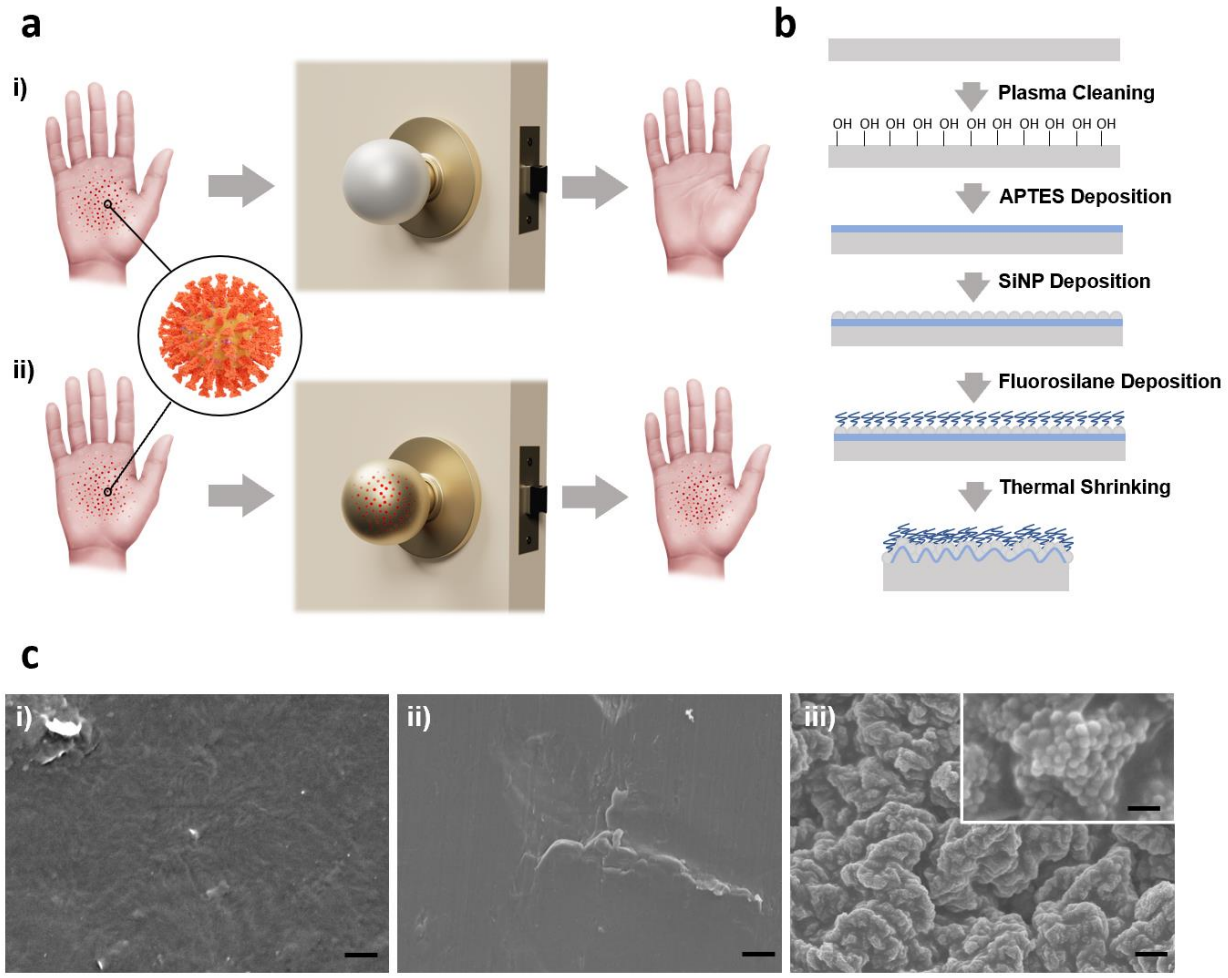

Figure 4-1: RepelWrap and its role in reducing viral transmission. (a) schematic illustration of person-to-person transfer of viruses through common (i) and RepelWrap-coated (ii) high touch surfaces. (b) Schematic diagram illustrating the manufacturing process of the RepelWrap (c) Scanning electron micrograph of i) polyethylene, ii) aluminum and iii) RepelWrap. The scale bars represent 1 µm. The inset provides a high magnification image of the surface with a scale bar of 100 nm.

To quantify the repellent properties of RepelWrap, we measured its static CA and CAH, and compared these metrics to other materials (polyethylene and aluminum) commonly used in high touch surfaces such as handles, railings, hand tools, and countertops. CA is a measure of the wettability of the surface and is used to assess the surface free energy,[243] whereas CAH measures the difference between advancing and receding CAs

and is used to assess the activation energy required for a droplet to slide on the surface.[244] RepelWrap showed superior hydrophobicity (water CA:153^{o} ± 3.6^{o}) compared to both polyethylene and aluminum (water CA:104^{o} ± 3.7^{o} and 94^{o} ± 1.8^{o} respectively, Figure 4-2a). The CA of the surfaces was also analyzed using hexadecane, glycerol and ethylene glycol to provide insight into different liquid surface interactions and to measure their level of wettability to the surface. Hexadecane in particular has a significantly lower surface tension than water (27.47 mN/m *vs.* 72 mN/m) and only interacts with itself and surfaces through dispersive forces, unlike water that interacts with surfaces through dipole-dipole interactions and hydrogen bonding.[245] These properties make hexadecane more efficient at wetting and contaminating surfaces, and make it suitable for quantifying the molecular interaction of dispersive forces at a surface. RepelWrap displayed superior performance in repelling hexadecane (hexadecane CA: 124^{o} +/- 1.6^{o}) compared to the control surfaces (hexadecane CA: polyethylene 35^{o} +/- 7.2^{o} and aluminum 10^{o} +/- 2.6^{o}). RepelWrap showed superior CA of 153.6^{o} ± 1.3^{o} for glycerol and 141.6^{o} ± 2.7^{o} for ethylene glycol, compared to the control surfaces of aluminum (glycerol CA: 42.0^{o} ± 1.9^{o} and ethylene glycol CA: 24.8^{o} ± 1.3^{o}) and polyethylene (glycerol CA: 92.9^{o} ± 3.6^{o} and ethylene glycol CA: 83.2^{o} ± 3.7^{o}). Additionally, RepelWrap exhibited much lower CAH with various liquids in comparison to the control surfaces (Figure 4-2a). A SA of < 5^{o} (5 µL) was also seen on the RepelWrap for both water and glycerol; however sliding was not observed with ethylene glycol and hexadecane due to pinning of the liquid droplets into the surface structure. SA is a measure of droplet mobility[98] and strongly correlates with CAH, with low SA being strongly correlated to repellency.[113] The strong repellency of all the test liquids (all CA > 90^{o} and CAH < 20^{o})[246] observed here are the result of the formation of Cassie-

Baxter wetting states on the micro and nanoscale features of the surface (Figure 4-1c i),[119] which are not present on the planar surfaces of polyethylene and aluminum (Figure 4-1c ii, iii).[54] In order to confirm that all solutions were in the Cassie-Baxter wetting state on the surface of the RepelWrap, the fractional wetting of the surface was calculated for both water (0.122) and hexadecane (0.299). Values of fractional wetting smaller than one, as observed here, represent Cassie-Baxter wetting.[247,248] Furthermore, modulation of the SiNP size (27 nm, 100 nm and 200 nm diameter) was used to tune the scale of the micro and nano-structures (Supplementary Figure 4-3). Comparison of the three surfaces showed that the increase in scale results in a decrease in the CA (Supplementary Figure 4-3d) and an increase in the CAH (Supplementary Figure 4-3e) for all probing liquids. This ability to control the wettability for all probing liquids also allows for the easy tunability of the surfaces wetting for relevant applications. Furthermore, it was previously determined that a significant portion of the hexadecane performance was due to the presence of fluorine groups (FS) on the surface, making the combination of the physical structure and the chemical modification essential for repellency.[54]

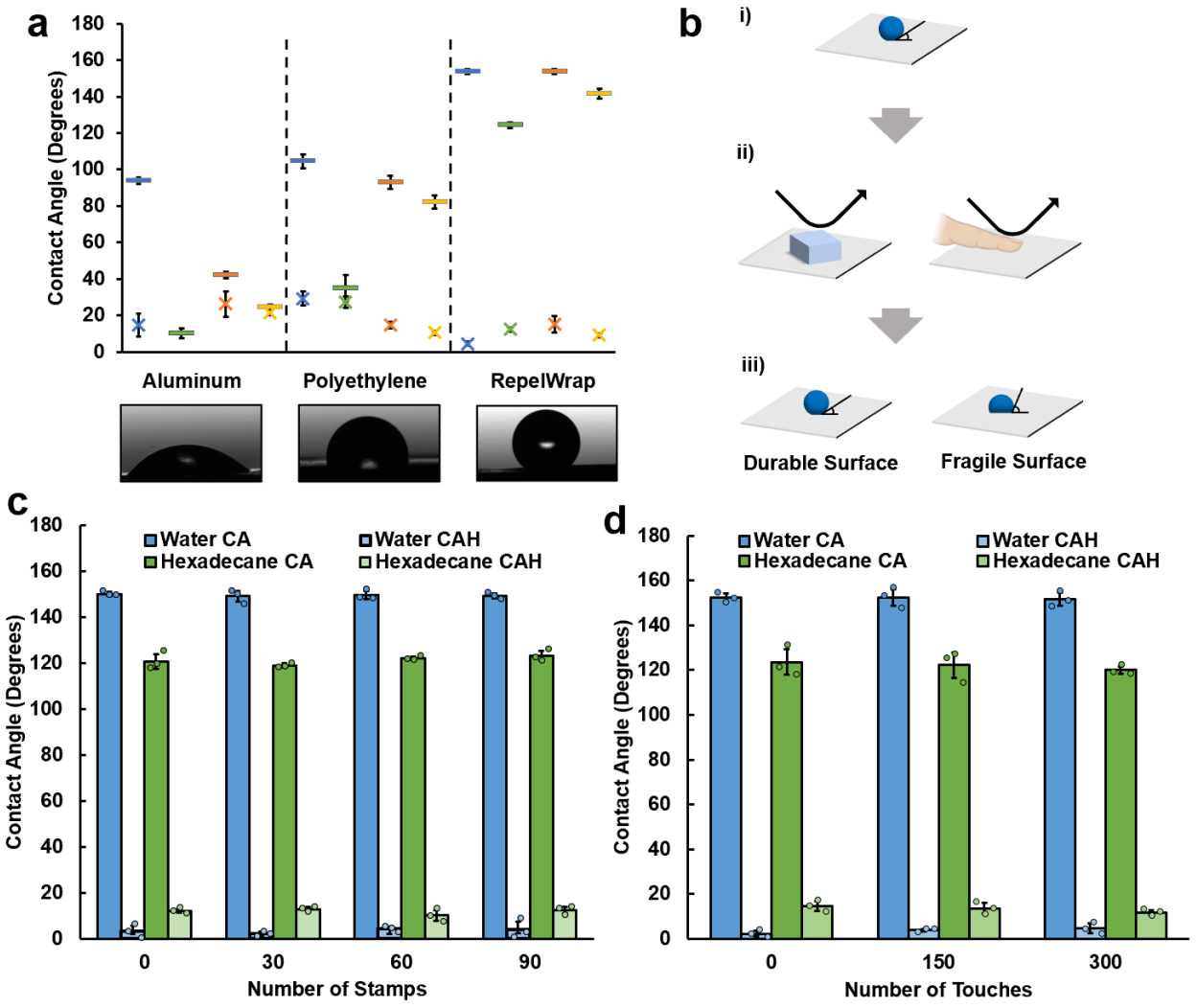

Figure 4-2: Evaluation of surface repellency and durability. (a) Graph displaying the contact angle (bars) and contact angle hysteresis (cross) of different surfaces with water (blue), hexadecane (green), glycerol (orange), and ethylene glycol (yellow). Images of water CA are inserted blow. (b) Schematic representation of the stability testing experiments where the contact angle of a newly fabricated surface was evaluated (i), the surface was physically contacted using an elastomeric stamp or a human finger (ii), and the physical characteristics of the surface were re-evaluated (iii). (c) Graph demonstrating the change in contact angle and contact angle hysteresis of water and hexadecane after repeated contact with an elastomeric stamp. (d) Graph demonstrating the change in contact angle and contact angle hysteresis of water and hexadecane after repeated touches with a human finger. All error bars represent the standard deviation from the mean.

To determine the stability and resiliency of RepelWrap, we re-evaluated the repellent properties of the surfaces before and after repeated contact with both elastomeric stamps and a human finger (Figure 4-2c, 4-2d). For the elastomeric stamp experiments, the water CA of the surfaces was measured every 30 stamps, each with a duration of 10 s and force of 699 ±1 mN, up to a total 90 stamps. There was no measurable change in the hydrophobicity (~150^o CA and >5^o CAH) and oleophobicity (~120^o CA and > 15^o CAH for Hexadecane) of the surfaces upon repeated stamping demonstrating the robustness of RepelWrap (Figure 4-2c). For the finger touch experiment, the surfaces were pressed with a force of 10793 ±1213 mN for roughly 1s, with a time delay of 1-2 s between the touches. The CA was measured after every 150 touches, and no significant change in repellency of water (~150^o CA and >5^o CAH) or hexadecane (~120^o CA and > 15^o CAH) was observed for the maximum number of touches that was assessed (Figure 4-2d), further demonstrating the resiliency of the surfaces against frequent usage on high touch surfaces (Figure 4-2b). The shear stability of the surface was also quantified to better understand how forces parallel to the surface will impact the wettability. After shearing of the surface with 200g and 500g weights no significant change was seen in the wettability of the surface, however after shearing with 1000g weight there was a significant decrease in the CA (by 20^o ± 2.5^o and 36.4^o ± 15.7^o) and increase in the CAH (by 27.4^o ± 7.1^o and 15.7^o ± 8.8^o) for both water and hexadecane respectively. From Supplementary Figure 4-5 it is also clear that the effects of shearing have a greater effect on the wetting of hexadecane, as greater variation in the CA measurement was observed for all shear cases compared to the control. The sustained CA (>150^o) and SA (<10^o) of water have been well reported for hierarchical wrinkled structures for various deformations

(stretching, bending and torsion) as well as abrasion and compression of the surface.[88,89] We have also previously shown that it is possible to cover objects with different form factors using the shrinking process involved in the fabrication of RepelWrap.[54] The surface structure after both repeated stamping and touching with a finger was also investigated using SEM (Supplementary Figure 4-3). These images show slight damage/crushing on the peak of the hierarchical wrinkle structure, however the internal deeper re-entrant structure of the wrinkles, which is mainly responsible for the formation and stability of Cassie-Baxter wetting states,[119] remains intact. Similar structural damage to hierarchical wrinkled microstructures have been observed in the past, which was paralleled with a decrease in the water CA from 160^{o} to 147^{o}.[89]

4.4.2 Evaluation of RepelWrap in reducing viral contamination using an enveloped virus (HSV-2) as a model

Once it was determined that the RepelWrap remains repellent following frequent touching, as is the case with high touch surfaces, we sought to determine whether the liquid repellent properties of the RepelWrap (high CA with various liquids and low SA)[54] can be translated to viral repellency (Figure 4-3). For this purpose, viral quantification was performed for HSV-2 (diameter of ~125 nm).[249] This pathogen was chosen because it contained a phospholipid envelope and had a similar size as SARS-CoV-2 (diameter of 60-140 nm)[250], allowing it to be used as a surrogate model to evaluate the potential applicability of RepelWrap against the spread of COVID-19. The assay was performed by first contaminating an elastomeric stamp with a solution of Dulbecco's Minimum Eagle Medium (DMEM) containing the virus (1.33×10^5 pfu/mL), then stamping the surfaces with

the stamp to mimic contamination with the human touch, and finally incubating the contaminated surface with cell growth media used in the viral quantification assay (Figure 3a). It is important to note that DMEM has a similar viscosity (0.94 cP) and CA (152.3^{o} ± 3^{o}) on RepelWrap as water, while the CAH of DMEM differs significantly from water (35^{o} ± 5^{o}). This indicates that interactions between DMEM droplets on contaminated surfaces should have slightly higher wetting and attractive properties compared to water droplets during contact transmission of viruses. The virus titer present in the media was quantified using the vero-cell plaque assay (Figure 4-3b), in which the number of developed viral plaques were counted for different serial dilution factors (10-fold) and used to calculate the viral titer. The potential antiviral properties of the FS molecule and surface coating was also investigated (in solution and on planar surfaces) to ensure that the reduced surface contamination of viruses was due to the repellent properties of the hierarchical wrinkled structure. These control experiments demonstrated no measurable decreases in the viral titer in the presence of FS indicating the importance of the hierarchical structuring of RepelWrap in viral repellency (Supplementary Figure 4-1). It is evident from the abovementioned assay that RepelWrap is far less susceptible to becoming contaminated after contact, showing more than 4 logs reduction in HSV-2 titer compared to aluminum and polyethylene (Figure 4-3b).

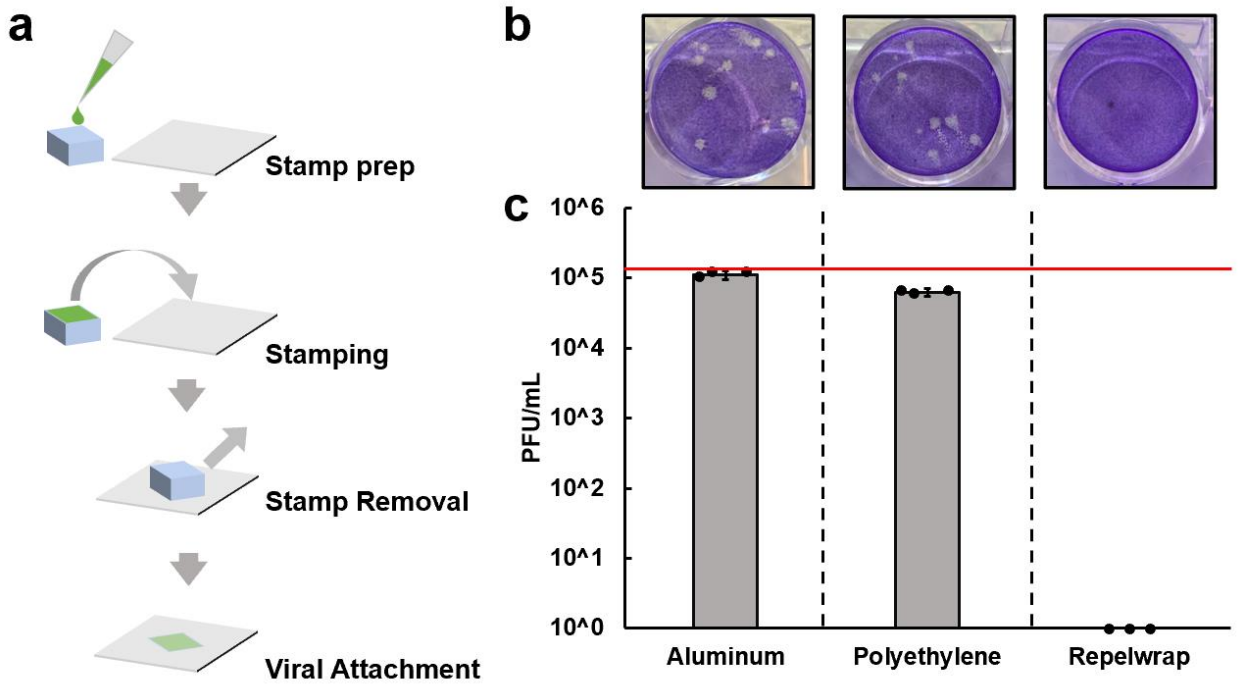

Figure 4-3: Evaluation of the viral titer of RepelWrap after exposure to stamps contaminated with HSV-2. (a) schematic showing the stamp-based surface contamination assay (b) image showing the plaque assay performed on the three surfaces (c) Quantification of viral load on different surfaces after contamination using the stamping technique depicted in (a), the red line represents the concentration of viruses deposited onto the stamp prior to contact with the surface.

4.4.3 RepelWrap significantly reduces contamination with coronaviruses

Given the remarkable ability of RepelWrap in reducing contamination with HSV-2, we sought to answer whether it would also be possible to reduce contamination caused by HuCoV-229E (diameter of 80-120 nm)[251], a coronavirus from the same family as SARS-CoV-2, which is responsible for the COVID-19 pandemic. As such, the abovementioned stamping assay was used to contaminate RepelWrap and control surfaces with HuCoV-229E, and the viral titer transferred to the surfaces was quantified using an endpoint dilution assay in which the serial dilution at which 50% cell lysis occurred was used to calculate the initial viral titre, *via* the Reed-Muench method.[242] Similar to the HSV-2

experiment, RepelWrap reduced the viral titer by 4-logs compared to aluminum and polyethylene, confirming its high performance in repelling viruses. To further analyse the ability of the RepelWrap in reducing contamination on high touch surfaces, a multi-touch version of the assay was performed using HuCov-229E, in which the surfaces were stamped three consecutive times (each with a viral titer of $9.80x10^5$ TCID50/mL) with 1 min intervals between stampings. The comparison of the single- and multi-touch experiments shows a 0.33- and 0.16-log increase in contamination on the polyethylene and aluminum (Figure 4-4a), respectively, after the two additional touches. Remarkably repeated contact with a contaminated surface causes no increase in the viral titer measured on the RepelWrap. This, in conjunction with the maintained liquid repellency (~150^o) after repeated physical contact (Figure 4-2c, 4-2d), show that the repellent properties sustain after repeated exposure to both contamination and mechanical strain.

The ability of RepelWrap in repelling contamination is further confirmed using electron microscopy (Figure 4-4b). Scanning electron microscopy show clusters of viruses adhered to both polyethylene and aluminum; however, no visible contamination is observed across the RepelWrap (Figure 4-4b). To further confirm that the contamination seen in Figure 4b is in fact the viral particles (and not crystalized culture solution), control surfaces were contaminated with culture solution with and without the virus (Supplementary Figure 4-4). Unlike the virus contaminated surfaces, the particles of crystallized culture media on the control surface were much more sparsely distributed across the surface and much larger in diameter (500 nm – 5 µm) then the viral particles (diameter ~100 nm) seen in Figure 4-4b. These findings are in strong agreement with the

viral quantification assay and highlight the superior performance of RepelWrap for repelling viruses when coming in contact with fomites.

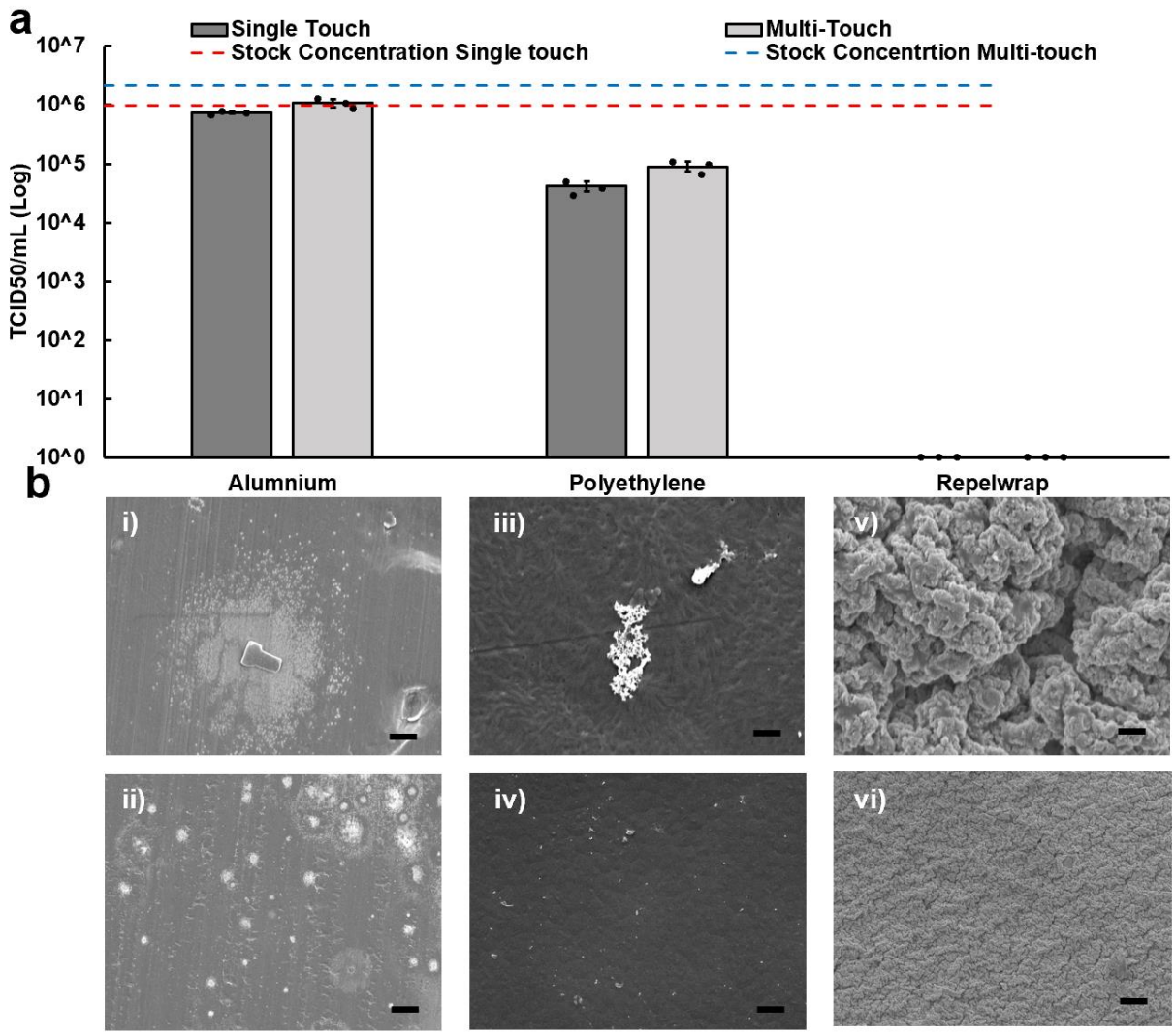

Figure 4-4: Evaluation of the viral titer of RepelWrap after exposure to stamps contaminated with HuCoV-229E (a) The amount of viral titer measured on surfaces after contact with stamps contaminated with HuCov-229E. The red and blue line shows the total concentration of viral samples deposited on the stamp before contact with the surface. (b) SEMs of aluminum (i, ii), polyethylene (iii, iv) and RepelWrap (v, vi) after contact with contaminated HuCov-229E stamps. The scale bars represent 1 µm (i, iii, v) and 10 µm (ii, iv, vi).

4.5 Conclusion

In this work, a contact transfer viral quantification assay was developed to investigate the interaction of viruses with RepelWrap, a highly repellent hierarchically structured surface. The quantification of the viral contamination was conducted with both DNA (HSV) and RNA (HuCov-229E) viruses. RepelWrap repelled various liquids (water CA 153º and Hexadecane CA 124º) and maintained its repellent properties after repeated physical contact with both elastomeric stamps and a human finger. When brought into physical contact with stamps contaminated with viruses, RepelWrap showed little to no contamination with HSV-2 or HuCov-229E, while other materials commonly used in high touch surfaces (aluminum and polyethylene) showed significant contamination. These repellent properties were retained after repeated contact with contaminated stamps, whereas the common surfaces displayed an increase in the amount of contamination.

We attribute the virus repellency of RepelWrap to the reduced interaction of virus-containing water droplets with the surface, reduced interaction of viral capsid proteins and biomolecules with the surface, or a combination of both.[252,253] It is possible that moisture mediates the suspension and transfer of viral particles to high touch surfaces;[254] as such, superhydrophobic surfaces that are highly effective in repelling water are less likely to get contaminated. Alternatively, reduced interaction/adsorption of viral capsid proteins in the presence of super-hydrophobic wetting states could reduce the adhesion of viruses from stamps to RepelWrap.[227] Similar mechanisms have also been used to explain the reduced formation of biofilms[54] and blood clots[238] on hydrophobic given that protein adsorption is the first step in these processes.[253] The adsorption of proteins to a surface is strongly related to the chemical properties, surface charge, surface structure, and the

hydrophilicity/hydrophobicity of the surface, the most significant of these effects are the long-range electrostatic interactions and hydrophobic effect,[255] and as such the unique properties of the RepelWrap could attribute to reduce protein adhesion.[113,252,253] More research is needed to better understand the exact mechanisms at play for the interaction of viruses with these class of surfaces. Better understanding of these interactions may also help to develop new classes of surfaces for preventing the spread and survivability of pathogens on surfaces.[227,256]

4.6 Acknowledgments

This work was supported by Natural Sciences and Engineering Research Council of Canada, Ontario Early Researcher Awards, IDEaS Grant from the Department of National Defence, and McMaster COVID-19 funding. The electron microscopy was carried out at the Canadian Center for Electron Microscopy (CCEM), a national facility supported by the NSERC and McMaster University. R.M. was the recipient of the Ontario Graduate Scholarship. L.S. is Tier II Canada Research Chair in Miniaturized Biomedical Devices.

4.7 Supplementary Information

4.7.1 Inactivation of viruses from Fluorosilane

The infectivity of the FS molecule and surface coating was also investigated (in solution and on planar surfaces) to ensure that the reduced surface contamination of viruses was due to the repellent properties of the hierarchical wrinkled structure. These control experiments demonstrated no measurable decreases in the viral titer in the presence of

FS indicating the importance of the hierarchical structuring of RepelWrap in viral repellency (Figure S1). No difference between the samples (Figure S1), all conditions look similar so no inhibitory effect by FS in HSV-2 infection in cell culture for both FS solutions and modified surfaces. This experiment was repeated two times and the results were consistent.

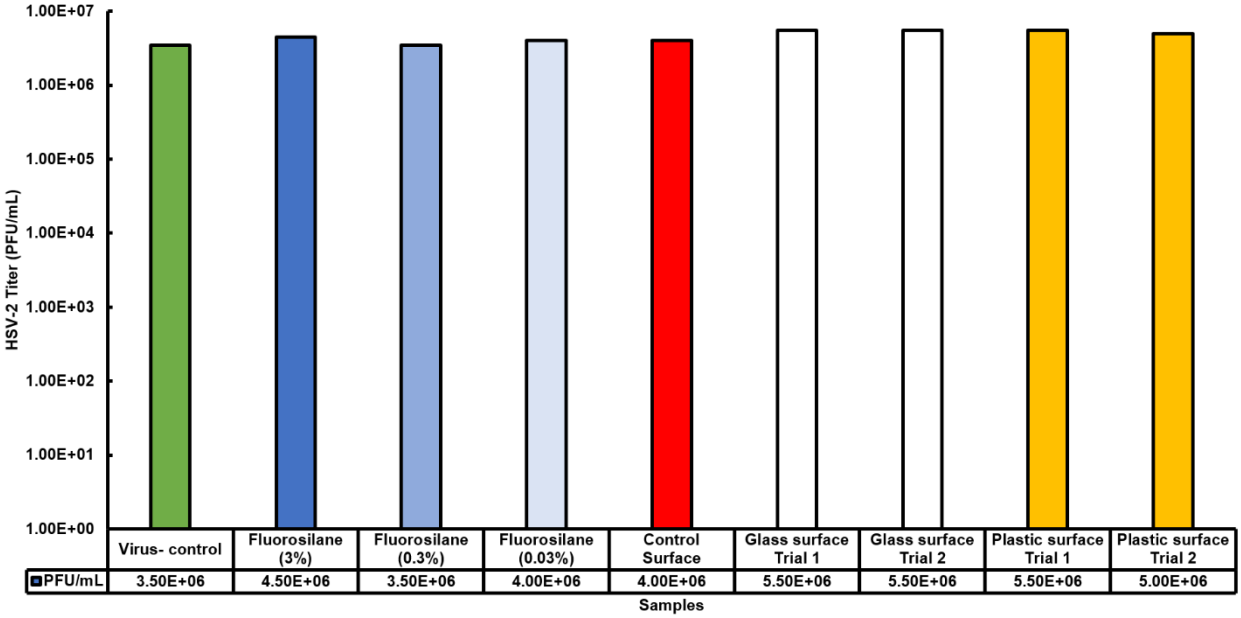

Supplementary Figure 4-1: Effect of fluorosilane on HSV-2 proliferation. Various concentrations (3%, 0.3%, 0.03%) of fluorosilane solution (blue) and different surfaces(unmodified glass (red), fluorosilane modified glass (white) and fluorosilane modified polyethylene (yellow)) after incubation with 6µL of 10^6 pfu/mL virus solution for 20min.

4.7.2 Partial wetting of surface structure with different liquids

The following process was used to determine whether the RepelWrap is in a Cassie-Baxter wetting state while wetting with hexadecane. The wetting of a surface under Cassie-Baxter wetting state is governed by the following equation[257]:

$$\cos(\theta_{CB}) = \varphi_s(1 + \cos(\theta_Y)) - 1 \text{ (Equation 4.1)}$$

Where θ_{CB}, θ_Y and φ_s are the Cassie-Baxter CA, the Young CA and the fractional wetting of the surface. Rearranging, we get the following equation for the fractional wetting of the surfaces for a given liquid[247]:

$$\varphi_s = \frac{(1+\cos(\theta_{CB}))}{(1+\cos(\theta_Y))} \text{ (Equation 4.2)}$$

For a surface sustaining Cassie Baxter wetting state, the fractional wetting will be $0 < \varphi_s < 1$. Values closer to 0 will represent a smaller amount of wetted surface area while values closer to 1 will represent a higher amount of wetted surface area. Values of $\varphi_s \geq 1$would represent more than 100% surface wetting and are not modeled by Cassie Baxter Wetting. In this case, other models such as Wenzel wetting should be used to analyze surface wettability of rough surfaces. [52,247] Since the surface of the SiNPs is coated in a FS monolayer, the CA found for water and hexadecane of planar FS PO surface from previous work (96 ^{o} ± 3.8^{o} for water and 62^{o} ± 2.4^{o} for hexadecane)[238] represents the Young CA of the RepelWrap surface. The values of θ_{CB} found in Figure 3-2a result in the fractional wetting (φ_s) for water and hexadecane of 0.122 and 0.299 respectively.

4.7.3 Tunable Wetting with change in nanoparticle size

To tune the surface structure of RepelWrap, we varied the diameter (27 nm, 100 nm and 200 nm) of its SiNP building blocks. The formation of wrinkled microstructures is governed by the following equation.

$$\lambda = \frac{\pi\, t_f}{\sqrt{\varepsilon_c}} \text{ (Equation 4.3)}$$

In which λ, ε_c and t_f are the wavelength of the wrinkle structure, the critical strain of the system and thickness of the thin film, respectively. Considering this equation, we

hypothesized that an increase in the NP size would increase the thickness of the buckling thin film, which would in turn increase the wavelength and amplitude of the wrinkled microstructure. Such predicted change in surface morphology is evident in the SEM images obtained from surfaces created from SiNPs of various diameters (Supplementary Figure 4-3a, 4-3b, 4-3c)). The increased wrinkle size in conjunction with the larger size of NPs increases the overall feature sizes observed on the hierarchical structures, which in turn reduces the CA of surfaces built using larger SiNPs (Supplementary Figure 4-3d). Further wetting analysis also showed an increase in the CAH of the larger structured surfaces (Supplementary Figure 4-3e), which reduced the repellency of the surfaces created using larger SiNPs.

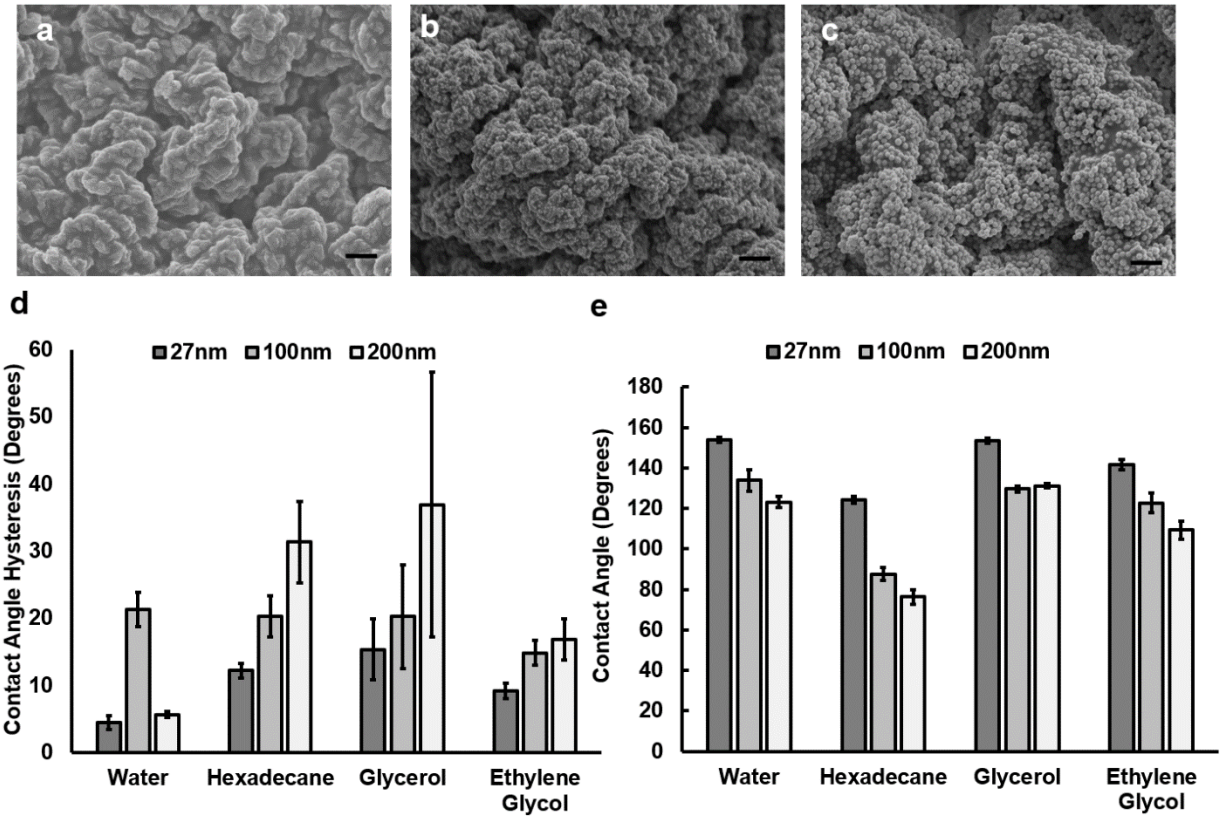

Supplementary Figure 4-2: SEM images of RepelWrap surfaces created from nanoparticles having diameters of a) 27 nm, b) 100 nm and c) 200 nm. Scale bar represents 1 µm. (d), (e)Wettability analysis of RepelWrap surfaces created from nanoparticles in (a)-(c).

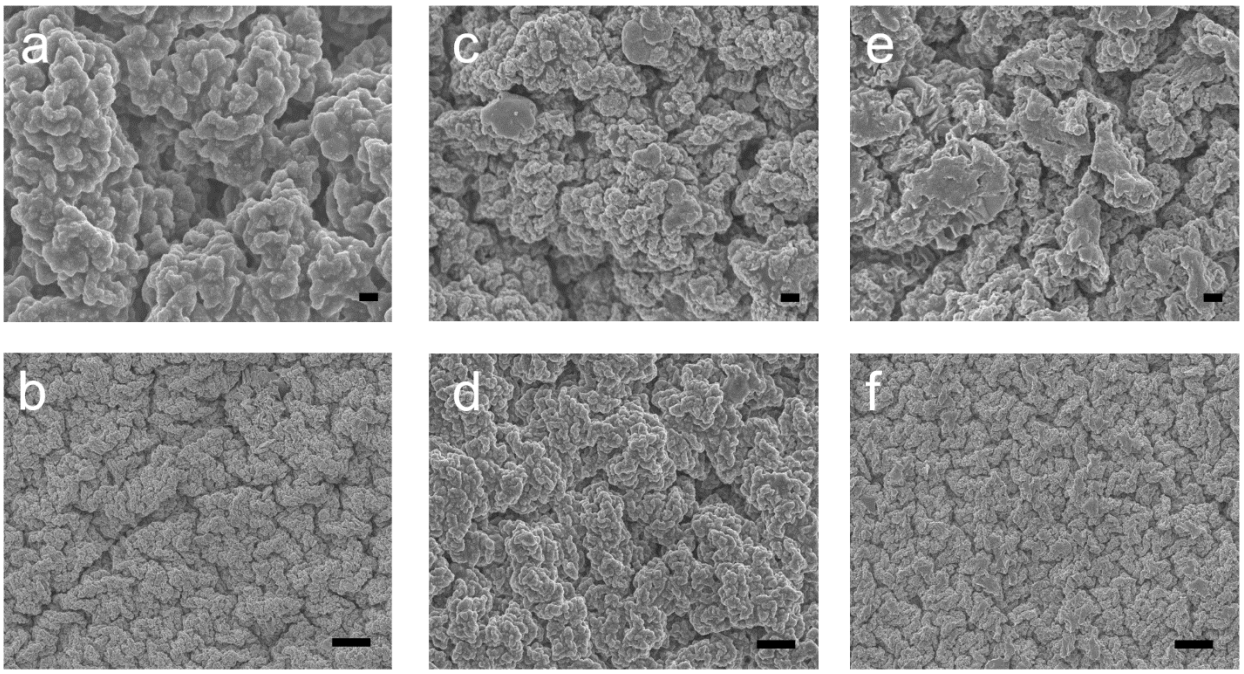

Supplementary Figure 4-3: Surface structure before (a,b) and after repeated stamping (c,d) and repeated touching with a finger (e,f) for 90 and 300 times respectively. The scale represents 1 µm (a,c,e) and 10 µm (b,d,f)

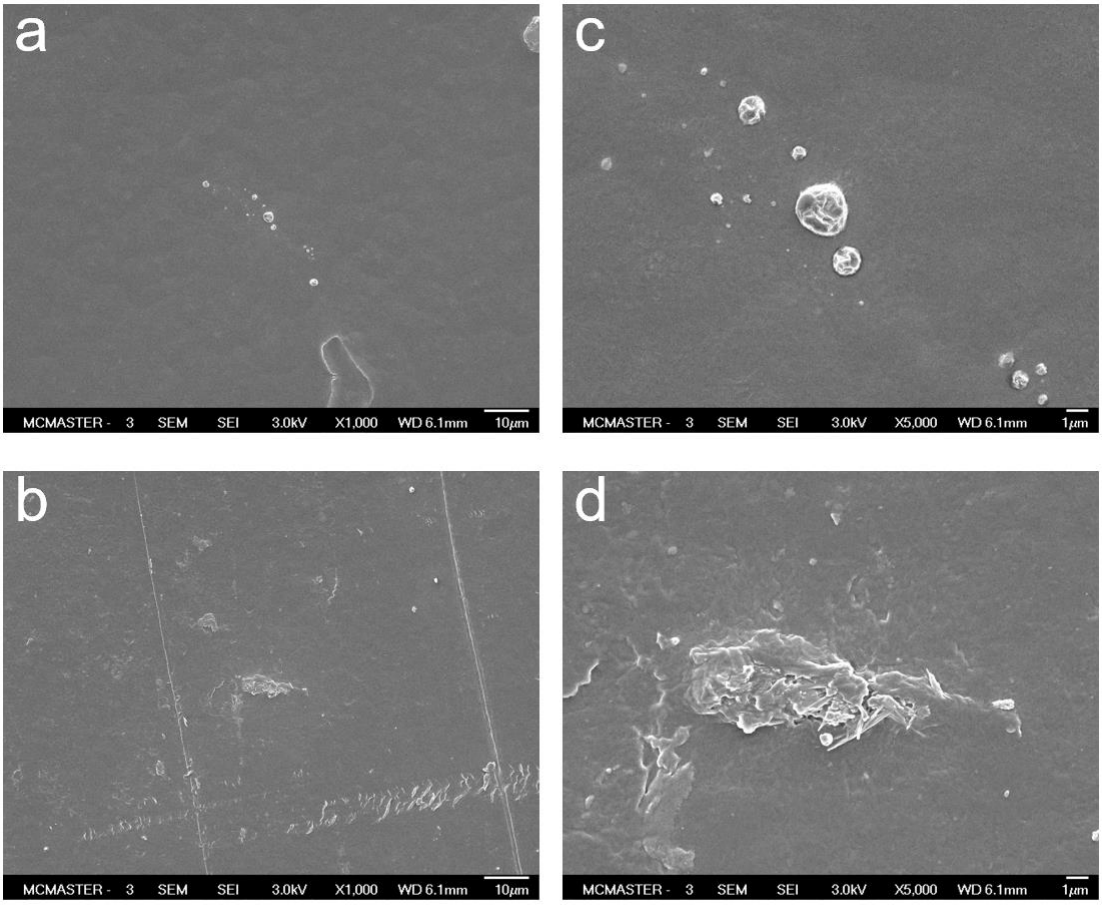

Supplementary Figure 4-4: Polyethylene Surface after stamping with culture media at two separate locations demonstrating debris (a,c) and surface defects (b,d).

4.7.4 Surface Durability to shearing

To measure the durability of the surface to sheering, the CA and CAH of water and hexadecane was measured before and after various masses were dragged across the surface.[89,258,259] The bottom of all weights was wrapped in a nitril glove such as to replicate the surface texture seen in the finger touch durability assay (Figure 3-2d). Each mass was dragged over each surface five times before the CA and CAH were measured (Supplementary Figure 4-5).

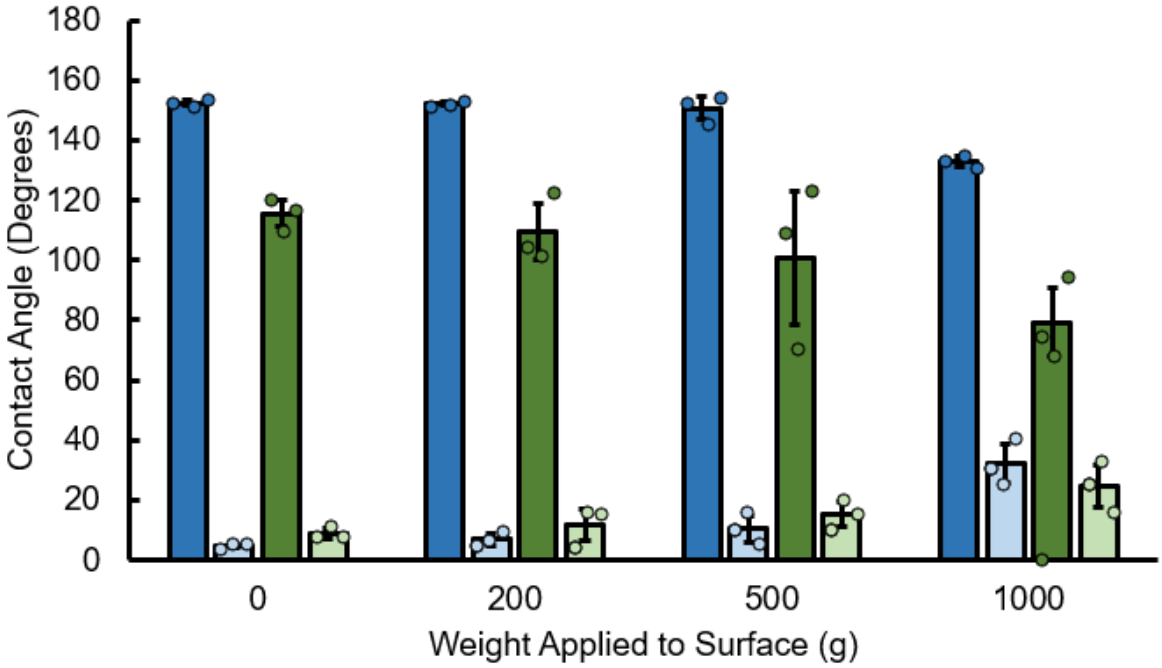

Supplementary Figure 4-5: Contact angle after surface sheering with different weights

Chapter 5 A Super-Omniphobic and Photoactive Surface Presents Antimicrobial Properties by Repelling and Killing Pathogens

Preface:

In chapter 4, we characterized the ability of the repellent surface to prevent the adhesion of viral pathogens, and their durability to a large number of repeated touches. In this chapter, we focus on creating a dual-functional material capable of both repelling (Objective III) and killing bacterial contaminates which adhere to the surface (Objective IV). A deeper investigation into the adhesion of bacterial pathogens was done with multiple pathogenic bacteria strains (*E. coli*, *B. subtilis*, *P. aeruginosa* and MRSA), both individually and in conjunction. Photoactive TiO_2 was integrated into the hierarchically structured repellent to enable the dual-functionality properties. The photoactive antimicrobial properties of the repellant surfaces were tested with and without light exposure. The performance of the dual-functional properties was additionally characterized under biofouling conditions with bacteria latent fecal matter, showing sustained pathogen repellency and antimicrobial effects. We also developed a more rapid manufacturing method than those used in the previous chapters (Objective I) in order to make the process more amenable to commercialization and large volume processing.

Methodology:

The aim of this chapter is to integrate photoactive materials into the surface structure of the omniphobic coating, enabling the surface to both repel pathogens as well as photoactively decontaminate the surface. An additional motivation behind modifying the repellent surfaces with photoactive materials was to improve manufacturing as photoactive metal oxides have different linking chemistry than that of the previous

nanomaterial's materials used. The methods discussed in the previous chapter, while easily scalable, require very long incubation times to properly coat the polymer substrate. Dip-coating the surfaces with TiO_2 nanoparticles was the method of choice, bringing down the manufacturing time of the hierarchical structures from roughly 24 hours to under 20 minutes.

To examine the transmission of bacteria on the surfaces, a similar stamping assay was conducted to the one described in the previous chapter (chapter 2), however an agar (3%) stamp was used instead of PDMS. The hydrophilic and hydrogel nature of agar stamps allowed for better absorption of the pathogens on their surface, resulting in the transfer of relatively equal amounts of contamination between the surfaces. After contamination of the surfaces, they were washed in phosphate buffer solution and 10-fold serial dilutions were performed. The dilutions were then plated using the tear drop method, allowing simultaneous plating and quantification of the number of colonies in the solution. To quantify the transfer on the different substrates, the number of bacteria cultured was compared directly to the number of bacteria deposited on the stamp before contamination. The latter method was then employed for the UV exposure assay, wherin surfaces were exposed to UV light for different lengths of time, after stamping and before washing of the substrates. Different types of bacterial species with varying cellular structures (Gram-positive or Gram-negative) and cell shapes (rod or spherical) were investigated. Furthermore, the testing of mixed cocktails of bacteria was also performed, as contaminated surfaces often have more the one pathogen present on their surface. It was also found that the fecal samples used also contained multiple different strains of bacteria.

Due to the extremely high liquid repellent properties of the superomniphobic surfaces, the measurement of the contact angle and contact angle hysteresis was quite challenging, as droplets would often roll off the surface before a measurement could be taken. One challenge in the photoactivity assays was the drying up of the transmitted bacteria on the surface, which increased the variances in the results, specifically on the control substrates. To solve this issue, the surfaces were incubated in phosphate buffer solution, in light and dark conditions, which led to more consistent and less variable results. Overall, the assays performed to test the transmittance and photoactive deactivation of pathogens validated the surfaces' strong ability to both repel and kill pathogens.

Authors: Roderick MacLachlan, Farhaan Kanji, Sadman Sakib, Shadman Kahn, Cedric Pattyn, Tohid F. Didar and Leyla Soleymani

Publication: To be submitted in 2023

5.1 Abstract

Nosocomial (healthcare acquired) infections place significant burdens on both the cost associated with and quality of patient care in hospitals. Reducing the spread and prevalence of these infections is achievable by reducing the number of contaminated surfaces within healthcare environments. Herein we report a dual functional surface, with photoactive TiO_2 integrated into the repellant hierarchical structures (OmniKill). To quantify the pathogen repellent properties of the OmniKill wrap, we developed a touch-based assay, capable of simulating the transfer of individual pathogens, multiple pathogens and pathogen laten fecal matter from hands to environmental surfaces. These

films were capable of repelling significant amounts of bacterial pathogens, 2.77-log (99.8%) reduction in transmission for all tested strains (*E. coli*, *B. subtilis*, *P. aeruginosa* and MRSA). As a result of the photoactive material in the surface structure the omniphobic coating was capable of further reducing the viability of pathogens on the surface showing a 2.43-log (99.6%) reduction in viable bacteria on the surface after 1 hour of light exposure. In addition, we also showed that these anti pathogenic effects (both repellence and deactivation of pathogens) were not affected by more complex biological contaminates such as feces. These findings show the potential use of dual functional material in reducing the physical transmission of bacterial pathogens in healthcare setting.

5.2 Introduction

Contamination of surfaces with pathogens plays a significant role in the transmission of infectious diseases, accounting for a significant amount of nosocomial infections worldwide.[20,141,260] Surfaces within our environment may become contaminated through a variety of pathways: deposition of respiratory droplets,[230] direct physical contact with contaminating secretions or biological materials,[261,262] and direct physical contact with other contaminated inanimate materials,[260] after which physical contact may result in the transmission of the contaminating pathogens to uninfected hosts/individuals. Disinfection and hygiene protocols are commonly used in healthcare environments to reduce the risk of surface-mediated pathogen transmission.[20] However, surfaces cleaned with traditional disinfectants are only able to remain sterile for a short period after cleaning and are vulnerable to recontamination.[20] Additionally, hygiene may be

ineffective when materials are heavily contaminated,[64] especially if the minimum infective dose for a specific pathogen is low.[263] As a result, antipathogenic coatings and materials have gain much attention over the past decade as a viable solution to address surface contamination.

Antipathogenic coatings can typically be broken down into biocide-releasing, contact-killing, or pathogen-repelling coatings.[62,65] Although purely antipathogenic (biocide-releasing or contact-killing) properties can significantly reduce the concentrations of infectious pathogens on surfaces, it is well established that they suffer from the depletion of antipathogenic agents,[62] buildup of dead pathogens and biological debris ,[62] and the development antimicrobial resistance.[141] These factors result in the buildup of viable pathogens on surfaces, which can later be transmitted though physical contact.

An alternative to solely antipathogenic coatings is pathogen-repellant materials, which inhibit the adhesion of microbial and pathogenic agents to the surface. Pathogen repellant surface technologies can be separated into two distinct categories liquid-infused coatings and air-infused coatings.[38] Liquid-infused surface coatings function through the infusion of a lubricating liquid into the surface structure or chemical coating.[184,264–266] This lubricating liquid layer is typically selected to be immiscible with the contaminating media (oil lubricant for water repulsion), which reduces the adhesion of the contaminate to the surface.[38,181,267] Air-infused coatings function by trapping air pockets within the surface structure, which inhibit the homogenous wetting of the solid surface.[36] The resulting unique wetting state of the air-infused coatings, also known as Cassie-Baxter states, is responsible for the observed superhydrophobic and oleophobic properties of these materials.[54,125] Generally, both classes of surfaces are manufactured

to have rough surfaces with high surface areas and are typically either porous, micro-structured, nano-structured, or hierarchically structured.[36,54,264] For both liquid- and air-infused surfaces, the presence of hierarchically structured surface topography has shown significant increase in liquid repellency and robustness of the surface properties.[38,268] The hierarchical structure used for liquid-infused surfaces helps retain larger amounts of the lubricating liquid within the structure,[35] while for air-infused surfaces the hierarchical structure helps to increase the stability of the air pockets within the surface.[125] Hierarchically structured surfaces also have the added benefit of significantly reducing the area of interaction between the solid surface and pathogens, significantly decreasing pathogen adhesion/contamination.[52]

Even though repellant materials significantly reduce the spread and proliferation of pathogens in a variety of environments,[54,269] they suffer from several shortcomings. In particular, liquid-infused coatings, despite recent progress for long-term lubricant retention,[233,266] might not be appropriate for high-touch surfaces due to the slippery nature of the coating.[35] Air-infused surface coatings are limited by the stability of the air-pockets trapped within the surface structure.[36] In submerged environments, the stability of the air pockets is dependent on the hydrostatic pressure, air diffusion, and shear flow near the surface; whereas in open air droplet impingement, mechanical abrasion, and chemical contamination are critically important.[36] More specifically, in case of coating degradation, there is a decrease in repellent properties of the air-infused surfaces, which increases the susceptibility of the surface to pathogen contamination[50] due to the formation of pathogen adhesion sites. Furthermore, pathogen repellent surfaces cannot provide the complete elimination of pathogen adhesion to their surfaces and their

repellency breaks down when the pathogen concentration exceeds a certain threshold value.[50]

These issues can be resolved through the addition of antipathogenic materials into the repellant coating, allowing for any adhered pathogens to be deactivated, resulting in the material retaining its low levels of pathogen contamination.[31] Coatings with the ability to both repel and kill pathogens are classified as dual-functional materials and have significant upside to the traditional pathogen-repellent or anti-pathogenic material coatings.[63,264,270]

The current strategies used to develop dual-functional materials, with both pathogen-repelling and antipathogenic properties include the co-deposition of repellent and antipathogenic materials such as co-polymers,[63,270] fluorinated metal oxide nanoparticles,[50,66] and fluorinated transition metal nanoparticles,[41,67,271] the impregnation or loading of repellant coating with anti-pathogenic material,[41] the use of switchable surfaces that change from repellent to pathogen killing states,[61,69,270] and the use of photoactive materials within the repellant coatings.[31,66,68] Dual-functionality achieved through co-deposition of repellent and antipathogenic materials is usually manufactured by the polymerization of an antiadhesive and antipathogenic monomer to form polymer brushes.[63] While co-deposition and loading methods allow for the simultaneous repulsion and killing of pathogens, the two properties on the monomers are naturally contradictory in function, since anti-adhesion components repel pathogens, while antipathogenic components attract pathogens in order to deactivate them.[63] As a result, creating material systems which allow for control over when desired materials properties (anti-pathogenic or pathogen-repellent) are expressed are of great benefit to

long term functionality of the coating. Switchable dual-functional surfaces can address this, allowing for switching between pathogen repellent and anti-pathogenic state, which is typically triggered through external stimuli such as temperature[75], humidity, and hydration,[69,76] light,[66,68] or gas exposure (ex. CO_2).[61,270] Furthermore, the use of photoactive materials into repellent surface structure allows for control over the production of anti-pathogenic agents. When disinfection is required, the coating can be stimulated with light, producing reactive oxygen species capable of deactivation pathogens,[151] allowing the surface to spend most of it working time in the pathogen-repellant state.

Herein, we developed a hierarchically structured air-infused omniphobic wrap integrated with photoactive TiO_2 nanoparticles (NPs) named OmniKill. We then characterized the dual-functional properties of OmniKill and studied its role in reducing the surface mediated transmission of pathogens. The pathogen repellency and anti-pathogenic properties of the superhydrophobic and omniphobic versions of the wrap were characterized using a touch transfer assay that modeled the physical transmission of pathogens from contaminated hands (modelled by an agar stamp) to high touch surfaces. Using this approach, we were able to characterize the surface mediated transmission of the surfaces with single and multiple pathogens, as well as under real-life conditions. We designed an experiment in which human finger mimicked by a stamp was contaminated with mouse feces, which was used to transfer contamination on secondary surfaces. Our study helped develop a new material system for reducing surface-mediated transmission of pathogens using repel and kill mechanisms and led to

a number of critical assays for modeling and studying surface-mediated transmission of pathogens with a single or multiple pathogens.

5.3 Methods

Functionalization of Polymer substrate with NP: Polyolefin (PO, Cryovac D-955) was cut into 15 mm discs and subsequently cleaned with ethanol and milli-Q water and dried with compressed air. The PO substrates were then exposed to oxygen-plasma in an expanded plasma cleaner (Harrick Plasma) 150W Radio Frequency (RF) power for 3 min. TiO_2(P25) nanoparticles were then deposited on the surface via Dip coating at a pull rate of 1-2 mm/s. TiO_2 NPs were prepared by adding 60 mg of P25-TiO_2 NP (~21 nm) to 30 mL of Milli-Q water, creating a 2 g/L suspension of TiO_2. Following the deposition of TiO_2 the surfaces were washed with Milli-Q water and dried with compressed air.

Fluorosilanization of Surfaces: 75 mL of anhydrous ethanol was heated to 55^o C for 30 min at which point 200 uL of 1 M HCl and 75 uL of FS making a 0.5 wt% solution. This was allowed to mix for 10 mins. The surfaces were then exposed to oxygen-plasma again for 3 min and subsequently placed into the FS solution for 1 hour. After the FS deposition the surfaces were washed in water for 5min and left to dry overnight. The wrap was then sonicated in ethanol for 10min and dried with compressed air. They were then shrunk via thermal shrinking at 145^{o}C in an oven for 10min.

Surface characterization: SEM and EDX imaging was performed on a JEOL 70000F. Samples were coated with 5-10 nm of platinum before imaging. CA and CAH measurements were taken on a KRUSS DSA30S Drop Shape Analyzer (Hamburg,

Germany) with droplets of water (5 µL), glycerol (5 µL), formamide (5 µL), ethylene Glycol (5 µL) and hexadecane (5 µL).

Surface Durability Characterization: The protocol for the touch durability test[269] and mechanical abrasion test[272] are found elsewhere. A 200g weight was used as the mechanical load for both the touch and mechanical abrasion durability tests.

Bacteria touch transfer assay: a 3 % (v/v) agar solution was prepared. This solution was heated in a microwave for 2 min. Hot agar suspension was then poured into 10 cm petri dishes and let cool at room temperature for 30 min. Stamps were then cut out using 6 mm biopsy punches (Integra Miltex Disposable Biopsy Punch 6mm and Thermo-Fisher). In each stamp, 10 uL of overnight bacteria culture was placed and allowed to incubate for 30 min. By the end of the incubation period, all water was adsorbed into the agar or evaporated, leaving behind a bacterial film. Surfaces were disinfected with 70% ethanol for 5 min and then left to dry for 30 min to ensure that no bacteria were present on the surface before stamping. The bacteria contaminated stamps were then placed into contact with the test surfaces for 10 s before being washed with 500 µL of PBS. This wash solution was then used for dilution and plating.

Multifactorial touch transfer Assay: Mixed bacteria culture was prepared by creating an overnight culture of each bacteria strain. 100 µL of the overnight bacteria culture were added to 10mL of tryptic soy broth (TSB) media and mixed thoroughly. Contaminated Agar stamps were prepared as previously described with this mixed culture solution. After Plating of the bacterial dilutions the cells were differentiate though their individually distanced colony morphologies (Supplementary Figure 5-6). *E. coli* was GPF expressing and could be distinguish by a bright green colour (Supplementary Figure 5-6b), *B. subtills*

and *P. aeruginosa* were distinguished by a white colony and MRSA was distinguished by a yellow colony. The *B. subtilis* and *P. aeruginosa* we then further distinguished by the colony morphology with the former having solid edges while the latter has clear edges.

Fixation of bacteria for SEM: Surfaces were contaminated using the same method described for the bacterial touch transfer assay. However instead of washing in 500 µL of PBS the surfaces were placed into a 2.5 % (v/v) glutaraldehyde solution for 60 min. the surfaces were then exposed to solutions of increasing ethanol concentrations (30 %, 50 %, 70 %, 80 % and 100 % (v/v)) for 10 min. surface were then left to dry for 30 min in ambient conditions.

Stamp-UV Assay: surfaces were contaminated using the same method described for the bacterial touch transfer assay. After contamination the surfaces were placed into a 48-well plate and covered in 500 µL of PBS. The surfaces were then exposed to UV light for 0, 10, 20, 30 and 60 min. When exposure was complete the 500 µL was removed and transferred to a 1.5 mL microtube and subsequently followed by the contaminated surface and vortexed for 10 s. This solution was then used for dilution and platting.

Fecal Transfer Assay: Mouse fecal samples were collected from the Farncombe Family Digestive Health Research Institute (Hamilton, Canada). Two pellets of either bacteria containing, or sterile mouse feces was placed into a 1.5 mL tube, to which 500 µL of phosphate buffer solution was added. This tube was then left to sit for 10min before shaking vigorously and vertexing at the max speed for 30 s. this process was repeated three times to create a suspension of fecal water. 20 µL of this solution was then placed on each stamp and let dry for 10 min. The stamping and plating procedure followed that of the Bacterial touch Transfer Assay.

Sequencing of Bacteria in Mouse Feces: To identify the bacterial colonies, the colonies were subcultured on Tryptic Soy Broth (TSB) agar to yield pure cultures. V3V4 16S rRNA PCR gene amplification was performed at the Surette laboratory (Hamilton, ON). Sanger DNA sequencing was performed at Mobix (Hamilton, ON). The DNA sequences were matched to corresponding bacteria using the National Center for Biotechnology Information's nucleotide collection database and the megablast program (Sayers et al, 2022).

5.4 Results and Discussion

5.4.1 Manufacturing and Wettability of the Omniphobic Wrap

The OmniKill Wraps were fabricated by first depositing the photoactive TiO_2 NPs on a PO wrap. This was achieved by exposing the wrap to oxygen plasma (3 min, 50 W) to induce a dense layer of hydroxyl groups on the surface (Figure 5-1a). The functionalized polymer sheet was then modified by dip-coating through submerging it into an aqueous suspension TiO_2 NPs (~21 nm) and then quickly removing it to deposit a thin layer of the NPs on the wrap. The TiO_2 NPs are attached/bound to the surface through condensation reaction.[134,273] This process was accelerated by baking the coated surface at 60^{o}C for 10 min (Figure 5-1a, ii). Following the formation of the TiO_2 NP layer, the surfaces were treated with FS (1.5 h, 0.5 wt%) in order to reduce the surface energy (Figure 5-1c).[54,269] The final microstructure of the wrap was formed by thermally shrinking the polymer at 145^{o}C, which resulted in buckling of the thin film and the formation of hierarchical structures with micro-scale and nano-scale features (Figure 5-1a, iv). Such buckling of NP thin films is expected as the NP act as a stiff layer, capable of buckling under a critical

strain.[129] The size and geometry of the buckled microstructure is dependent on the density of the NP film, with denser films resulting in larger buckling wavelengths.[129] Scanning Electron Microscopy (SEM) and Energy Dispersive Spectroscopy (EDS) images of the surface show great uniformity in both surfaces structure and coverage of the surface with fluorine groups (Supplementary Figure 5-1).

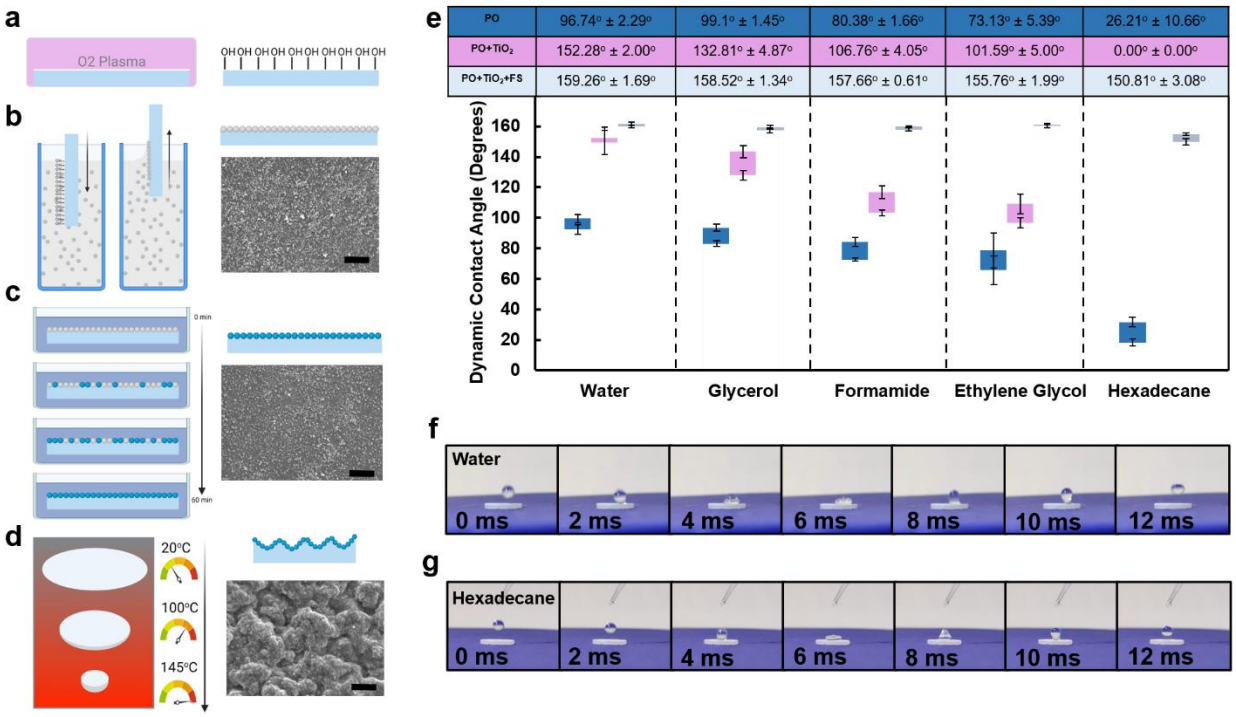

Figure 5-1: Fabrication and characterization of the OmniKill Wrap. a) Schematic diagram depicting the manufacturing process of the OmniKill Wrap: i) oxygen Plasma treatment of the polyolefin substrate, ii) dip-coating of the substrate into a TiO_2 nanoparticle suspension, iii) fluorosilanization of nanoparticles on the substrate, and iv) formation of microstructure through shrinking of the polymer substrate, along with the corresponding SEM images. e) Surface repellency of the OmniKill Wrap with various liquids (water, glycerol, ethylene glycol, formamide and hexadecane). The static contact angles for each liquid are denoted in the table above the graph while the colour boxes in the graph represent the contact angle hysteresis. Dynamics of liquids bouncing on the surface of OmniKill Wrap using f) water and g) hexadecane. Scale bars on the SEM images are 3 µm.

To quantify the wettability and omniphobicity (CA > 150^o and CAH < 10^o for all test liquids)[46] of the functionalized wraps, we examined its interaction with various liquids with a wide range of surface tension, surface tension components (dispersive, polar) and viscosity (Supplementary Table 5-1). The PO substrate displayed CA of 96.7^o±2.3^o (water), 99.4^o±1.5^o (glycerol), 80.4^o±1.7^o (formamide), 73.1^o ± 5.3^o (ethylene glycol) and 26.2^o± 10.7^o (hexadecane). Following the formation of the hierarchical structures made from TiO_2 NPs (PO+TiO_2), the wrap displayed superhydrophobic properties and a significant increase in the CAs of water (152.3^o ± 2.0^o), glycerol (132.8^o ± 4.9^o), formamide (106.8^o ± 4.1^o) and ethylene glycol (101.6^o ± 5.0^o). Interestingly the hexadecane CA of ~0^o, displayed a breakdown of the Cassie-Baxter wetting states with the decrease in liquid surface tension (Figure 5-1e). This was further evident as the fraction of surface wetting was increased with decreasing surface tension (Supplementary Figure 5-3) for the PO+TiO_2 surface, displaying a direct transition of the Cassie-Baxter wetting states into Wenzel states with decrease in surface tension. The addition of FS increased the liquid repellency of the wrap for every tested liquid (water 159.3^o ± 1.7^o, glycerol: 158.5^o ± 1.3^o , formamide: 157.7^o ± 0.6^o , ethylene glycol: 155.76^o ± 2.0^o , hexadecane: 150.8^o ± 3.1^o), achieving omniphobic wetting.[46] The most significant change in wettability for the PO + TiO_2+ FS was seen with hexadecane, with an increase in over 150^o compared to PO + TiO_2, which is due to the FS modification, as the PO+TiO_2 and PO+TiO_2+FS surface have the same topography. The Cassie-Baxter state on the PO+TiO_2+FS surfaces was significantly more stable than the PO+TiO_2 surfaces maintaining a solid fraction of wetting of less than 16.5% for all liquids (Supplementary Figure 5-3). This indicates that adding FS causes the droplets of various liquids not to transition to Wenzel wetting states, which

is likely due to a large energy barrier between the solid/vapor and solid/liquid interfaces at the surface.[274]

Even though the static CA is an important metric for surface wettability, interactions in the real world are rarely static. Therefore, we also tested the surfaces under dynamic wetting states though measurements of the CAH. The CAH of the tested liquids on the PO surface ranged from 6.9º-13.5º, the lowest hysteresis being for water and the largest being for hexadecane. The PO+TiO_2 showed a larger variation in CAH (2.7º - 12.3º), with the smallest being water and the largest being ethylene glycol. Due to the high wettability of the Hexadecane on the PO+TiO_2 surface, the CAH of hexadecane was unmeasurable. The PO+TiO_2+FS surface had a significant decrease in CAH when compared to PO+TiO_2, showing a CAH of less than 2º for all liquids excluding hexadecane, which had a CAH of 5.0º ± 1.4º (Figure 5-1e). To further characterize wettability under dynamic conditions, 5 μL droplets (water and hexadecane) were dropped onto various surfaces. The PO surfaces did not show any detachment of either water (SV 1) or the hexadecane (SV 2) droplets after impact with the material. On PO+TiO_2 surfaces, water (SV 3) droplets fully detached from the surface after impact, but hexadecane (SV 4) fully wetted the surface. For the PO+TiO_2+FS surface, both water (Figure 5-1f, SV 5) and hexadecane (Figure 5-1g, SV6) droplets bounced off of the surface due to the high static CA and low CAH, displaying robust Cassie-Baxter wetting when droplets were moving at high speeds.[97,275] The repellency of the PO+TiO_2+FS surface toward both high and low surface tension liquids indicates wide range repellency[36] and points to the potential for pathogen repellency.[31]

The durability of OmniKill Wrap was analyzed by observing the change in surface wettability after mechanical stress, including compression caused by frequent touching and mechanical abrasion. After compressing the surface 100 and 200 times with a human touch, no visible change in water wettability was seen (Supplementary Figure 5-4a); however, the CA of hexadecane was significantly decreased after 200 touches, falling by 17.7% to below 150^{o} ($124.5^{+}\pm 17.4^{o}$ after 200 touches). Mechanical abrasion showed a decrease in both the superhydrophobic and oleophobic properties after 10 abrasion cycles reducing the water and hexadecane CA by 5.0% and 23.6% respectively (SI Figure 5-4b).

5.4.2 Interaction of Omniphobic Hierarchical structures with Pathogens

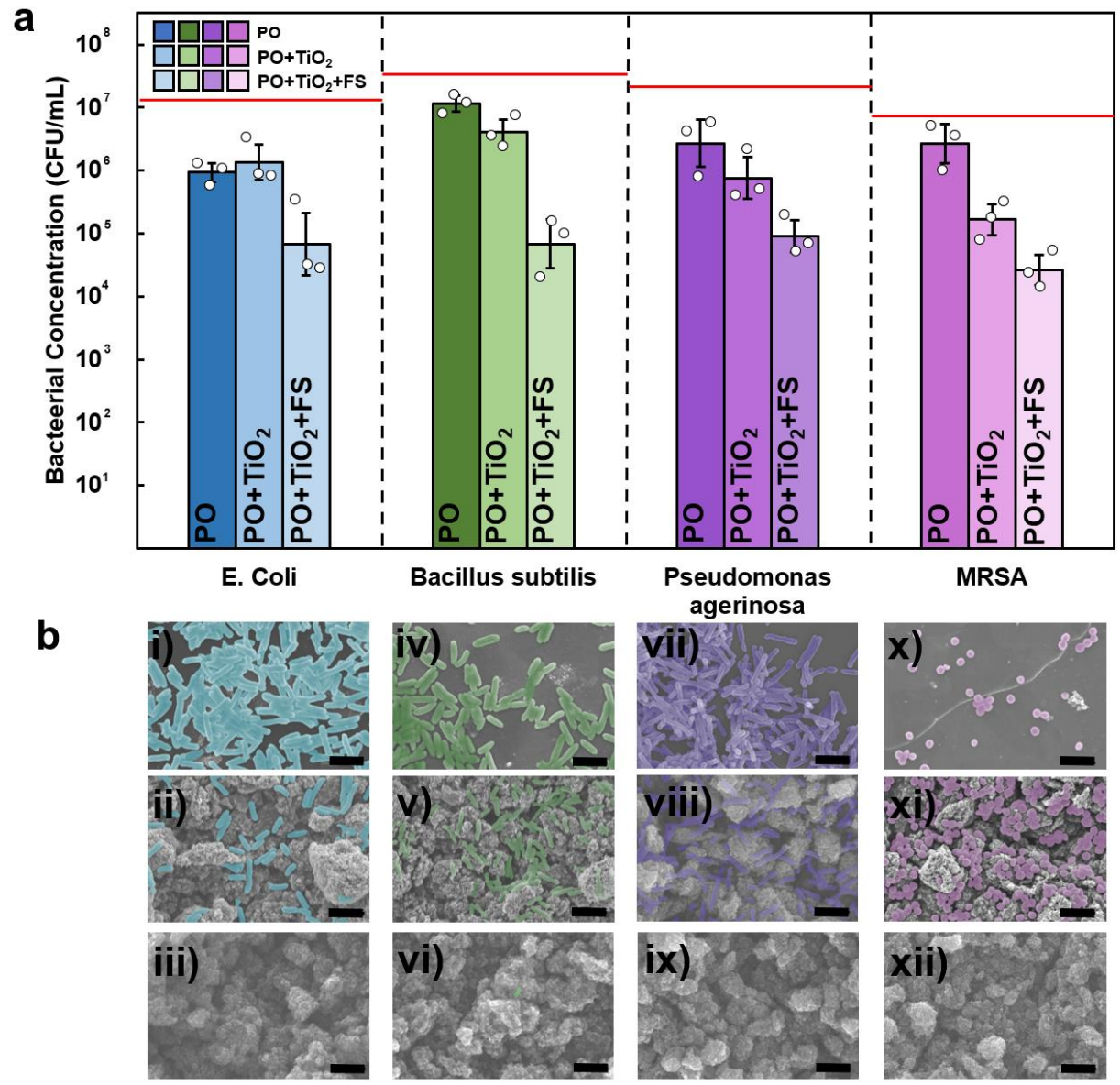

Figure 5-2: Characterization of the pathogen repellency of the OmniKill Wrap. a) Log-plot depicting the number of bacteria transferred between a contaminated stamp and sterile surface after physical contact. Red lines indicate the initial concentration of bacteria on the contaminating stamp. b) SEMs of bacteria (*E. coli*; i, ii, iii. *B. subtilis*; iv, v, vi. *P. aeruginosa*; vii, viii, ix. MRSA; x, xi, xii) on surface after contamination through physical contact. Scale bars on the SEM images are 3μm.

Once the liquid repellency of the PO+TiO_2+FS surface was characterized, we investigated whether omniphobicity translated to bacteria repellency. To quantify the amount of bacteria that could be transmitted between a contaminated and a clean surface, agar stamps were contaminated with overnight culture of various bacteria and pressed into the clean surfaces. After stamping, the surfaces were washed with 500 uL of Phosphate Buffer Silane (PBS) and serial dilution was performed to count the number of bacteria transferred to the surface. Following the stamping assay, the PO surface showed a reduction in the transfer of bacteria to its surface of 1.5-log, 1.34-log, 0.88-log, and 0.52-log *for Escherichia coli* (*E. coli)*, *Bacillus Subtills* (*B. subtilis)*, *Pseudomonas aeruginosa* (*P. aeruginosa)* and Methicillin Resistant *Staphylococcus aureus* (MRSA), respectively from the initial concentration of the bacteria present on the stamp (Figure 5-2a). This high degree of contamination is further evident from the SEM of the PO surface after contamination with each bacterial strain. These images show individual bacteria as well as large aggregates spread over the entire surface (Figure 5-2b (i, iv, vii, x)). The PO+TiO_2 surface had slightly improved repellency displaying a 1.34-log, 1.80-log, 1.43-log, and 1.72-log for *E. coli*, *B. subtilis*, *P. aeruginosa* and MRSA reduction, respectively from the initial concentration of bacteria. The SEM of the PO+TiO_2 surface reveals that the surfaces are only contaminated with individual bacterium and not with large aggregates. Interestingly, most of these contaminating bacteria are found within the groves of the surface microstructure (Figure 5-2b (ii,v,viii,xi)). Additionally, there appears to be a difference in the contamination level seen by spherical and rod-shaped bacteria. For surfaces contaminated with MRSA, rod shaped and Gram-positive, we saw much more bacteria hidden within the structure, compared to the other rod-shaped bacteria,

which is in line with previous work.[54] The PO+TiO_2+FS surface displayed a reduction of 2.65 log, 3.57-log, 2.35-log, and 2.52-log for *E. coli*, *B. subtilis*, *P. aeruginosa* and MRSA from the initial concentration of bacterial. This is the highest reduction seen with the tested surfaces and is reflected in the SEM images of the PO+TiO_2+FS surface after contamination, which show little to no bacterial contamination for all strains used in this study (Figure 5-2b (iii, vi, ix and xii)).

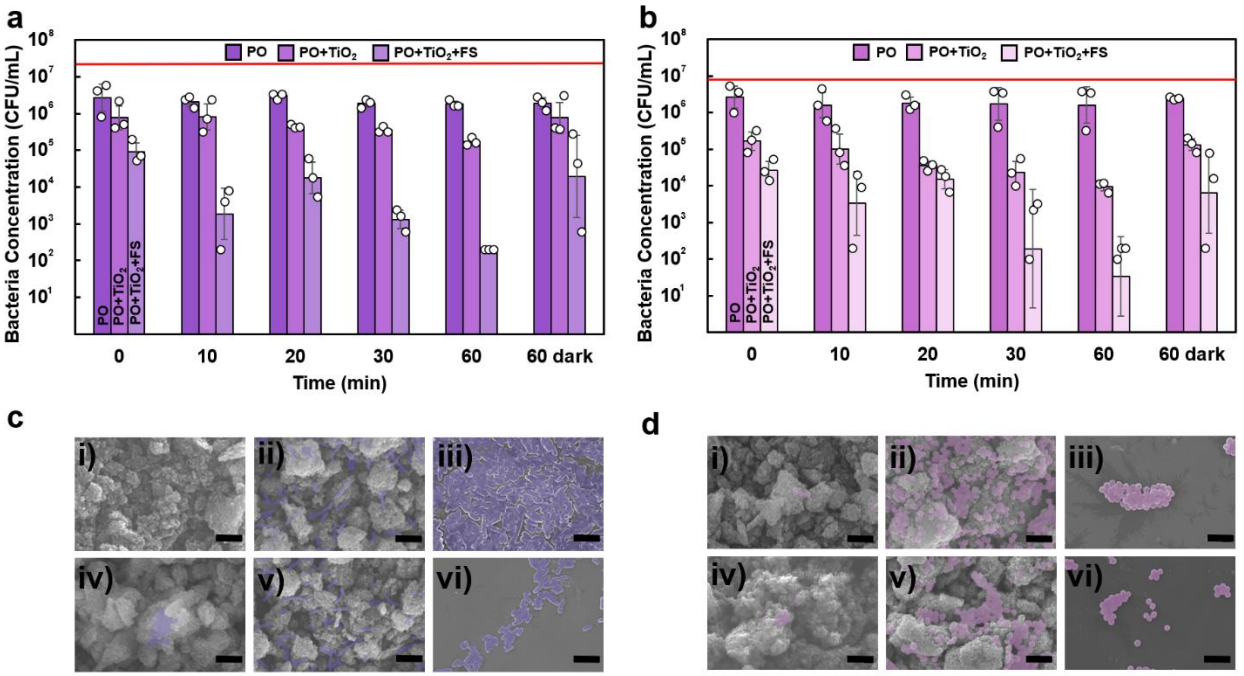

Figure 5-3: Antimicrobial properties due to the photoactivity of TiO_2. Concentration of live a) *P. aeruginosa* and b) MRSA on the surfaces after exposure to UV light. Red lines indicate the initial concentration of bacteria on the stamp before contamination. SEMs of the surfaces contaminated with c) *P. aeruginosa* and d) MRSA after 1h exposure to UV light; i) PO+TiO_2+FS, ii) PO+TiO_2, iii) PO, and in the dark; iv) PO+TiO_2+FS, v) PO+TiO_2, vi) PO. Scale bars on the SEM images represent 3 μm.

Light-induced bacterial deactivation was measured on both PO+TiO_2 and PO+TiO_2+FS surfaces by exposing them to ultraviolet (UV) light after contamination with bacteria through stamping. More specifically, the surfaces were contaminated with *P. aeruginosa*

(Gram-negative) and MRSA (Gram-positive) *via* stamping, they were then exposed to low amounts of UV light for up to 60 min, and finally they were washed with 500 μL of PBS and the 100 μL was cultured to determine the amount of live bacteria present on the surfaces following contamination and light exposure. For both tested bacteria, no change bacteria concentration was seen on the PO surfaces after 60 min of exposure to UV light. On the other hand, the PO+TiO_2 surfaces showed a reduction of 0.65 log (*P. aeruginosa*) and 1.24-log (*MRSA*) in the number of viable transmitted pathogens. Interestingly, the PO+TiO_2+FS surfaces showed an even greater reduction in the number of bacteria, 2.65-log for *P. aeruginosa* and 2.21-log for *MRSA* compared to the initial number of transferred bacteria, after a 60 min light exposure. From the inoculating concentration on the stamps, this presents a 5.0-log and 4.74-log reduction in *P. aeruginosa* and MRSA concentration, respectively. Even though both PO+TiO_2 and PO+TiO_2+FS surfaces showed reductions in viable bacteria concentration after 60 min of light exposure, no real change in the bacterial concentration was seen on either surface after 60 min of incubation in the dark, indicating that this reduction is related to the photoactivity of TiO_2. This reduction in viable bacteria on the surface is generally attributed to photocatalysis and the formation of oxygen radicals on the surface of TiO_2.[151] It is well established that the formation of free reactive oxygen species by TiO_2 causes oxidative stress to the inter- and extra-cellular components of bacteria, which ultimately leads to their deactivation.[31,151] Omniphobic and superhydrophobic surfaces have been shown to prevent bacteria from forming protective biofilms,[54,264] which leaves the bacteria more vulnerable to damage from their environment.[276] Without the protective biofilm, the oxygen radicals produced by the TiO_2 on the surface can more easily interact with the bacterial cell membrane, causing

irreversible damage to the bacteria.[151] Additionally there is evidence in the literature that alkylsilane and fluoroalkylsilanes may increase the rate and efficiency of oxygen radical formation.[277] The combination of poor surface environment for bacterial attachment and proliferation, and enhanced production of oxygen radicals enabled by the combination of TiO_2 and silanes on the PO+TiO_2+FS surface, explains its superior bactericidal effects of this surface.

5.4.3 Testing of Anti-Pathogenic Properties in Real-World Conditions

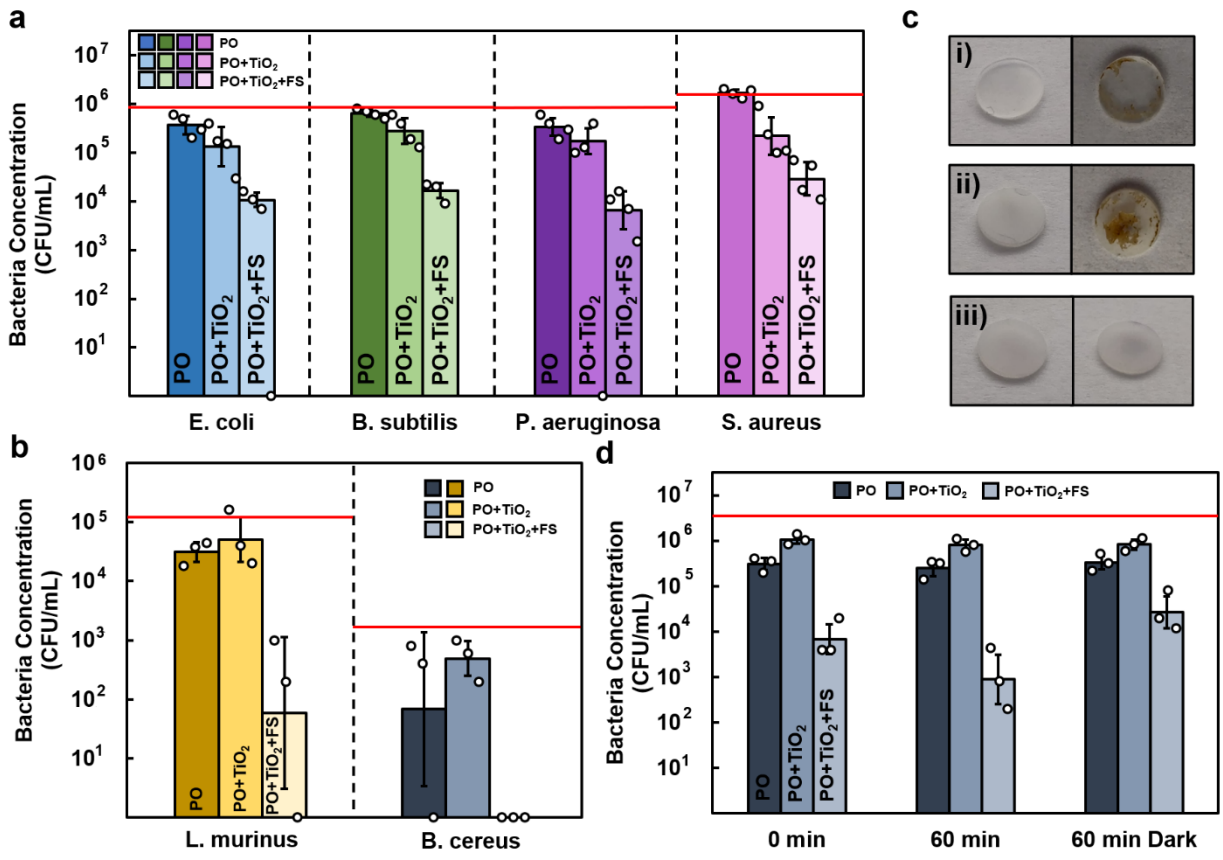

Figure 5-4: Multi-pathogen assay characterizing the simultaneous contamination of surfaces with multiple bacteria. a) contamination of the surfaces using the stamp assay inoculated with a mixed culture of *E. coli*, *B. subtilis*, *P. aeruginosa* and MRSA. b) contamination of the surfaces with mouse feces containing two types of bacteria (Bacillus cereus and Lactobacillus murinus. c) images showing the staining of i) PO, ii) PO+TiO_2

and iii) PO+TiO_2+FS with mouse feces before (left) and after (right) contact with the contaminated stamp. d) decontamination of the surfaces with UV light after contamination with feces containing Bacillus cereus. Red lines indicate the initial concentration on the stamp prior to contamination.

The surfaces were also tested under simultaneous contamination form multiple bacteria introduced from 1) a stamp contaminated with a mixed culture of *E. coli*, *B. subtilis*, *P. aeruginosa* and MRSA, and 2) a stamp contaminated with mouse feces containing *Bacillus cereus* and *Lactobacillus murinus*. After physical contact with the mixed-culture contaminated stamps, the PO, PO+TiO_2 and PO+TiO_2+FS surface displayed a reduction of 0.53-log, 1.16-log and 2.15-log reduction in *total* bacterial adhesion (Supplementary Figure 5-5) compared to the initial concentration of bacteria on the stamp. The concentration of each individual strain was also determined by analyzing the colony morphology as discussed in the methods section. After differentiating the colonies (Supplementary Figure 5-6) a reduction of 1.96-log (*E. coli*), 1.52-log (*B. subtilis*), 1.93-log (*P. aeruginosa*), 1.56-log (*S. aureus*) compared to the initial concentrations of each individual bacteria on the stamp, was seen on the PO+TiO_2+FS (Figure 5-4a). This was very similar to that of the individual bacterial results seen in Figure 5-2a, indicating that the deposition of multiple strains of bacteria at once does not significantly affect their adhesion.

To determine the ability of OmniKill Wrap in reducing real-life cross contamination caused by a surface (*e.g*. human hand) contaminated with biological materials (*e.g.* feces), we used stamps that mimicked the human hands and were soiled with mouse feces. Following the contamination with mouse feces and subsequent washing and culture, two distinct colony morphologies were seen on the agar plates (large white colonies with

smooth edges and small clear colonies with rough edges) (Supplementary Figure 5-7). To determine what bacterial strains these colonies represented, 16S rRNA amplicon sequencing was done. It was determined that the strains present in the mouse feces were *Bacillus cereus* and *Lactobacillus murinus*. We saw a reduction of 1.2, 0.46, and 3.15-log in *Bacillus cereus* concentration for PO, PO+TiO_2 and PO+TiO_2+FS surfaces compared to initial concentration of bacteria in the fecal matter. For *Lactobacillus murinus*, a reduction of 0.57, 0.36 and 3.29-log was also seen for the PO, PO+TiO_2 and PO+TiO_2+FS surfaces compared to initial concentration of the fecal bacteria on the stamp, respectively (Figure 5-4b). The bacterial contamination was also seen visually on the surfaces contaminated with feces-soiled stamps (Figure 5-4c). The PO+TiO_2+FS surface showed the least amount of visible contamination compared than the other surfaces, which is in line with the viability results. These results indicate that the OmniKill Wrap is effective in reducing the transfer of contamination from intermediate surfaces.

The deactivation of pathogens transferred from the feces was quantified by exposing contaminated surfaces to UV irradiation for 1 hour (Figure 5-4d). No reduction in bacterial contamination was seen for the PO or PO+TiO_2 surfaces after the 1 hour of light exposure. The PO+TiO_2+FS surface displayed a reduction of 0.89-log, which was lower than the 2.21-log and 2.65-log seen for the bacteria suspended in growth media (MRSA and *P. aeruginosa*). The lack of decontamination on the PO+TiO_2 substrates (Figure 5-4d), compared to the bacteria in growth media (Figure 5-3), and the reduced decontamination seen on the PO+TiO_2+FS, is likely a result of the fecal matter acting as a protective barrier between the oxygen radicles generated by the surface and the bacteria.

5.6 Conclusion

We created two highly repellent and photoactive surface which were distinguished by their superhydrophobic and omniphobic properties. After characterization and classification of their liquid repellency, we quantified the pathogen repellency and found significant reduction in the physical adsorption of bacteria/pathogens to the omniphobic vs superhydrophobic surfaces. An average of 2.77-log (omniphobic) vs 1.57-log (superhydrophobic) of the pathogens remained on the contaminating surface after physical contact. After contamination of the surface an enhanced pathogen deactivation under UV light exposure on the fluorinated TiO_2 vs the TiO_2 was observed. After exposure to UV the OmniKill Wrap was able to reduce the number of viable bacteria by 4.74-log (MRSA) and 5.0-log (*P. aeruginosa*) from the initial concentration of bacteria on the stamp, while the non-fluorinated substrates were only able to reduce the pathogen concentrations by 1.24-log (MRSA) and 0.65-log (*P. aeruginosa*). This increase in the deactivation of the OmniKill wrap was attributed to the poor environment of the omniphobic surface for bacteria attachment and proliferation, allowing the bacteria to be more susceptible to damage from oxygen radicles generated by the surface, or the increased generation of ROS seen by FS modified TiO_2.

Additionally, the real-world interaction of the surfaces was analyzed through contamination with bacteria latent feces, which is a commonly found contaminate in health care environments. A significant decrease in the repellency of the PO+TiO_2 surface was seen under the fecal contamination, showing less then half a log reduction in the bacteria contamination and clear visible contamination of the surface with feces. The OmniKill wrap on the other hand preformed significantly better, retaining the high

repellency in the presence of feces, showing a reduction of 3.22-log vs 0.405-log on the PO+TiO_2 compared to the initial number of pathogens in the feces. The OmniKill wrap also showed deactivation of the transmitted fecal bacteria (reduction of 0.89-log) under UV irradiation, while the non-fluorinated TiO_2 was unable to change the concentration after contamination. Overall the combination of omniphobic properties vs superhydrophobic properties in combination with controllable antipathogenic effects, were found to be superior. The combination of omniphobicity and photoactivity was able to passively and effectively reduce various different forms pathogenic contamination, during and after a contamination event, significantly reducing the exposure of physical pathogen transmission between people and surfaces.

5.7 Acknowledgements

The electron microscopy was carried out at the Canadian Center for Electron Microscopy (CCEM), a national facility supported by the NSERC and McMaster University. R.M. was the recipient of the Ontario Graduate Scholarship. L.S. is Tier II Canada Research Chair in Miniaturized Biomedical Devices.

5.8 Supplementary Information

5.8.1 EDX Data on the surfaces

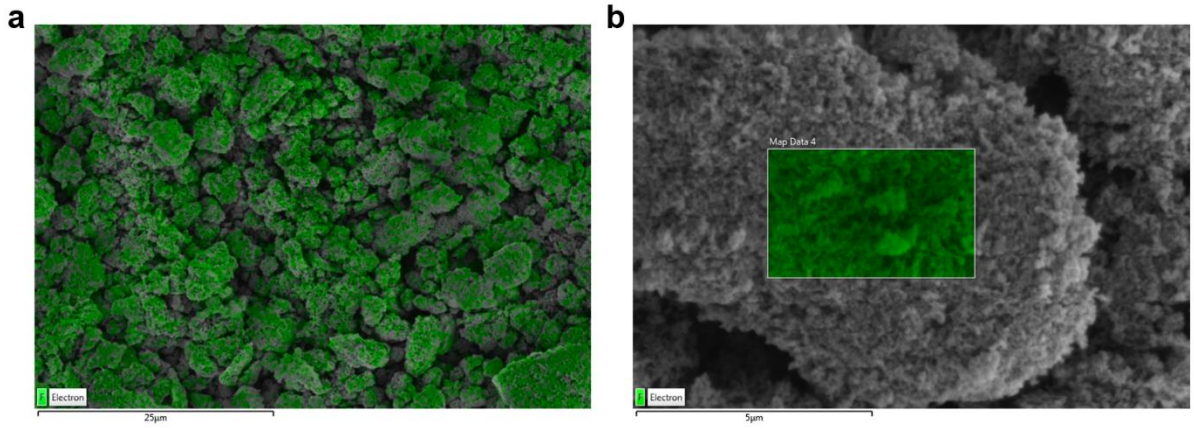

Supplementary Figure 5-1: EDS images of the Fluorine coverage of the a) microstructure and b) nanostructure

5.8.2 Properties of Probing Liquids

Supplementary Table 5-1: Surface Tension Components of Probe Liquids

Liquid	γ	γ^{LW}	γ^{+}	γ^{-}	μ
Water	72.8	22.6	25.5	25.5	0.01
Glycerol	63.4	40.6	3.92	57.4	648
Formamide	58.2	36	2.28	39.9	3.23
Ethylene Glycol	48	29	3	30.1	18.376
Hexadecane	27.5	27.5	0	0	3.454

5.8.3 Fraction of Surface Wetting

To determine the fraction of wetting the following equation was derived from the Cassie-Baxter wetting equation, as seen in previous work.[269] To determine the fraction of surface wetting the CA of the surface before the presence or in the absence of the microstructure is needed (Supplementary Figure 5-2). The resulting fractions of surface wetting for each surface were plotted against each probing liquids total surface tension (Supplementary Figure 5-3). The blue data, which represents the TiO_2 without the presence of FS shows

a significant increase in the wetting of the surface with a decrease in liquid surface tension and thus as poor omniphobicity. The TiO_2 surface with the FS however show very little change in the fraction of wetting with the tested probing liquids and thus display very good omniphobicity.

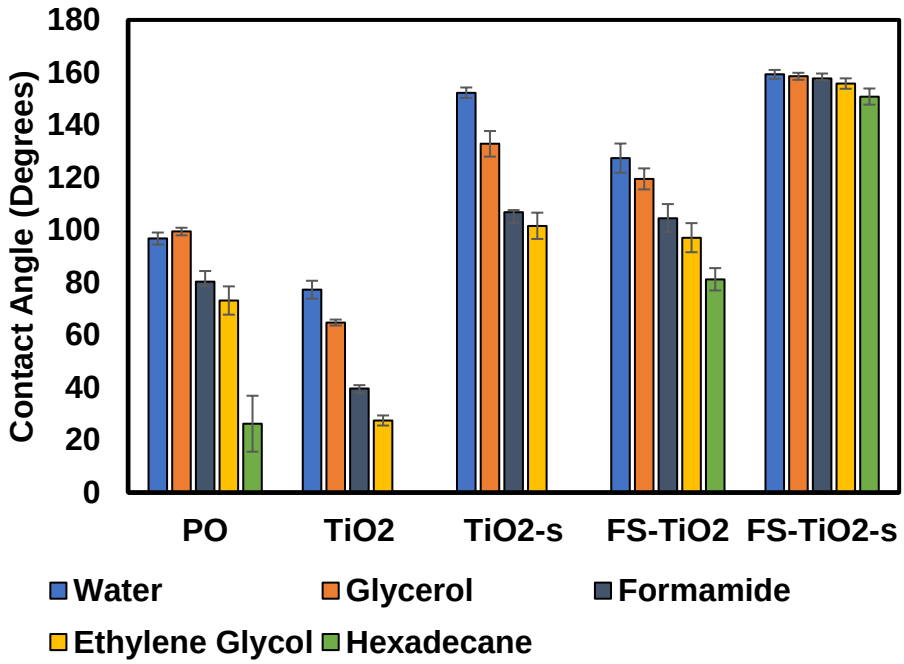

Supplementary Figure 5-2: Static Contact angle for surface before and after formation of the microstructure.

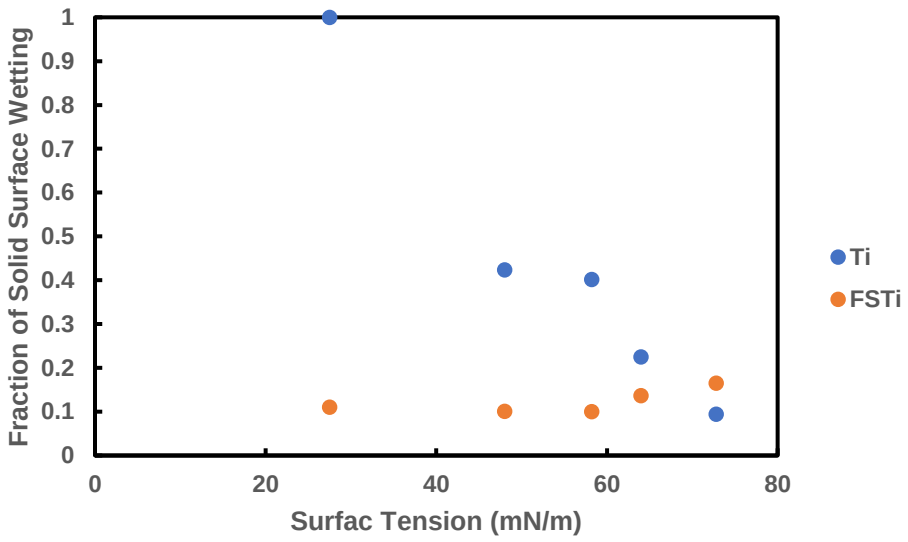

Supplementary Figure 5-3: Fraction of surface wetting for PO+TiO_2 and PO+TiO_2+FS surfaces

5.8.4 Surface Durability

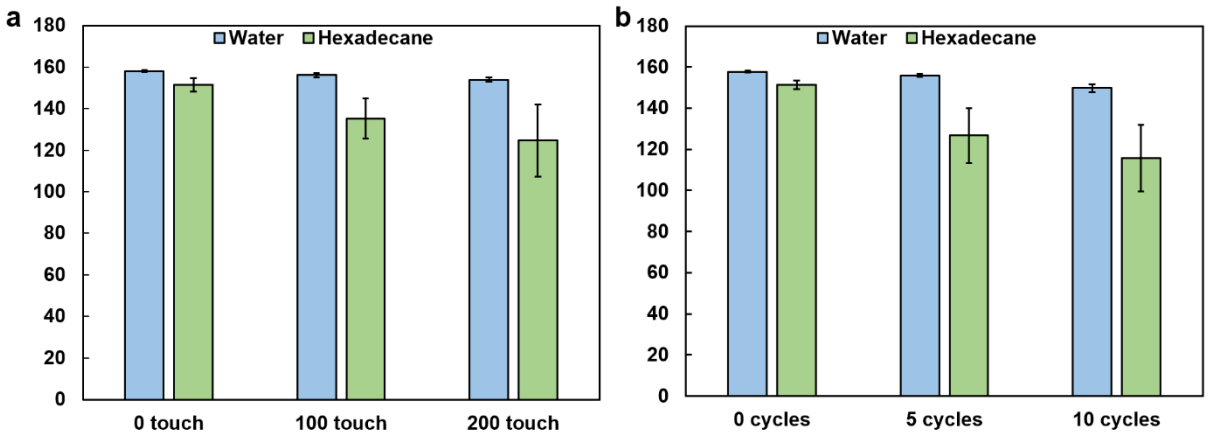

Supplementary Figure 5-4: Stability of the omniphobic properties to a) surface compression and b) mechanical abrasion.

5.8.5 Mixed Bacteria Transfer Assay

After measuring the initial number of colonies, the agar plates were left to grow for an additional 24-36h. At this point the difference in morphology between the different strains became clear. The bacteria we platted on Tryptic Soy Broth (TSB) plates and TSB Nalidixic Acid (TSB-NXA) plates. The TSB plates showed growth for all bacteria, *E. coli* was GPF expressing and could be distinguish by a bright green colour (Supplementary Figure 5-5b), *B. subtills* and *P. aeruginosa* were distinguished by a white colony and MRSA was distinguished by a yellow colony. The *B. subtilis* and *P. aeruginosa* we then further distinguished by the colony morphology with the former having solid edges while the latter has clear edges. The MRSA and *P. aeruginosa* we also cultured on TSB-NXA plates in case they were out competed buy the *E. coli* and *B. subtilis*. The MRSA concentrations did not seem to vary between the two plates however the *P. aeruginosa* grew better on the TSB-NXA plates (Supplementary Figure 5-5a).

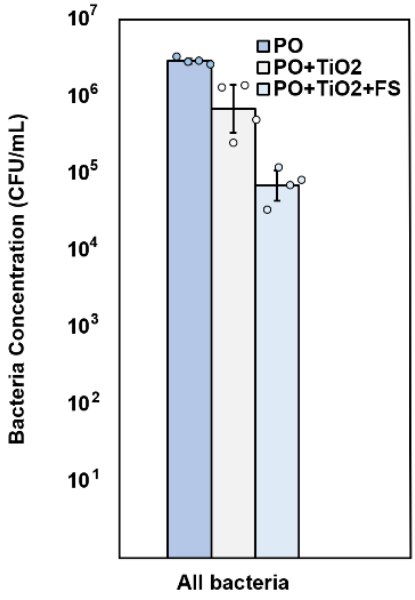

Supplementary Figure 5-5: Total contamination of Surface After mixed assay transfer.

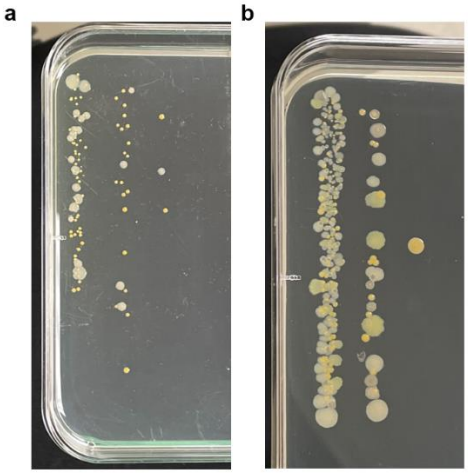

Supplementary Figure 5-6: Different colony morphologies of the various bacterial strains, a) TSB-NXA plates and b) TSB plates.

5.8.6 Determination of Fecal Bacteria Strains

After platting of the feces onto TSB agar plates two-three distinct colony morphologies were seen. Two of them had larger spherical shapes with a white or a beige colour, the third was smaller, clear and had a much less spherical shape (Supplementary Figure 5-7). These distinct colonies were then individually grown in TSB media overnight and then sent for PCR sequencing to determine what each individual bacterium was. The results of the PCR came back and reported the clear colony was Bacillus cereus the white colony was Rothia terrae and the Beige colony was Lactobacillus murinus.

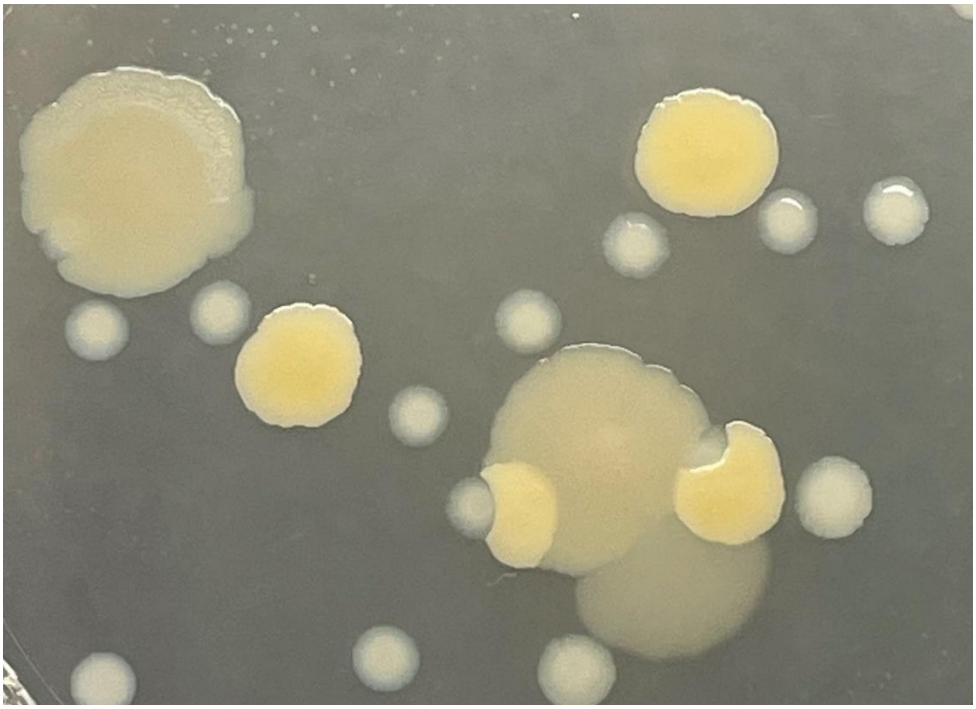

Supplementary Figure 5-7: Different colonies found in mouse fecal samples

The following are the results of each colonies sequencing:

Clear colony:

NNNNNNNtgcgcgTGCCTAATACaTGCaAGTCGAaCGAAACTTCTTTAtNccGAGTGCTTGCACTCACCGATAAAgaGTT

GAGTGGCGAACGGGTGAGTAACACGTGGGCAACCTGCCCAAAAGAGGGGGATAACACTTGGAAACAGGTGCTAATACCGC

ATAACCATAGTTACCGCATGGTAACTATGTAAAAGGTGGCTATGCTACCGCTTTTGGATGGGCCCGCGGCGCATTAGCTA

GTTGGTGGGGTAAAGGCTTACCAAGGCAATGATGCGTAGCCGAACTGAGAGGTTGATCGGCCACATTGGGACTGAGACAC

GGCCCAAACTCCTACGGGAGGCAGCAGTAGGGAATCTTCCACAATGGGCGAAAGCCTGATGGAGCAACGCCGCGTGGGTG

AAGAAGGTCTTCGGATCGTAAAACCCTGTTGTTAGAGAAGAAAGTGCGTGAGAGTAACTGTTCACGTTTCGACGGTATCT

AACCAGAAAGCCACGGCTAACTACGTGCCAGCAGCCGCGGTAATACGTAGGTGGCAAGCGTTATCCGGATTTATTGGGCG

TAAAGGGAACGCAGGCGGTCTTTTAAGTCTGATGTGAAAGCCTTCGGCTTAACCG
GAGTAGTGCATTGGAAACTGGGAGA

CTTGAGTGCAGAAGAGGAGAGTGGAACTCCATGTGTAGCGGTGAAATGCGTAGAT
ATATGGAAGAACACCAGTGGCGAAA

GCGGCTCTCTGGTCTGTAACTGACGCTGAgGTTCGAAAGCGTGGGTAGCAAACAG
GATTAGATACCCTGGTAGTCCACGC

CGTAAACGATGAATGCTAAGTGTTGGAGGGTTTCCGCCCTTCAGTGCTGCAGCTAA
CGCAATAAGCATTCCGCCTGGGGA

GTACGACCGCAAGGTTGAAACTCAAAGGAATTGAACgG

White colony:

NNNNNNNgTGNcgcgTGCTTAANACATGCaAGTCGAACGATGAaGACCGGTGCTTGC
ACTGGTTGGATtAGTGGCGAACG

GGTGAGTAATACGTGAGTAACCTGCCTTTGACTCTGGGATAAGCCTTGGAAACGA
GGTCTAATACCGGATATGACACAGT

TTCGCATGAAATCTGTGTGGAAAGGGTTTGTACTGGTTTTAGATGGGCTCACGGCC
TATCAGCTTGTTGGTGGGGTAATG

GCTCACCAAGGCGACGACGGGTAGCCGGCCTGAGAGGGTGACCGGCCACACTG
GGACTGAGACACGGCCCAGACTCCTAC

GGGAGGCAGCAGTGGGGAATATTGCACAATGGGCGCAAGCCTGATGCAGCGACG
CCGCGTGAGGGATGACGGCCTTCGGG

TTGTAAACCTCTTTCAGCAGGGGAGAAGCGAAAGTGACGGTACCTGCAGAAGAAG
CGCCGGCTAACTACGTGCCAGCAGC

CGCGGTAATACGTAGGGCGCGAGCGTTGTCCGGAATTATTGGGCGTAAAGAGCTT
GTAGGCGGTTTGTCGCGTCTGCTGT

GAAAGCCCGGGGCTTAACTCCGGGTTTGCAGTGGGTACGGGCTAACTAGAGTGCA
GTAGGGGAGACTGGAATTCCTGGTG

TAGCGGTGGAATGCGCAGATATCAGGAGGAACACCGATGGCGAAGGCAGGTCTC
TGGGCTGTAACTGACGCTGAGAAGCG

AAAGCATGGGGAGCGAACAGGATTAGATACCCTGGTAGTCCATGCCGTAAACGTT
GGGCACTAGGTGTGGGGGACATTCC

ACGTTTTCCGCGCCGTAGCTAACGCATTAAGTGCCCCGCCTGGGGAGTACGGTCG
CAAGGCTAAAACTCAAAGGATTGAA

CNGG

Beige colony:

NNNNNNNNNTGcgcgtGCCTAATACaTGCaGTCGAGCGaNTGNattAAGAGCTTGCTCTTATGAAGTTAGCGGCGGacGG

GTGAGTAACACGTGGGTAACCTGCCCATAAGACTGGGATAACTCCGGGAAACCGGGGCTAATACCGGATAACATTTTGAA

CCGCATGGTTCGAAATTGAAAGGCGGCTTCGGCTGTCACTTATGGATGGACCCGCGTCGCATTAGCTAGTTGGTGAGGTA

ACGGCTCACCAAGGCAACGATGCGTAGCCGACCTGAGAGGGTGATCGGCCACACTGGGACTGAGACACGGCCCAGACTCC

TACGGGAGGCAGCAGTAGGGAATCTTCCGCAATGGACGAAAGTCTGACGGAGCAACGCCGCGTGAGTGATGAAGGCTTTC

GGGTCGTAAAACTCTGTTGTTAGGGAAGAACAAGTGCTAGTTGAATAAGCTGGCACCTTGACGGTACCTAACCAGAAAGC

CACGGCTAACTACGTGCCAGCAGCCGCGGTAATACGTAGGTGGCAAGCGTTATCCGGAATTATTGGGCGTAAAGCGCGCG

CAGGTGGTTTCTTAAGTCTGATGTGAAAGCCCACGGCTCAACCGTGGAGGGTCATTGGAAACTGGGAGACTTGAGTGCAG

AAGAGGAAAGTGGAATTCCATGTGTAGCGGTGAAATGCGTAGAGATATGGAGGAACACCAGTGGCGAAgGCGACTTTTCT

GGTCTGTAACTGACACTGAGGCGCGAAAGCGTGGGGAGCAACAGGATTAgATACCCTGGTAGTCCACGCCGTAAACGATG

AGTGCTAAGTGTTAGAGGGTTTTCCGCCCTTTAGTGCTGANGTTAACGCATTAAAGCACTCCGNCTGGGGAGTACGGCCG

CAAGGCTGAAACTCAaANGAatTNGACGGN

Chapter 6 Summary, Conclusions, Limitations, and Future Work

Preface:

This final chapter summarizes the work done in the thesis, as well as discuss the impact of this on the development of antipathogenic and pathogen repellant materials. This will finish off with a discussion of the limitations of the current work and opportunities for future improvements.

6.1 Thesis Summary

The goal of this thesis was to develop and investigate the use of omniphobic surfaces in reducing the physical contamination of surfaces with biological contaminates. Photoactive TiO_2 was integrated into the hierarchical structures to create an additional layer of protection against surface contamination. This study provides insight into the physical adhesion of pathogens to omniphobic surfaces in open-air environments and the dual functional effects of photoactive materials integrated into the surface of repellent structures.

Solution-based and layer-by-layer manufacturing techniques were chosen due to low-cost, scalability, and uniformity. The structural properties and chemical composition of the hierarchical structures were analyzed using scanning electron microcopy (SEM) and energy dispersed spectroscopy (EDS). Liquid repellent properties were characterized through contact angle (CA) and contact angle hysteresis (CAH) measurements with liquids of various surface tensions, including water and hexadecane. The resistance to biological contaminates was analyzed through exposure to blood fouling and pathogen transmission assays. Blood staining and coagulation studies were used to assess the repellent surfaces resistance to blood fouling. Transmission assays as well as SEM

imaging were used to quantify both the quantity of transmitted viral and bacterial pathogens on the repellent surfaces and their antimicrobial effects.

We have demonstrated that repellent materials, with omniphobic properties, can repel a wide variety of biological contaminates including blood, fecal matter, bacteria, and viruses. Modification of the surface structure with photoactive materials was also found to add another layer of antipathogenic effects allowing the surfaces to both repel and kill pathogens.

6.2 Thesis Conclusions

1) Hierarchically structured wrinkled surfaces were developed through solution-based and dip coating methods, resulting in inexpensive and scalable deposition of NP films. These methods allow for the easy tuning of the structure geometry by changing parameters like the size of deposited NPs and the amount of strain applied to the film. The topography of the surface structure can be tailored by changing the size of nano particles used (200 nm-12 nm), with smaller particles allowing for smaller nano and micro scale features, which results in stronger omniphobic properties. The hierarchically structured wrinkled surfaces displayed homogeneous and robust omniphobic wetting properties showing CA > 150^{o} and SA < 5^{o} for water and hexadecane.
2) We investigated the effect of surface texture over multiple length scales (ie. hierarchical structures) in their resistance to biofouling. The hierarchically structured wrinkled omniphobic surface showed significant improvements in anti-

biofouling properties compared to the same micro- and nano-scale features on their own, with a greater than 90% reduction in the adherence of blood to the surface. The presence of hieratical structures also had significant impact on the wettability of the surface structures, with the hierarchical structures (water CA $149.9^{o} \pm 3.7^{o}$) having much stronger liquid repellent properties then the micro (water CA $78^{o} \pm 5.1^{o}$) and nano (water CA $127^{o} \pm 9.4^{o}$) structures. Under dynamic conditions blood cells were unable to adhere to the repellant surface (this was verified though SEM imaging of the surface after flow), while non-hierarchical surface structures were heavily contaminated with blood cells. It is evident from this work that hierarchy in the surface topography is critical in producing strong and robust omniphobic and anti-biofouling properties, under static and dynamic conditions.

3) We showed that hierarchically structured omniphobic surface significantly reduce the physical adsorption of pathogens in open-air environments. The presence of hierarchical surface structures has a significant impact on the interacting surface area of the solid interface, limiting the cohesive interaction of liquids and pathogens with the surface. In this respect, a reduction of greater than 2-log was shown by hierarchical structures with all pathogens. Omniphobic hierarchical structures reduced the adsorption similarly for several pathogenic bacteria species with differing cell morphologies (rod and spherical) and cell membrane structure (Gram-negative and Gram-positive). The strongest pathogen repellant properties were seen for viral pathogens, which showed a roughly 5-log reduction in the adsorption when compared to non-hierarchical materials.

4) Omniphobicity was found to be superior to superhydrophobicity in repelling all forms of biological contamination in open-air environments. Differences in the pathogenic adhesion of bacteria on superhydrophobic vs omniphobic hierarchical structured surfaces was seen from SEM of their surfaces after contamination. Surfaces with only superhydrophobic properties, and no repellency to oils, trap bacterial pathogens inside their surface structures, resulting in higher amounts of pathogen adhesion. Bacterial culture also supported these observations with the omniphobic surface showing a 2.15-log reduction in contact transmission compared to the 1.16-log reduction seen on the superhydrophobic surfaces. Moreover, omniphobic surface structures showed significantly reduced surface biofouling with feces, when compared to superhydrophobic surfaces, which were significantly contaminated. While both have shown reduction in the adhesion of isolated pathogens, superhydrophobic surfaces were unable to prevent the contamination of pathogens when fecal matter was present.
5) Photoactive materials (TiO_2) were integrated into the surface structure of a hierarchically structured omniphobic coating, showing robust dual functional (pathogen repellent and anti-pathogenic) effects. The photoactive hierarchal strictures displayed strong omniphobic (water and hexadecane CA of $159.3^o \pm 1.7^o$ and $150.8^o \pm 3.1^o$ respectively) repellent properties, and displayed no antimicrobial effects under dark conditions. Illumination of the surface with ultraviolet light was able to further reduce the number of physically transferred bacteria from a contaminated stamp by an additional ~2.43-log compared to dark conditions. The combination of highly repellant and photoactive materials significantly reduced

pathogen contamination, compared to the individual effects of these properties, allowing for a combined total reduction in contamination of ~4.87-log.

6.3 Contributions to the Field

The work described in this thesis has led to the following contributions to the field:

Scalable all-solution process for the manufacturing of tunable superhydrophobic and oleophobic materials

Techniques to develop hierarchically structure surfaces with high liquid repellency commonly depend on photolithography,[117] reactive ion etching,[45] electrospinning,[117,278] electrochemical etching/ anodizing,[279,280] and laser ablation[118] in order to create their surface structures. These manufacturing processes suffer from several draw backs including difficulty to scale to large areas and substrate/material restriction.[281] The development of manufacturing methods described here, which utilize the layer-by-layer deposition of NPs[129] and fluorinate coatings onto pre-strained polymer substrates, allows for the inexpensive and scalable functionalizing of superhydrophobic and omniphobic materials. Additionally, these methods allow for the easy coating of pre-strained polymer substrates that have the ability to shrink and conform to any shape, which allows for the easy application of liquid repellent coatings in various areas and environments. Furthermore, manufacturing parameters including NP size (12 nm-200 nm), NP materials (AuNP, SiNP and TiO_2 NP) and chemical modifications (OTS, FS) can be varied to achieve different levels of repellency (liquid and pathogen), geometry of the surface

structure and material properties (such as photoactivity) of the surfaces, as seen throughout the work.

Quantification of the physical transmission of individual pathogens and the simultaneous transmission of multiple different pathogens to surfaces

The quantification of pathogen repellency is typically achieved through biofilm growth assays,[54] inhibition zone assays[282–284] and aqueous/spray contamination assays.[73,285] These methods replicate the adherence of pathogens in aqueous environments or are limited to the testing of individual pathogens at one time, all of which do not simulate the real-world physical transmission of pathogens between surfaces in open air environments. We developed a touch transfer assay which simulated the transmission of pathogens from human fingers to various test materials. The stamps used in this assay were easily functionable with a wide range of individual pathogens and combinations of different pathogens, which allow for the high throughput screening of the pathogen transmission to different materials. This will permit researchers to sample/simulate various contamination conditions and environments, ultimately aiding in the design of repellent surfaces that are tailored for specific situations. This work also displayed one of the first examples of omniphobic surface preventing the physical transmission and adsorption of viral pathogens under physical contact with contaminated solid interfaces.

Enhanced Repellency of omniphobic vs superhydrophobic surfaces

The adhesion of pathogens to surfaces with poor wettability has demonstrated a large disconnect between what is seen experimentally and what is expected theoretically,[95] with theoretical models suggesting that pathogen adhesion should be promoted to these

surfaces while experimentally this is not the case. To this extent, we tested the differences in pathogen adhesion for repellent surfaces with only superhydrophobic (super repellent to only water) properties and those with omniphobic (super repellent to all liquids) properties. We demonstrated that both superhydrophobic and omniphobic materials can significantly reduce the adhesion of virus (both RNA and DNA) and bacteria (both Gram-negative and Gram-positive) pathogens, which the omniphobic materials showing improved performance. The benefit of omniphobic *versus* superhydrophobic surfaces was further evident through SEM of the surface, which showed that a significant portion of the contamination of bacterial pathogens on superhydrophobic surfaces were found trapped within the repellant surface structure. The superhydrophobic material also lost all repellent properties under contamination with bacteria latent fecal matter, while the omniphobic materials were able to maintain the pathogen repellency.

Light stimulated antipathogenic properties integrated into omniphobic surface structures

While pathogen repellent materials have shown a great ability to prevent the initial adhesion of pathogens to their surface,[31,42,54] they suffer from some significant drawbacks. Specifically, damage or defects to the surface structure will lead to a buildup of contaminants,[50] environmental instability in the repelling phenomena,[35,36] and breakdown in repellency at sufficiently large pathogen concentrations.[50] In this work, we explored the use of photoactive NPs that are integrated into the hierarchical structure of the omniphobic material to address these issues. This was achieved by the addition of TiO_2 into the surface structure, which displayed both reduced adhesion of pathogens through physical contact and surface decontamination under UV exposure. The reduced adhesion of pathogens resulted from the hierarchical and omniphobic structures made by

the Fluorinated TiO_2 NPs, while the self-decontaminating properties arose from the photoactivity of the TiO_2 NPs in the surface. Interestingly, the combination of the photoactive material and omniphobic properties displayed an enhancement of antipathogenic effects of the surface under light exposure, which was not seen on the superhydrophobic versions of the surface.

6.4 Future Work

Mechanistic study on the adhesion of pathogens to surface with superhydrophobic and omniphobic properties

In chapter 2, we discussed the mechanisms of pathogen adhesion and the different models which have been developed in order to select and design materials capable of preventing and/or significantly reducing this adhesion. The issue with the discussed models is that they only describe the interaction of pathogenic particles with planar smooth surfaces. In fact, it is well understood in the literature that there is a disconnect between adhesion predicted observed on superhydrophobic and omniphobic surfaces.[95] This disconnect arises as the hydrophobic interactions between the pathogens and the solid-liquid interfaces of superhydrophobic and omniphobic surfaces predict that these materials should favor the adhesion of pathogens.[95] However, in both chapter 4 and 5 this was not observed, and similar observations of superhydrophobic and omniphobic surface pathogen repelling properties have also been seen throughout the literature.[42,54,95,271] In order to better characterize the interaction of pathogen-surface adhesion on superhydrophobic and omniphobic materials, an in-depth study comparing

the adhesion of various pathogens with different wetting states and material surface energies should be conducted.

With the methods of creating tunable wrinkled hierarchical structures employed throughout this work, we can create surfaces with a variety of wetting properties; hydrophobic-oleophobic, superhydrophobic-oleophilic, superhydrophobic and oleophobic, and omniphobic, which all have similar surface structure. By combining this with the pathogen touch transfer assay we have developed, we can directly compare the number of pathogens transferred to the surface with their wettability, and look for models which describe the observed pathogen transfer to these surfaces. Specifically, we can use the wettability data to determine the surface tension components of both the bacteria and the repellant materials, which has been done extensively with planar materials in order to relate wettability and pathogen adhesion.[37,109] Gaining a better understanding of the physical interactions and mechanisms of pathogen adhesion at hierarchically structured repellent interfaces may lead to improved or new methods or approaches in reducing the adhesion of pathogens to surfaces.

Integrating visible light adsorbing photoactive materials into omniphobic surfaces

In chapter 5 we integrated photoactive TiO_2 into the hierarchical structure of the repellant surfaces. These showed great performance in reducing the contamination of pathogens, under both physical contact and light exposure. However, the TiO_2 was only able to decontaminate the surface under exposure to UV light, which has a few draw backs; low-levels or lack of ambient UV light in the environment will limit the antimicrobial properties

of surfaces and UV light can be damaging to human eyes, depending on the intensity. To address these issues the use of visible light adsorbing photoactive materials should be used, which will allow for the passive and continuous decontamination of the surface from ambient light in the environment.

One way to achieve this would be to modify the integrated TiO_2 NP so they are visible light adsorbent. This can be done by functionalizing the TiO2 NP with catechol ligands.[134] Catechol's are benzene derivatives with two adjacent hydroxyl groups,[286] and are known for their great adhesive and oxidative properties.[286–288] Catechol based molecules readily bond to metal oxides and have been used extensively in photoelectron chemistry to change the light absorption of TiO_2.[289] Particularly, the catechol's 3,4-dihydroxybenzaldehyde (DHBA) and Caffeic Acid have shown to significantly shift the absorption spectra of TiO_2,[273,290] as well have shown to significantly increase the photocurrent generation.[290] Furthermore, catechols have been used for antimicrobial coatings as catechol oxidation produces significant ROS,[291] making them excellent candidates for dual-functional surfaces.

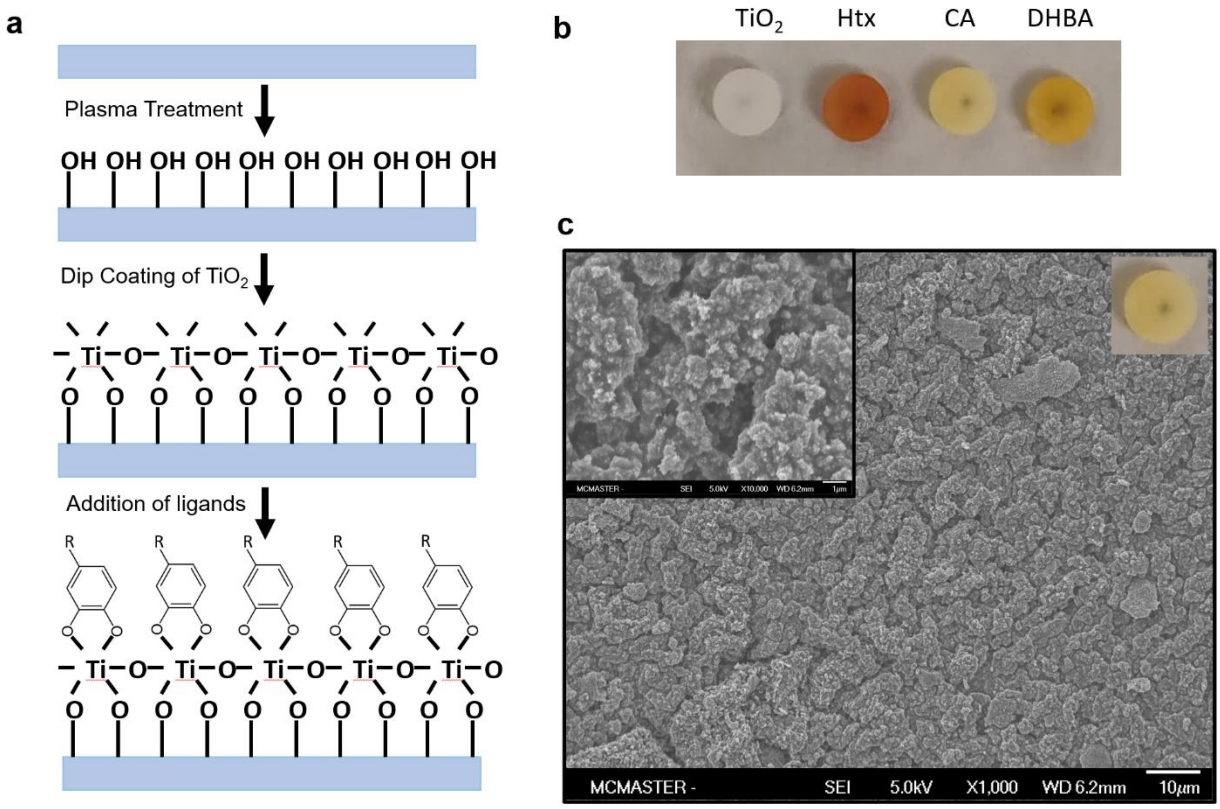

Figure 6-1: Modification of TiO_2 coated PO with catechols a) Schematic of the surface manufacturing b) TiO_2 surface modified with different catechols c) SEM of CA modified TiO_2 surface.

Following the dip-coating of TiO_2 NP as seen in chapter 5, we can create a uniform TiO_2 film which can be easily functionalized by submerging it in the catechol solution for 30s (Figure 6-1a). Figure 6-1b shows the TiO_2 surface with three different catechol modifications (Hematoxylin (red), DHBA (orange) and CA (yellow)), to which the shift in the adsorption spectra can be seen visually with the change in colour of the surface. These catechol modified surfaces also all show superhydrophobicity and a robust wrinkled microstructure when shrunk (Figure 6-1c).

Wrinkling without shrinking

One of the key issues with the designed material systems in this work is the requirement for a prestrained polymer substrate in order to form the hierarchical wrinkled microstructure. In order to create the hierarchical surface structure, the substrates were heated above the glass transition temperature, causing them to shrink significantly, with the PS substrates used in chapter 2 shrinking by 60% and the PO substrates used in chapter 4 and 5 shrinking by 90%. This process results in a significant increase in the cost of manufacturing for these materials because the final usable surface area of the coating is significantly lower than that of the functionalized polymer film. To solve this issue, investigations should be done into creating a manufacturing method of hierarchical wrinkles which do not require the straining of the polymer substrate in order to form. To create spontaneous wrinkles without thermal shrinking of the polymer substrate, the following techniques have been developed:

1) Wrinkling of Hydrogel Films: Generally, the wrinkles are induced by generating internal stress and strain throughout the hydrogel film. This has been achieved in two main ways: curing of the film during dehydration of the hydrogel[130] and photo-cross-linking of the hydrogel at the surface.[292,293] In the first case, partial dehydration of the film is done (through vacuum and heat exposure) creating a strain gradient across the film. The surface is then exposed to UV light until the hydrogel is fully cured, causing the film to hold the wrinkle structure. In the second case, photo initiators are diffused into the surface and activated with UV light. This results in cross linking and stiffening of the upper portions of the film, creating a strain gradient and wrinkling formation at the surface.[292,293]

2) Wrinkling of polyelectrolyte multilayer films: In this process, two polyelectrolyte chains are deposited simultaneously onto the substrate surface. The electrostatic interactions of these chains can cause instability within the film.[294] These instabilities can be exaggerated by swelling the films, which creates significant internal stresses resulting in the formation of wrinkles.[295] Once swollen, these layers can be crosslinked together, allowing the film to hold its wrinkled structure.[294–296]

These processes involve creating internal stress/strain gradients throughout the coating, which causes the formation of the micro wrinkle structure. Combining these wrinkling methods with the NP functionalization and fluorination process discussed throughout this thesis may result in unique and easy to manufacture hierarchical and repellant surface structures.

6.5 References

(1) Kramer, A.; Schwebke, I.; Kampf, G. How Long Do Nosocomial Pathogens Persist on Inanimate Surfaces? A Systematic Review. *BMC Infect. Dis.* **2006**, *6* (1), 1–8. https://doi.org/10.1186/1471-2334-6-130/TABLES/3.

(2) Casadevall, A.; Pirofski, L. A. What Is a Pathogen? *https://doi.org/10.1080/078538902317338580* **2009**, *34* (1), 2–4. https://doi.org/10.1080/078538902317338580.

(3) Khan, H. A.; Ahmad, A.; Mehboob, R. Nosocomial Infections and Their Control Strategies. *Asian Pac. J. Trop. Biomed.* **2015**, *5* (7), 509–514. https://doi.org/10.1016/J.APJTB.2015.05.001.

(4) Inweregbu, K.; Dave, J.; Pittard, A. Nosocomial Infections. *Contin. Educ. Anaesthesia, Crit. Care Pain* **2005**, *5* (1), 14–17. https://doi.org/10.1093/BJACEACCP/MKI006.

(5) Vasickova, P.; Pavlik, I.; Verani, M.; Carducci, A. Issues Concerning Survival of Viruses on Surfaces. *Food and Environmental Virology*. Nature Publishing Group March 2010, pp 24–34. https://doi.org/10.1007/s12560-010-9025-6.

(6) Wang, C. C.; Prather, K. A.; Sznitman, J.; Jimenez, J. L.; Lakdawala, S. S.; Tufekci, Z.; Marr, L. C. Airborne Transmission of Respiratory Viruses. *Science (80-.).* **2021**, *373* (6558). https://doi.org/10.1126/SCIENCE.ABD9149/ASSET/9C00F9CB-FB7F-479D-BF56-5719BE0142E9/ASSETS/IMAGES/LARGE/SCIENCE.ABD9149-F5.JPG.

(7) Pierce, A. K.; Sanford, J. P. Bacterial Contamination of Aerosols. *Arch. Intern. Med.* **1973**, *131* (1), 156–159. https://doi.org/10.1001/ARCHINTE.1973.00320070152017.

(8) Oswin, H. P.; Haddrell, A. E.; Otero-Fernandez, M.; Cogan, T. A.; Mann, J. F. S.; Morley, C. H.; Hill, D. J.; Davidson, A. D.; Finn, A.; Thomas, R. J.; Reid, J. P. Measuring Stability of Virus in Aerosols under Varying Environmental Conditions. *Aerosol Sci. Technol.* **2021**, *55* (12), 1315–1320. https://doi.org/10.1080/02786826.2021.1976718/SUPPL_FILE/UAST_A_1976718_SM8800.PDF.

(9) Weber, T. P.; Stilianakis, N. I. Inactivation of Influenza A Viruses in the Environment and Modes of Transmission: A Critical Review. *Journal of Infection*. J Infect November 2008, pp 361–373. https://doi.org/10.1016/j.jinf.2008.08.013.

(10) Boone, S. A.; Gerba, C. P. Significance of Fomites in the Spread of Respiratory and Enteric Viral Disease. *Applied and Environmental Microbiology*. American Society for Microbiology March 15, 2007, pp 1687–1696. https://doi.org/10.1128/AEM.02051-06.

(11) Sattar, S. A.; Khalid Ijaz, M.; Gerba, C. P. Spread of Viral Infections by Aerosols. *Crit. Rev. Environ. Sci. Technol.* **1987**, *17* (2), 89–131. https://doi.org/10.1080/10643388709388331.

(12) Killingley, B.; Nguyen-Van-Tam, J. Routes of Influenza Transmission. *Influenza Other Respi. Viruses* **2013**, *7*, 42–51. https://doi.org/10.1111/irv.12080.

(13) Cheng, C. H.; Chow, C. L.; Chow, W. K. Trajectories of Large Respiratory Droplets in Indoor Environment: A Simplified Approach. *Build. Environ.* **2020**, *183*, 107196. https://doi.org/10.1016/j.buildenv.2020.107196.

(14) Jaradat, Z. W.; Ababneh, Q. O.; Sha, S. T.; Alkofahi, A. A.; Assaleh, D.; Al Shara, A. Methicillin Resistant Staphylococcus Aureus and Public Fomites: A Review. **2020**. https://doi.org/10.1080/20477724.2020.1824112.

(15) Wißmann, J. E.; Kirchhoff, L.; Brüggemann, Y.; Todt, D.; Steinmann, J.; Steinmann, E. Microorganisms Persistence of Pathogens on Inanimate Surfaces: A Narrative Review. **2021**. https://doi.org/10.3390/microorganisms9020343.

(16) Joshi, M.; Kaur, S. NOSOCOMIAL INFECTION : SOURCE AND PREVENTION. *Int. J. Pharm. Sci. Res.* **2019**, *10* (January), 1613–1624. https://doi.org/10.13040/IJPSR.0975-8232.10(4).1613-24.

(17) Bandara, H. M. H. N.; Samaranayake, L. P. Emerging Strategies for Environmental Decontamination of the Nosocomial Fungal Pathogen Candida Auris. *J. Med. Microbiol.* **2022**, *71*, 1548. https://doi.org/10.1099/jmm.0.001548.

(18) Kollef, M. H.; Torres, A.; Shorr, A. F.; Martin-Loeches, I.; Micek, S. T. Nosocomial Infection. *Crit. Care Med.* **2021**, *49* (2), 169–187. https://doi.org/10.1097/CCM.0000000000004783.

(19) Kotwal, G.; Cannon, J. L. Environmental Persistence and Transfer of Enteric Viruses. *Curr. Opin. Virol.* **2014**, *4*, 37–43. https://doi.org/10.1016/J.COVIRO.2013.12.003.

(20) Kim, M. J.; Linstadt, R. T. H.; Ahn Ando, K.; Ahn, J. Gemini-Mediated Self-Disinfecting Surfaces to Address the Contact Transmission of Infectious Diseases. *Langmuir* **2022**, *38* (6), 2162–2173. https://doi.org/10.1021/ACS.LANGMUIR.1C03401/ASSET/IMAGES/LARGE/LA1C03401_0009.JPEG.

(21) Parveen, N.; Chowdhury, S.; Goel, S. Environmental Impacts of the Widespread Use of Chlorine-Based Disinfectants during the COVID-19 Pandemic. *Environ. Sci. Pollut. Res.* **2022**, *29* (57), 85742–85760. https://doi.org/10.1007/S11356-021-18316-2/TABLES/1.

(22) Rideout, K.; Teschke, K.; Dimich-Ward, H.; Kennedy, S. M. Considering Risks to Healthcare Workers from Glutaraldehyde Alternatives in High-Level Disinfection. *J. Hosp. Infect.* **2005**, *59* (1), 4–11. https://doi.org/10.1016/j.jhin.2004.07.003.

(23) Kuchinka, J.; Willems, C.; Telyshev, D. V.; Groth, T. Control of Blood Coagulation by Hemocompatible Material Surfaces—A Review. *Bioeng. 2021, Vol. 8, Page 215* **2021**, *8* (12), 215. https://doi.org/10.3390/BIOENGINEERING8120215.

(24) Wu, X. H.; Liew, Y. K.; Mai, C. W.; Then, Y. Y. Potential of Superhydrophobic Surface for Blood-Contacting Medical Devices. *Int. J. Mol. Sci. 2021, Vol. 22,*

Page 3341 **2021**, *22* (7), 3341. https://doi.org/10.3390/IJMS22073341.

(25) Biran, R.; Pond, D. Heparin Coatings for Improving Blood Compatibility of Medical Devices. *Adv. Drug Deliv. Rev.* **2017**, *112*, 12–23.

(26) Jokinen, V.; Kankuri, E.; Hoshian, S.; Franssila, S.; Ras, R. H. A. Superhydrophobic Blood-Repellent Surfaces. *Adv. Mater.* **2018**, *30* (24), 1705104. https://doi.org/10.1002/adma.201705104.

(27) Wada, T.; Ishihama, K.; Yonemitsu, K.; Sumioka, S.; Yamada, C.; Higuchi, M.; Kogo, M. Blood Contamination of Environmental Surfaces in Outpatient Oral Surgery Operatory. *Asian J. Oral Maxillofac. Surg.* **2010**, *22* (1), 12–16. https://doi.org/10.1016/J.AJOMS.2009.07.001.

(28) Hota, B. Contamination, Disinfection, and Cross-Colonization: Are Hospital Surfaces Reservoirs for Nosocomial Infection?

(29) Obenza, A.; Cruz, P.; Buttner, M.; Woodard, D. Microbial Contamination on Ambulance Surfaces: A Systematic Literature Review. *J. Hosp. Infect.* **2022**, *122*, 44–59. https://doi.org/10.1016/j.jhin.2021.12.020.

(30) Song, L.; Sun, L.; Zhao, J.; Wang, X.; Yin, J.; Luan, S.; Ming, W. Synergistic Superhydrophobic and Photodynamic Cotton Textiles with Remarkable Antibacterial Activities. **2019**. https://doi.org/10.1021/acsabm.9b00149.

(31) Imani, S. M.; Ladouceur, L.; Marshall, T.; Maclachlan, R.; Soleymani, L.; Didar, T. F. *Antimicrobial Nanomaterials and Coatings: Current Mechanisms and Future Perspectives to Control the Spread of Viruses Including SARS-CoV-2*; American Chemical Society, 2020; Vol. 14, pp 12341–12369. https://doi.org/10.1021/acsnano.0c05937.

(32) Hori, K.; Matsumoto, S. Bacterial Adhesion: From Mechanism to Control. *Biochem. Eng. J.* **2010**, *48* (3), 424–434. https://doi.org/10.1016/J.BEJ.2009.11.014.

(33) Katsikogianni, M.; Missirlis, Y. F.; Harris, L.; Douglas, J. Concise Review of Mechanisms of Bacterial Adhesion to Biomaterials and of Techniques Used in Estimating Bacteria-Material Interactions. *Eur. Cells Mater.* **2004**, *8*, 37–57. https://doi.org/10.22203/eCM.v008a05.

(34) Stiefel, U.; Donskey, C. J. The Role of the Intestinal Tract As a Source for Transmission of Nosocomial Pathogens. **2004**.

(35) Kim, P.; Kreder, M. J.; Alvarenga, J.; Aizenberg, J. Hierarchical or Not? Effect of the Length Scale and Hierarchy of the Surface Roughness on Omniphobicity of Lubricant-Infused Substrates. *Nano Lett.* **2013**, *13* (4), 1793–1799.

(36) Wang, T.; Wang, Z. Liquid-Repellent Surfaces. *Langmuir* **2022**, *38* (30), 9073–9084. https://doi.org/10.1021/ACS.LANGMUIR.2C01533/ASSET/IMAGES/MEDIUM/LA2C01533_0009.GIF.

(37) Oss, C. J. van. *Interfacial Forces in Aqueous Media*; 2006.

(38) Villegas, M.; Zhang, Y.; Abu Jarad, N.; Soleymani, L.; Didar, T. F. Liquid-Infused Surfaces: A Review of Theory, Design, and Applications. *ACS Nano* **2019**, *13* (8), 8517–8536.

(39) Nokes, J. M.; Liedert, R.; Kim, M. Y.; Siddiqui, A.; Chu, M.; Lee, E. K.; Khine, M. Reduced Blood Coagulation on Roll-to-Roll, Shrink-Induced Superhydrophobic Plastics. *Adv. Healthc. Mater.* **2016**, *5* (5), 593–601. https://doi.org/10.1002/ADHM.201500697.

(40) Tesler, A. B.; Kim, P.; Kolle, S.; Howell, C.; Ahanotu, O.; Aizenberg, J. Extremely Durable Biofouling-Resistant Metallic Surfaces Based on Electrodeposited Nanoporous Tungstite Films on Steel. *Nat. Commun.* **2015**, *6* (1), 1–10. https://doi.org/10.1038/ncomms9649.

(41) Lee, J.; Yoo, J.; Kim, J.; Jang, Y.; Shin, K.; Ha, E.; Ryu, S.; Kim, B. G.; Wooh, S.; Char, K. Development of Multimodal Antibacterial Surfaces Using Porous Amine-Reactive Films Incorporating Lubricant and Silver Nanoparticles. *ACS Appl. Mater. Interfaces* **2019**. https://doi.org/10.1021/ACSAMI.8B20092/ASSET/IMAGES/LARGE/AM-2018-20092Z_0006.JPEG.

(42) Khan, S.; Jarad, A.; Ladouceur, L.; Rachwalski, K.; Bot, V.; Shakeri, A.; Maclachlan, R.; Sakib, S.; Weitz, J. I.; Brown, E. D.; Soleymani, L.; Didar, T. F.; Khan, S.; Jarad, N. A.; Ladouceur, L.; Bot, V.; Soleymani, L.; Didar, T. F.; Rachwalski, K.; Brown, E. D.; Shakeri, A.; Maclachlan, R.; Sakib, S.; Weitz, J. I. 2108112 (1 of 12) Transparent and Highly Flexible Hierarchically Structured Polydimethylsiloxane Surfaces Suppress Bacterial Attachment and Thrombosis Under Static and Dynamic Conditions. **2022**. https://doi.org/10.1002/smll.202108112.

(43) Yong, J.; Chen, F.; Yang, Q.; Huo, J.; Hou, X. Superoleophobic Surfaces. *Chem. Soc. Rev.* **2017**, *46* (14), 4168–4217. https://doi.org/10.1039/C6CS00751A.

(44) Rolo, L. I.; Caç, A. I.; nio Queimada, A. J.; Marrucho, I. M.; P Coutinho, J. A. Surface Tension of Heptane, Decane, Hexadecane, Eicosane, and Some of Their Binary Mixtures. **2002**. https://doi.org/10.1021/je025536.

(45) Mazumder, P.; Jiang, Y.; Baker, D.; Carrilero, A.; Tulli, D.; Infante, D.; Hunt, A. T.; Pruneri, V. Superomniphobic, Transparent, and Antireflection Surfaces Based on Hierarchical Nanostructures. *Nano Lett.* **2014**, *14* (8), 4677–4681. https://doi.org/10.1021/nl501767j.

(46) Pan, S.; Kota, A. K.; Mabry, J. M.; Tuteja, A. Superomniphobic Surfaces for Effective Chemical Shielding. *J. Am. Chem. Soc.* **2013**, *135* (2), 578–581. https://doi.org/10.1021/JA310517S/SUPPL_FILE/JA310517S_SI_005.AVI.

(47) Huang, X.; Chrisman, J. D.; Zacharia, N. S. Omniphobic Slippery Coatings Based on Lubricant-Infused Porous Polyelectrolyte Multilayers. *ACS Macro Lett.* **2013**, *2* (9), 826–829.

https://doi.org/10.1021/MZ400387W/SUPPL_FILE/MZ400387W_SI_007.MPG.

(48) Badv, M.; Imani, S. M.; Weitz, J. I.; Didar, T. F. Lubricant-Infused Surfaces with Built-In Functional Biomolecules Exhibit Simultaneous Repellency and Tunable Cell Adhesion. *ACS Nano* **2018**, *12* (11), 10890–10902. https://doi.org/10.1021/ACSNANO.8B03938/SUPPL_FILE/NN8B03938_SI_003.AVI.

(49) Yu, M.; Liu, M.; Hou, Y.; Fu, S.; Zhang, L.; Li, M.; Wang, D. Facile Fabrication of Biomimetic Slippery Lubricant-Infused Transparent and Multifunctional Omniphobic Surfaces Chemical Routes to Materials. *J Mater Sci* **2020**, *55*, 4225–4237. https://doi.org/10.1007/s10853-019-04243-8.

(50) Ren, T.; Yang, M.; Wang, K.; Zhang, Y.; He, J. CuO Nanoparticles-Containing Highly Transparent and Superhydrophobic Coatings with Extremely Low Bacterial Adhesion and Excellent Bactericidal Property. *ACS Appl. Mater. Interfaces* **2018**, *10* (30), 25717–25725. https://doi.org/10.1021/ACSAMI.8B09945/ASSET/IMAGES/LARGE/AM-2018-09945W_0002.JPEG.

(51) Jiang, R.; Hao, L.; Song, L.; Tian, L.; Fan, Y.; Zhao, J.; Liu, C.; Ming, W.; Ren, L. Lotus-Leaf-Inspired Hierarchical Structured Surface with Non-Fouling and Mechanical Bactericidal Performances. *Chem. Eng. J.* **2020**, *398*, 125609. https://doi.org/10.1016/j.cej.2020.125609.

(52) Wang, T.; Huang, L.; Liu, Y.; Li, X.; Liu, C.; Handschuh-Wang, S.; Xu, Y.; Zhao, Y.; Tang, Y. Robust Biomimetic Hierarchical Diamond Architecture with a Self-Cleaning, Antibacterial, and Antibiofouling Surface. *Cite This ACS Appl. Mater. Interfaces* **2020**, *12* (21), 24432–24441. https://doi.org/10.1021/acsami.0c02460.

(53) Ozkan, E.; Mondal, A.; Singha, P.; Douglass, M.; Hopkins, S. P.; Devine, R.; Garren, M.; Manuel, J.; Warnock, J.; Handa, H. Fabrication of Bacteria-and Blood-Repellent Superhydrophobic Polyurethane Sponge Materials. *Cite This ACS Appl. Mater. Interfaces* **2020**, *12*, 51160–51173. https://doi.org/10.1021/acsami.0c13098.

(54) Imani, S. M.; Maclachlan, R.; Rachwalski, K.; Chan, Y.; Lee, B.; McInnes, M.; Grandfield, K.; Brown, E. D.; Didar, T. F.; Soleymani, L. Flexible Hierarchical Wraps Repel Drug-Resistant Gram-Negative and Positive Bacteria. *ACS Nano* **2020**, *14* (1), 454–465. https://doi.org/10.1021/acsnano.9b06287.

(55) Schlaich, C.; Cuellar Camacho, L.; Yu, L.; Achazi, K.; Wei, Q.; Haag, R. Surface-Independent Hierarchical Coatings with Superamphiphobic Properties. *ACS Appl. Mater. Interfaces* **2016**, *8* (42), 29117–29127. https://doi.org/10.1021/ACSAMI.6B08487/SUPPL_FILE/AM6B08487_SI_003.MPG.

(56) Doll, K.; Fadeeva, E.; Schaeske, J.; Ehmke, T.; Winkel, A.; Heisterkamp, A.; Chichkov, B. N.; Stiesch, M.; Stumpp, N. S. Development of Laser-Structured Liquid-Infused Titanium with Strong Biofilm-Repellent Properties. *ACS Appl.*

Mater. Interfaces **2017**, *9* (11), 9359–9368. https://doi.org/10.1021/ACSAMI.6B16159/SUPPL_FILE/AM6B16159_SI_001.PDF.

(57) Leslie, D. C.; Waterhouse, A.; Berthet, J. B.; Valentin, T. M.; Watters, A. L.; Jain, A.; Kim, P.; Hatton, B. D.; Nedder, A.; Donovan, K.; Super, E. H.; Howell, C.; Johnson, C. P.; Vu, T. L.; Bolgen, D. E.; Rifai, S.; Hansen, A. R.; Aizenberg, M.; Super, M.; Aizenberg, J.; Ingber, D. E. A Bioinspired Omniphobic Surface Coating on Medical Devices Prevents Thrombosis and Biofouling. *Nat. Biotechnol.* **2014**, *32* (11), 1134–1140. https://doi.org/10.1038/nbt.3020.

(58) Liu, J.; Ye, L.; Sun, Y.; Hu, M.; Chen, F.; Wegner, S.; Mailänder, V.; Steffen, W.; Kappl, M.; Butt, H. J. Elastic Superhydrophobic and Photocatalytic Active Films Used as Blood Repellent Dressing. *Adv. Mater.* **2020**, *32* (11). https://doi.org/10.1002/ADMA.201908008.

(59) Ting Shiu, H.; Goss, B.; Lutton, C.; Crawford, R.; Xiao, Y. Formation of Blood Clot on Biomaterial Implants Influences Bone Healing. https://doi.org/10.1089/ten.teb.2013.0709.

(60) Liu, S.; Zheng, J.; Hao, L.; Yegin, Y.; Bae, M.; Ulugun, B.; Taylor, T. M.; Scholar, E. A.; Cisneros-Zevallos, L.; Oh, J. K.; Akbulut, M. Dual-Functional, Superhydrophobic Coatings with Bacterial Anticontact and Antimicrobial Characteristics. *ACS Appl. Mater. Interfaces* **2020**, *12* (19), 21311–21321. https://doi.org/10.1021/ACSAMI.9B18928/ASSET/IMAGES/LARGE/AM9B18928_0006.JPEG.

(61) Chu, Y.; Wang, Y.; Liu, A.; Chen, G.; Li, W.; Wang, X.; Chu, H.; Wang, L. Dual-Functional Anti-Pathogen Coatings. *Adv. Mater. Interfaces* **2022**, *9* (28), 2200865. https://doi.org/10.1002/ADMI.202200865.

(62) Ding, X. X. K.; Duan, S.; Ding, X. X. K.; Liu, R.; Xu, F.-J. J. F.-J.; Ding, X. X. K.; Duan, S.; Ding, X. X. K.; Xu, F.-J. J. F.-J.; Liu, R. Versatile Antibacterial Materials: An Emerging Arsenal for Combatting Bacterial Pathogens. *Adv. Funct. Mater.* **2018**, *28* (40), 1802140. https://doi.org/10.1002/ADFM.201802140.

(63) Zou, Y.; Zhang, Y.; Yu, Q.; Chen, H. Dual-Function Antibacterial Surfaces to Resist and Kill Bacteria: Painting a Picture with Two Brushes Simultaneously. *J. Mater. Sci. Technol.* **2021**, *70*, 24–38. https://doi.org/10.1016/J.JMST.2020.07.028.

(64) Page, K.; Wilson, M.; Parkin, I. P. Antimicrobial Surfaces and Their Potential in Reducing the Role of the Inanimate Environment in the Incidence of Hospital-Acquired Infections. *J. Mater. Chem.* **2009**, *19* (23), 3819–3831. https://doi.org/10.1039/B818698G.

(65) Yu, Q.; Wu, Z.; Chen, H. Dual-Function Antibacterial Surfaces for Biomedical Applications. *Acta Biomater.* **2015**, *16* (1), 1–13. https://doi.org/10.1016/J.ACTBIO.2015.01.018.

(66) Mishra, J. R.; Samal, S. K.; Mohanty, S.; Nayak, S. K. Polyvinylidene Fluoride

(PVDF)/Ag@TiO2 Nanocomposite Membrane with Enhanced Fouling Resistance and Antibacterial Performance. *Mater. Chem. Phys.* **2021**, *268*, 124723. https://doi.org/10.1016/J.MATCHEMPHYS.2021.124723.

(67) Jarad, N. A.; Imran, H.; Imani, S. M.; Didar, T. F.; Soleymani, L.; Jarad, N. A.; Imani, S. M.; Didar, T. F.; Soleymani, L.; Imran, H. Fabrication of Superamphiphobic Surfaces via Spray Coating; a Review. *Adv. Mater. Technol.* **2022**, *7* (10), 2101702. https://doi.org/10.1002/ADMT.202101702.

(68) Santos, M. R. E.; Mendonça, P. V.; Branco, R.; Sousa, R.; Dias, C.; Serra, A. C.; Fernandes, J. R.; Magalhães, F. D.; Morais, P. V.; Coelho, J. F. J. Light-Activated Antimicrobial Surfaces Using Industrial Varnish Formulations to Mitigate the Incidence of Nosocomial Infections. *ACS Appl. Mater. Interfaces* **2021**, *13* (6), 7567–7579. https://doi.org/10.1021/ACSAMI.0C18930/ASSET/IMAGES/LARGE/AM0C18930_0006.JPEG.

(69) Cheng, G.; Xue, H.; Zhang, Z.; Chen, S.; Jiang, S. A Switchable Biocompatible Polymer Surface with Self-Sterilizing and Nonfouling Capabilities. *Angew. Chemie* **2008**, *120* (46), 8963–8966. https://doi.org/10.1002/ANGE.200803570.

(70) Fu, Y.; Yang, Y.; Xiao, S.; Zhang, L.; Huang, L.; Chen, F.; Fan, P.; Zhong, M.; Tan, J.; Yang, J. Mixed Polymer Brushes with Integrated Antibacterial and Antifouling Properties. *Prog. Org. Coatings* **2019**, *130*, 75–82. https://doi.org/10.1016/J.PORGCOAT.2019.01.038.

(71) Zou, Y.; Lu, K.; Lin, Y.; Wu, Y.; Wang, Y.; Li, L.; Huang, C.; Zhang, Y.; Brash, J. L.; Chen, H.; Yu, Q. Dual-Functional Surfaces Based on an Antifouling Polymer and a Natural Antibiofilm Molecule: Prevention of Biofilm Formation without Using Biocides. *ACS Appl. Mater. Interfaces* **2021**, *13* (38), 45191–45200. https://doi.org/10.1021/ACSAMI.1C10747/ASSET/IMAGES/LARGE/AM1C10747_0007.JPEG.

(72) Gao, C.; Wang, Z.; Jiao, Z.; Wu, Z.; Guo, M.; Wang, Y.; Liu, J.; Zhang, P. Enhancing Antibacterial Capability and Osseointegration of Polyetheretherketone (PEEK) Implants by Dual-Functional Surface Modification. *Mater. Des.* **2021**, *205*, 109733. https://doi.org/10.1016/J.MATDES.2021.109733.

(73) Yan, S.; Luan, S.; Shi, H.; Xu, X.; Zhang, J.; Yuan, S.; Yang, Y.; Yin, J. Hierarchical Polymer Brushes with Dominant Antibacterial Mechanisms Switching from Bactericidal to Bacteria Repellent. *Biomacromolecules* **2016**, *17* (5), 1696–1704. https://doi.org/10.1021/ACS.BIOMAC.6B00115/SUPPL_FILE/BM6B00115_SI_001.PDF.

(74) Yang, H.; Li, G.; Stansbury, J. W.; Zhu, X.; Wang, X.; Nie, J. Smart Antibacterial Surface Made by Photopolymerization. *ACS Appl. Mater. Interfaces* **2016**, *8* (41), 28047–28054. https://doi.org/10.1021/ACSAMI.6B09343/ASSET/IMAGES/MEDIUM/AM-2016-09343Q_0011.GIF.

(75) Wei, T.; Tang, Z.; Yu, Q.; Chen, H. Smart Antibacterial Surfaces with Switchable Bacteria-Killing and Bacteria-Releasing Capabilities. *ACS Appl. Mater. Interfaces* **2017**, *9* (43), 37511–37523. https://doi.org/10.1021/ACSAMI.7B13565.

(76) Koh, E.; Taek Lee, Y. Development of Humidity and PH Responsive Ligand Brush Porous Nanocapsules for Self-Controlled Antibacterial Properties without Cytotoxicity. *Appl. Surf. Sci.* **2021**, *562*, 150133. https://doi.org/10.1016/J.APSUSC.2021.150133.

(77) AF, H.; TS, H.; VN, P. Colloid Particle Formulations for Antimicrobial Applications. *Adv. Colloid Interface Sci.* **2017**, *249*, 134–148. https://doi.org/10.1016/J.CIS.2017.05.012.

(78) He, J.; Kumar, A.; Khan, M.; Lo, I. M. C. Critical Review of Photocatalytic Disinfection of Bacteria: From Noble Metals- and Carbon Nanomaterials-TiO2 Composites to Challenges of Water Characteristics and Strategic Solutions. *Sci. Total Environ.* **2021**, *758*, 143953. https://doi.org/10.1016/J.SCITOTENV.2020.143953.

(79) Mano, T.; Nishimoto, S.; Kameshima, Y.; Miyake, M. Water Treatment Efficacy of Various Metal Oxide Semiconductors for Photocatalytic Ozonation under UV and Visible Light Irradiation. *Chem. Eng. J.* **2015**, *264*, 221–229. https://doi.org/10.1016/J.CEJ.2014.11.088.

(80) Oise Immel, F.; Bauda, P.; Pagnout, C. Insight into the Primary Mode of Action of TiO 2 Nanoparticles on Escherichia Coli in the Dark B ´ Enédicteen´enédicte Sohm. *Proteomics* **2015**, *15*, 98–113. https://doi.org/10.1002/pmic.201400101.

(81) Zhuo, J. Photoactive Chemicals for Antimicrobial Textiles. *Antimicrob. Text.* **2016**, 197–223. https://doi.org/10.1016/B978-0-08-100576-7.00011-0.

(82) Gabardo, C. M.; Zhu, Y.; Soleymani, L.; Moran-Mirabal, J. M. Bench-Top Fabrication of Hierarchically Structured High-Surface-Area Electrodes. *Adv. Funct. Mater.* **2013**, *23* (24), 3030–3039. https://doi.org/10.1002/adfm.201203220.

(83) Gabardo, C. M.; Kwong, A. M.; Soleymani, L. Rapidly Prototyped Multi-Scale Electrodes to Minimize the Voltage Requirements for Bacterial Cell Lysis. *Analyst* **2015**, *140* (5), 1599–1608. https://doi.org/10.1039/c4an02150a.

(84) Rahmawan, Y.; Moon, M.-W.; Kim, K.-S.; Lee, K.-R.; Suh, K.-Y. Wrinkled, Dual-Scale Structures of Diamond-Like Carbon (DLC) for Superhydrophobicity. *Langmuir* **2010**, *26* (1), 484–491. https://doi.org/10.1021/la902129k.

(85) Zhang, W.; Gao, J.; Deng, Y.; Peng, L.; Yi, P.; Lai, X.; Lin, Z. Tunable Superhydrophobicity from 3D Hierarchically Nano-Wrinkled Micro-Pyramidal Architectures. *Adv. Funct. Mater.* **2021**, *31* (24), 2101068. https://doi.org/10.1002/ADFM.202101068.

(86) Scarratt, L. R. J.; Hoatson, B. S.; Wood, E. S.; Hawkett, B. S.; Neto, C. Durable Superhydrophobic Surfaces via Spontaneous Wrinkling of Teflon AF. **2016**. https://doi.org/10.1021/acsami.5b12165.

(87) Li, Y.; Dai, S.; John, J.; Carter, K. R. Superhydrophobic Surfaces from Hierarchically Structured Wrinkled Polymers. *ACS Appl. Mater. Interfaces* **2013**, *5* (21), 11066–11073. https://doi.org/10.1021/AM403209R/ASSET/IMAGES/MEDIUM/AM-2013-03209R_0010.GIF.

(88) Chu, Z.; Jiao, W.; Huang, Y.; Ding, G.; Zhong, X.; Yan, M.; Zheng, Y.; Wang, R. FDTS-Modified SiO2/RGO Wrinkled Films with a Micro-Nanoscale Hierarchical Structure and Anti-Icing/Deicing Properties under Condensation Condition. *Adv. Mater. Interfaces* **2020**, *7* (1), 1901446.

(89) Chen, T.-L.; Huang, C.-Y.; Xie, Y.-T.; Chiang, Y.-Y.; Chen, Y.-M.; Hsueh, H.-Y. Bioinspired Durable Superhydrophobic Surface from a Hierarchically Wrinkled Nanoporous Polymer. *ACS Appl. Mater. Interfaces* **2019**, *11*, 40875–40885. https://doi.org/10.1021/acsami.9b14325.

(90) Lee, W. K.; Jung, W. Bin; Nagel, S. R.; Odom, T. W. Stretchable Superhydrophobicity from Monolithic, Three-Dimensional Hierarchical Wrinkles. *Nano Lett.* **2016**, *16* (6), 3774–3779. https://doi.org/10.1021/ACS.NANOLETT.6B01169/SUPPL_FILE/NL6B01169_SI_006.AVI.

(91) Yun, G. T.; Jung, W. Bin; Oh, M. S.; Jang, G. M.; Baek, J.; Kim, N. I.; Im, S. G.; Jung, H. T. Springtail-Inspired Superomniphobic Surface with Extreme Pressure Resistance. *Sci. Adv.* **2018**, *4* (8), 4978–5002. https://doi.org/10.1126/SCIADV.AAT4978/SUPPL_FILE/AAT4978_SM.PDF.

(92) Chibowski, E. Surface Free Energy of a Solid from Contact Angle Hysteresis. *Adv. Colloid Interface Sci.* **2003**, *103* (2), 149–172. https://doi.org/10.1016/S0001-8686(02)00093-3.

(93) Gusnaniar, N.; van der Mei, H. C.; Qu, W.; Nuryastuti, T.; Hooymans, J. M. M.; Sjollema, J.; Busscher, H. J. Physico-Chemistry of Bacterial Transmission versus Adhesion. *Adv. Colloid Interface Sci.* **2017**, *250*, 15–24. https://doi.org/10.1016/J.CIS.2017.11.002.

(94) Hwang, G. B.; Page, K.; Patir, A.; Nair, S. P.; Allan, E.; Parkin, I. P. The Anti-Biofouling Properties of Superhydrophobic Surfaces Are Short-Lived. *ACS Nano* **2018**, *12*, 46. https://doi.org/10.1021/acsnano.8b02293.

(95) Liu, L.; Xiao, Z.; Liu, Y.; Li, X.; Yin, H.; Volkov, A.; He, T. Understanding the Fouling/Scaling Resistance of Superhydrophobic/Omniphobic Membranes in Membrane Distillation. *Desalination* **2021**, *499*, 114864. https://doi.org/10.1016/J.DESAL.2020.114864.

(96) Marmur, A. Hydro- Hygro- Oleo- Omni-Phobic? Terminology of Wettability Classification. *Soft Matter* **2012**, *8* (26), 6867–6870. https://doi.org/10.1039/C2SM25443C.

(97) Wang, H.; Zhang, Z.; Wang, Z.; Zhao, J.; Liang, Y.; Li, X.; Ren, L. Improved Dynamic Stability of Superomniphobic Surfaces and Droplet Transport on

Slippery Surfaces by Dual-Scale Re-Entrant Structures. *Chem. Eng. J.* **2020**, *394*, 124871. https://doi.org/10.1016/J.CEJ.2020.124871.

(98) Pierce, E.; Carmona, F. J.; Amirfazli, A. Understanding of Sliding and Contact Angle Results in Tilted Plate Experiments. *Colloids Surfaces A Physicochem. Eng. Asp.* **2008**, *323* (1–3), 73–82. https://doi.org/10.1016/j.colsurfa.2007.09.032.

(99) Janssen, D.; De Palma, R.; Verlaak, S.; Heremans, P.; Dehaen, W. Static Solvent Contact Angle Measurements, Surface Free Energy and Wettability Determination of Various Self-Assembled Monolayers on Silicon Dioxide. *Thin Solid Films* **2006**, *515* (4), 1433–1438. https://doi.org/10.1016/J.TSF.2006.04.006.

(100) Bhushan, B.; Hansford, D.; Lee, K. K. Surface Modification of Silicon and Polydimethylsiloxane Surfaces with Vapor-Phase-Deposited Ultrathin Fluorosilane Films for Biomedical Nanodevices. *J. Vac. Sci. Technol. A Vacuum, Surfaces, Film.* **2006**, *24* (4), 1197. https://doi.org/10.1116/1.2167077.

(101) Mannelli, I.; Reigada, R.; Suárez, I.; Janner, D.; Carrilero, A.; Mazumder, P.; Sagués, F.; Pruneri, V.; Lakadamyali, M. Functionalized Surfaces with Tailored Wettability Determine Influenza A Infectivity. *ACS Appl. Mater. Interfaces* **2016**, *8* (24), 15058–15066. https://doi.org/10.1021/acsami.6b02779.

(102) Hornyak, G. L.; Rao, A. K. Fundamentals of Nanoscience (and Nanotechnology). *Nanosci. Dermatology* **2016**, 15–29. https://doi.org/10.1016/B978-0-12-802926-8.00002-1.

(103) Jiaqiang, E.; Jin, Y.; Deng, Y.; Zuo, W.; Zhao, X.; Han, D.; Peng, Q.; Zhang, Z. Wetting Models and Working Mechanisms of Typical Surfaces Existing in Nature and Their Application on Superhydrophobic Surfaces: A Review. *Adv. Mater. Interfaces* **2018**, *5* (1), 1701052. https://doi.org/10.1002/ADMI.201701052.

(104) Zhang, X.; Shi, F.; Niu, J.; Jiang, Y.; Wang, Z. Superhydrophobic Surfaces: From Structural Control to Functional Application. *J. Mater. Chem.* **2008**, *18* (6), 621–633. https://doi.org/10.1039/B711226B.

(105) Teisala, H.; Butt, H. J. Hierarchical Structures for Superhydrophobic and Superoleophobic Surfaces. *Langmuir* **2019**, *35* (33), 10689–10703. https://doi.org/10.1021/ACS.LANGMUIR.8B03088/ASSET/IMAGES/LARGE/LA-2018-03088C_0002.JPEG.

(106) Yoon, Y.; Kim, D.; Lee, J.-B. Hierarchical Micro/Nano Structures for Super-Hydrophobic Surfaces and Super-Lyophobic Surface against Liquid Metal. **2014**. https://doi.org/10.1186/s40486-014-0003-x.

(107) Chen, X.; Kong, L.; Dong, D.; Yang, G.; Yu, L.; Chenand, J.; Zhang, P. Fabrication of Functionalized Copper Compound Hierarchical Structure with Bionic Superhydrophobic Properties. *J. Phys. Chem. C* **2009**, *113* (14), 5396–5401. https://doi.org/10.1021/JP809616D/SUPPL_FILE/JP809616D_SI_001.PDF.

(108) Mallick, D.; Gupta, D.; Sharma, S. Transfer of Bacteria between Fabric and Surrogate Skin. *Am. J. Infect. Control* **2022**, *50* (7), 758–763.

https://doi.org/10.1016/j.ajic.2021.10.040.

(109) R Moreira, J. M.; Simões, M.; Melo, L. F.; Mergulhão, F. J. Escherichia Coli Adhesion to Surfaces-a Thermodynamic Assessment. https://doi.org/10.1007/s00396-014-3390-x.

(110) Ubbink, J.; Schär-Zammaretti, P. Colloidal Properties and Specific Interactions of Bacterial Surfaces. *Curr. Opin. Colloid Interface Sci.* **2007**, *12* (4–5), 263–270. https://doi.org/10.1016/J.COCIS.2007.08.004.

(111) Yang, K.; Shi, J.; Wang, L.; Chen, Y.; Liang, C.; Yang, L.; Wang, L. N. Bacterial Anti-Adhesion Surface Design: Surface Patterning, Roughness and Wettability: A Review. *J. Mater. Sci. Technol.* **2022**, *99*, 82–100. https://doi.org/10.1016/J.JMST.2021.05.028.

(112) Crick, C. R.; Ismail, S.; Pratten, J.; Parkin, I. P. An Investigation into Bacterial Attachment to an Elastomeric Superhydrophobic Surface Prepared via Aerosol Assisted Deposition. *Thin Solid Films* **2011**, *519* (11), 3722–3727. https://doi.org/10.1016/J.TSF.2011.01.282.

(113) Zhang, X.; Wang, L.; Levänen, E. Superhydrophobic Surfaces for the Reduction of Bacterial Adhesion. *RSC Advances*. Royal Society of Chemistry August 14, 2013, pp 12003–12020. https://doi.org/10.1039/c3ra40497h.

(114) De Los Santos Pereira, A.; Sheikh, S.; Blaszykowski, C.; Pop-Georgievski, O.; Fedorov, K.; Thompson, M.; Rodriguez-Emmenegger, C. Antifouling Polymer Brushes Displaying Antithrombogenic Surface Properties. *Biomacromolecules* **2016**, *17* (3), 1179–1185. https://doi.org/10.1021/ACS.BIOMAC.6B00019/SUPPL_FILE/BM6B00019_SI_003.AVI.

(115) Movafaghi, S.; Leszczak, V.; Wang, W.; Sorkin, J. A.; Dasi, L. P.; Popat, K. C.; Kota, A. K. Hemocompatibility of Superhemophobic Titania Surfaces. *Adv. Healthc. Mater.* **2017**, *6* (4), 1600717. https://doi.org/10.1002/adhm.201600717.

(116) Wu, S. Polymer Interface and Adhesion. *Polym. Interface Adhes.* **2017**, 1–630. https://doi.org/10.1201/9780203742860/POLYMER-INTERFACE-ADHESION-SOUHENG-WU.

(117) Tuteja, A.; Choi, W.; Mabry, J. M.; McKinley, G. H.; Cohen, R. E.; A, T.; W, C.; JM, M.; GH, M.; RE, C. Robust Omniphobic Surfaces. *Proc. Natl. Acad. Sci. U. S. A.* **2008**, *105* (47), 18200–18205.

(118) A, P.; S, M.; W, W.; S, S.; AP, Y.; AK, K. Fabrication of Nanostructured Omniphobic and Superomniphobic Surfaces with Inexpensive CO 2 Laser Engraver. *ACS Appl. Mater. Interfaces* **2017**, *9* (31), 25656–25661. https://doi.org/10.1021/ACSAMI.7B06924.

(119) Kota, A. K.; Kwon, G.; Tuteja, A. The Design and Applications of Superomniphobic Surfaces. *NPG Asia Materials*. Nature Publishing Group 2014. https://doi.org/10.1038/am.2014.34.

(120) Wang, D.; Wang, X.; Liu, X.; Zhou, F. Engineering a Titanium Surface with Controllable Oleophobicity and Switchable Oil Adhesion. *J. Phys. Chem. C* **2010**, *114* (21), 9938–9944. https://doi.org/10.1021/JP1023185/ASSET/IMAGES/MEDIUM/JP-2010-023185_0002.GIF.

(121) Leng, B.; Shao, Z.; De With, G.; Ming, W. Superoleophobic Cotton Textiles. *Langmuir* **2009**, *25* (4), 2456–2460. https://doi.org/10.1021/LA8031144/SUPPL_FILE/LA8031144_SI_003.WMV.

(122) Nosonovsky, M.; Bhushan, B. Why Re-Entrant Surface Topography Is Needed for Robust Oleophobicity. https://doi.org/10.1098/rsta.2016.0185.

(123) Yamaguchi, M. Microfabrication of Re-Entrant Surface with Hydrophobicity/Oleophobicity for Liquid Foods. *Sci. Reports 2020 101* **2020**, *10* (1), 1–7. https://doi.org/10.1038/s41598-020-59149-2.

(124) Lee, W.-K.; Engel, C. J.; Huntington, M. D.; Hu, J.; Odom, T. W. Controlled Three-Dimensional Hierarchical Structuring by Memory-Based, Sequential Wrinkling. *Nano Lett* **2015**, *15*, 43. https://doi.org/10.1021/acs.nanolett.5b02394.

(125) Pan, R.; Cai, M.; Liu, W.; Luo, X.; Chen, C.; Zhang, H.; Zhong, M. Extremely High Cassie–Baxter State Stability of Superhydrophobic Surfaces via Precisely Tunable Dual-Scale and Triple-Scale Micro–Nano Structures. *J. Mater. Chem. A* **2019**, *7* (30), 18050–18062. https://doi.org/10.1039/C9TA04484A.

(126) Moradi, S.; Hadjesfandiari, N.; Toosi, S. F.; Kizhakkedathu, J. N.; Hatzikiriakos, S. G. Effect of Extreme Wettability on Platelet Adhesion on Metallic Implants: From Superhydrophilicity to Superhydrophobicity. *ACS Appl. Mater. Interfaces* **2016**, *8* (27), 17631–17641. https://doi.org/10.1021/acsami.6b03644.

(127) Gabardo, C. M.; Hosseini, A.; Soleymani, L. A New Wrinkle in Biosensors: Wrinkled Electrodes Could Be a Breakthrough for Lab-on-A-Chip Devices. *IEEE Nanotechnol. Mag.* **2016**, *10* (2), 6–18. https://doi.org/10.1109/MNANO.2016.2539999.

(128) Adams-McGavin, R. C.; Chan, Y.; Gabardo, C. M.; Yang, J.; Skreta, M.; Fung, B. C.; Soleymani, L. Nanoporous and Wrinkled Electrodes Enhance the Sensitivity of Glucose Biosensors. *Electrochim. Acta* **2017**, *242*, 1–9. https://doi.org/10.1016/J.ELECTACTA.2017.04.108.

(129) Gabardo, C. M.; Yang, J.; Smith, N. J.; Adams-McGavin, R. C.; Soleymani, L. Programmable Wrinkling of Self-Assembled Nanoparticle Films on Shape Memory Polymers. *ACS Nano* **2016**, *10* (9), 8829–8836. https://doi.org/10.1021/acsnano.6b04584.

(130) González-Henríquez, C. M.; Medel-Molina, G. E.; Rodríguez-Umanzor, F. E.; Terraza Inostroza, C.; Sarabia-Vallejos, M. A.; Rodríguez-Hernández, J. Thermoresponsive Microwrinkled Hydrogel Surfaces with Modulated Chemical Composition. *Polymer (Guildf).* **2021**, *231*, 124109. https://doi.org/10.1016/J.POLYMER.2021.124109.

(131) Tan, Y.; Hu, B.; Song, J.; Chu, Z.; Wu, W. Bioinspired Multiscale Wrinkling Patterns on Curved Substrates: An Overview. *Nano-Micro Lett. 2020 121* **2020**, *12* (1), 1–42. https://doi.org/10.1007/S40820-020-00436-Y.

(132) Gabardo, C. M.; Adams-McGavin, R. C.; Vanderfleet, O. M.; Soleymani, L. Rapid Prototyping of Microfluidic Devices with Integrated Wrinkled Gold Micro-/Nano Textured Electrodes for Electrochemical Analysis. *Analyst* **2015**, *140* (16), 5781–5788. https://doi.org/10.1039/C5AN00774G.

(133) Schedl, A. E.; Neuber, C.; Fery, A.; Schmidt, H. W. Controlled Wrinkling of Gradient Metal Films. *Langmuir* **2018**, *34* (47), 14249–14253. https://doi.org/10.1021/ACS.LANGMUIR.8B03123/ASSET/IMAGES/LARGE/LA-2018-031235_0006.JPEG.

(134) Sadowski, R.; Wach, A.; Buchalska, M.; Kuśtrowski, P.; Macyk, W. Photosensitized TiO2 Films on Polymers – Titania-Polymer Interactions and Visible Light Induced Photoactivity. *Appl. Surf. Sci.* **2019**, *475*, 710–719. https://doi.org/10.1016/J.APSUSC.2018.12.286.

(135) Søndergaard, R. R.; Hösel, M.; Krebs, F. C. Roll-to-Roll Fabrication of Large Area Functional Organic Materials. *J. Polym. Sci. Part B Polym. Phys.* **2013**, *51* (1), 16–34. https://doi.org/10.1002/POLB.23192.

(136) Kumar, V.; Elfving, A.; Koivula, H.; Bousfield, D.; Toivakka, M. Roll-to-Roll Processed Cellulose Nanofiber Coatings. *Ind. Eng. Chem. Res.* **2016**, *55* (12), 3603–3613. https://doi.org/10.1021/acs.iecr.6b00417.

(137) Chung, J. Y.; Nolte, A. J.; Stafford, C. M. Surface Wrinkling: A Versatile Platform for Measuring Thin-Film Properties. *Adv. Mater.* **2011**, *23* (3), 349–368. https://doi.org/10.1002/ADMA.201001759.

(138) Jung, W.-B.; Cho, K. M.; Lee, W.-K.; Odom, T. W.; Jung, H.-T. Universal Method for Creating Hierarchical Wrinkles on Thin-Film Surfaces. *ACS Appl. Mater. Interfaces* **2017**, *10* (1), 1347–1355. https://doi.org/10.1021/ACSAMI.7B14011.

(139) Beyth, N.; Houri-Haddad, Y.; Domb, A.; Khan, W.; Hazan, R. Alternative Antimicrobial Approach: Nano-Antimicrobial Materials. *Evidence-based Complement. Altern. Med.* **2015**, *2015*. https://doi.org/10.1155/2015/246012.

(140) Hadjikakou, S. K.; Banti, C. N.; Rossos, A. K. Antimicrobial Materials with Medical Applications.

(141) Cloutier, M.; Mantovani, D.; Rosei, F. Antibacterial Coatings: Challenges, Perspectives, and Opportunities. *Trends Biotechnol.* **2015**, *33* (11), 637–652. https://doi.org/10.1016/J.TIBTECH.2015.09.002.

(142) Sun, D.; Babar Shahzad, M.; Li, M.; Wang, G.; Xu, D. Antimicrobial Materials with Medical Applications. *https://doi.org/10.1179/1753555714Y.0000000239* **2014**, *30* (B2), B90–B95. https://doi.org/10.1179/1753555714Y.0000000239.

(143) Li, R.; Chen, T.; Pan, X. Metal-Organic-Framework-Based Materials for Antimicrobial Applications. *ACS Nano* **2021**, *15* (3), 3808–3848.

https://doi.org/10.1021/ACSNANO.0C09617/ASSET/IMAGES/LARGE/NN0C09617_0016.JPEG.

(144) M, V.; RE, D.; P, H.; M, E.-D. Contact Killing and Antimicrobial Properties of Copper. *J. Appl. Microbiol.* **2018**, *124* (5), 1032–1046. https://doi.org/10.1111/JAM.13681.

(145) Jeevanandam, J.; Krishnan, S.; Hii, Y. S.; Pan, S.; Chan, Y. S.; Acquah, C.; Danquah, M. K.; Rodrigues, J. Synthesis Approach-Dependent Antiviral Properties of Silver Nanoparticles and Nanocomposites. *J. Nanostructure Chem. 2021 125* **2022**, *12* (5), 809–831. https://doi.org/10.1007/S40097-021-00465-Y.

(146) Govind Bharadwaj M R Sai Ganesh Jithin Vishnu Karthik V Shankar Balakrishnan Shankar R Rajesh, V. S. Antiviral Properties of Copper and Its Alloys to Inactivate Covid-19 Virus: A Review. *BioMetals 34*. https://doi.org/10.1007/s10534-021-00339-4.

(147) Galdiero, S.; Falanga, A.; Vitiello, M.; Cantisani, M.; Marra, V.; Galdiero, M. Molecules Silver Nanoparticles as Potential Antiviral Agents. *Molecules* **2011**, *16*, 8894–8918. https://doi.org/10.3390/molecules16108894.

(148) Guldiren, D.; Aydın, S. Antimicrobial Property of Silver, Silver-Zinc and Silver-Copper Incorporated Soda Lime Glass Prepared by Ion Exchange. *Mater. Sci. Eng. C* **2017**, *78*, 826–832. https://doi.org/10.1016/J.MSEC.2017.04.134.

(149) Jassby, D.; Farner Budarz, J.; Wiesner, M. Impact of Aggregate Size and Structure on the Photocatalytic Properties of TiO 2 and ZnO Nanoparticles. *Environ. Sci. Technol* **2012**, *46*, 48. https://doi.org/10.1021/es202009h.

(150) Cho, M.; Chung, H.; Choi, W.; Yoon, J. Linear Correlation between Inactivation of E. Coli and OH Radical Concentration in TiO2 Photocatalytic Disinfection. *Water Res.* **2004**, *38* (4), 1069–1077. https://doi.org/10.1016/J.WATRES.2003.10.029.

(151) Kumaravel, V.; Nair, K. M.; Mathew, S.; Bartlett, J.; Kennedy, J. E.; Manning, H. G.; Whelan, B. J.; Leyland, N. S.; Pillai, S. C. Antimicrobial TiO2 Nanocomposite Coatings for Surfaces, Dental and Orthopaedic Implants. *Chem. Eng. J.* **2021**, *416*. https://doi.org/10.1016/J.CEJ.2021.129071.

(152) Rahimi, N.; Pax, R. A.; Gray, E. M. A. Review of Functional Titanium Oxides. I: TiO2 and Its Modifications. *Prog. Solid State Chem.* **2016**, *44* (3), 86–105. https://doi.org/10.1016/J.PROGSOLIDSTCHEM.2016.07.002.

(153) Wang, K.; Paszkiewicz, O.; Vincent, M.; Henkiel, P.; Kowalski, D.; Kowalska, E.; Markowska-Szczupak, A. Evaluation of Antifungal Properties of Titania P25. *Micromachines 2022, Vol. 13, Page 1851* **2022**, *13* (11), 1851. https://doi.org/10.3390/MI13111851.

(154) Selishchev, D.; Stepanov, G.; Sergeeva, M.; Solovyeva, M.; Zhuravlev, E.; Komissarov, A.; Richter, V.; Kozlov, D. Inactivation and Degradation of Influenza A Virus on the Surface of Photoactive Self-Cleaning Cotton Fabric Functionalized with Nanocrystalline TiO2. *Catalysts* **2022**, *12* (11), 1298.

https://doi.org/10.3390/CATAL12111298/S1.

(155) Habibi-Yangjeh, A.; Asadzadeh-Khaneghah, S.; Feizpoor, S.; Rouhi, A. Review on Heterogeneous Photocatalytic Disinfection of Waterborne, Airborne, and Foodborne Viruses: Can We Win against Pathogenic Viruses? *J. Colloid Interface Sci.* **2020**, *580*, 503–514. https://doi.org/10.1016/J.JCIS.2020.07.047.

(156) Soo Joung, Y.; Buie, C. R. Electrophoretic Deposition of Unstable Colloidal Suspensions for Superhydrophobic Surfaces. **2011**, *27*, 4156–4163. https://doi.org/10.1021/la200286t.

(157) Zhu, P.; Kong, T.; Tang, X.; Wang, L. Well-Defined Porous Membranes for Robust Omniphobic Surfaces via Microfluidic Emulsion Templating. *Nat. Commun.* **2017**, *8* (May). https://doi.org/10.1038/ncomms15823.

(158) Wu, W.; Wang, X.; Wang, D.; Chen, M.; Zhou, F.; Liu, W.; Xue, Q. Alumina Nanowire Forests via Unconventional Anodization and Super-Repellency plus Low Adhesion to Diverse Liquids. *Chem. Commun.* **2009**, No. 9, 1043–1045. https://doi.org/10.1039/b818633b.

(159) Xu, L.-C.; Bauer, J. W.; Siedlecki, C. A. Proteins, Platelets, and Blood Coagulation at Biomaterial Interfaces. *Colloids Surfaces B Biointerfaces* **2014**, *124*, 49–68.

(160) Sask, K. N.; Zhitomirsky, I.; Berry, L. R.; Chan, A. K. C.; Brash, J. L. Surface Modification with an Antithrombin–Heparin Complex for Anticoagulation: Studies on a Model Surface with Gold as Substrate. *Acta Biomater.* **2010**, *6* (8), 2911–2919. https://doi.org/https://doi.org/10.1016/j.actbio.2010.02.043.

(161) Hansson, K. M.; Tosatti, S.; Isaksson, J.; Wetterö, J.; Textor, M.; Lindahl, T. L.; Tengvall, P. Whole Blood Coagulation on Protein Adsorption-Resistant PEG and Peptide Functionalised PEG-Coated Titanium Surfaces. *Biomaterials* **2005**, *26* (8), 861–872.

(162) Heath, D. E.; Cooper, S. L. Design and Characterization of PEGylated Terpolymer Biomaterials. *J. Biomed. Mater. Res. Part A* **2010**, *94* (4), 1294–1302.

(163) Tsai, W.-B.; Chen, Y.-H.; Chien, H.-W. Collaborative Cell-Resistant Properties of Polyelectrolyte Multilayer Films and Surface PEGylation on Reducing Cell Adhesion to Cytophilic Surfaces. *J. Biomater. Sci. Polym. Ed.* **2009**, *20* (11), 1611–1628.

(164) Ishihara, K. Blood-Compatible Surfaces with Phosphorylcholine-Based Polymers for Cardiovascular Medical Devices. *Langmuir* **2018**, *35* (5), 1778–1787.

(165) Lin, P. H.; Chen, C.; Bush, R. L.; Yao, Q.; Lumsden, A. B.; Hanson, S. R. Small-Caliber Heparin-Coated EPTFE Grafts Reduce Platelet Deposition and Neointimal Hyperplasia in a Baboon Model. *J. Vasc. Surg.* **2004**, *39* (6), 1322–1328.

(166) Heyligers, J. M. M.; Verhagen, H. J. M.; Rotmans, J. I.; Weeterings, C.; de Groot, P. G.; Moll, F. L.; Lisman, T. Heparin Immobilization Reduces Thrombogenicity of Small-Caliber Expanded Polytetrafluoroethylene Grafts. *J. Vasc. Surg.* **2006**, *43*

(3), 587–591.

(167) Seib, F. P.; Herklotz, M.; Burke, K. A.; Maitz, M. F.; Werner, C.; Kaplan, D. L. Multifunctional Silk–Heparin Biomaterials for Vascular Tissue Engineering Applications. *Biomaterials* **2014**, *35* (1), 83–91.

(168) Zhao, J.; Chen, Y.; Yang, S.; Wu, S.; Zeng, R.; Wu, H.; Zhang, J.; Zha, Z.; Tu, M. Improving Blood-Compatibility via Surface Heparin-Immobilization Based on a Liquid Crystalline Matrix. *Mater. Sci. Eng. C* **2016**, *58*, 133–141.

(169) Yang, Z.; Wang, J.; Luo, R.; Maitz, M. F.; Jing, F.; Sun, H.; Huang, N. The Covalent Immobilization of Heparin to Pulsed-Plasma Polymeric Allylamine Films on 316L Stainless Steel and the Resulting Effects on Hemocompatibility. *Biomaterials* **2010**, *31* (8), 2072–2083.

(170) Hoshi, R. A.; Van Lith, R.; Jen, M. C.; Allen, J. B.; Lapidos, K. A.; Ameer, G. The Blood and Vascular Cell Compatibility of Heparin-Modified EPTFE Vascular Grafts. *Biomaterials* **2013**, *34* (1), 30–41.

(171) Hiob, M. A.; She, S.; Muiznieks, L. D.; Weiss, A. S. Biomaterials and Modifications in the Development of Small-Diameter Vascular Grafts. *ACS Biomater. Sci. Eng.* **2017**, *3* (5), 712–723.

(172) Oonishi, H. Orthopaedic Applications of Hydroxyapatite. *Biomaterials* **1991**, *12* (2), 171–178.

(173) Chu, P. K.; Chen, J. Y.; Wang, L. P.; Huang, N. Plasma-Surface Modification of Biomaterials. *Mater. Sci. Eng. R Reports* **2002**, *36* (5–6), 143–206.

(174) Vallieres, K.; Petitclerc, É.; Laroche, G. Covalent Grafting of Fibronectin onto Plasma-treated PTFE: Influence of the Conjugation Strategy on Fibronectin Biological Activity. *Macromol. Biosci.* **2007**, *7* (5), 738–745.

(175) Santos, M.; Bilek, M. M. M.; Wise, S. G. Plasma-Synthesised Carbon-Based Coatings for Cardiovascular Applications. *Biosurface and Biotribology* **2015**, *1* (3), 146–160.

(176) De Agostini, A. I.; Watkins, S. C.; Slayter, H. S.; Youssoufian, H.; Rosenberg, R. D. Localization of Anticoagulantly Active Heparan Sulfate Proteoglycans in Vascular Endothelium: Antithrombin Binding on Cultured Endothelial Cells and Perfused Rat Aorta. *J. Cell Biol.* **1990**, *111* (3), 1293–1304.

(177) Badv, M.; Imani, S. M.; Weitz, J. I.; Didar, T. F. Lubricant-Infused Surfaces with Built-In Functional Biomolecules Exhibit Simultaneous Repellency and Tunable Cell Adhesion. *ACS Nano* **2018**, acsnano.8b03938. https://doi.org/10.1021/acsnano.8b03938.

(178) Imani, S. M.; Badv, M.; Shakeri, A.; Yousefi, H.; Yip, D.; Fine, C.; Didar, T. F. Micropatterned Biofunctional Lubricant-Infused Surfaces Promote Selective Localized Cell Adhesion and Patterning. *Lab Chip* **2019**, *19* (19), 3228–3237. https://doi.org/10.1039/c9lc00608g.

(179) Osborne, M.; Aryasomayajula, A.; Shakeri, A.; Selvaganapathy, P. R.; Didar, T. F. Suppression of Biofouling on a Permeable Membrane for Dissolved Oxygen Sensing Using a Lubricant-Infused Coating. *ACS Sensors* **2019**, *4* (3), 687–693. https://doi.org/10.1021/ACSSENSORS.8B01541.

(180) Badv, M.; Alonso-Cantu, C.; Shakeri, A.; Hosseinidoust, Z.; Weitz, J. I.; Didar, T. F. Biofunctional Lubricant-Infused Vascular Grafts Functionalized with Silanized Bio-Inks Suppress Thrombin Generation and Promote Endothelialization. *ACS Biomater. Sci. Eng.* **2019**, *5* (12), 6485–6496. https://doi.org/10.1021/acsbiomaterials.9b01062.

(181) Badv, M.; Weitz, J. I.; Didar, T. F. Lubricant-Infused PET Grafts with Built-In Biofunctional Nanoprobes Attenuate Thrombin Generation and Promote Targeted Binding of Cells. *Small* **2019**, *15* (51), 1905562. https://doi.org/10.1002/smll.201905562.

(182) Hosseini, A.; Villegas, M.; Yang, J.; Badv, M.; Weitz, J. I.; Soleymani, L.; Didar, T. F. Conductive Electrochemically Active Lubricant-Infused Nanostructured Surfaces Attenuate Coagulation and Enable Friction-Less Droplet Manipulation. *Adv. Mater. Interfaces* **2018**, *1800617*, 1–10. https://doi.org/10.1002/admi.201800617.

(183) Villegas, M.; Cetinic, Z.; Shakeri, A.; Didar, T. F. Fabricating Smooth PDMS Microfluidic Channels from Low-Resolution 3D Printed Molds Using an Omniphobic Lubricant-Infused Coating. *Anal. Chim. Acta* **2018**, *1000*, 248–255. https://doi.org/10.1016/j.aca.2017.11.063.

(184) Badv, M.; Jaffer, I. H.; Weitz, J. I.; Didar, T. F. An Omniphobic Lubricant-Infused Coating Produced by Chemical Vapor Deposition of Hydrophobic Organosilanes Attenuates Clotting on Catheter Surfaces. **2017**, *7* (1). https://doi.org/10.1038/s41598-017-12149-1.

(185) Qin, H.; Sun, C.; He, C.; Wang, D.; Cheng, C.; Nie, S.; Sun, S.; Zhao, C. High Efficient Protocol for the Modification of Polyethersulfone Membranes with Anticoagulant and Antifouling Properties via in Situ Cross-Linked Copolymerization. *J. Memb. Sci.* **2014**, *468*, 172–183. https://doi.org/10.1016/j.memsci.2014.06.006.

(186) Li, L.; Cheng, C.; Xiang, T.; Tang, M.; Zhao, W.; Sun, S.; Zhao, C. Modification of Polyethersulfone Hemodialysis Membrane by Blending Citric Acid Grafted Polyurethane and Its Anticoagulant Activity. *J. Memb. Sci.* **2012**, *405–406*, 261–274. https://doi.org/10.1016/j.memsci.2012.03.015.

(187) Li, Z.; Nguyen, B. L.; Cheng, Y. C.; Xue, J.; MacLaren, G.; Yap, C. H. Durable, Flexible, Superhydrophobic and Blood-Repelling Surfaces for Use in Medical Blood Pumps. *J. Mater. Chem. B* **2018**, *6* (39), 6225–6233. https://doi.org/10.1039/C8TB01547C.

(188) Ware, C. S.; Smith-Palmer, T.; Peppou-Chapman, S.; Scarratt, L. R. J.; Humphries, E. M.; Balzer, D.; Neto, C. Marine Antifouling Behavior of Lubricant-

Infused Nanowrinkled Polymeric Surfaces. *ACS Appl. Mater. Interfaces* **2018**, *10* (4), 4173–4182.

(189) Dramé, A.; Darmanin, T.; Dieng, S. Y.; Taffin de Givenchy, E.; Guittard, F. Superhydrophobic and Oleophobic Surfaces Containing Wrinkles and Nanoparticles of PEDOT with Two Short Fluorinated Chains. *RSC Adv.* **2014**, *4* (21), 10935–10943. https://doi.org/10.1039/C3RA47479H.

(190) Shillingford, C.; MacCallum, N.; Wong, T.-S.; Kim, P.; Aizenberg, J. Fabrics Coated with Lubricated Nanostructures Display Robust Omniphobicity. *Nanotechnology* **2013**, *25* (1), 14019. https://doi.org/10.1088/0957-4484/25/1/014019.

(191) Saha, S.; Chan, Y.; Soleymani, L. Enhancing the Photoelectrochemical Response of DNA Biosensors Using Wrinkled Interfaces. *ACS Appl. Mater. Interfaces* **2018**, *10* (37), 31178–31185. https://doi.org/10.1021/acsami.8b12286.

(192) Zhu, Z.; Zhu, T.; Liu, Z. Raman Scattering Enhancement Contributed from Individual Gold Nanoparticles and Interparticle Coupling. *Nanotechnology* **2004**, *15* (3), 357–364. https://doi.org/10.1088/0957-4484/15/3/022.

(193) Li, D.; Neumann, A. . Contact Angles on Hydrophobic Solid Surfaces and Their Interpretation. *J. Colloid Interface Sci.* **1992**, *148* (1), 190–200. https://doi.org/10.1016/0021-9797(92)90127-8.

(194) Crawford, R. J.; Webb, H. K.; Truong, V. K.; Hasan, J.; Ivanova, E. P. Surface Topographical Factors Influencing Bacterial Attachment. *Adv. Colloid Interface Sci.* **2012**, *179–182*, 142–149. https://doi.org/10.1016/j.cis.2012.06.015.

(195) Nakae, H.; Inui, R.; Hirata, Y.; Saito, H. Effects of Surface Roughness on Wettability. *Acta Mater.* **1998**, *46* (7), 2313–2318.

(196) Yan, L.; Wang, K.; Wu, J.; Ye, L. Hydrophobicity of Model Surfaces with Closely Packed Nano-and Micro-Spheres. *Colloids Surfaces A Physicochem. Eng. Asp.* **2007**, *296* (1–3), 123–131.

(197) Nosonovsky, M. Multiscale Roughness and Stability of Superhydrophobic Biomimetic Interfaces. *Langmuir* **2007**, *23* (6), 3157–3161. https://doi.org/10.1021/la062301d.

(198) Vazquez, G.; Alvarez, E.; Navaza, J. M. Surface Tension of Alcohol Water + Water from 20 to 50 .Degree.C. *J. Chem. Eng. Data* **1995**, *40* (3), 611–614. https://doi.org/10.1021/je00019a016.

(199) Ensikat, H. J.; Ditsche-Kuru, P.; Neinhuis, C.; Barthlott, W.; Editors, G.; Barthlott, W.; Koch, K. Superhydrophobicity in Perfection: The Outstanding Properties of the Lotus Leaf. *Beilstein J. Nanotechnol* **2011**, *2*, 152–161. https://doi.org/10.3762/bjnano.2.19.

(200) van Oeveren, W. Obstacles in Haemocompatibility Testing. *Scientifica (Cairo).* **2013**, *2013*, 392584. https://doi.org/10.1155/2013/392584.

(201) Parhi, P.; Golas, A.; Vogler, E. A. Role of Proteins and Water in the Initial Attachment of Mammalian Cells to Biomedical Surfaces: A Review. *J. Adhes. Sci. Technol.* **2010**, *24* (5), 853–888.

(202) Badv, M.; Imani, S. M.; Weitz, J. I.; Didar, T. F. Lubricant-Infused Surfaces with Built-in Functional Biomolecules Exhibit Simultaneous Repellency and Tunable Cell Adhesion. *ACS Nano* **2018**, *12* (11), 10890–10902.

(203) Shakeri, A.; Imani, S. M.; Chen, E.; Yousefi, H.; Shabbir, R.; Didar, T. F. Plasma-Induced Covalent Immobilization and Patterning of Bioactive Species in Microfluidic Devices. *Lab Chip* **2019**, *19* (18), 3104–3115.

(204) *Elcometer 1542 Cross Hatch Adhesion Tester*.

(205) Fatanat Didar, T.; Foudeh, A. M.; Tabrizian, M. Patterning Multiplex Protein Microarrays in a Single Microfluidic Channel. **2011**. https://doi.org/10.1021/ac2025877.

(206) Otter, J. A.; Donskey, C.; Yezli, S.; Douthwaite, S.; Goldenberg, S. D.; Weber, D. J. Transmission of SARS and MERS Coronaviruses and Influenza Virus in Healthcare Settings: The Possible Role of Dry Surface Contamination. *Journal of Hospital Infection*. W.B. Saunders Ltd March 1, 2016, pp 235–250. https://doi.org/10.1016/j.jhin.2015.08.027.

(207) Li, H.; Wang, Y.; Ji, M.; Pei, F.; Zhao, Q.; Zhou, Y.; Hong, Y.; Han, S.; Wang, J.; Wang, Q.; Li, Q.; Wang, Y. Transmission Routes Analysis of SARS-CoV-2: A Systematic Review and Case Report. *Front. Cell Dev. Biol.* **2020**, *0*, 618. https://doi.org/10.3389/FCELL.2020.00618.

(208) Eslami, H.; Jalili, M. The Role of Environmental Factors to Transmission of SARS-CoV-2 (COVID-19). *AMB Express 2020 101* **2020**, *10* (1), 1–8. https://doi.org/10.1186/S13568-020-01028-0.

(209) Kampf, G.; Todt, D.; Pfaender, S.; Steinmann, E. Persistence of Coronaviruses on Inanimate Surfaces and Their Inactivation with Biocidal Agents. *J. Hosp. Infect.* **2020**, *104* (3), 246–251. https://doi.org/10.1016/J.JHIN.2020.01.022.

(210) Warnes, S. L.; Little, Z. R.; Keevil, C. W. Human Coronavirus 229E Remains Infectious on Common Touch Surface Materials. *MBio* **2015**, *6* (6). https://doi.org/10.1128/mBio.01697-15.

(211) Hasan, M. A.; Carmel Mary Esther, A.; Dey, A.; Mukhopadhyay, A. K. A Review on Coronavirus Survivability on Material's Surfaces: Present Research Scenarios, Technologies and Future Directions. *Surf. Eng.* **2020**, *36* (12), 1226–1239. https://doi.org/10.1080/02670844.2020.1833277.

(212) Wathore, R.; Gupta, A.; Bherwani, H.; Labhasetwar, N. Understanding Air and Water Borne Transmission and Survival of Coronavirus: Insights and Way Forward for SARS-CoV-2. *Sci. Total Environ.* **2020**, *749*, 141486. https://doi.org/10.1016/j.scitotenv.2020.141486.

(213) Sattar, S. A.; Springthorpe, V. S.; Karim, Y.; Loro, P. Chemical Disinfection of

Non-Porous Inanimate Surfaces Experimentally Contaminated with Four Human Pathogenic Viruses. *Epidemiol. Infect.* **1989**, *102* (3), 493–505. https://doi.org/10.1017/S0950268800030211.

(214) Warnes, S. L.; Keevil, C. W. Inactivation of Norovirus on Dry Copper Alloy Surfaces. *PLoS One* **2013**, *8* (9), 75017. https://doi.org/10.1371/journal.pone.0075017.

(215) Korant, B. D.; Kauer, J. C.; Butterworth, B. E. Zinc Ions Inhibit Replication of Rhinoviruses. *Nature* **1974**, *248* (5449), 588–590. https://doi.org/10.1038/248588a0.

(216) Lara, H. H.; Ayala-Nuñez, N. V.; Ixtepan-Turrent, L.; Rodriguez-Padilla, C. Mode of Antiviral Action of Silver Nanoparticles against HIV-1. *J. Nanobiotechnology* **2010**, *8*. https://doi.org/10.1186/1477-3155-8-1.

(217) Carrouel, F.; Viennot, S.; Ottolenghi, L.; Gaillard, C.; Bourgeois, D. Nanoparticles as Anti-Microbial, Anti-Inflammatory, and Remineralizing Agents in Oral Care Cosmetics: A Review of the Current Situation. *Nanomaterials*. MDPI AG January 1, 2020. https://doi.org/10.3390/nano10010140.

(218) Hsu, B. B.; Wong, S. Y.; Hammond, P. T.; Chen, J.; Klibanov, A. M. Mechanism of Inactivation of Influenza Viruses by Immobilized Hydrophobic Polycations. *Proc. Natl. Acad. Sci. U. S. A.* **2011**, *108* (1), 61–66. https://doi.org/10.1073/pnas.1017012108.

(219) Jo, H.; West, A. M.; Teska, P. J.; Oliver, H. F.; Howarter, J. A. Assessment of Early Onset Surface Damage from Accelerated Disinfection Protocol. *Antimicrob. Resist. Infect. Control* **2019**, *8* (1), 24. https://doi.org/10.1186/s13756-019-0467-9.

(220) National Institute for Occupational Safety and Health. *Hazard Communication for Disinfectants Used Against Viruses*. https://www.cdc.gov/niosh/topics/disinfectant/default.html (accessed 2021-04-05).

(221) Ishiguro, H.; Nakano, R.; Yao, Y.; Kajioka, J.; Fujishima, A.; Sunada, K.; Minoshima, M.; Hashimoto, K.; Kubota, Y. Photocatalytic Inactivation of Bacteriophages by TiO2-Coated Glass Plates under Low-Intensity, Long-Wavelength UV Irradiation. *Photochem. Photobiol. Sci.* **2011**, *10* (11), 1825–1829. https://doi.org/10.1039/c1pp05192j.

(222) Noyce, J. O.; Michels, H.; Keevil, C. W. Inactivation of Influenza A Virus on Copper versus Stainless Steel Surfaces. *Appl. Environ. Microbiol.* **2007**, *73* (8), 2748–2750. https://doi.org/10.1128/AEM.01139-06.

(223) Wu, Q.; Yang, C.; Su, C.; Zhong, L.; Zhou, L.; Hang, T.; Lin, H.; Chen, W.; Li, L.; Xie, X. Slippery Liquid-Attached Surface for Robust Biofouling Resistance. *ACS Biomater. Sci. Eng.* **2020**, *6* (1), 358–366. https://doi.org/10.1021/acsbiomaterials.9b01323.

(224) Jiang, J.; Zhang, H.; He, W.; Li, T.; Li, H.; Liu, P.; Liu, M.; Wang, Z.; Wang, Z.; Yao, X. Adhesion of Microdroplets on Water-Repellent Surfaces toward the

Prevention of Surface Fouling and Pathogen Spreading by Respiratory Droplets. *ACS Appl. Mater. Interfaces* **2017**, *9* (7), 6599–6608. https://doi.org/10.1021/acsami.6b15213.

(225) Shakeri, A.; Jarad, N. A.; Terryberry, J.; Khan, S.; Leung, A.; Chen, S.; Didar, T. F. Antibody Micropatterned Lubricant-Infused Biosensors Enable Sub-Picogram Immunofluorescence Detection of Interleukin 6 in Human Whole Plasma. *Small* **2020**, *16* (45), 2003844. https://doi.org/10.1002/SMLL.202003844.

(226) Siddiquie, R. Y.; Gaddam, A.; Agrawal, A.; Dimov, S. S.; Joshi, S. S. Anti-Biofouling Properties of Femtosecond Laser-Induced Submicron Topographies on Elastomeric Surfaces. *Langmuir* **2020**, *36* (19), 5349–5358. https://doi.org/10.1021/acs.langmuir.0c00753.

(227) Galante, A. J.; Haghanifar, S.; Romanowski, E. G.; Shanks, R. M. Q. Q.; Leu, P. W. Superhemophobic and Antivirofouling Coating for Mechanically Durable and Wash-Stable Medical Textiles. **2020**, *12* (19), 22120–22128. https://doi.org/10.1021/acsami.9b23058.

(228) Cao, Y.; Jana, S.; Tan, X.; Bowen, L.; Zhu, Y.; Dawson, J.; Han, R.; Exton, J.; Liu, H.; McHale, G.; Jakubovics, N. S.; Chen, J. Antiwetting and Antifouling Performances of Different Lubricant-Infused Slippery Surfaces. *Langmuir* **2020**, *36* (45), 13396–13407. https://doi.org/10.1021/acs.langmuir.0c00411.

(229) He, X.; Tian, F.; Bai, X.; Yuan, C.; Wang, C.; Neville, A. Biomimetic Lubricant-Infused Titania Nanoparticle Surfaces via Layer-by-Layer Deposition to Control Biofouling. *Appl. Surf. Sci.* **2020**, *515*, 146064. https://doi.org/10.1016/J.APSUSC.2020.146064.

(230) Wang, Z.; Yi, B.; Wu, M.; Lv, D.; He, M.-L. M.; Liu, M.; Yao, X.; Wang, Z.; Yi, B.; Wu, M.; Lv, D.; He, M.-L. M.; Yao, X.; Liu, M. Bioinspired Supramolecular Slippery Organogels for Controlling Pathogen Spread by Respiratory Droplets. *Adv. Funct. Mater.* **2021**, *31* (34), 2102888. https://doi.org/10.1002/ADFM.202102888.

(231) Villegas, M.; Alonso-Cantu, C.; Rahmani, S.; Wilson, D.; Hosseinidoust, Z.; Didar, T. F. Antibiotic-Impregnated Liquid-Infused Coatings Suppress the Formation of Methicillin-Resistant Staphylococcus Aureus Biofilms. *ACS Appl. Mater. Interfaces* **2021**, *13* (24), 27774–27783. https://doi.org/10.1021/ACSAMI.0C19355.

(232) Li, J.; Ueda, E.; Paulssen, D.; Levkin, P. A. Slippery Lubricant-Infused Surfaces: Properties and Emerging Applications. *Adv. Funct. Mater.* **2019**, *29* (4), 1802317. https://doi.org/10.1002/ADFM.201802317.

(233) Kasapgil, E.; Badv, M.; Cantú, C. A.; Rahmani, S.; Erbil, H. Y.; Sakir, I. A.; Weitz, J. I.; Hosseini-Doust, Z.; Didar, T. F.; Anac Sakir, I.; Weitz, J. I.; Hosseini-Doust, Z.; Didar, T. F. Polysiloxane Nanofilaments Infused with Silicone Oil Prevent Bacterial Adhesion and Suppress Thrombosis on Intranasal Splints. **2021**, *7* (2), 541–552.

(234) Lafuma, A.; Quéré, D. *Superhydrophobic States*; 2003; Vol. 2, pp 457–460.

https://pubmed.ncbi.nlm.nih.gov/12819775/ (accessed 2021-03-03).

(235) Wenzel, R. N. Resistance of Solid Surfaces to Wetting by Water. *Ind. Eng. Chem.* **1936**, *28* (8), 988–994. https://doi.org/10.1021/ie50320a024.

(236) Cassie, A. B. D.; Baxter, S. Wettability of Porous Surfaces. *Trans. Faraday Soc.* **1944**, *40* (0), 546–551. https://doi.org/10.1039/tf9444000546.

(237) Pan, S.; Guo, R.; Björnmalm, M.; Richardson, J. J.; Li, L.; Peng, C.; Bertleff-Zieschang, N.; Xu, W.; Jiang, J.; Caruso, F. Coatings Super-Repellent to Ultralow Surface Tension Liquids. *Nat. Mater. 17*. https://doi.org/10.1038/s41563-018-0178-2.

(238) Imani, S. M.; Maclachlan, R.; Chan, Y.; Shakeri, A.; Soleymani, L.; Didar, T. F. Hierarchical Structures, with Submillimeter Patterns, Micrometer Wrinkles, and Nanoscale Decorations, Suppress Biofouling and Enable Rapid Droplet Digitization. *Small* **2020**, *16* (50), 2004886. https://doi.org/10.1002/smll.202004886.

(239) Li, W.; Wang, Y.; Tang, X.; Yuen, T. T. T.; Han, X.; Li, J.; Huang, N.; Chan, J. F. W.; Chu, H.; Wang, L. Liquid Repellency Enabled Antipathogen Coatings. *Mater. Today Bio* **2021**, *12*. https://doi.org/10.1016/j.mtbio.2021.100145.

(240) Zhu, P.; Wang, Y.; Chu, H.; Wang, L. Superhydrophobicity Preventing Surface Contamination as a Novel Strategy against COVID-19. *J. Colloid Interface Sci.* **2021**, *600*, 613–619. https://doi.org/10.1016/J.JCIS.2021.05.031.

(241) McDermott, M.; Smiley, J.; Brais, L. Immunity in the Female Genital Tract after Intravaginal Vaccination with Attenuated Simplex Virus Type II (HSV-2). *Fed. Proc.* **1984**, *43* (6), 747–753.

(242) REED, L. J.; MUENCH, H. A SIMPLE METHOD OF ESTIMATING FIFTY PER CENT ENDPOINTS12. *Am. J. Epidemiol.* **1938**, *27* (3), 493–497. https://doi.org/10.1093/oxfordjournals.aje.a118408.

(243) McHale, G.; Shirtcliffe, N. J.; Newton, M. I. Contact-Angle Hysteresis on Super-Hydrophobic Surfaces. *Langmuir* **2004**, *20* (23), 10146–10149. https://doi.org/10.1021/la0486584.

(244) Gao, L.; Mccarthy, T. J. Contact Angle Hysteresis Explained. **2006**. https://doi.org/10.1021/la060254j.

(245) Graupe, M.; Koini, T.; Kim, H. I.; Garg, N.; Miura, Y. F.; Takenaga, M.; Perry, S. S.; Lee, T. R. Self-Assembled Monolayers of CF3-Terminated Alkanethiols on Gold. In *Colloids and Surfaces A: Physicochemical and Engineering Aspects*; Elsevier Science Publishers B.V., 1999; Vol. 154, pp 239–244. https://doi.org/10.1016/S0927-7757(98)00902-9.

(246) Arunachalam, S.; Das, R.; Nauruzbayeva, J.; Domingues, E. M.; Mishra, H. Assessing Omniphobicity by Immersion. *J. Colloid Interface Sci.* **2019**, *534*, 156–162. https://doi.org/10.1016/J.JCIS.2018.08.059.

(247) Tommaso Baldacchini, †; James E. Carey, †; Ming Zhou, †,‡ and; Eric Mazur*, †; Baldacchini, T.; Carey, J. E.; Zhou, M.; Mazur, E. Superhydrophobic Surfaces Prepared by Microstructuring of Silicon Using a Femtosecond Laser. *Langmuir* **2006**, *22* (11), 4917–4919.

(248) Wang, W.; Zhang, Y.; Chen, T.; Sun, X.; Mei, X.; Cui, J. Wettability and Stability of Wetting States for the Surfaces with Reentrant Structures. *J. Phys. Chem. C* **2020**, *124* (52), 28479–28487. https://doi.org/10.1021/acs.jpcc.0c07472.

(249) Wang, J. J.; Yuan, S.; Zhu, D.; Tang, H.; Wang, N.; Chen, W.; Gao, Q.; Li, Y.; Wang, J. J.; Liu, H.; Zhang, X.; Rao, Z.; Wang, X. Structure of the Herpes Simplex Virus Type 2 C-Capsid with Capsid-Vertex-Specific Component. *Nat. Commun.* **2018**, *9* (1), 1–10. https://doi.org/10.1038/s41467-018-06078-4.

(250) Bar-On, Y. M.; Flamholz, A.; Phillips, R.; Milo, R. SARS-CoV-2 (COVID-19) by the Numbers. *Elife* **2020**, *9*.

(251) Liu, D. X.; Liang, J. Q.; Fung, T. S. Human Coronavirus-229E, -OC43, -NL63, and -HKU1 (Coronaviridae). In *Encyclopedia of Virology*; Elsevier, 2021; pp 428–440. https://doi.org/10.1016/b978-0-12-809633-8.21501-x.

(252) Zhu, H.; Guo, Z.; Liu, W. Adhesion Behaviors on Superhydrophobic Surfaces. *Chem. Commun.* **2014**, *50* (30), 3900–3913. https://doi.org/10.1039/c3cc47818a.

(253) Chen, H.; Yuan, L.; Song, W.; Wu, Z.; Li, D. *Biocompatible Polymer Materials: Role of Protein-Surface Interactions*; Pergamon, 2008; Vol. 33, pp 1059–1087. https://doi.org/10.1016/j.progpolymsci.2008.07.006.

(254) Rzezutka, A.; Cook, N.; Rzeżutka, A.; Cook, N. *Survival of Human Enteric Viruses in the Environment and Food*; 2004; Vol. 28, pp 441–453. https://doi.org/10.1016/j.femsre.2004.02.001.

(255) Armanious, A.; Aeppli, M.; Jacak, R.; Refardt, D.; Thérè Se Sigstam, T.; Kohn, T.; Sander, M. Viruses at Solid−Water Interfaces: A Systematic Assessment of Interactions Driving Adsorption. *Environ. Sci. Technol* **2016**, *50*, 45. https://doi.org/10.1021/acs.est.5b04644.

(256) Meguid, S. A.; Elzaabalawy, A. Potential of Combating Transmission of COVID-19 Using Novel Self-Cleaning Superhydrophobic Surfaces: Part I—Protection Strategies against Fomites. *Int. J. Mech. Mater. Des.* **2020**, *16* (3), 423–431. https://doi.org/10.1007/s10999-020-09513-x.

(257) de Leon, A.; Advincula, R. C. Conducting Polymers with Superhydrophobic Effects as Anticorrosion Coating. *Intell. Coatings Corros. Control* **2015**, 409–430. https://doi.org/10.1016/B978-0-12-411467-8.00011-8.

(258) Ke, Q.; Fu, W.; Jin, H.; Zhang, L.; Tang, T.; Zhang, J. Fabrication of Mechanically Robust Superhydrophobic Surfaces Based on Silica Micro-Nanoparticles and Polydimethylsiloxane. *Surf. Coatings Technol.* **2011**, *205* (21–22), 4910–4914. https://doi.org/10.1016/J.SURFCOAT.2011.04.073.

(259) Groten, J.; Rgen Rü, J. Surfaces with Combined Microscale and Nanoscale

Structures: A Route to Mechanically Stable Superhydrophobic Surfaces? **2013**. https://doi.org/10.1021/la304641q.

(260) Stephens, B.; Azimi, P.; Thoemmes, M. S.; Heidarinejad, M.; Allen, J. G.; Gilbert, J. A. Microbial Exchange via Fomites and Implications for Human Health. *Curr. Pollut. Reports* **2019**, *5* (4), 198–213. https://doi.org/10.1007/S40726-019-00123-6/FIGURES/1.

(261) Julian, T. R.; MacDonald, L. H.; Guo, Y.; Marks, S. J.; Kosek, M.; Yori, P. P.; Pinedo, S. R.; Schwab, K. J. Fecal Indicator Bacteria Contamination of Fomites and Household Demand for Surface Disinfection Products: A Case Study from Peru. *Am. J. Trop. Med. Hyg.* **2013**, *89* (5), 869–872. https://doi.org/10.4269/AJTMH.12-0425.

(262) Boone, S. A.; Gerba, C. P. Significance of Fomites in the Spread of Respiratory and Enteric Viral Disease. *Appl. Environ. Microbiol.* **2007**, *73* (6), 1687–1696. https://doi.org/10.1128/AEM.02051-06/ASSET/F25F792F-BC40-4985-A2D5-96990F95B1E4/ASSETS/GRAPHIC/ZAM0060776300003.JPEG.

(263) Griffith, C. J.; Cooper, R. A.; Gilmore, J.; Davies, C.; Lewis, M. An Evaluation of Hospital Cleaning Regimes and Standards. *J. Hosp. Infect.* **2000**, *45* (1), 19–28. https://doi.org/10.1053/JHIN.1999.0717.

(264) Zhang, P.; Lin, L.; Zang, D.; Guo, X.; Liu, M. Designing Bioinspired Anti-Biofouling Surfaces Based on a Superwettability Strategy. *Small* **2017**, *13* (4), 1503334. https://doi.org/10.1002/SMLL.201503334.

(265) Shakeri, A.; Yousefi, H.; Jarad, N. A.; Kullab, S.; Al-Mfarej, D.; Rottman, M.; Didar, T. F. Contamination and Carryover Free Handling of Complex Fluids Using Lubricant-Infused Pipette Tips. *Sci. Reports 2022 121* **2022**, *12* (1), 1–10. https://doi.org/10.1038/s41598-022-18756-x.

(266) Afonso, E.; Bayat, F.; Ladouceur, L.; Khan, S.; Martínez-Gómez, A.; Weitz, J. I.; Hosseinidoust, Z.; Tiemblo, P.; García, N.; Didar, T. F. Highly Stable Hierarchically Structured All-Polymeric Lubricant-Infused Films Prevent Thrombosis and Repel Multidrug-Resistant Pathogens. *ACS Appl. Mater. Interfaces* **2022**, *14* (48), 53535–53545. https://doi.org/10.1021/ACSAMI.2C17309/SUPPL_FILE/AM2C17309_SI_004.PDF.

(267) Yousefi, H.; Samani, S. E.; Khan, S.; Prasad, A.; Shakeri, A.; Li, Y.; Filipe, C. D. M.; Didar, T. F. LISzyme Biosensors: DNAzymes Embedded in an Anti-Biofouling Platform for Hands-Free Real-Time Detection of Bacterial Contamination in Milk. *ACS Nano* **2022**, *16* (1), 29–37. https://doi.org/10.1021/ACSNANO.1C05766/ASSET/IMAGES/LARGE/NN1C05766_0005.JPEG.

(268) Verho, T.; Bower, C.; Andrew, P.; Franssila, S.; Ikkala, O.; Ras, R. H. A. Mechanically Durable Superhydrophobic Surfaces. *Adv. Mater.* **2011**, *23* (5), 673–678. https://doi.org/10.1002/ADMA.201003129.

(269) Maclachlan, R.; Vahedi, F.; Imani, S. M.; Ashkar, A. A.; Didar, T. F.; Soleymani, L. Pathogen-Repellent Plastic Warp with Built-In Hierarchical Structuring Prevents the Contamination of Surfaces with Coronaviruses. **2022**, *14* (9). https://doi.org/10.1021/acsami.1c21476.

(270) Li, W.; Zhan, Y.; Amirfazli, A.; Siddiqui, A. R.; Yu, S. Recent Progress in Stimulus-Responsive Superhydrophobic Surfaces. *Prog. Org. Coatings* **2022**, *168*, 106877. https://doi.org/10.1016/J.PORGCOAT.2022.106877.

(271) Abu Jarad, N.; Rachwalski, K.; Bayat, F.; Khan, S.; Shakeri, A.; MacLachlan, R.; Villegas, M.; Brown, E. D.; Soleymani, L.; Didar, T. F. An Omniphobic Spray Coating Created from Hierarchical Structures Prevents the Contamination of High-Touch Surfaces with Pathogens. *Small* **2023**, 2205761. https://doi.org/10.1002/SMLL.202205761.

(272) Tian, X.; Verho, T.; Ras, R. H. A. Moving Superhydrophobic Surfaces toward Real-World Applications. *Science (80-.).* **2016**, *352* (6282), 142–143. https://doi.org/10.1126/SCIENCE.AAF2073/ASSET/65CC3A4D-03CC-4545-B11C-52702CCF0532/ASSETS/GRAPHIC/352_142_F2.JPEG.

(273) Sakib, S.; Hosseini, A.; Zhitomirsky, I.; Soleymani, L. Photoelectrochemical IL-6 Immunoassay Manufactured on Multifunctional Catecholate-Modified TiO2Scaffolds. *ACS Appl. Mater. Interfaces* **2021**, *13* (43), 50851–50861. https://doi.org/10.1021/ACSAMI.1C18240/SUPPL_FILE/AM1C18240_SI_001.PDF.

(274) Murakami, D.; Jinnai, H.; Takahara, A. Wetting Transition from the Cassie-Baxter State to the Wenzel State on Textured Polymer Surfaces. *Langmuir* **2014**, *30* (8), 2061–2067. https://doi.org/10.1021/LA4049067/SUPPL_FILE/LA4049067_SI_004.AVI.

(275) Im, M.; Im, H.; Lee, J. H.; Yoon, J. B.; Choi, Y. K. A Robust Superhydrophobic and Superoleophobic Surface with Inverse-Trapezoidal Microstructures on a Large Transparent Flexible Substrate. *Soft Matter* **2010**, *6* (7), 1401–1404. https://doi.org/10.1039/B925970H.

(276) Roilides, E.; Simitsopoulou, M.; Katragkou, A.; Walsh, T. J. How Biofilms Evade Host Defenses. *Microbiol. Spectr.* **2015**, *3* (3). https://doi.org/10.1128/MICROBIOLSPEC.MB-0012-2014.

(277) Zhang, T.; Lin, P.; Wei, N.; Wang, D. Enhanced Photoelectrochemical Water-Splitting Property on TiO2 Nanotubes by Surface Chemical Modification and Wettability Control. *ACS Appl. Mater. Interfaces* **2020**, *12* (17), 20110–20118. https://doi.org/10.1021/ACSAMI.0C03051/ASSET/IMAGES/LARGE/AM0C03051_0008.JPEG.

(278) Yang, G.; Li, X.; He, Y.; Ma, J.; Ni, G.; Zhou, S. From Nano to Micro to Macro: Electrospun Hierarchically Structured Polymeric Fibers for Biomedical Applications. *Prog. Polym. Sci.* **2018**, *81*, 80–113. https://doi.org/10.1016/J.PROGPOLYMSCI.2017.12.003.

(279) Wu, W.; Wang, X.; Wang, D.; Chen, M.; Zhou, F.; Liu, W.; Xue, Q. Alumina Nanowire Forests via Unconventional Anodization and Super-Repellency plus Low Adhesion to Diverse Liquids. *Chem. Commun.* **2009**, No. 9, 1043–1045. https://doi.org/10.1039/B818633B.

(280) Hizal, F.; Rungraeng, N.; Lee, J.; Jun, S.; Busscher, H. J.; Van Der Mei, H. C.; Choi, C. H. Nanoengineered Superhydrophobic Surfaces of Aluminum with Extremely Low Bacterial Adhesivity. *ACS Appl. Mater. Interfaces* **2017**, *9* (13), 12118–12129. https://doi.org/10.1021/ACSAMI.7B01322/SUPPL_FILE/AM7B01322_SI_001.PDF.

(281) Chu, Z.; Seeger, S. Superamphiphobic Surfaces. *Chem. Soc. Rev.* **2014**, *43* (8), 2784–2798. https://doi.org/10.1039/C3CS60415B.

(282) Chauhan, P.; Kumar, A.; Bhushan, B. Self-Cleaning, Stain-Resistant and Anti-Bacterial Superhydrophobic Cotton Fabric Prepared by Simple Immersion Technique. **2018**. https://doi.org/10.1016/j.jcis.2018.09.087.

(283) Suryaprabha Mathur Gopalakrishnan Sethuraman, T. Fabrication of Copper-Based Superhydrophobic Self-Cleaning Antibacterial Coating over Cotton Fabric. *Cellulose 24*. https://doi.org/10.1007/s10570-016-1110-z.

(284) Görgülüer, H.; Çakıroğlu, B.; Özacar, M. Ag NPs Deposited TiO2 Coating Material for Superhydrophobic, Antimicrobial and Self-Cleaning Surface Fabrication on Fabric. *J. Coatings Technol. Res.* **2020**, *18* (2), 569–579. https://doi.org/10.1007/s11998-020-00412-6.

(285) Müller, R.; Eidt, A.; Hiller, K. A.; Katzur, V.; Subat, M.; Schweikl, H.; Imazato, S.; Ruhl, S.; Schmalz, G. Influences of Protein Films on Antibacterial or Bacteria-Repellent Surface Coatings in a Model System Using Silicon Wafers. *Biomaterials* **2009**, *30* (28), 4921–4929. https://doi.org/10.1016/J.BIOMATERIALS.2009.05.079.

(286) Razaviamri, S.; Wang, K.; Liu, B.; Lee, B. P.; Schnabelrauch, M. Molecules Catechol-Based Antimicrobial Polymers. **2021**. https://doi.org/10.3390/molecules26030559.

(287) Kim, S.; Moon, J. M.; Choi, J. S.; Cho, W. K.; Kang, S. M. Mussel-Inspired Approach to Constructing Robust Multilayered Alginate Films for Antibacterial Applications. *Adv. Funct. Mater.* **2016**, *26* (23), 4099–4105. https://doi.org/10.1002/ADFM.201600613.

(288) Saiz-Poseu, J.; Mancebo-Aracil, J.; Nador, F.; Busqué, F.; Ruiz-Molina, D. The Chemistry behind Catechol-Based Adhesion. *Angew. Chemie Int. Ed.* **2019**, *58* (3), 696–714. https://doi.org/10.1002/ANIE.201801063.

(289) Sakib, S.; Bakhshandeh, F.; Saha, S.; Soleymani, L.; Zhitomirsky, I. Surface Functionalization of Metal Oxide Semiconductors with Catechol Ligands for Enhancing Their Photoactivity. **2021**. https://doi.org/10.1002/solr.202100512.

(290) Sakib, S.; Pandey, R.; Soleymani, L.; Zhitomirsky, I. Surface Modification of TiO 2 for Photoelectrochemical DNA Biosensors . *Med. DEVICES SENSORS* **2020**, *3* (2). https://doi.org/10.1002/MDS3.10066.

(291) Pinnataip, R.; Lee, B. P. Oxidation Chemistry of Catechol Utilized in Designing Stimuli-Responsive Adhesives and Antipathogenic Biomaterials. *ACS Omega* **2021**, *6* (8), 5113–5118. https://doi.org/10.1021/ACSOMEGA.1C00006/ASSET/IMAGES/LARGE/AO1C00006_0004.JPEG.

(292) Jang, S.; Moon, J.; Cho, H.; Joo, C. W.; Lee, J.; Shin, J. W.; Park, S. K.; Cho, N. S.; Yang, S. Y.; Kwon, B. H. Spontaneously Formed Organic Wrinkle Structure for Top-Emitting Organic Light Emitting Diodes. *J. Ind. Eng. Chem.* **2019**, *80*, 490–496. https://doi.org/10.1016/J.JIEC.2019.08.033.

(293) Um, E.; Cho, Y. K.; Jeong, J. Spontaneous Wrinkle Formation on Hydrogel Surfaces Using Photoinitiator Diffusion from Oil-Water Interface. *ACS Appl. Mater. Interfaces* **2021**, *13* (13), 15837–15846. https://doi.org/10.1021/ACSAMI.1C00449/SUPPL_FILE/AM1C00449_SI_002.AVI.

(294) Kim, Y. H.; Lee, Y. M.; Lee, J. Y.; Ko, M. J.; Yoo, P. J. Hierarchical Nanoflake Surface Driven by Spontaneous Wrinkling of Polyelectrolyte/Metal Complexed Films. *ACS Nano* **2012**, *6* (2), 1082–1093. https://doi.org/10.1021/NN203226K/SUPPL_FILE/NN203226K_SI_003.WMV.

(295) Li, Y.; Li, X.; Guo, W.; Wu, M.; Sun, J. Chemistry Spontaneous Wrinkling of Layer-by-Layer Assembled Polyelectrolyte Films for Humidity-Responsive Superhydrophobicity. **2016**, *59*, 1568–1573. https://doi.org/10.1007/s11426-016-0243-7.

(296) Chen, X.; Ren, K.; Chen, J.; Wang, J.; Zhang, H.; Ji, J. Self-Wrinkling Polyelectrolyte Multilayers: Construction, Smoothing and the Underlying Mechanism. *Phys. Chem. Chem. Phys.* **2016**, *18* (45), 31168–31174. https://doi.org/10.1039/C6CP05419F.

Appendix A: Formation of Hierarchical wrinkled structure on PO substrates

The work in this section describes and discusses the results of my contributions to the work published in ACS Nano on December 13, 2019, which was led by Sara M. Imani. The repellent surface described in chapter 3, while displaying excellent blood repellent properties, suffered from a few drawbacks including non-flexible substrate after shrinking and expensive AuNP. To address this the substrate was switched from PS to PO, which maintains its flexibility after shrinking. The PO substrate also had substantially higher strain compared to the PS, shrinking to 10% of its original area compared to the 40% of the PS. Comparison of the hierarchical structure of the PO and PS surface can be found in Figure A-1.

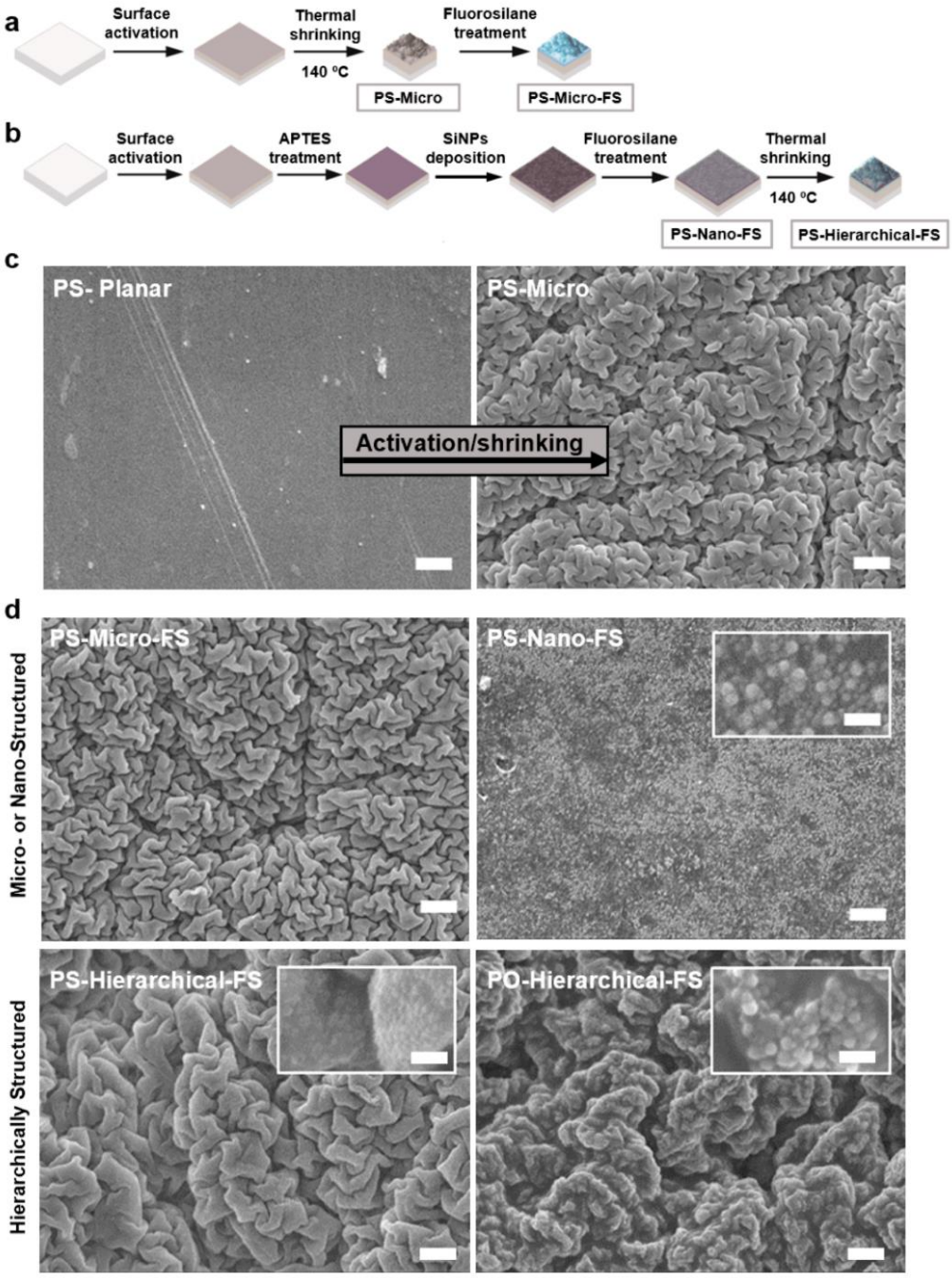

Figure A-1: Schematic illustrating the process for fabricating omniphobic surfaces and wraps. a) Steps for creating microstructured surfaces (PS-Micro and PS-Micro-FS). b) Steps for creating nanostructured surfaces (PS-Nano-FS) and hierarchical surfaces (PS-Hierarchical-FS). Similar process is done for producing PO-Hierarchical-FS. c) Corresponding scanning electron microscopy (SEM) images to each processing step with high magnification insets showing the visible nanostructures (27nm SiNPs). The scale bars on larger SEM images represent 1um and for the insets represent 100nm. The insets provide high magnification representative image from the imaged substrate.

After the desired surface structure was achieved, the wetting properties of the wraps were compared to the original PS surface structures made in chapter 3. The hierarchically wrinkled structures on the PO substrates showed similar properties to that of the PS surface, displaying contact angle of $154^{o}\pm4^{o}$, $124^{o}\pm2^{o}$ and $142^{o}\pm5^{o}$ for water, blood, and hexadecane respectively. Additionally, the PO substrate also maintained its liquid repellent properties under deformation, allowing it to conform around objects without losing its repellent properties. Further, characterization of the surface wettability under dynamic conditions was also conducted in this work, as seen with the slow-motion snap shots (Figure A-1b) and measurements of the advancing/receding contact angles and contact angle hysteresis (Figure A-1c). The omniphobic surface here showed great antiwetting properties under dynamic conditions, as impact water droplets were able to completely detach from the surface after impact (Figure A-1b), indicating robust superhydrophobic wetting states.

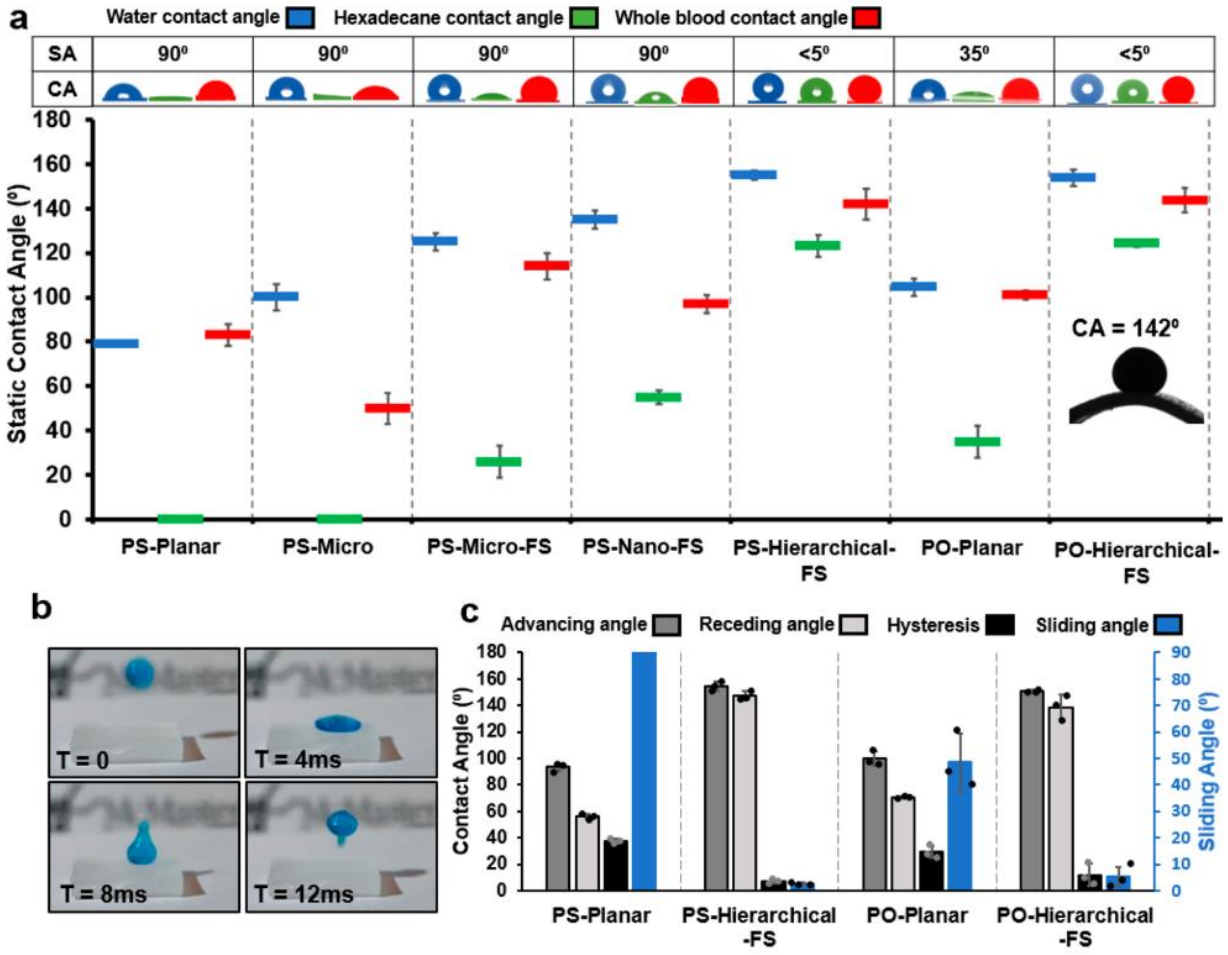

Figure A-2: Surface repellency and assessment of omniphobicity. a) Graph showing the contact angle of different surfaces for water, hexadecane, and blood as test liquids. Table showing sliding angles for water on various surfaces (SA represents sliding angle) and representative colour-coded image of the contact angle (CA represents contact angle). The inset shows the blood contact angle on a bent PO-Hierarchical-FS, showing he robustness of the surface upon bending. b) slow-motion snapshots of 10uL droplet on PO-hierarchical-FS at 4ms intervals. c) Advancing/receding contact angles, contact angle hysteresis and calculated sliding angle. Error bars represent standard deviation from the mean for at least three samples. The “dot” represents the individual data points leading to the averages plotted as bars.